UNDRAINED RESPONSE OF SATURATED SANDS WITH EMPHASIS ON LIQUEFACTION AND CYCLIC MOBILITY

by

JIN-CHING CHERN

B.S., National Taiwan University, 1968

M.E., Asian Institute of Technology, 1971

M.A.Sc., The University of British Columbia, 1981

A THESIS SUBMITTED IN PARTIAL FULFILMENT OF

THE REQUIREMENTS FOR THE DEGREE OF

DOCTOR OF PHILOSOPHY

in

THE FACULTY OF GRADUATE STUDIES

DEPARTMENT OF CIVIL ENGINEERING

We accept this thesis as conforming

to the required standard

THE UNIVERSITY OF BRITISH COLUMBIA

January, 1985

In presenting this thesis in partial fulfilment of the requirements for an advanced degree at the University of British Columbia, I agree that the Library shall make it freely available for reference and study. I further agree that permission for extensive copying of this thesis for scholarly purposes may be granted by the head of my department or by his or her representatives. It is understood that copying or publication of this thesis for financial gain shall not be allowed without my written permission.

Department of Civil Engineering

The University of British Columbia
1956 Main Mall
Vancouver, Canada
V6T 1Y3

Date February 15, 1985

ABSTRACT

An experimental investigation of the undrained monotonic and cyclic loading behaviour of a saturated angular sand and a rounded sand under triaxial conditions is presented. These studies are aimed at obtaining a unified approach to the undrained behaviour of sand spanning from strain softening (termed liquefaction or limited liquefaction) to strain hardening response and linking the cyclic loading behaviour to the monotonic loading behaviour. It is also aimed at investigating the differences in undrained loading behaviour of sand with different particle angularity.

Under monotonic loading, the strain softening response is initiated and terminated at two distinct values of effective stress ratio termed critical effective stress ratio state (CSR) and phase transformation state (PT), regardless of the relative density and consolidation stress conditions. For strain hardening response, the start of dilation also occurs at the same effective stress ratio of PT for strain softening response. It is shown that the unique steady state line concept for liquefaction is also valid for limited liquefaction. The PT states for strain hardening response, however, form a series of lines, which are function of initial void ratio, merging into the unique steady state line as the consolidation stresses increase.

A 3-D effective stress state behavioural model is developed, which enables prediction of the anticipated undrained loading behaviour (strain softening or strain hardening) from the knowledge of the initial state of the sand. It is shown that a complete specifications of initial state of sand, i.e., void ratio, confining pressure and static shear, is required to predict the type of undrained response, especially for angular sand.

Under cyclic loading, if liquefaction develops, the CSR, effective stress ratio at PT state and steady state line are the same as those observed under monotonic loading. If cyclic mobility develops, the effective stress ratio at PT state is also the same as that observed under monotonic loading. Thus, the 3-D effective stress state diagram provides a link between monotonic and cyclic loading behaviour, and is used to develop the criteria for the occurrence of liquefaction and cyclic mobility. The influences of void ratio and confining pressure on the cyclic loading behaviour are similar to those for the monotonic loading behaviour. However, the influence of static shear on cyclic loading behaviour can be completely different depending on whether liquefaction or cyclic mobility is developed.

The undrained loading behaviour of rounded sand is similar to that of the angular sand. However, for the range of consolidation stresses of interest, the initial relative density alone provides a good single parameter characterizing the initial state of the sand, and hence its anticipated response.

TABLE OF CONTENTS

TABLE OF CONTENTS (cont'd)

TABLE OF CONTENTS (cont'd)

LIST OF FIGURES

LIST OF FIGURES (Continued)

LIST OF FIGURES (Continued)

LIST OF FIGURES (Continued)

LIST OF FIGURES (Continued)

LIST OF FIGURES (Continued)

NOTATIONS

A_1, A_2	area of top chamber and bottom chamber of air loading piston
A_r	area of the loading ram
A_s	sample area
a_{max}	maximum ground surface acceleration
B	Skempton's pore pressure parameter
c	critical effective stress ratio constant = $(\sigma_1'/\sigma_3')_{CSR}$
CSR	critical effective stress ratio
CT	characteristic threshold
D_r	relative density
D_{rc}	relative density after consolidation
D_{ri}	initial relative density of specimen as prepared (under initial effective stress of 0.2 kgf/cm^2)
e	void ratio
e_c	void ratio after consolidation
e_i	initial void ratio of specimen as prepared (under initial effective stress of 0.2 kgf/cm^2)
g	gravitational acceleration
K	bias relay constant
K_c	consolidation stress ratio = $\sigma_{1c}'/\sigma_{3c}'$
m	magnification factor of pressure amplifier
N	number of stress cycles
$p, p_1, p_2, \bar{p}$	air pressures
p'	= 1/2 $(\sigma_1' + \sigma_3')$
PT	phase transformation

q	$= 1/2\ (\sigma_1' - \sigma_3')$
R	magnification factor of ratio relay
s	signal pressure
SSL	steady state line
S_{up}	undrained peak shear strength
S_{us}	undrained steady state shear strength
ΔS_{up}	shear stress increment to peak shear strength under undrained monotonic loading
u	pore pressure
Δu	excess pore pressure
ε_a	axial strain
ϕ'	angle of internal friction
σ_1', σ_3'	major and minor effective pricipal stresses
σ_1	major total principal stress
$\Delta\sigma_1', \Delta\sigma_3'$	major and minor effective prinpcipal stress increments
$\sigma_{1c}', \sigma_{3c}'$	major and minor effective principal consolidation stresses
$(\sigma_{1c}')_{crit}$	critical consolidation stress
$\sigma_{1p}', \sigma_{3p}'$	major and minor effective principal stresses at peak strength
σ_d	deviator stress
σ_{dcy}	cyclic deviator stress
$\Delta\sigma_d$	deviator stress increment
τ_{cy}	cyclic shear stress = $\sigma_{dcy}/2$
τ_s	static shear stress

ACKNOWLEDGEMENTS

In presenting this thesis, the author wishes to express his gratitude to the University of British Columbia and National Research Council of Canada for financial support which made this investigation possible.

The author would also like to thank the following individuals:

- His supervisor, Dr. Y.P. Vaid, for his invaluable guidance and advice during the entire course of the research.
- Dr. P.M. Byrne, Dr. R.G. Campanella and Dr. W.D.L. Finn for their valuable comments.
- His colleagues for their valuable discussions, and Dr. P.K. Robertson for his suggestion in the manner of presenting part of the test results.
- The staff of the Civil Engineering Department Workshop for their technical assistance in fabricating the testing equipments.
- Mrs. Brenda Gillespie for her assistance in drafting the figures, and Mrs. Kelly Lamb for typing the manuscripts and final thesis.

And finally, the author deeply appreciates the support and consideration given to him by his wife during the entire course of his studies.

CHAPTER 1

INTRODUCTION

Undrained loading behaviour of saturated sands is of direct interest in practice where deposits of such materials may be subjected to rapid shearing. As a result of such loading, sand may develop large deformations, and for certain initial states may even flow like a frictional fluid. The undrained shearing could be due to cyclic earthquake loading or rapidly applied static loading such that practically no drainage occurs.

A large number of studies (e.g., Finn et al., 1971; Ishihara et al., 1975; Lee and Seed, 1967[1,2]; Seed and Lee, 1966; Seed et al., 1975) have been reported in literature concerning the large deformation developed in saturated sands under cyclic loading. The main emphasis in these studies has been on the resistance of sand to strain development, with little attention paid as to the mechanism which is responsible for this strain development. Most researchers attributed the developments of large deformation under cyclic loading to liquefaction. This phenomenon of developing large deformation under cyclic loading has apparently been called liquefaction, because these deformations are developed when a condition of transient zero effective stress occurs in the sand at some stage of the cyclic loading.

Large deformations can also occur in saturated sands under rapidly applied static loads. The development of such deformations under static loading conditions, which is a result of strain softening (temporary or permanent decrease in shear resistance with continued straining) undrained response of sand, has been treated separately as another

category of problem (e.g., Casagrande 1975, Castro 1969), and has also been termed liquefaction. This type of liquefaction response can not be explained within the framework of liquefaction as perceived under cyclic loading conditions.

It is now recognized, however, that the development of large deformation could be the result of transient zero effective stress condition developed at certain stage of the cyclic loading without any strain softening, or strain softening response developed under static or even cyclic loading conditions (Castro 1969; Seed, 1979). These two phenomena have been called cyclic mobility and liquefaction, respectively (Castro, 1969; Casagrande, 1975; Seed, 1979) and will also be referred to as such in this thesis. However, due to a lack of clear distinction as to which of the two phenomena is responsible for development of strain, considerable controversies have arisen regarding the influence of some factors, most notably the level of static shear, on the resistance to strain development in liquefaction and cyclic mobility (Casagrande, 1975; Castro and Poulos, 1977). A proper recognition of the mechanism of strain development (liquefaction or cyclic mobility) is vital for a rational explanation of some of the conflicting ideas regarding undrained response of sand (Vaid and Chern, 1983[1,2]).

Traditionally, the study of the phenomenon of liquefaction under monotonic loading has been carried out on sand which developed strain softening response with unlimited deformation (Castro, 1969). The concept of an eventual steady state of deformation has been advanced in relation to the sand during the state of liquefaction. The state of sand is characterized by its void ratio and the effective stress conditions.

Liquefaction is thus considered a phenomenon wherein a sand, which is consolidated to a state well above the steady state, develops large unidirectional deformation associated with strain softening response on undrained shearing, ultimately ending at steady state. Such a sand has been called contractive for which a unique steady state line, independent of the loading paths causing the steady state deformations, has been proposed (Castro, 1969; Castro and Poulos, 1977; Castro et al, 1982). Based on this perception of liquefaction, the development of large deformation is exclusively due to the occurrence of strain softening leading to steady state deformation. Liquefaction can not be induced in sand with initial state below the steady state line and such a sand is called dilative.

During cyclic loading, the deformation can develop either due to the occurrence of liquefaction or cyclic mobility (Castro, 1975; Vaid and Chern, 1983[2]). In most cyclic loading studies, however, predominant focus has tended to be on the response of dilative sand in which strain development occurs as a consequence of cyclic mobility (Seed and Lee, 1966; Lee and Seed, 1967). For certain initial states and cyclic stresses, a sand may develop limited liquefaction (strain softening response, but without unlimited strain) under cyclic loading (Vaid and Chern, 1983[1,2]). In such cases, cyclic mobility can occur after the occurrence of limited liquefaction, when cyclic loading is continued, which results in additional accumulation of strain. Thus, it is conceivable that liquefaction and cyclic mobility occur in different regimes of initial sand state. In between, both limited liquefaction and cyclic mobility can occur, and limited liquefaction always precedes cyclic mobility.

In the steady state approach to liquefaction (Castro, 1969; Castro et al., 1982), the void ratio and confining pressure have been used in a 2-D state diagram to separate the initial sand state into regions of liquefaction and dilative responses. Tests on sand are performed purposely for those initial states which induce liquefaction only. For states which develop dilative response in monotonic loading or cyclic mobility in cyclic loading are considered of no concern. Although the general influence of static shear stress on the occurrence of liquefaction has been identified, the static shear stress has never been incorporated as a part characterizing the initial state of sand in order to predict the occurrence of liquefaction. Only an arbitrary criterion, such as sand with an initial state well above and to the right of the steady state line is susceptible to liquefaction, has been proposed. No clear quantitative boundary for separating the initial states into regions of liquefaction and dilative response has been specified, and thus the influence of several factors on the undrained behaviour of sand can not be explained rationally. At present, no comprehensive and unified approach exists which covers the undrained behaviour of sand in both contractive (which includes limited liquefaction) and dilative regimes, and enables prediction of the undrained response from the knowledge of the initial sand state together with the nature of loading applied.

Most of the understanding in the undrained behaviour of saturated sand has been obtained from tests performed on natural sands with generally rounded particles and under relatively low confining pressures. Relative density has often been used as the sole criterion to separate the regions of development of liquefaction and cyclic mobility, without

any reference as to the particle angularity and consolidation stress condition. It is generally believed that sand with low relative density is susceptible to liquefaction, and that with high relative density can develop cyclic mobility only. However, there is a fair acceptance of the fact that sand behaviour is very much dependent on the particle characteristics and consolidation stress condition. Thus, it may not be prudent to predict behaviour of a sand by extrapolating the results obtained on another sand under relatively low consolidation stress and different consolidation stress conditions.

The first purpose of these investigations is to present a unified approach for the undrained behaviour of sand which spans between liquefaction with unlimited deformation on one side and dilative response on the other. This is done by an experimental study of the undrained monotonic loading behaviour which covers the whole spectrum of undrained response, i.e., from strain softening response associated with the development of unlimited strain on one end to strain hardening response on the other, using a wide range of initial sand states. Then, a comprehensive behavioural model for the sand is attempted, which enables prediction of the undrained monotonic loading behaviour from the knowledge of initial state of the sand. The link between undrained static and cyclic loading response is demonstrated within the framework of undrained monotonic loading behaviour, i.e. whether liquefaction or cyclic mobility will develop under cyclic loading conditions in sand which is characterized as contractive or dilative under undrained monotonic loading condition. Furthermore, additional cyclic loading criteria for liquefaction under cyclic loading is established even if liquefaction will be expected under monotonic loading. The behavioural model for the sand is also used to

explain the influence of factors (such as void ratio, confining pressure and static shear) on the undrained behaviour of saturated sand under both static and cyclic loading conditions in an attempt to clarify some contradictory conclusions in literature arisen primarily due to different perceptions of the phenomenon of liquefaction.

The second objective of the study is the investigation of the differences in the undrained response of sand with changes in particle angularity. This is achieved by comprehensive experimental studies over a large range of confining pressure on two sands having identical gradation and mineral composition, one angular and the other rounded. Behaviour of angular sands under high confining pressure is of utmost importance in the design of tailings dams where such sands are used. There is a growing trend towards building tailings dams of increasing height. Confining pressure up to 25.0 kgf/cm^2 (2450 kPa) could be encountered in such dams of 200 m height. Tailings dams of this height are either being constructed or under consideration in the future. The undrained behaviour of tailings sand under high confining pressure could have a dramatic difference from that of the rounded or subrounded sands.

CHAPTER 2

GENERAL ASPECTS OF UNDRAINED BEHAVIOUR OF SAND

Undrained response of saturated sand is traditionally considered separately under monotonic and cyclic loading conditions. Interest in monotonic loading has generally been related to undrained failure associated with flow slides. The characteristic feature of such behaviour is extremely large deformation under very small shear resistance. Conditions which could bring about such a response from soil could be rapid increase in stresses due to earthquake loading, shock loading or even static loading. Interest in cyclic undrained loading behaviour has been related to the susceptibility of sand to accumulate undesirable deformation during earthquake shaking.

Monotonic Loading Behaviour

The range of typical undrained triaxial compression behaviour of isotropically consolidated saturated sand under moderate confining pressure is shown in Fig. 2.1. The variations in stress-strain curves from type 1 to type 5 is associated with increasing relative density. These types of response have been reported by several investigators, such as Bishop, Webb and Skinner (1965), Bjerrum, Kringstad and Kummeneje (1961), Castro (1969), Castro et al. (1982) and Lee and Seed (1970). The same type of characteristic behaviour is also obtained if the sand is initially anisotropically consolidated.

Types 1, 2 and 3 are strain softening response - a behaviour associated with loss of shear resistance after the occurrence of a peak. Sand showing such behaviour is called contractive. Type 1 response has

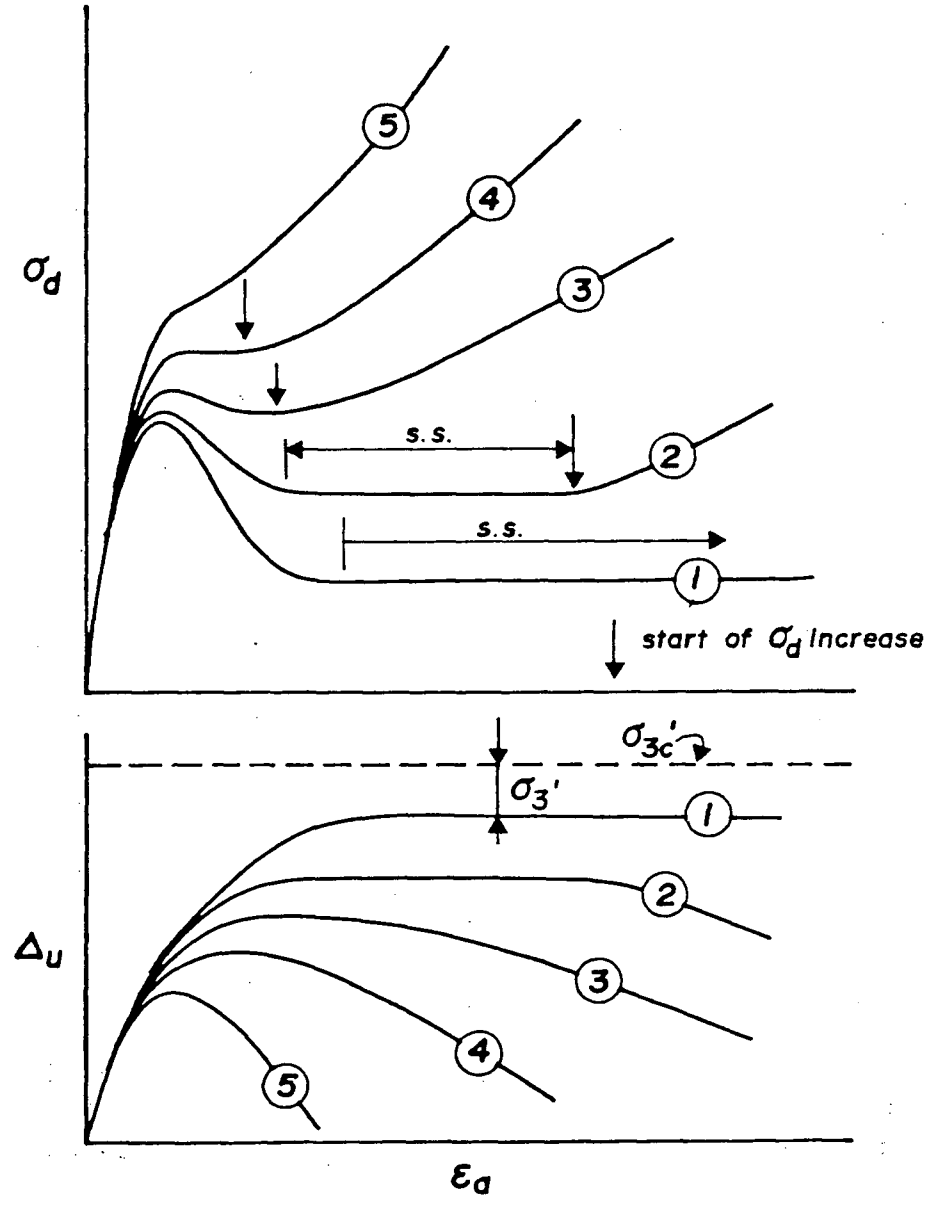

Fig. 2.1 Characteristic behaviour of saturated sand under undrained monotonic loading.

been called liquefaction by Castro (1969), Casagrande (1975) and Seed (1979). It is a strain softening response with unlimited unidirectional strain and will be called herein true liquefaction. The characteristic feature of this type of response is continued deformation at constant void ratio, confining stress and shear resistance, which has been called steady state deformation or flow deformation, since it resembles flow of fluid (Poulos, 1971; Castro, 1975; Vaid and Chern, 1983). However, the shear resistance during such deformation is of a frictional nature, instead of zero, as would be the case for a fluid.

Type 2 and 3 responses were called limited liquefacton by Castro (1969). Such types of response is thus strain softening with limited unidirectional strain. Instead of deforming continuously at reduced constant shear resistance, the shear resistance of sand increases with further deformation after attaining a minimum, and simultaneously the pore pressure decreases after attaining its maximum value. However, over some finite range of strain prior to the commencement of increase in shear resistance, the sand deforms at essentially constant void ratio, effective confining stress and shear resistance, which could be considered as the steady state condition of the case of true liquefaction. The difference in response represented by type 2 and type 3 is a lesser degree of strain softening and associated smaller strain until the start of increase in shear resistance or decrease in pore pressure in type 3 compared to that in type 2.

The arrows in Fig. 2.1 indicate the arrest of strain softening response, i.e., the start of increase in shear resistance and decrease in pore pressure with further straining. On effective stress path, this condition is reflected by a sharp turnaround of the effective stress

path. Such a condition has been called phase transformation (PT) state by Ishihara et al. (1975). After the PT state has been reached, the effective stress path approaches the undrained failure envelope rather quickly with further straining. A state of PT for true liquefaction (type 1 response) coincides with the attainment of steady state. The stress state then stays on the PT line while steady state deformation continues indefinitely.

Type 4 response is associated with a terminal case of strain softening response in which the degree of strain softening can be considered as zero. Such a behaviour is represented by a flat plateau in stress-strain curve over a certain strain range before the shear resistance starts to increase and pore pressure starts to decrease with further straining.

Type 5 response represents the strain hardening behaviour with no loss of shear resistance. Sand showing such behaviour is called dilative. For such a response, a sharp turnaround in the effective stress path is not well defined (see Fig. 2.2). However, the condition of start of decrease in pore pressure after its maximum value is well defined. Such a condition has been called characteristic threshold (CT) by Luong (1980), which is the same as the PT state described before. Luong further showed that this threshold occurs at the same effective stress ratio regardless of the relative density of sand. It represents the boundary between contractive and dilative regions of sand in effective stress space. Luong's conclusions were based on tests on one sand under low confining pressure only.

It may be pointed out that a sand exhibiting strain hardening response can develop strain softening response but only after large straining. Such type of response is illustrated schematically in Fig.

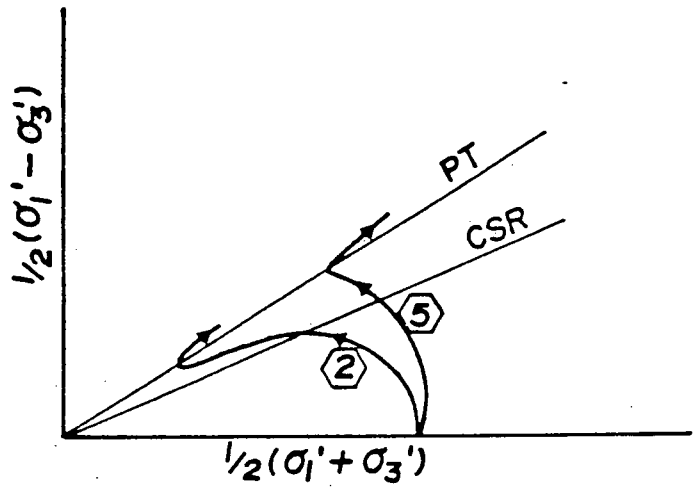

Fig. 2.2 Effective stress paths of contractive and dilative response.

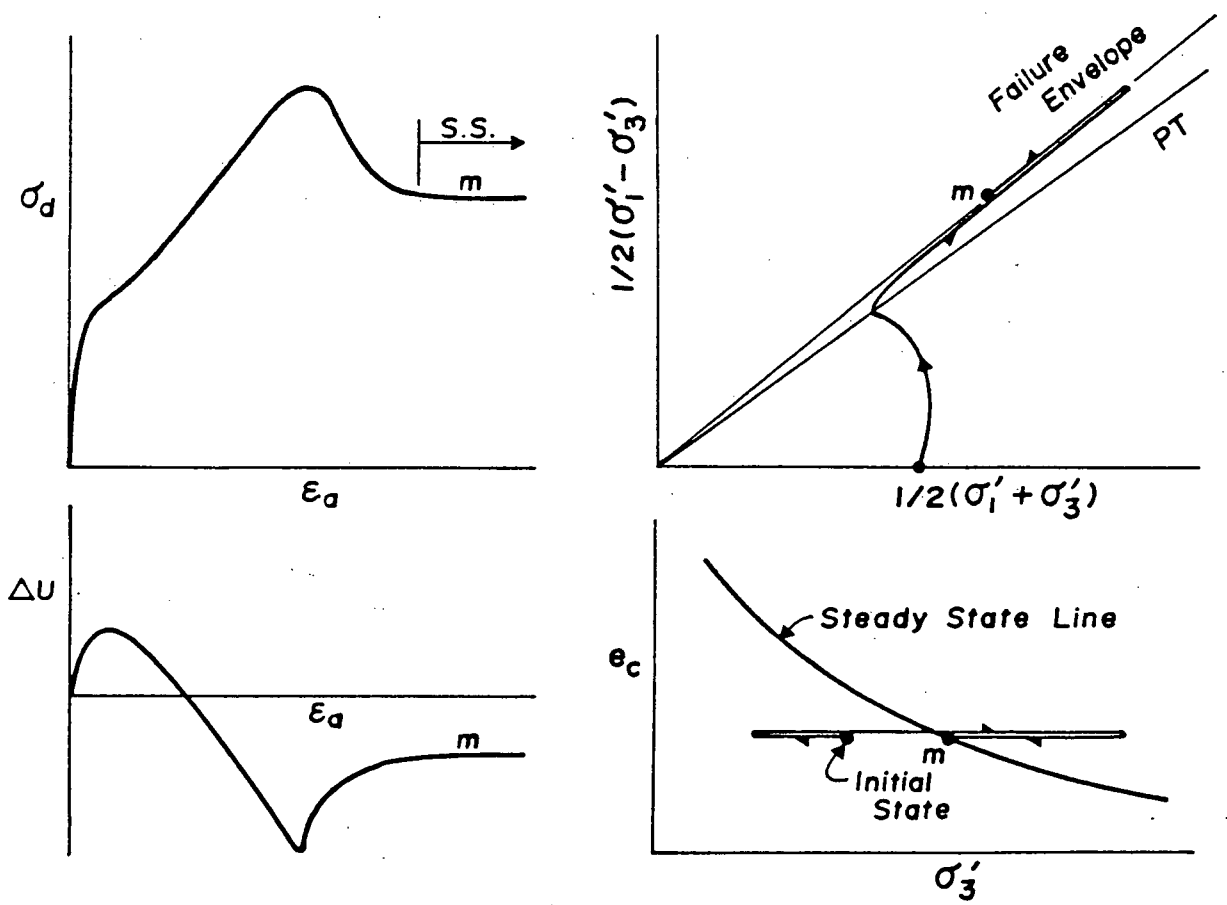

Fig. 2.3 Characteristic behaviour of dilative sand after large deformation.

2.3. After initial strain hardening response (Type 5), the sand dilates until the effective confining stress becomes high enough to cause contraction in the sand. The sand then develops a strain softening response ultimately leading to a state of constant effective confining stress and constant shear resistance. This was also termed steady state by Poulos (1981) and Castro et al. (1982). This type of strain softening response however can be induced only after very large straining, and the shear stress required to induce such response is well above the levels of practical interest and may even be greater than the drained strength. Moreover, the back pressure for the sand to sustain the negative excess pore pressure without causing cavitation is very high, which may seldom be encountered in practical cases. Therefore, this type of response is not considered in this investigation.

Predominant interest in monotonic loading behaviour has been with the occurrence of true liquefaction. Castro (1969), Castro et al. (1982) and Casagrande (1975) studied such behaviour in relation to the problem of flow slide. It has been shown by Castro (1969) that if sand undergoes true liquefaction, the effective confining stress and shear resistance during steady state deformation are uniquely related to void ratio, and that such relationship is independent of the initial consolidation stress condition. This unique line relating the void ratio with effective confining stress or shear resistance during steady state was called steady state line. Triaxial tests on several sands with rounded to angular particles under a wide range of confining pressure and consolidation stress ratio have been shown to support these concepts (Castro, 1969; Castro et al. 1982). However, the studies have been limited to compression mode only, and possible influence of stress path, e.g., triaxial

extension, was not considered. Only true liquefaction was considered and no attention was given to the treatment of range of behaviour described by response type 2 to type 5 (Fig. 2.1). Consideration was given only to relate parameters during steady state deformation. In particular, no quantitative attempt was made to assess whether such a response could occur for a known initial state of the sand. Only an arbitrary criterion, e.g., initial state above and significantly to the right of steady state line will cause true liquefaction, was proposed. Furthermore, in their approach the deformation is considered unlimited so that their design proposal are similar to a strength criterion. Many cases of limited liquefaction of practical interest (response type 2 to type 3) may exist where minimum strength available will be still substantial but deformation to mobilize such strength could be excessive and therefore unacceptable. Such cases were not considered by Castro within the framework of liquefaction.

Cyclic Loading Behaviour

Initial interest in undrained cyclic loading behaviour of sand was triggered by the extensive failure associated with saturated sand during Niigata and Alaska earthquakes of 1964. Consideration centered predominantly on the response of saturated sand under level ground, which will be subjected to reversing shear stresses on horizontal planes (Seed and Lee, 1966). The stress conditions on such soil elements are simulated in the laboratory by undrained cyclic simple shear or cyclic triaxial test on isotropically consolidated samples. The samples were subjected to constant amplitude cyclic shear stresses on horizontal plane in simple shear test or constant pulsating deviator loads in the triaxial test.

Continued cyclic loading results in the development of large strain and soil is said to have liquefied. Cyclic shear stress or deviator stress amplitude which causes a specified level of strain in a fixed number of stress cycles is called the resistance to liquefaction.

Liquefaction in cyclic loading has thus been defined as a strain criterion with no attention paid to the mechanism which is responsible for the development of strain. The phenomenon was called liquefaction because during some stage of the cyclic loading with shear stress reversal, a transient state of zero effective stress is reached when the applied shear stress in sand is zero. Zero effective stress in sand would imply zero shear resistance for a friction material and hence its equivalence with a liquid and the corresponding phenomenon liquefaction. The strain development during the increasing phase of the deviator stress in a cyclic triaxial test after a state of zero effective stress is reached is illustrated in Fig. 2.4. It may be noted that large deforma-

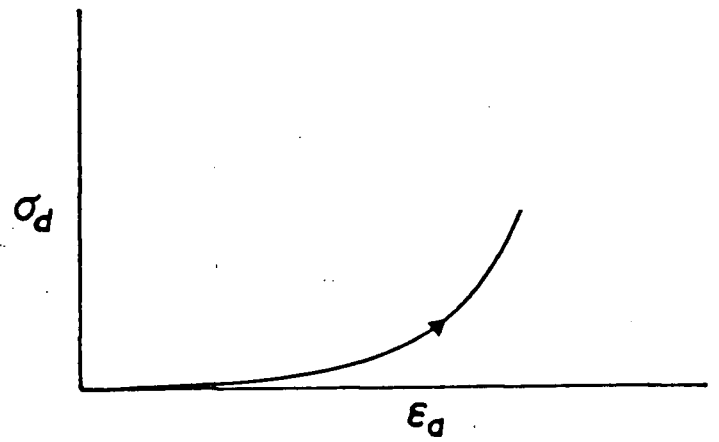

Fig. 2.4 Strain development on loading after the attainment of transient state of zero effective stress.

tion developed is not associated with strain softening.

Undrained cyclic loading of sand causes a progressive increase in pore pressure and cyclic deformation in saturated sand with increasing number of cycles, regardless of its relative density. However, two distinct types of response may be obtained with regard to the development of strain. In the first type of response, at some stage during cyclic loading the sample undergoes liquefaction. Castro (1969) has shown cases in which true liquefaction developed much in the same manner as those observed under monotonic loading (Fig. 2.5a). Vaid and Chern (1983[1,2]), however, have shown cases of cyclic loading of sand wherein limited liquefaction developed in the same way as that observed in type 2 and 3 response under monotonic loading (Fig. 2.5b). By making a detailed observation of the development of pore pressure and strain not only at the end of cycles of loading but also within cycles of loading, they clarified the possible mechanism of strain development during undrained cyclic loading.

Vaid and Chern showed that strain softening associated with limited liquefaction is initiated at a critical value of effective stress ratio (CSR) regardless of the void ratio or consolidation stress conditions of sand. Following the arrest of liquefaction (or strain softening), the subsequent unloading from the peak amplitude of cyclic deviator stress causes large increase in pore pressure bringing the sample close to the state of zero effective stress, but with very little change in deformation (Fig. 2.5b,c). Reloading in the extension region of the stress cycle causes the sample to undergo large deformation with its stress state moving along the undrained failure envelope. Subsequent unloading now, from the peak amplitude of deviator stress on extension side, once

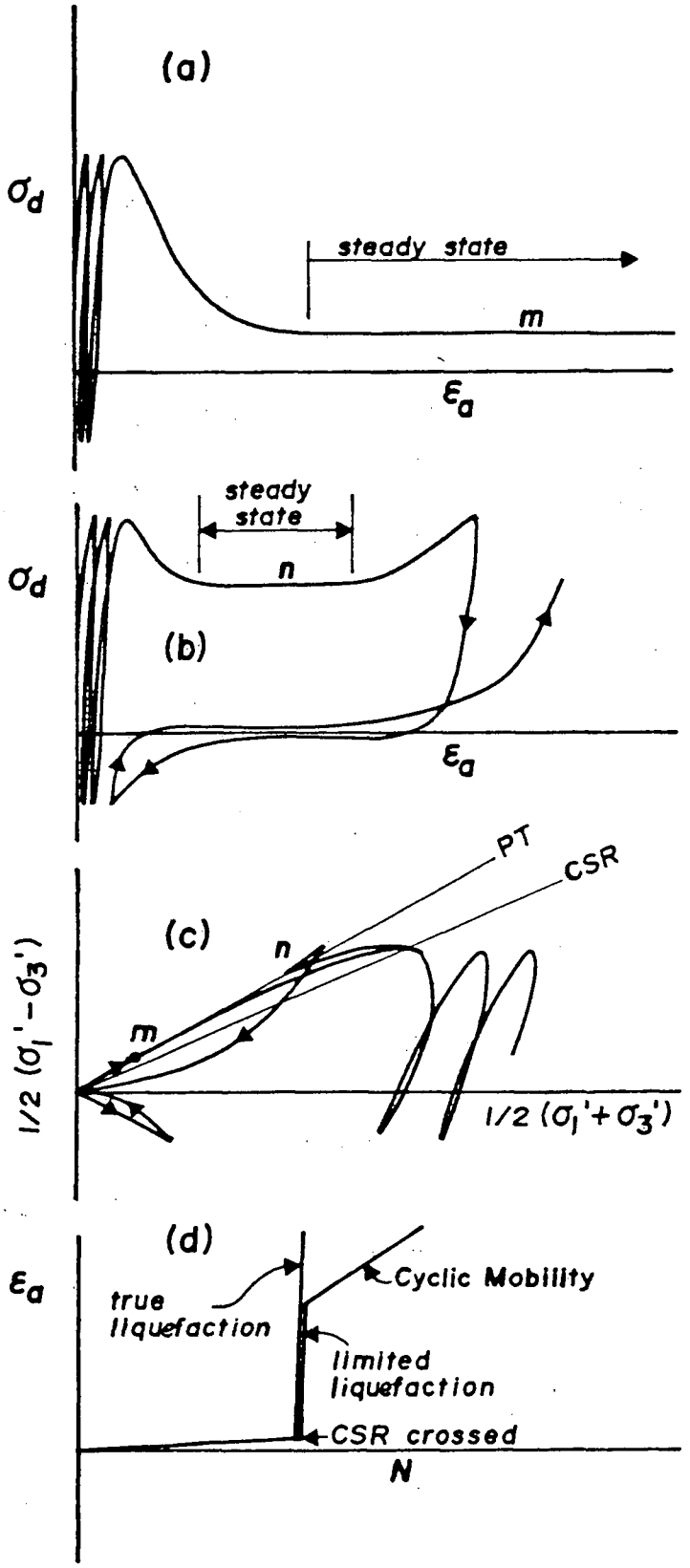

Fig. 2.5 Cyclic loading behaviour of contractive sand - true liquefaction and limited liquefaction.

again brings the sample to a state of zero effective stress, and further reloading into the compression region again causes the stress state moving along the failure envelope with large deformation developed. Repetition of this loading and unloading process causes a progressive increase in cyclic deformation following limited liquefaction. In such type of response the accumulation of strain with loading cycle is shown schematically in Fig. 2.5d.

In the second type of response, the sample develops progressive increase in pore pressure and cyclic deformation but at no stage is deformation associated with strain softening. Vaid and Chern (1983[1,2]) observed that such a sample develops very small deformation as long as its effective stress state stays below the stress ratio corresponding to the phase transformaton line (Fig. 2.6a,b). Significant amount of deformation is accumulated only when the stress state crosses the PT line during the loading phase. Unloading causes large increase in pore pressure bringing the sample close to the state of zero effective stress, but with very little change in deformation. Repetition of this phenomenon of stress state moving alternately into the region beyond the PT lines with cycles of loading ultimately results in a transient state of zero effective stress, and is responsible for further accumulation of deformation at a much faster rate. Strain accumulation with cycles of loading in this type of response is shown in Fig. 2.6c.

In this thesis the term liquefaction will be used only if sand deforms in a strain softening manner regardless of the nature of loading - monotonic or cyclic. This definition is consistent with that used by Castro (1969) except that it now encompasses limited liquefaction in addition to true liquefaction. The second type of response described

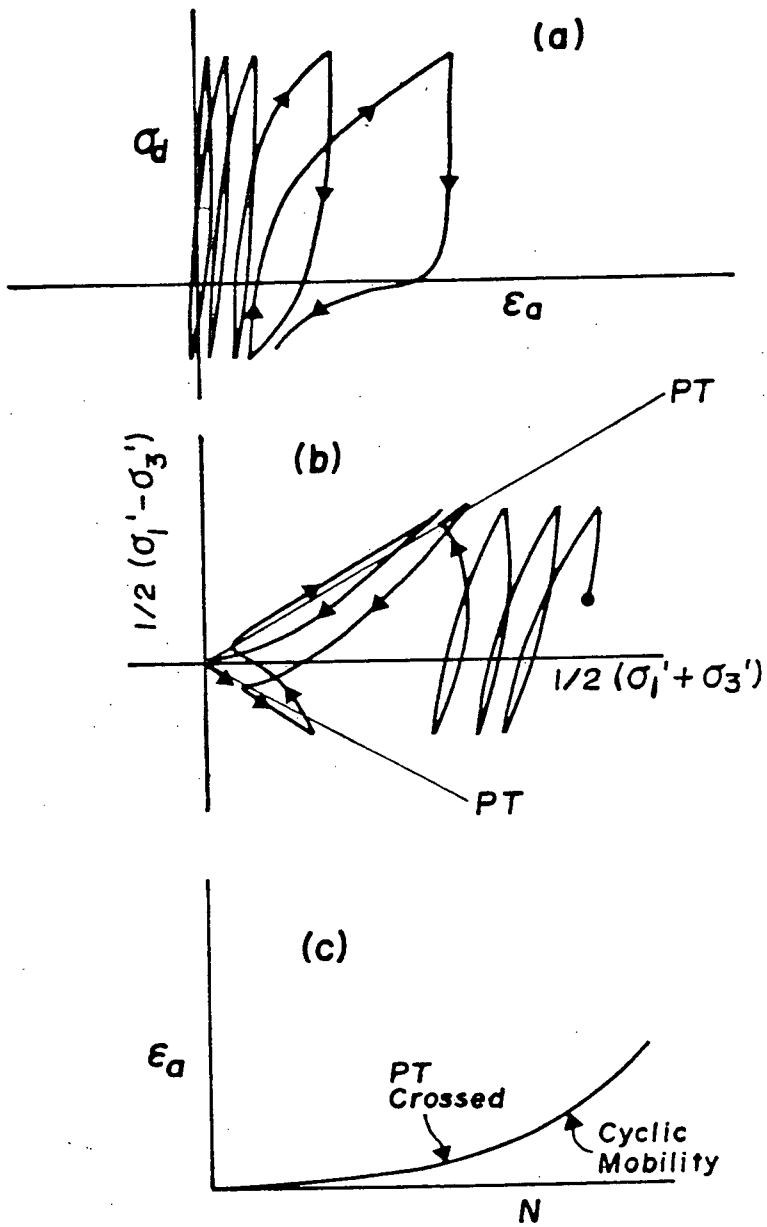

Fig. 2.6 Cyclic loading behaviour of dilative sand - cyclic mobility.

above, in which the deformation developed during cyclic loading is not associated with strain softening, will be called cyclic mobility. This definition of cyclic mobility is also after Castro (1969). Thus in the type of cyclic loading response illustrated in Fig. 2.5, the accumulation of deformation is partly due to limited liquefaction and partly to cyclic mobility following limited liquefaction.

It may be pointed out that the progressive increase in deformation of serious magnitude can develop when there is no shear stress reversal in sand with a certain level of static shear. During cyclic loading of such a sand, a state of transient zero effective stress is never realized and the association of term "liquefaction" to the response of this sand becomes ambiguous. Cyclic mobility is a more appropriate term in connection with the accumulation of all deformations under cyclic loading not associated with strain softening.

Since a specified strain development during cyclic loading could be due to liquefaction or cyclic mobility or the combination of two (Figs. 2.5 and 2.6), the term "resistance to liquefaction" used to designate resistance to cyclic loading will herein be called resistance to strain development under cyclic loading. However, if the specified strain development during cyclic loading is exclusively due to liquefaction only, then the term resistance to liquefaction will be used. If the strain development during cyclic loading is due to cyclic mobility only, then resistance to cyclic mobility will be used. These distinctions in definitions are necessary because various factors affect liquefaction and cyclic mobility response differently (Castro, 1969; Castro and Poulos, 1975; Vaid and Chern, 1983[1,2]).

Attempts to link the monotonic and cyclic loading behaviour have

been confined only to the illustration that strain softening occurs under cyclic loading much in the same manner as under monotonic loading. Castro (1969) and Castro et al. (1982) showed that the steady state line is unique under monotonic and cyclic loading conditions, which implies that the undrained stress paths have no effect on steady state line. A study on one sand at one confining pressure by Vaid and Chern (1983[1,2]) showed that the initiation of strain softening under monotonic and cyclic loading occur at a unique value of effective stress ratio. Also the arrest of strain softening occurs at a stress ratio corresponding to the phase transformation line. No comprehensive studies have been made to make general prediction of sand behaviour under cyclic loading from the known behaviour under monotonic loading. The role of void ratio, confining pressure and static shear on undrained cyclic loading behaviour are not clear and often contradictory, because of a lack of recognition of the mechanism of deformation under cyclic loading. It is the purpose of these investigations to present a unified approach for undrained response of sand, which will enable prediction of the type of undrained monotonic and cyclic loading behaviour from the knowledge of the initial state of the sand and the superimposed shear loading. It is also intended to clarify the role of various factors influencing the undrained response of saturated sand, including the effects of particle angularity.

CHAPTER 3

LABORATORY TESTING

3.1 Test Apparatus

All tests were conducted using the triaxial apparatus. The testing system consists of an instrumented triaxial cell and a loading system. The loading system is capable of monotonic consolidation under anisotropic stress conditions and cyclic loading under stress or strain controlled conditions.

3.1.1 Triaxial Apparatus

A schematic layout of the triaxial testing apparatus and the associated instrumentation is shown in Fig. 3.1. The triaxial cell was designed to test specimen with 6.4 cm diameter and 12.7 cm height.

It has long been recognized that frictionless end plattens cause more uniform deformation throughout the specimen and hence yield more reliable soil parameters. Use of frictionless end plattens however, is often complicated by the development of non-uniform expansion in the sample over its height, apart from the difficult sample preparation procedures involved and lateral sliding of sample off the platten during testing. Green (1969) performed a comprehensive study on the deformation modes of a Belgium sand by using frictionless end plattens. He found that the sample did not develop uniform lateral expansion during shear. The sample expanded predominantly either at the top or at the base, depending on the sample preparation procedures used. This non-uniform expansion was also obtained by Rowe and Barden (1964), Lee (1966) and by

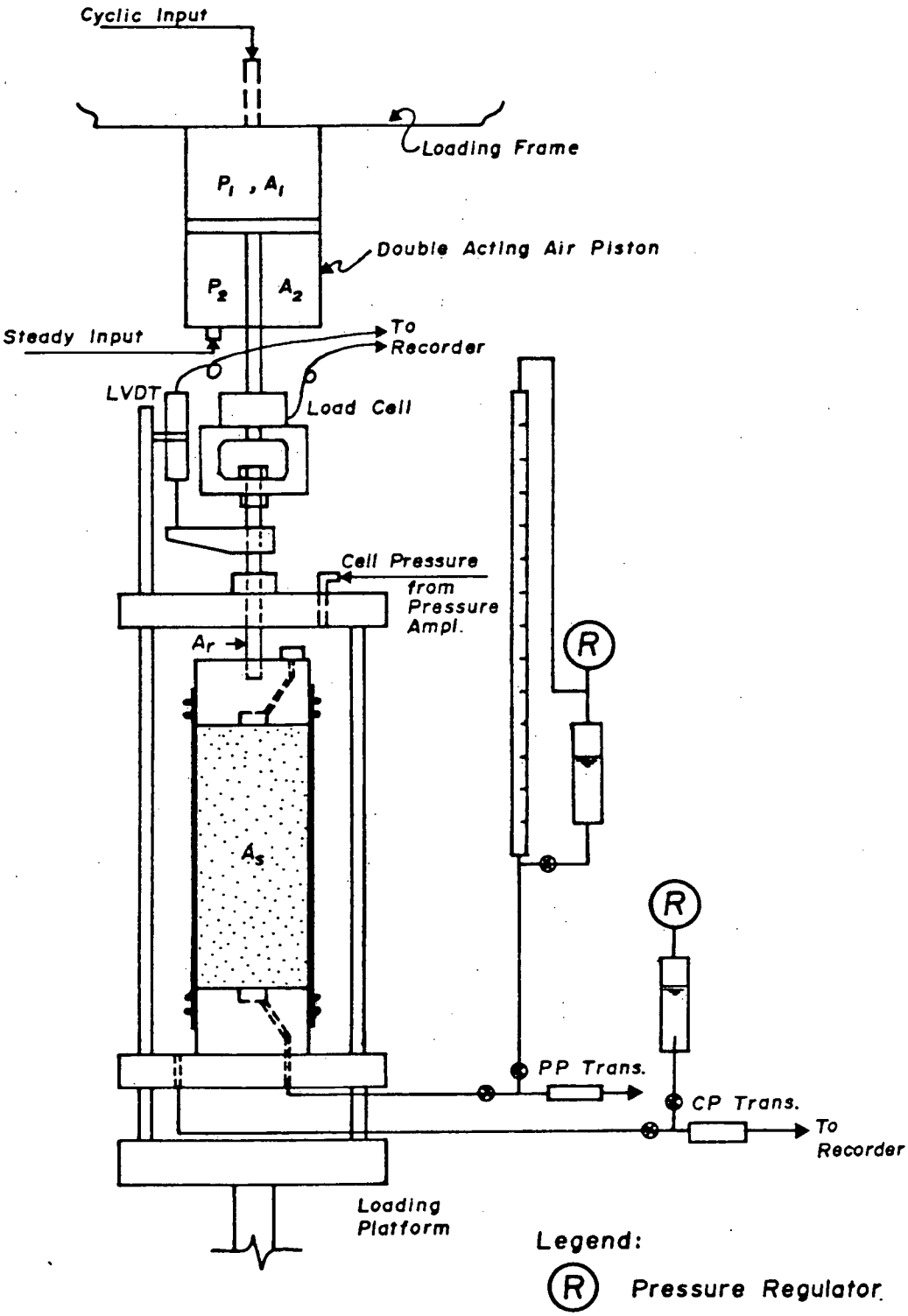

Fig. 3.1 Schematic layout of triaxial apparatus.

the writer in preliminary trials using the frictionless ends. The major factor influencing the mode of deformation appears to be the difference in the sand contact at the top and bottom sample-platten interfaces (Green, 1969). Although this may be reduced by forming a sample in two halves, as was done by Green, such a procedure is not possible to use for sample formed by the sedimentation technique.

Furthermore, most of the frictionless end plattens used have a slightly higher central portion for the porous disk in order to accommodate the thickness of the membranes and the grease on the outer portion. This technique serves to prevent the sample from sliding laterally off the end platten. Such a protrusion of stone into the sand sample may result in a complex stress and strain pattern within the sample, and hence may influence test results in an unknown manner.

Comprehensive studies have been made by Lee (1978) and Lee and Vernese (1978) on the influence of end restraint on the static and cyclic strength of sand. It was found that end restraint could have a significant effect on static and cyclic strength, but only in dilative dense soil. This effect appeared to be a direct function of dilation tendency of the soil. For loose sand, little or no effect of the type of end restraint was found. Such findings are also supported by recent studies of Castro et al. (1982) who investigated the effect of end restraint on the effective confining stress at steady state for two types of loose sands. No significant difference in results was found if frictionless ends were substituted for regular end plattens in both sands. Since the major objective of the intended study is the response of relatively loose sand, the choice was made in favour of regular end plattens for simplicity of test procedure. Nevertheless, the end restraint was kept to a

minimum by using polished anodized plattens with a small central 2 cm diameter porous discs for drainage.

3.1.2 Loading System

The loading system consists of two parts: the consolidation system and the cyclic loading system. This system is basically similar to that described by Chern (1981). However, considerable additional improvements were made to facilitate testing under high confining pressure and various anisotropic consolidation stress conditions.

Consolidation System

In order to simulate the field consolidation stress condition more closely, particularly under the sloping ground, an anisotropic consolidation system was developed. In the conventional method, anisotropic consolidation is either carried out incrementally in steps, or the sample is consolidated isotropically first and then deviator stress applied under drained condition until the desired $K_c = \sigma'_{1c}/\sigma'_{3c}$ ratio is obtained. The newly designed system enables the soil sample to be consolidated isotropically or anisotropically along any constant effective stress ratio path. This system is illustrated schematically in the lower left part of Fig. 3.2, whereas the details are shown in Fig. 3.3.

The consolidation system consists of a motorized pressure regulator, a pressure amplifier (if higher confining pressures are needed), a positive and negative bias relay and an adjustable ratio relay. In operating the system, an identical signal pressure, s, from the motorized regulator is fed into the pressure amplifier and the bias relay. The pressure amplifier simply magnifies the signal pressure by a constant ratio m (=

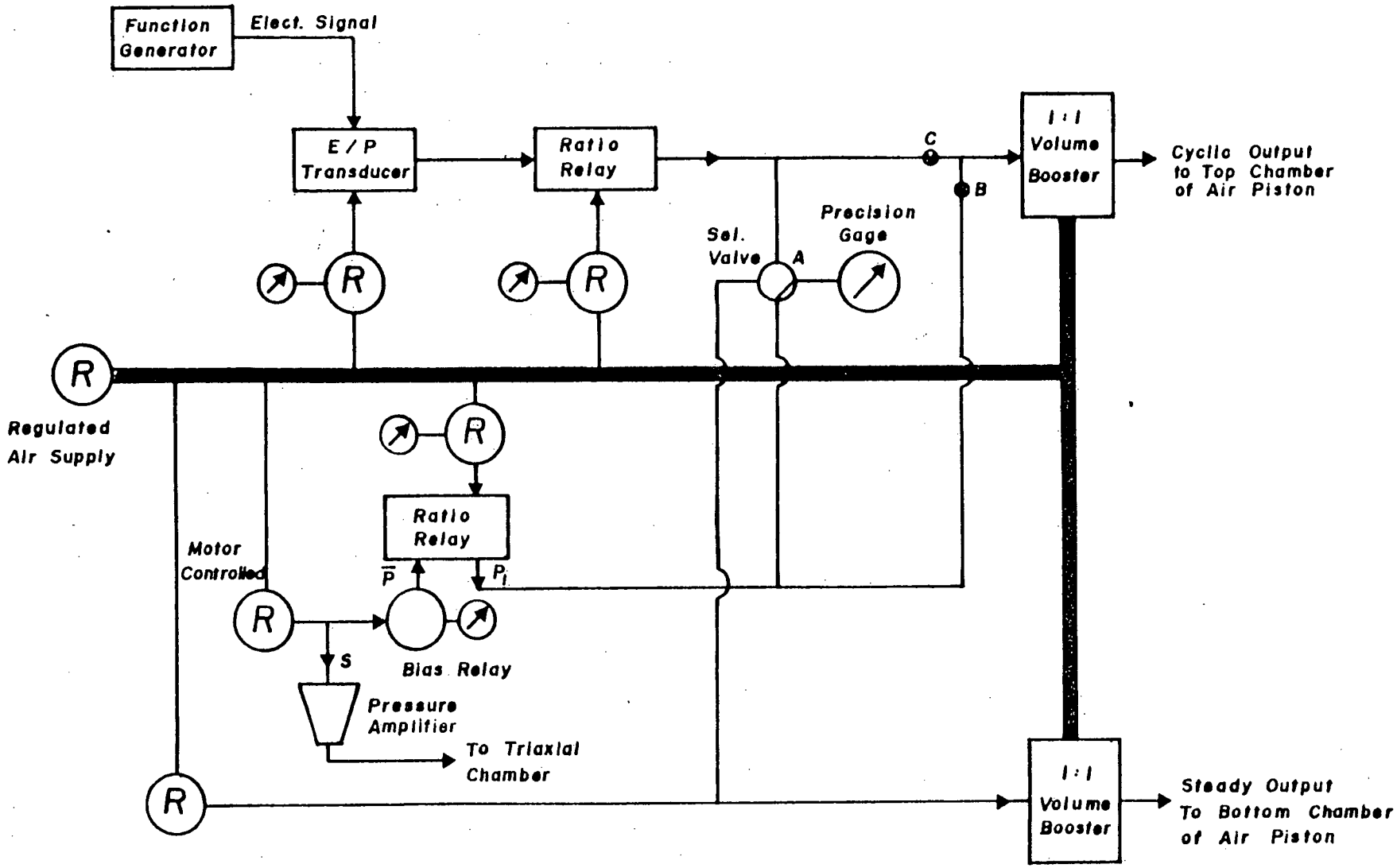

Fig. 3.2 Schematic layout of loading system.

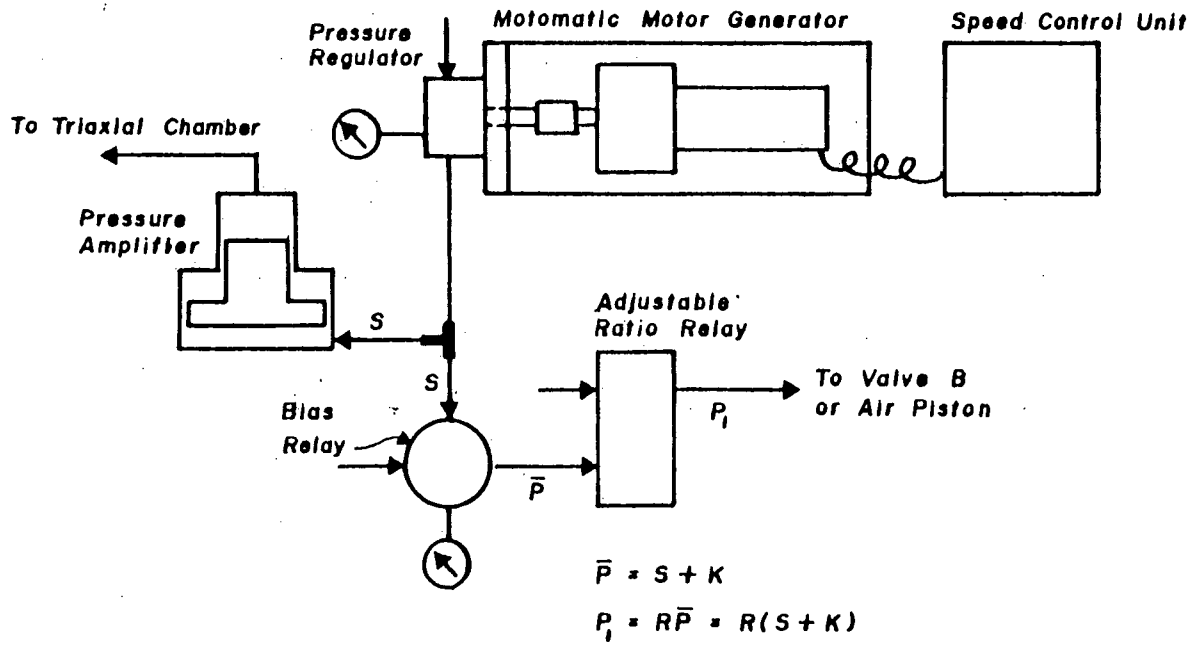

Fig. 3.3 Detailed layout of consolidation system.

4.167 in system designed) before feeding the output pressure into the triaxial chamber as cell pressure σ_3, i.e.,

$$\sigma_3 = m\ s$$

The bias relay adds a constant K (continuously adjustable) to the signal pressure and outputs a pressure

$$\bar{p} = s + K.$$

The pressure $\bar{p}$ when fed through the ratio relay gets multiplied by a factor R (continuously adjustable) and the output pressure

$$p_1 = R(s + K)$$

is fed to the top chamber of the air loading piston, either directly or through a volume booster.

For the given signal pressure s, the vertical stress σ_1 on the sample is given by (see Fig. 3.1)

$$\sigma_1 = \frac{1}{A_s}\left[R(s + K)A_1 - p_2A_2 - msA_r\right] + m\ s \qquad (3.1)$$

in which A_s = sample area,

A_1 = area of top chamber of air loading piston,

A_2 = area of bottom chamber of air loading piston,

A_r = area of the loading ram,

p_2 = steady input to the bottom chamber of air loading piston.

If the consolidation is desired under a K_c value, incremental changes in σ_1' and σ_3' are related by

$$\Delta\sigma_1'/\Delta\sigma_3' = K_c \tag{3.2}$$

Now

$$\Delta\sigma_1' = \Delta\sigma_1 - \Delta u \tag{3.3}$$

$$\Delta\sigma_3' = m\Delta s - \Delta u \tag{3.4}$$

Under drained conditions u = constant and thus $\Delta u = 0$. Therefore, from Eqs. 3-2, 3-3 and 3-4,

$$\Delta\sigma_1' = m\Delta s\ K_c \tag{3.5}$$

Substituting for $\Delta\sigma_1$ from Eq. 3-1 into Eq. 3-5, we get

$$\frac{1}{A_s}(R\Delta sA_1 - \Delta p_2 A_2 - m\Delta sA_r) + m\Delta s = m\Delta s\ K_c \tag{3.6}$$

If p_2 is held constant, $\Delta p_2 = 0$ and Eq. 3-6 reduces to

$$\frac{1}{A_s}(RA_1 - mA_r) + m = m\ K_c \tag{3.7}$$

from which the value of ratio relay R factor can be obtained in terms of the system constants for the desired K_c value. In this investigation, the input pressure p_2 in the bottom chamber of the air loading piston and the back pressure u were maintained constant. Therefore, knowing R factor of the ratio relay, the K factor of the bias relay can be obtained

from the relationship $\sigma_1' = K_c \sigma_3'$, i.e.,

$$\frac{1}{A_s}[R(s + K)A_1 - p_2A_2 - msA_r] + ms - u = K_c(ms-u) \qquad (3.8)$$

For any value of signal pressure s. Once the constant R on the ratio relay and constant K on the bias relay are selected, the sample can be consolidated continuously along the desired constant K_c ratio path.

A cohesionless soil sample has to be set up with some finite confinement, which makes its initial effective stress state hydrostatic. This hydrostatic stress was kept to a practical minimum of about 0.2 kgf/cm^2 (19.6 kPa) following the application of back pressure and prior to initiating the consolidation phase of loading. In order to avoid sudden change of stress state from initial hydrostatic stress of about 0.2 kgf/cm^2 (19.6 kPa) to the anisotropic stress condition, which may cause sudden buildup of excess pore presure and cause collapse of loose sample, the consolidation stress path was brought to approach the desired K_c path during the initial stage of consolidation (see Fig. 3.4). This is done by opening the valve B slowly and admitting the pressure p_1, to the air piston slowly.

Cyclic Loading System

Cyclic loading is applied by means of an electro-pneumatic (E/P) transducer driven by a function generator (Fig. 3.2). Due to the limited output pressure capability of the E/P transducers, an adjustable ratio relay was installed to magnify this pressure. Any desired cyclic load amplitude can be obtained by appropriate combination of piston size and multiplication factor of the ratio relay.

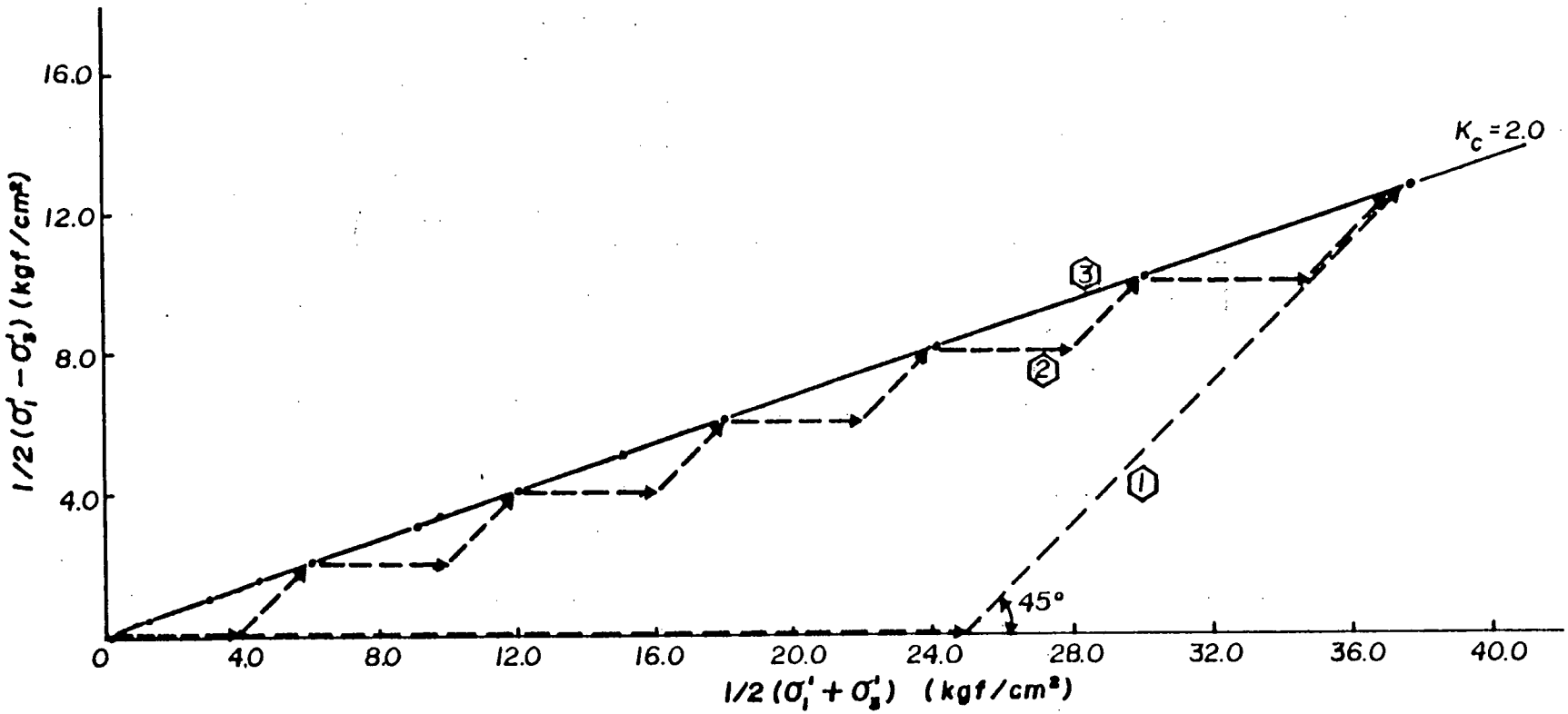

Fig. 3.4 Anisotropic consolidation stress paths.

In order to maintain a constant cyclic load amplitude when large sample deformation develops, a 1:1 pressure ratio volume booster relay was installed on both top and bottom chambers of the air piston. A large increase in air flow rate and exhausting rate reduced greatly the degradation of cyclic load pulse when large deformation developed.

After consolidation was completed, the pressure in the top chamber of the air piston was transferred to the cyclic loading system. With valve C closed, the pressure in the cyclic loading system was increased to the value equals to that in the consolidation system using the DC-offset on the function generator. A smooth transfer was then made by closing valve B and opening valve C.

3.2 Testing Procedures

3.2.1 Sample Preparation and Saturation

Test samples were formed by pluviating sand in deaired water which filled the sample cavity formed by a membrane lined split mold. While depositing sand, the tip of the pouring nozzle was always submerged and maintained at a constant height of about 1 cm above the sedimented sand surface. The pouring tip was traversed laterally over the plan area of sample in order to form a loose uniform sand deposit. All samples were formed loose in this manner. Higher initial densities, if required, were obtained by densification after the loading cap was in place. Densification was achieved by tappings on the base of the triaxial cell with a soft hammer while maintaining a gentle pressure on the loading cap. The detailed sample preparation techniques have been described previously by Chern (1981). These techniques are believed to yield samples of uniform

density throughout (Vaid and Finn, 1979).

During the process of sample set up in the loading frame and checking for saturation, the main emphasis was to first bring all samples to a state of constant effective stress prior to consolidation. This value of effective stress was about 0.2 kgf/cm^2 (19.6 kPa), which was the confining pressure after the sample was formed. The careful sample preparation technique, which involved sedimentation by mutual transfer of sand with water without contacting air, resulted in virtually saturated samples with B value greater than 0.99.

Other sample preparation techniques, e.g., moist or dry compaction, frequently give rise to nonuniformities in density over the height of the sample (Castro, 1969). Moreover, they require application of full vacuum to the sample in order to remove the air trapped to facilitate saturation with high back pressure. Such procedures result in unknown volume changes in the samples and hence an uncertainty in the estimation of void ratio of the sample. Furthermore, cell pressure has to be applied before the sample is percolated with water in order to dissolve or drive out the air trapped in the sample. Thus, the sample first experiences an effective stress of more than 1.0 kgf/cm^2 (98 kPa) depending on the level of cell pressure applied, followed by a loss of this effective stress when vacuum is released at one end during the process of saturation. Hence the sample gets consolidated and then rebounded causing stress history effects in addition to unknown volume changes. This volume change may be significant when the water is allowed to percolate into the sample. Very large volume change can take place especially if the sand contains some fines. In any case, the exact amount of volume change is difficult to estimate due to inherent anisotropy of the pluviated samples even

though the axial deformation is monitored.

The sample preparation technique adopted in this investigation is believed to yield more uniform samples, the effective stress prior to initiating consolidation was kept identical in all samples at a very low value (0.2 kgf/cm^2) and no arbitrary effective stress history was imparted to the samples. Consolidation was started from this initial effective stress state. A complete record of volume changes of samples was kept and hence errors in the estimation of void ratio at the end of consolidation were eliminated. Such errors, together with those associated with sample preparation by tamping, are especially important in the study of undrained response of loose samples under relatively low consolidation pressure.

After the sample had been saturated, the triaxial cell was centered on the loading platform, and the sample loading ram was connected to the loading piston rod. The sample was now ready for consolidation. Anisotropic consolidation, if required, was achieved by raising the cell pressure and axial load simultaneously in a preset ratio as described in Section 3.1.2. The cell pressure was increased at a constant rate of about 0.5 kgf/cm^2 (49 kPa) per minute by the motorized regulator until the desired cell pressure was achieved. During the process of consolidation, the volume change, axial deformation and axial load were monitored at discrete levels of confining pressure. A typical monotonic consolidation stress path for K_c ratio of 2.0 is illustrated by path 3 in Fig. 3.4. In the conventional procedure of anisotropic consolidation, the sample would be first consolidated isotropically and then sheared under drained condition to the desired value of K_c ratio. This is generally carried out in one step or in multiple steps as illustrated by paths 1

and 2 respectively in Fig. 3.4. A monotonic anisotropic consolidation is superior to the conventional technique, because of the possible influence of stress path during consolidation on the subsequent undrained behaviour.

When the consolidation pressure reached the desired value, the drainage line was kept open for a period of time until the secondary consolidation, if any, was complete. The time required for this phase depends on the type and the level of consolidation stress used. For both rounded and angular sands consolidated to low consolidation pressure, this waiting period was very short. However, for angular tailings sand under high consolidation stresses, a period of more than 20 minutes elapsed before the volume change got stabilized. During consolidation, the sample was always kept under stress controlled condition until the next stage of loading.

3.2.2 Methods of Loading

Two types of tests, i.e., monotonic and cyclic loading test, were performed in order to study the undrained behaviour of sands. In each type of test, either strain controlled or stress controlled loading was applied. All tests were performed using the conventional triaxial stress path, i.e., the cell pressure was maintained constant during shear.

Undrained Monotonic Loading

Generally, undrained strain softening behaviour has been studied by testing samples under stress controlled conditions (Castro, 1969; Castro et al., 1982). The dead weight system or air piston loading system can be used for this purpose.

It was found that the dead weight system is not suitable for investigating behaviour of sand that developed limited liquefaction. This is due to the impact on the sample after occurrence of steady state deformation and the sample moving beyond the state of PT with accompanied increase in its resistance. The impact force on the sample was due to the large inertia force in dead weights at PT state. As an example, the actual load acting on the sample during and after strain softening is shown in Fig. 3.5 together with pore pressure response and axial deformation. High frequency vibrations occurred in the sample, causing a complicated stress-strain history after steady state deformation. The data for this test were recorded on an oscillographic recorder.

In contrast to the dead weight system, air piston loading is a low inertia system. Such a loading system was found to influence the test results if sand undergoes strain softening on account of interaction of sample characteristics with that of the loading system. It was found that the steady state strength and strain potential (amount of strain from peak until PT state) could vary depending on the piston size, position of the piston cylinder and the presence of volume booster. An example of such an interaction is illustrated by the results of tests on two identical sand samples in Fig. 3.6. The samples were loaded identically except that for one sample the volume of air in the air piston prior to the occurrence of strain softening response was larger than for the other.

It was found in preliminary studies that the steady state strength and strain potential obtained under strain controlled conditions were comparable to those obtained using the dead weight system. This was also observed by Castro et al. (1982). For these reasons, all monotonic

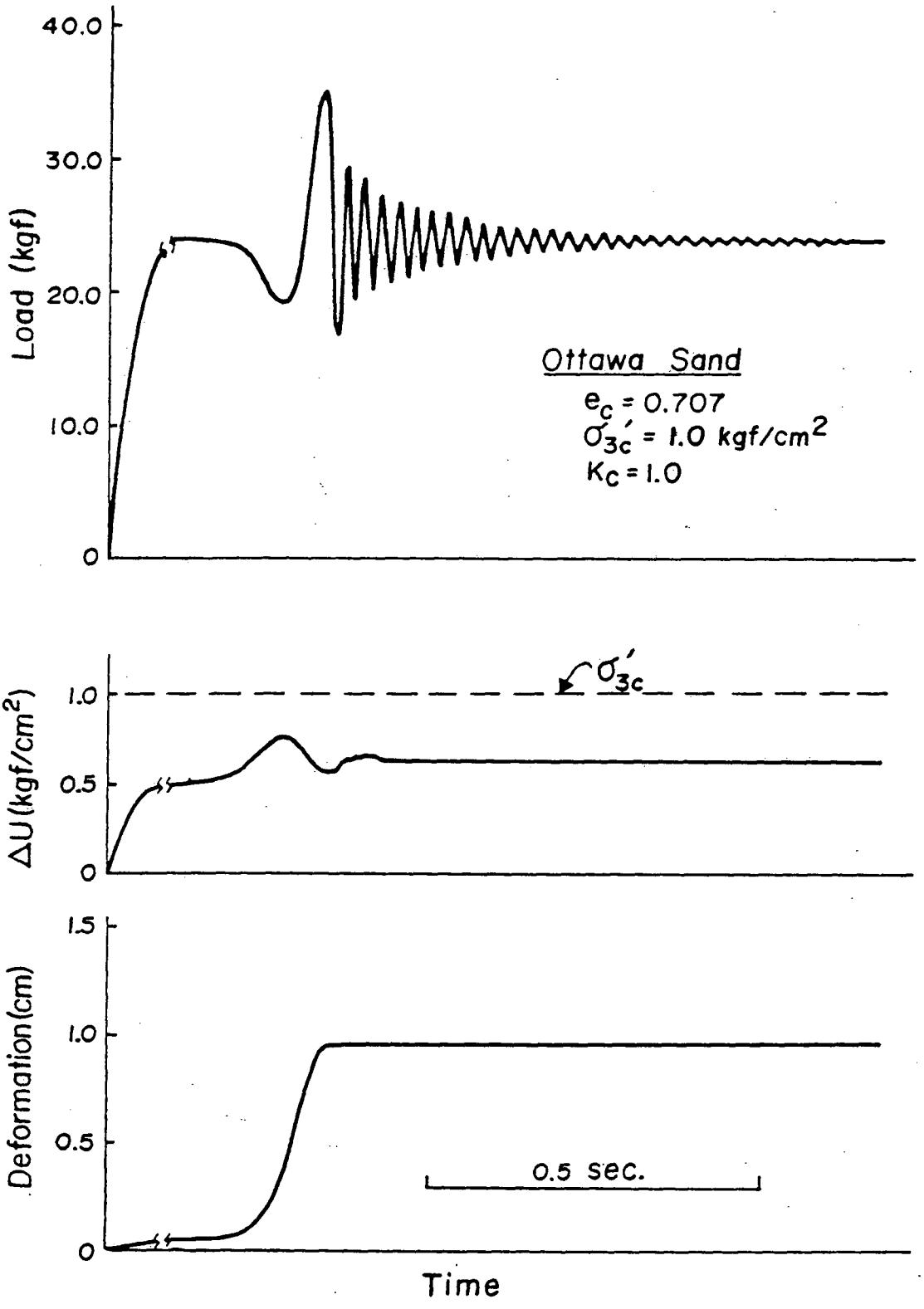

Fig. 3.5 Undrained monotonic loading response with limited liquefaction using dead weight loading.

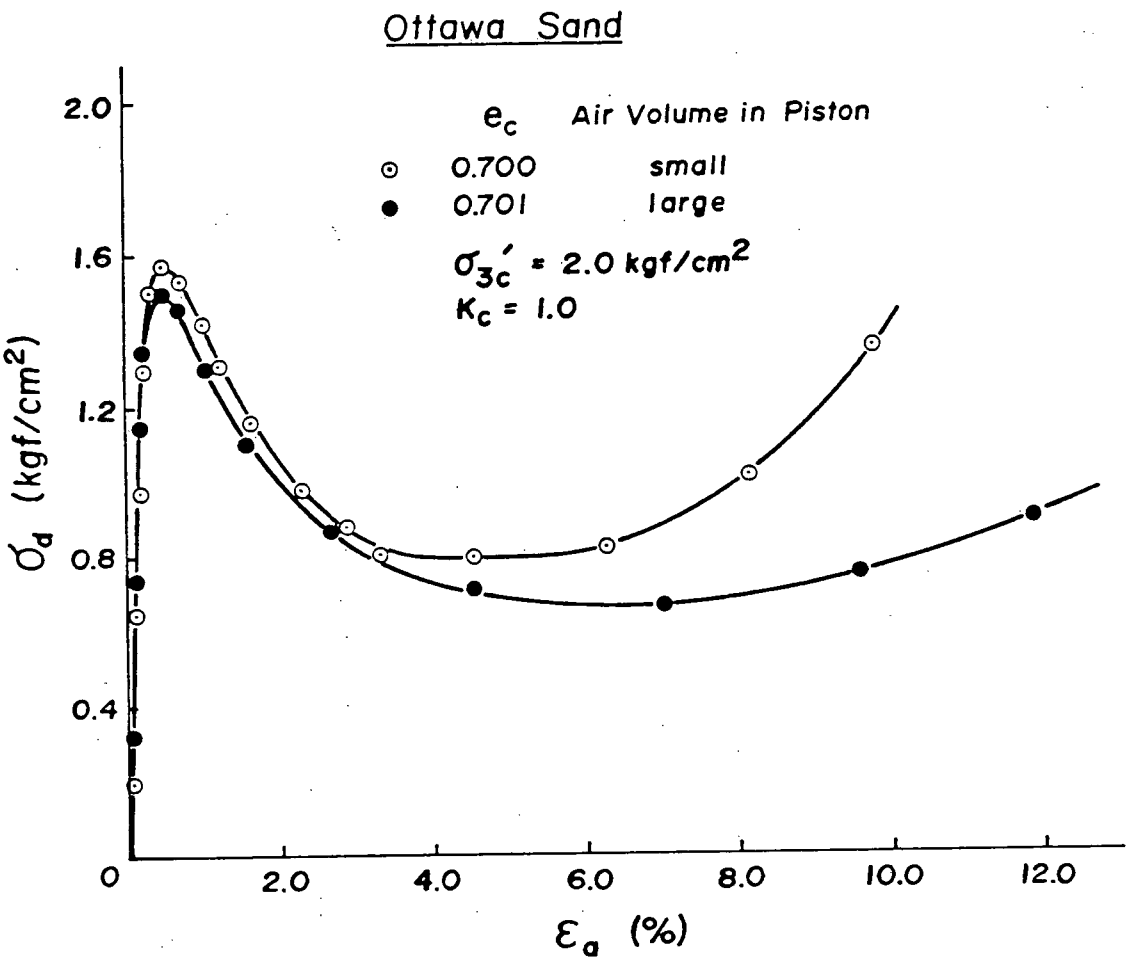

Fig. 3.6 Influence of the pneumatic loading system on the strain softening behaviour.

loading tests were performed by using strain controlled loading system. However, it should be noted that the interaction of the sample with the stress controlled loading system occurs in samples which developed strain softening response only. For samples which developedstrain hardening response, both the stress controlled and strain controlled tests should yield the same result.

After consolidation was completed, the loading platform was raised or lowered until the piston rod contacted the loading crosshead. With drainage line closed, the sample was loaded monotonically under strain controlled conditions. Axial strain rate of about 1.0% per minute was used in all tests. During the process of loading, axial load, pore pressure, cell pressure and axial deformation were monitored continuously by transducers and records obtained on a four pen chart recorder.

Undrained Cyclic Loading

Cyclic loading tests were performed in order to obtain the effective confining stress and shear strength at PT state under cyclic loading condition, and also to assess the resistance to cyclic loading in terms of strain development.

For reasons described above, only strain controlled loading was used to obtain the steady state strength parameters under cyclic loading. It was achieved manually by loading and unloading in the strain controlled machine maintaining constant stress amplitudes. The strain rate used in these tests was similar to that used in the monotonic loading tests.

3.3 Testing Program

Four types of triaxial tests were performed:

1. IC-U - Isotropically Consolidated Undrained Monotonic Loading Tests.
2. AC-U - Anisotropically Consolidated Undrained Monotonic Loading Tests.
3. IC-U_{cy} - Isotropically Consolidated Undrained Cyclic Loading Tests.
4. AC-U_{cy} - Anisotropically Consolidated Undrained Cyclic Loading Tests.

Most of the monotonic loading tests were performed in the compression mode. However, a limited number of monotonic loading tests were also carried out in the extension mode in order to illustrate possible differences due to the two modes of loading. The main purpose of this testing program was to establish a unified picture of the undrained behaviour of sand under monotonic and cyclic loading conditions, and the manner in which the void ratio, consolidation stress ratio, level of confining pressure and amplitude of cyclic loading influence this behaviour. Tests were carried out on samples having the same initial void ratio while varying the consolidation stress ratio K_c and confining pressure level σ'_{3c}. Five series of test with initial relative denstiy varying from 15% to 70% for angular tailings sand and three series of test with initial relative density varying from 30% to 45% for rounded Ottawa sand were performed. The consolidation stress ratios were varied from 1.0 to 2.0 under wide range of consolidation pressure from 2.0 kgf/cm^2 (196 kPa) to 25.0 kgf/cm^2 (2450 kPa).

Two types of cyclic loading test were performed. One type of tests were carried out to examine, under cyclic loading conditions, the applicability of steady state concept established under monotonic loading condition. In order to observe the steady state deformation under cyclic

loading condition, only initially loose samples consolidated to K_c ratio of 2.0 and subjected to consolidation pressure ranging from 2.0 kgf/cm^2 (196 kPa) to 25.0 kgf/cm^2 (2450 kPa) were tested for both sands. As explained previously, these tests were carried out under strain controlled conditions in order to eliminate the influence of sample characteristics - loading system interaction on test results. The other type of tests were carried out to obtain the resistance to cyclic strain development or cyclic mobility. These tests were performed using the conventional stress controlled cyclic loading technique. For each sand, two series of tests were performed. In one series, the sample states after consolidation were so chosen that steady state deformation was expected under monotonic loading condition. These tests consisted of sample with the same void ratio after consolidation and consolidation stress σ'_{3c} while the consolidation stress ratio K_c was varied from 1.0 to 2.0. In the second series, the sample states after consolidation were chosen such that they were well below the steady state line from monotonic loading tests and hence no liquefaction but the development of cyclic mobility was anticipated. Again, the samples were prepared with the same void ratio after consolidation and consolidation stress σ'_{3c} while the consolidation stress ratio K_c was varied from 1.0 to 2.0. The main purpose of these two series of tests was to show the influence of static shear on resistance to liquefaction and cyclic mobility.

In addition, several tests were performed to simulate the phenomenon of spontaneous liquefaction. The details of such testing will be given in Section 5.6.

3.4 Material Tested

Two sands were used in this laboratory testing program. One was Ottawa sand C-109, which has been used extensively in the laboratory studies of undrained cyclic loading behaviour at UBC and elsewhere. The other was a mine tailings sand. The tailings sand was specially screened. The fraction retained on #60 sieve was virtually all quartz and the grain size distribution almost identical to that of Ottawa sand. Thus, the two sands represented sands which differed only in their particle shape, and therefore provided a direct assessment of the influence of particle angularity on the undrained behaviour.

3.4.1 Soil Description

Ottawa Sand

Ottawa sand is a natural sand processed by Ottawa Silica Company, Ottawa, Illinois. It meets the ASTM Designation C-109. It is a clean, uniform, medium sand with rounded particles. The grain size distribution of the sand is shown in Fig. 3.7. The sand has a maximum and minimum void ratios of 0.82 and 0.50 respectively, according to standard test method ASTM D2049. The lowest relative density of water pluviated sand after isotropic consolidation to σ'_{3c} = 2.0 kgf/cm^2 (196 kPa) was about 32.0%.

Mine Tailings Sand

Mine tailings sand was obtained from a copper mining operation in Peachland, British Columbia. It constituted the coarse fraction used in building the embankment for tailings impoundment. The sand consists of

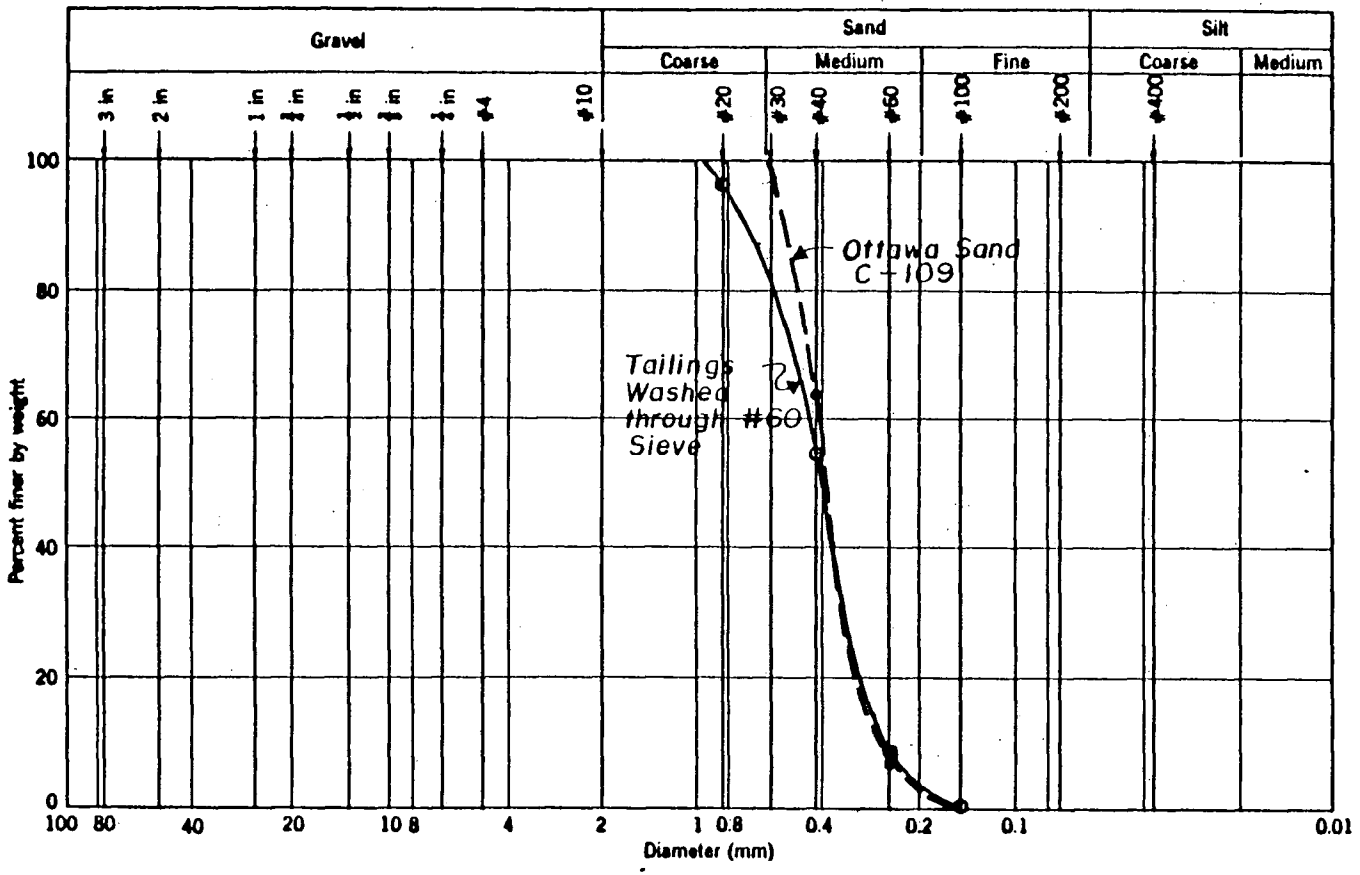

Fig. 3.7 Grain size distribution curves of sands tested.

about 80-85% of quartz, 10-15% of mica, traces of chalopyrite and feldspar and has angular particles.

The tailigns sand was washed through #60 sieve in order to remove the fines and mica presented. Removal of these fines brought both the mineral composition and the gradation curve of the fraction retained on #60 sieve very similar to that of the Ottawa sand C-109. The gradation curve of the sand is shown in Fig. 3.7. It may be noted that the grain size distribution of the two sands are essentially identical. This permits the influence of particle angularity on undrained behaviour to be isolated without introducing additional variables in the form of gradation and mineral content. The maximum and minimum void ratios of the tailings sand were found to be 1.060 and 0.688 respectively, according to standard test method ASTM D2049. The loosest relative density of water pluviated sand after isotropic consolidation to σ'_{3c} = 2.0 kgf/cm^2 (196 kPa) was about 25.0%.

3.4.2 Consolidation Characteristics

The consolidation characteristics of sands were determined at several initial void ratios e_i and consolidation stress conditions. The relationships between void ratio after consolidation e_c and major consolidation stress σ'_{1c} for tailings sand are shown in Fig. 3.8. Similar results for Ottawa sand are shown in Fig. 3.9.

It may be noted that considerable volume reduction occurs on application of high confining pressure during consolidation of angular tailings sand (Fig. 3.8). However, the volume reduction is much less for rounded Ottawa sand under similar stress levels. Larger compressibility of angular sand is a consequence of easy breakage of sharp edges of

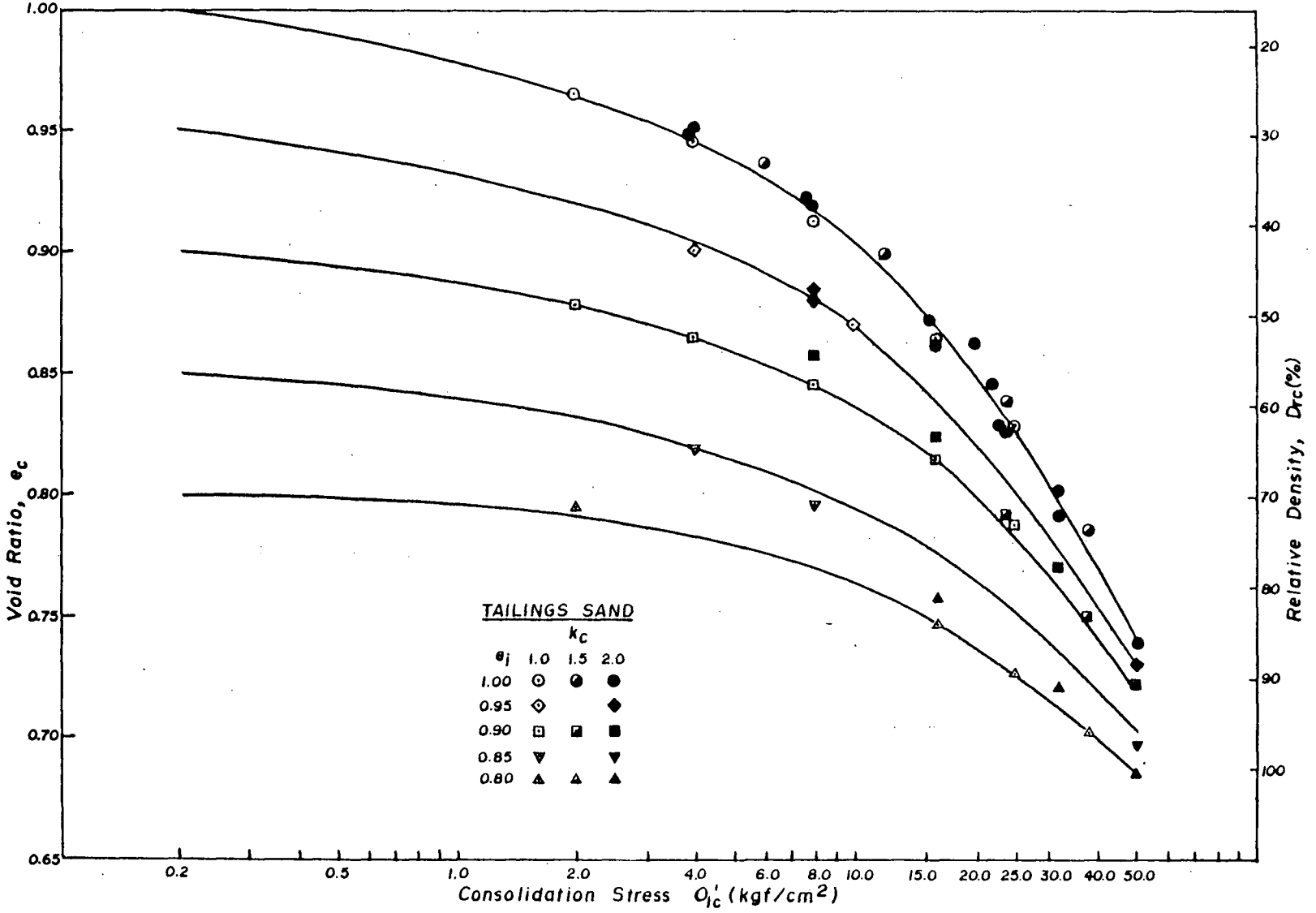

Fig. 3.8 Consolidation characteristics of tailings sand.

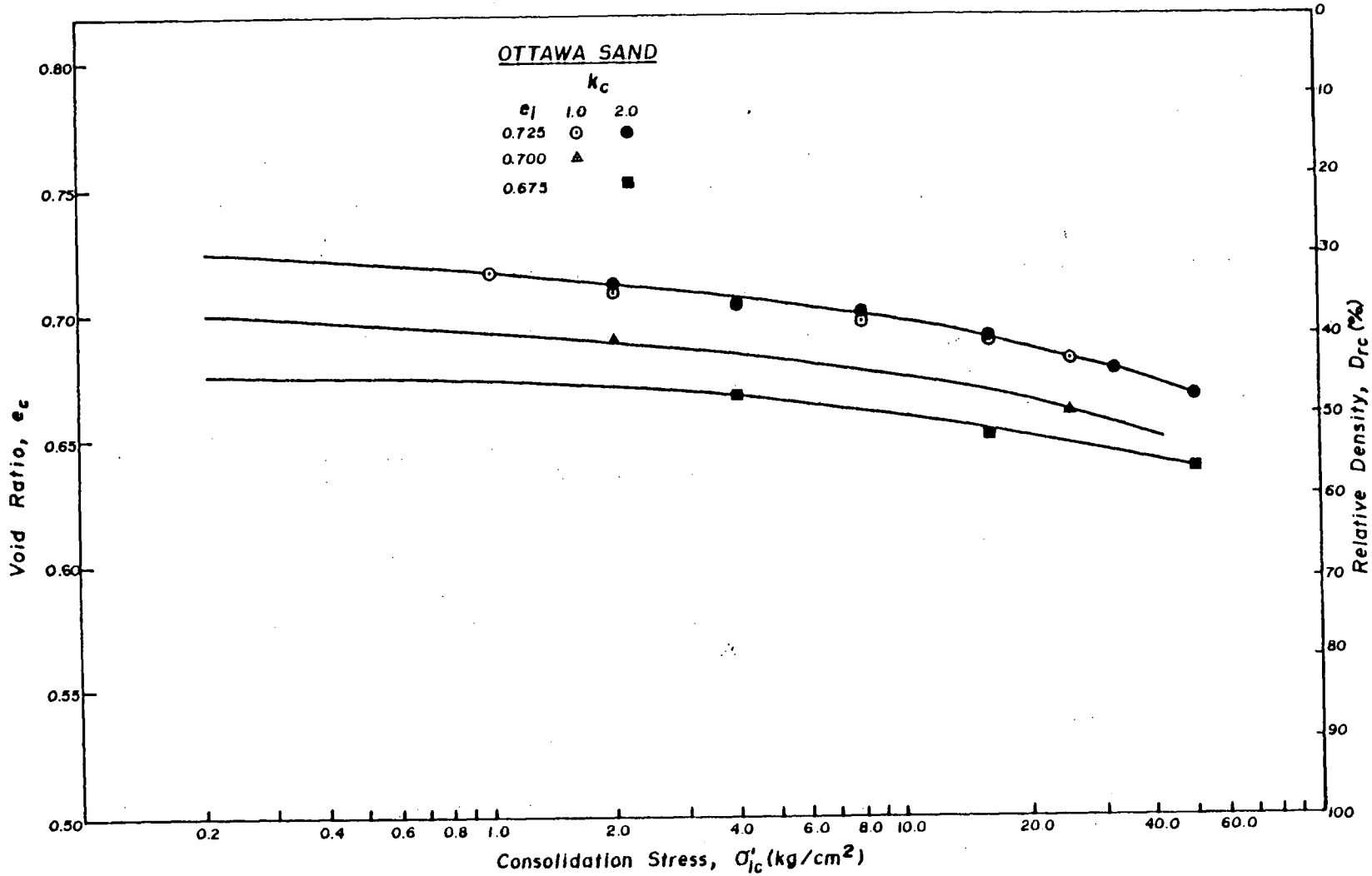

Fig. 3.9 Consolidation characteristics of Ottawa sand.

particles under high consolidation stresses, which makes the particles to move into a more compact arrangement. As expected, the volume reduction for a given stress increment decreases with increasing initial density. However, the consolidation curves with various initial void ratios tend to converge under high consolidation pressure. This is particularly apparent in the case of tailings sand. It appears that under very high confining pressure the final void ratio may be more or less independent of the initial void ratio of the sample.

It may also be noted in Figs. 3.8 and 3.9 that for a given initial void ratio the final void ratio after consolidation is a function only of the major principal consolidation stress σ'_{1c}, regardless of the consolidation stress ratio K_c. Such consolidation behaviour of sand has also been observed for Sacramento River sand over an even larger range of consolidation stress ratio and confining stress level by Lee and Seed (1970). This characteristic behaviour may be used to estimate the final void ratio of sand after consolidation once the initial void ratio and consolidation stress conditions are known. As will be discussed in Section 5.1.4, the curves in Figs. 3.8 and 3.9 give a very good basis for preparing samples to a desired final void ratio under a wide range of consolidation stress conditions. In this manner the final void ratio could be reproduced with variation of less than 1.6% in relative density. For a given e_i, the unique e_c vs. σ'_{1c} consolidation characteristics of sand may also have significant importance in determining the in-situ void ratio as construction proceeds if the initial placement void ratio can be estimated. This is especially true if the sand is loose. Sampling of loose sand is known to always cause densification and hence gives higher strength estimate, which could be unsafe for design purposes.

It should be pointed out that the unique consolidation relationships of sand discussed above are restricted for water pluviated sand and under normal consolidation only. Other sample preparation procedures, e.g., moist tamping, dry compaction, etc., which may impart to the sample a complex stress history, may not result in such relationships. This will be especially critical for a sand with rounded particles in which the total volume change during consolidation is generally very small.

CHAPTER 4

UNDRAINED MONOTONIC LOADING BEHAVIOUR

Undrained triaxial compression tests were carried out on both sands using confining pressure σ'_{3c} ranging from 2.0 to 25.0 kgf/cm^2 (196 to 2450 kPa) and K_c values from 1.0 to 2.0. For each sand, samples were formed at a fixed initial void ratio e_i and a series of tests performed after consolidation to various levels of σ'_{3c} and K_c values. Similar series of tests were then repeated on samples formed at another fixed initial void ratio. In this manner, five initial void ratio states for tailings sand and three initial void ratio states for Ottawa sand were covered. This enabled investigation of undrained behaviour which covered a full spectrum of initial states e_c, σ'_{3c} and K_c, of sand.

Only limited number of tests were performed under triaxial extension mode. The objective was to show possible influence of loading path on the undrained behaviour.

4.1 Typical Undrained Monotonic Loading Behaviour

Stress-strain and pore pressure response together with effective stress paths for some selected tests on both sands incorporating a range of end of consolidation states are shown in Figures 4.1 to 4.10. It may be noted that the range of observed undrained response covers the full range of behaviour described by type 1 to 5 in Chapter 2. In the subsequent discussions, the magnitude of axial strain from peak until the phase transformaton state (start of pore pressure decrease) for strain softening response will be designated as strain potential. With this

definition, true liquefaction corresponds to an unlimited strain potential.

Tailings Sand Test Results

Typical stress-strain and pore pressure response of initially loose samples of tailings sand consolidated to low (2.0 kgf/cm^2), moderate (8.0 kgf/cm^2), and high (25.0 kgf/cm^2) confining pressures σ'_{3c} are shown in Fig. 4.1a,b,c. The corresponding effective stress paths are shown in Fig. 4.2.

Isotropically consolidated sample under low confining pressure did not develop strain softening response (Fig. 4.1a) even though the relative density was only 25%. Instead, the sample developed a deviator stress plateau over a small range of strain before the shear resistance started increasing once again due to dilation with further straining. It may also be seen that the stress-strain curve after the plateau was much flatter than that in the initial stage of loading. This is the typical type 4 response described in Chapter 2.

Anisotropically consolidated sample under the same confining pressure, on the other hand, developed a slight strain softening even though its relative density was higher than that of isotopically consolidated sample (Fig. 4.1a). Small strain softening was associated with a small strain potential of less than 2%. The sample deformed in a manner characterized as limited liquefaction, except that the strain potential was very small. This is the typical type 3 response described in Chapter 2.

When the confining pressure was increased to 8.0 kgf/cm^2 (784 kPa), both isotropically and anisotropically consolidated samples developed strain softening response (Fig. 4.1b) even though relative densities were

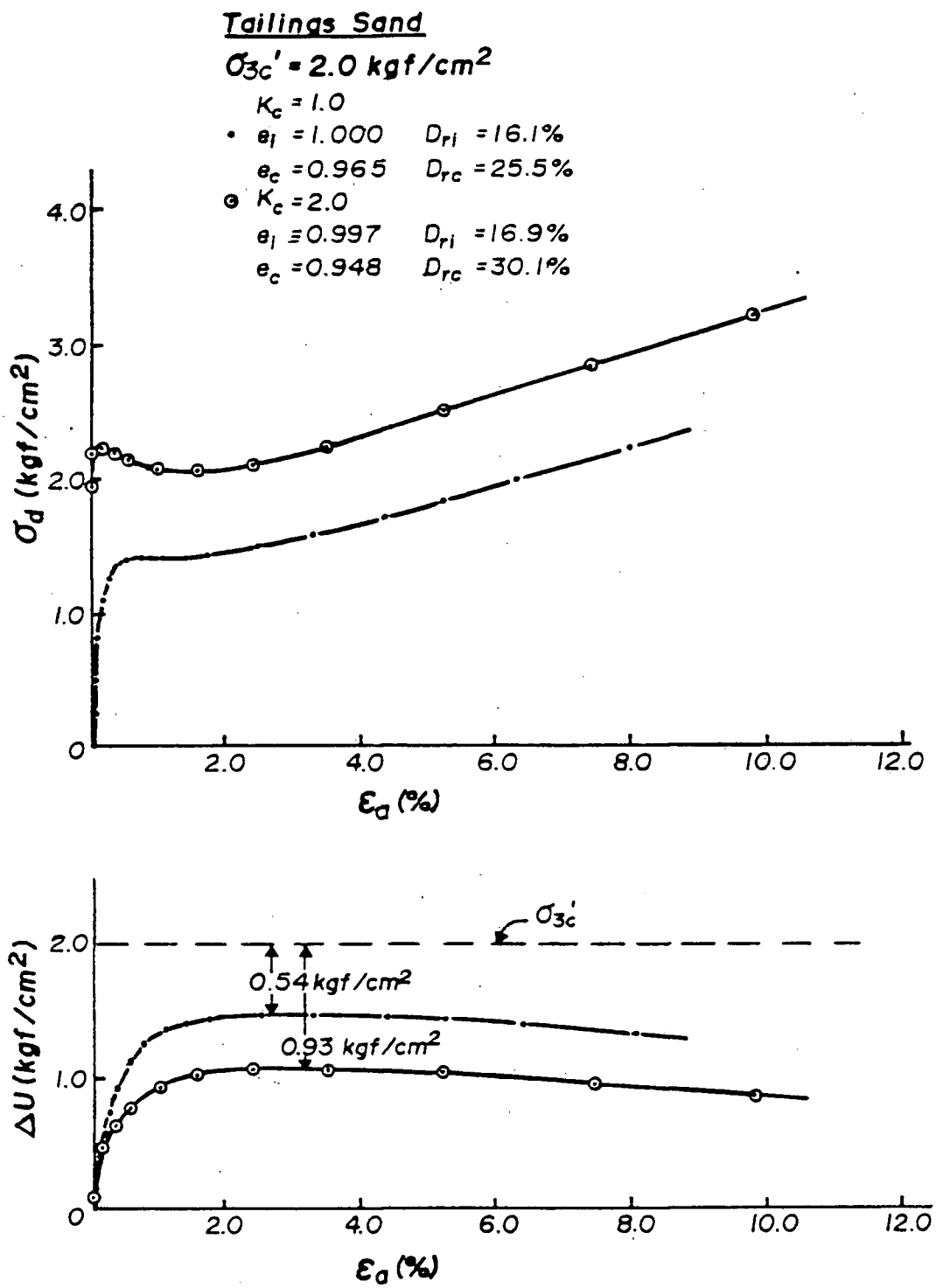

Fig. 4.1a Undrained monotonic compression loading behaviour of initially loose tailings sand under low confining pressure.

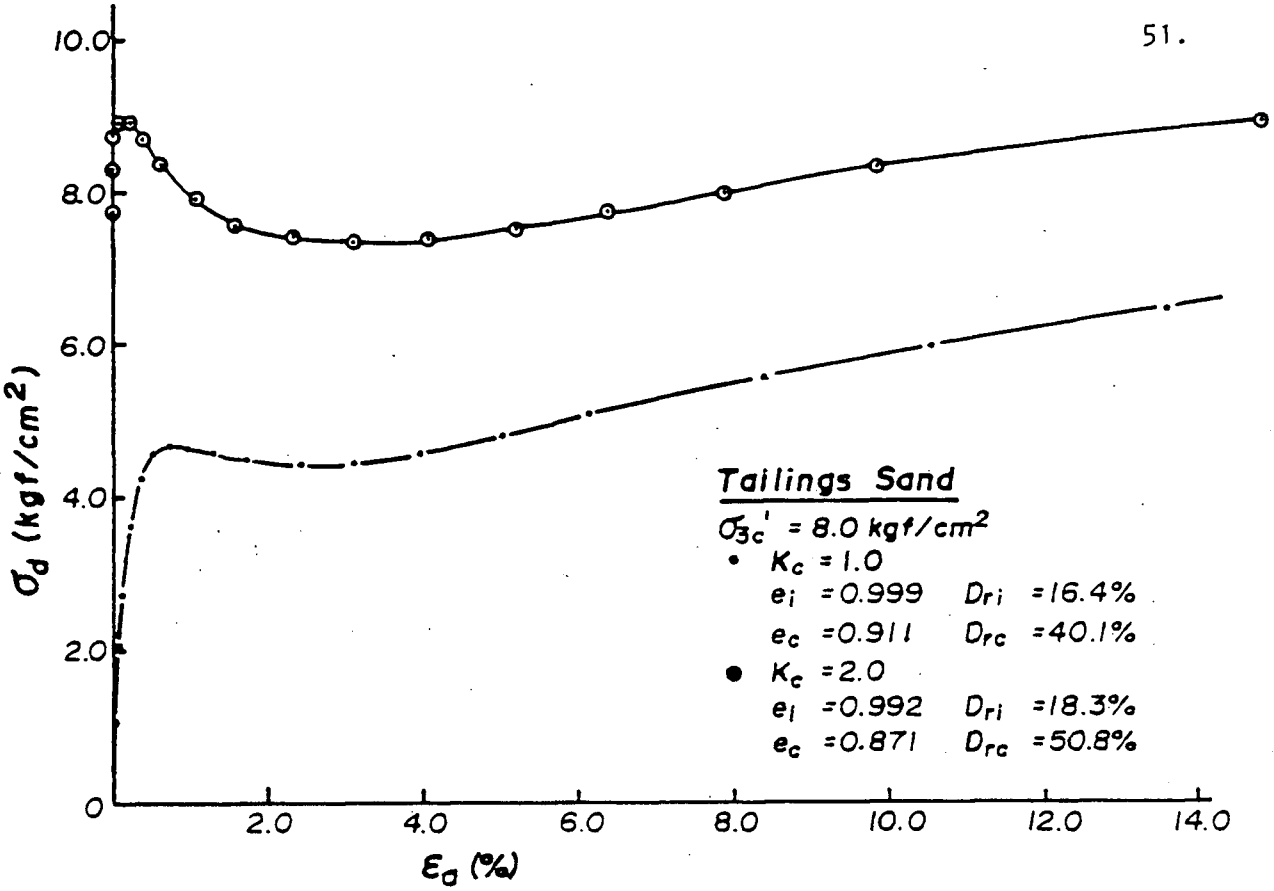

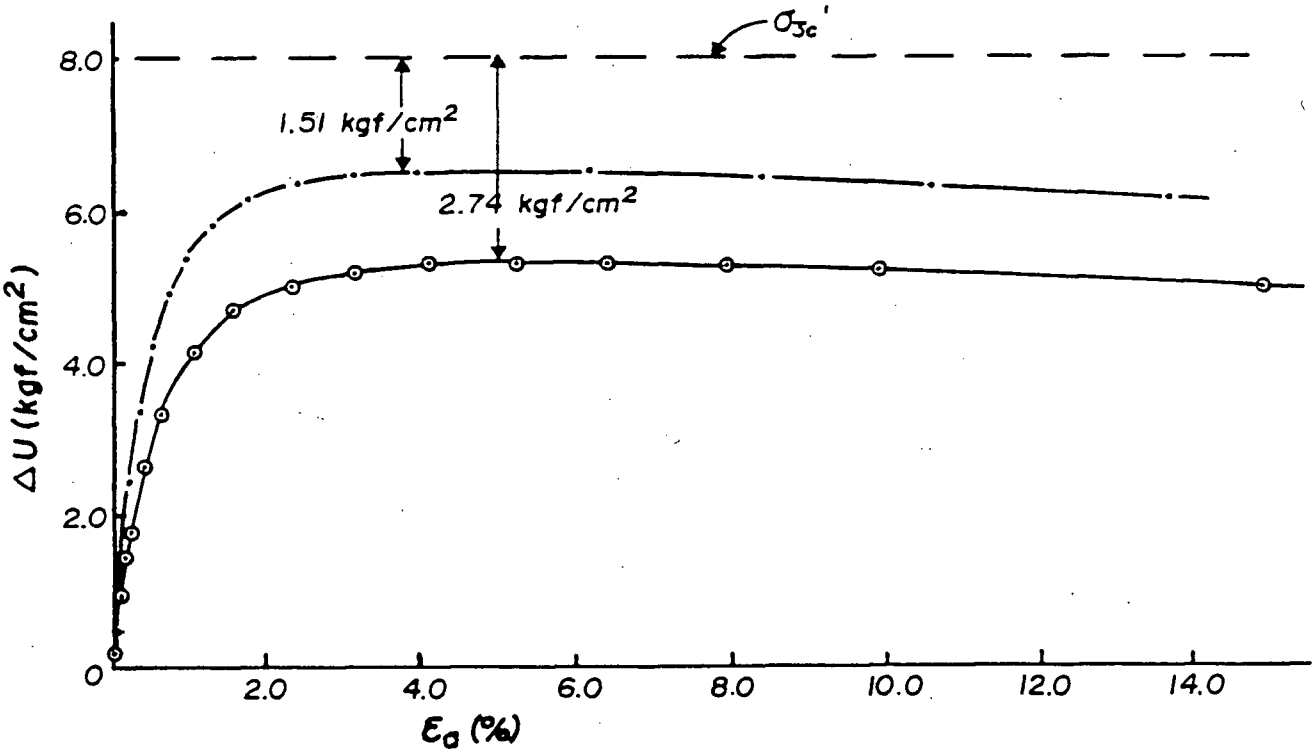

Fig. 4.1b Undrained monotonic compression loading behaviour of initially loose tailings sand under moderate confining pressure.

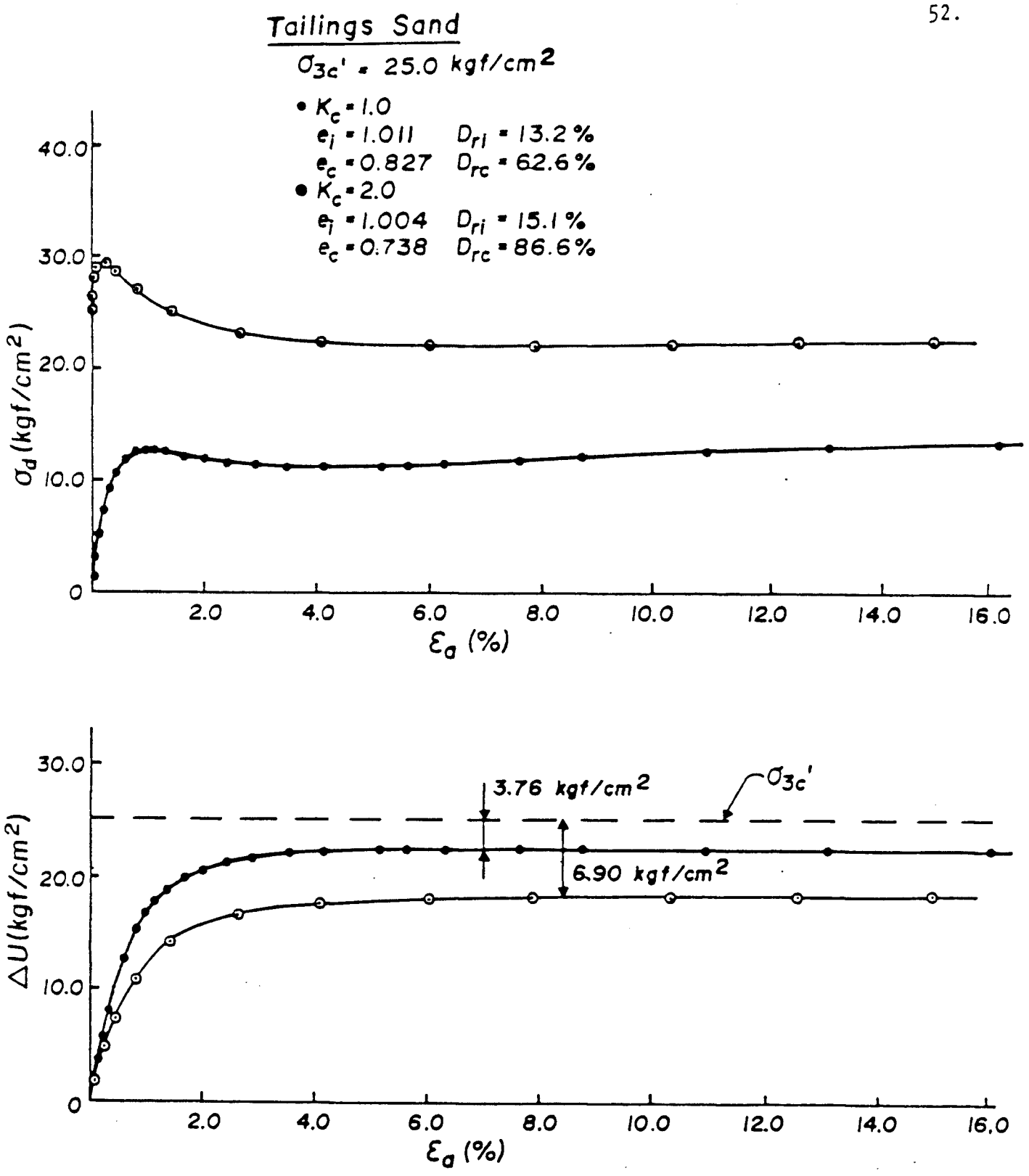

Fig. 4.1c Undrained monotonic compression loading behaviour of initially loose tailings sand under high confining pressure.

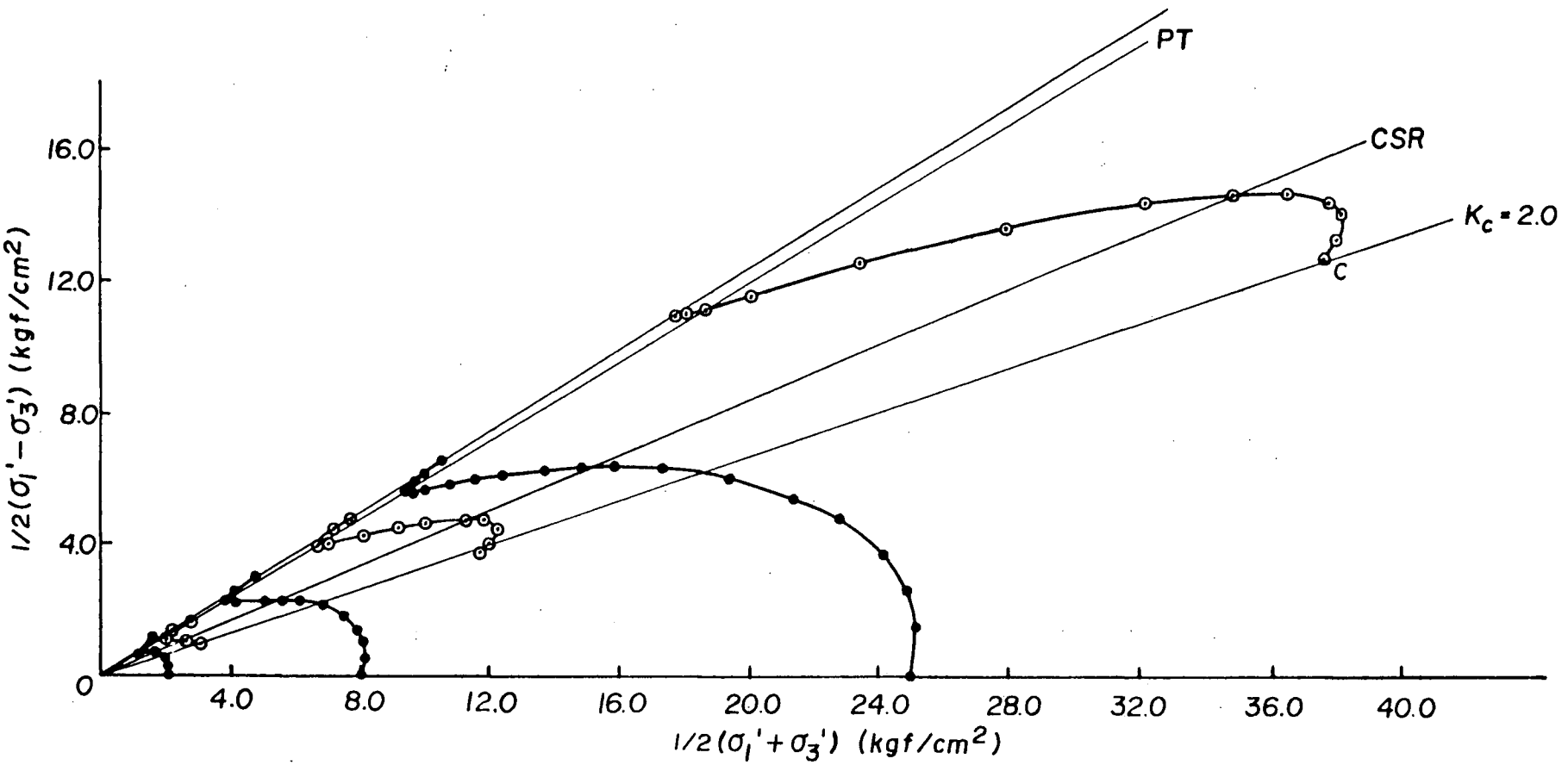

Fig. 4.2 Effective stress paths of undrained monotonic compression loading response of initially loose tailings sand.

much higher than those under the lower confining pressure. Both samples deformed in the same manner with steady state conditions over a moderate range of strain, before regaining strength due to dilation with further straining. These correspond to type 2 response described in Chapter 2. It may be noted that anisotropically consolidated sample, which simulates soil element with initial shear bias, developed more severe loss of strength and larger strain potential than the isotropically consolidated one, even though its final relative density was higher. Furthermore, its shear resistance during steady state was slightly less than the initial static shear stress after consolidation.

Under high confining pressure of 25.0 kgf/cm^2 (2450 kPa), both samples behaved in a manner similar to those under moderate confining pressure (Fig. 4.1c). Despite their much higher relative densities, they developed a severe loss of shear resistance and larger strain potential than samples at moderate confining pressure. The loss in resistance was especially severe for anisotropically consolidated sample. Its shear resistance was reduced to a value considerably less than the initial static shear stress, and the sample deformed continuously with unlimited strain potential. Although the relative density is very high (86.6%), its behaviour is the same as the true liquefaction developed in very loose sand (type 1 response), with the difference that relatively high shear resistance was still retained during steady state deformation.

Typical stress-strain and pore pressure responses of initially dense samples under moderate and high confining pressures is shown in Fig. 4.3a,b and the effective stress paths in Fig. 4.4.

Isotropically consolidated sample under moderate confining pressure of 8.0 kgf/cm^2 (784 kPa) developed type 5 strain hardening response (Fig.

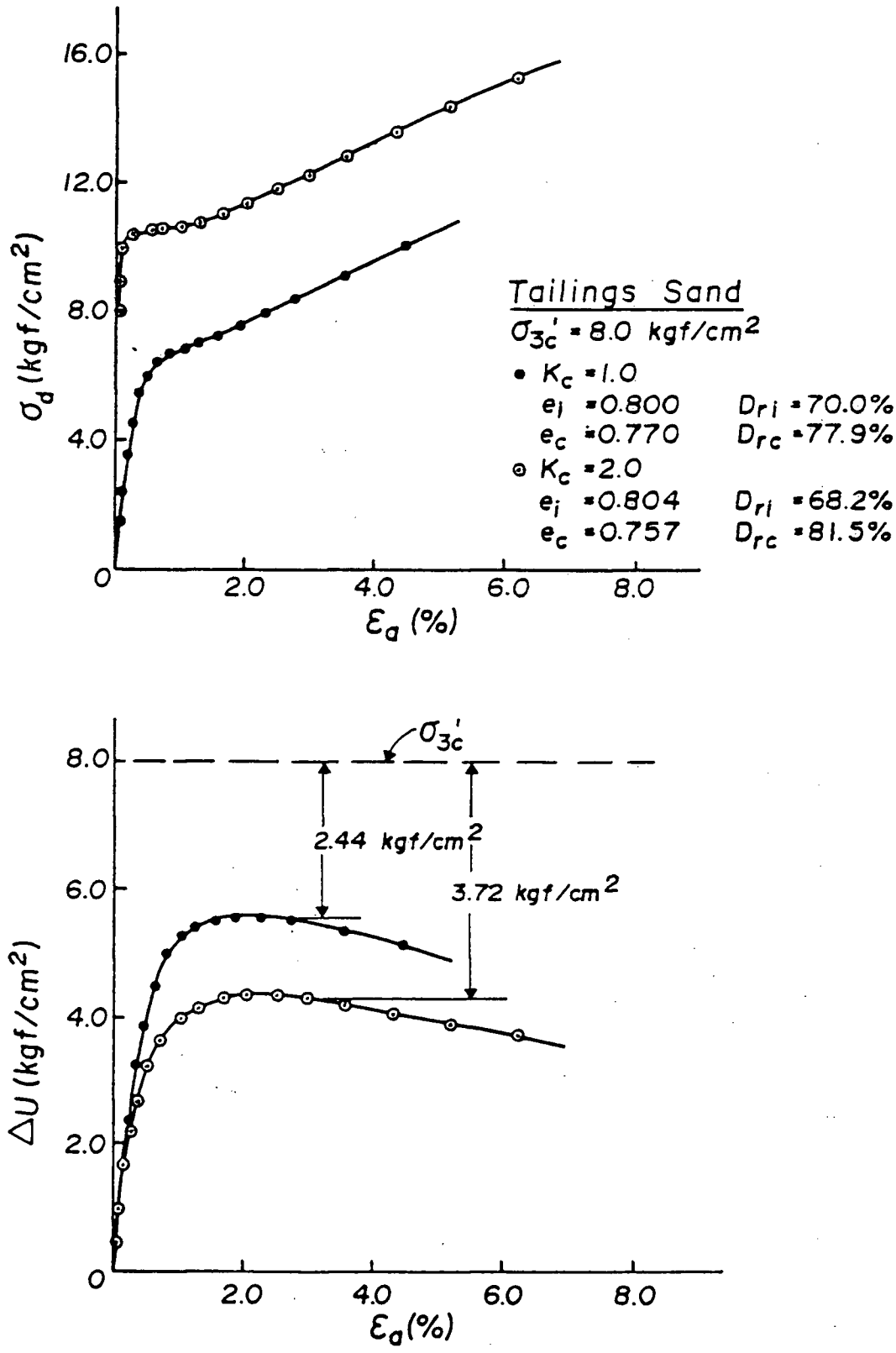

Fig. 4.3a Undrained monotonic compression loading behaviour of initially dense tailings sand under moderate confining pressure.

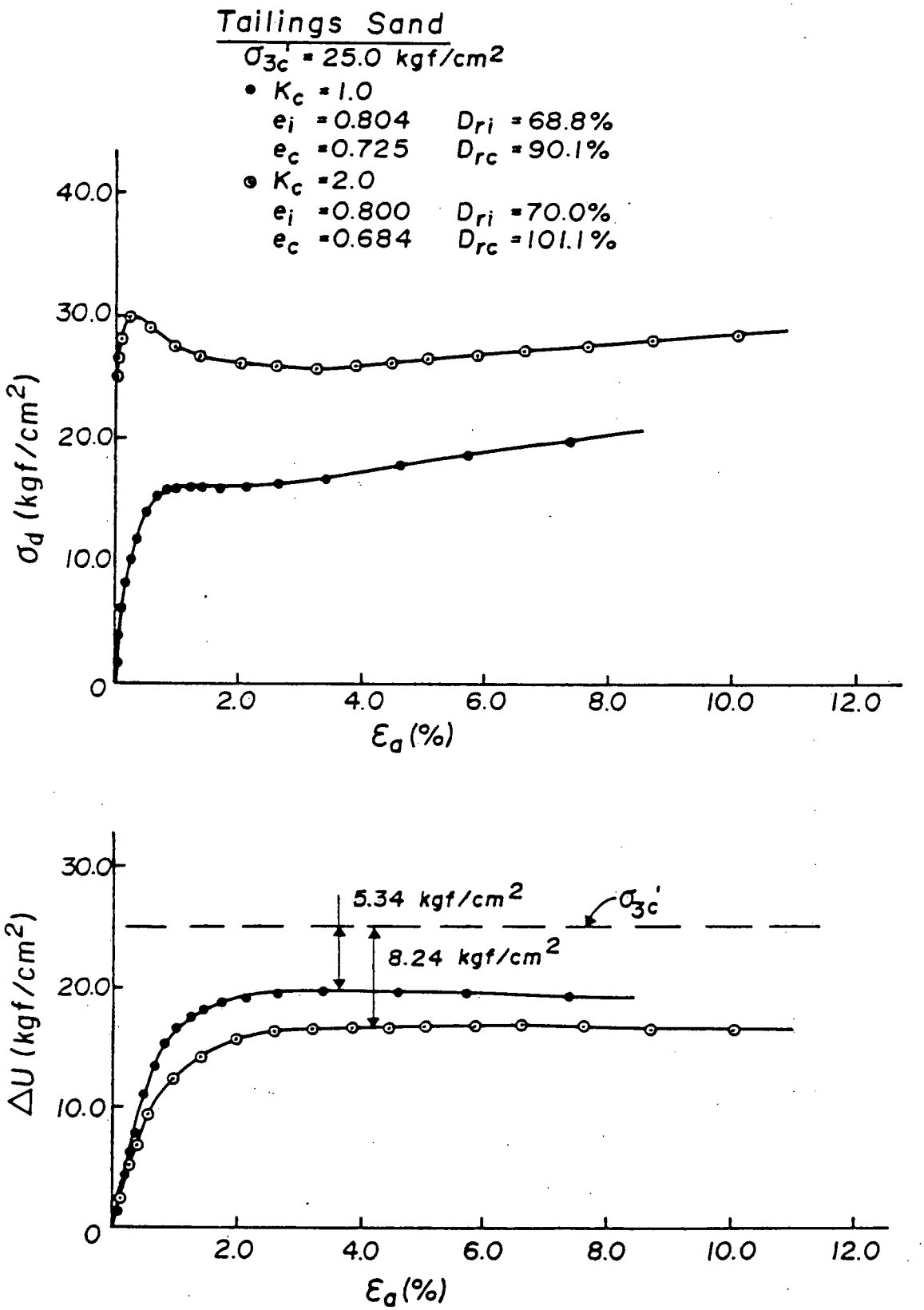

Fig. 4.3b Undrained monotonic compression loading behaviour of initially dense tailings sand under high confining pressure.

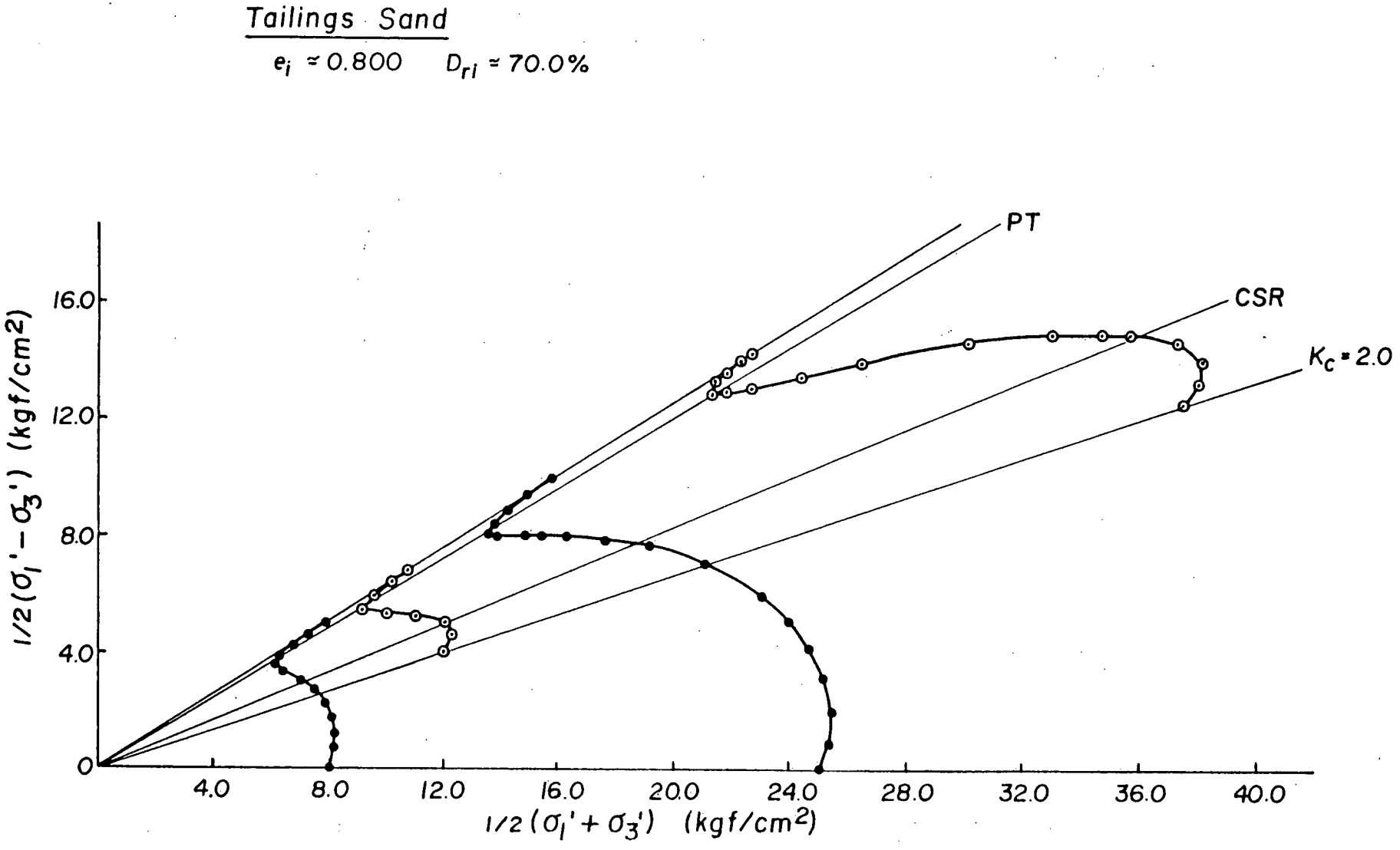

Fig. 4.4 Effective stress paths of undrained monotonic compression loading response of initially dense tailings sand.

4.3a), whereas anisotropically consolidated sample developed type 4 response. When the confining pressure was increased to 25.0 kgf/cm^2 (2450 kPa), both isotropically and anisotropically consolidated samples developed more contractive tendancy even though their relative densities were much higher than those under moderate confining pressure. For isotropically consolidated samples, the response changed from type 5 under moderate confining pressure to type 4 under high confining pressure, while that of anisotropically consolidated samples transformed from type 4 to type 2 as the confining pressure increased by the same magnitude.

Typical test results for an initially loose sample under low confining pressure of 1.84 kgf/cm^2 (180 kPa) subjected to monotonic extension loading are shown in Fig. 4.5. The sample developed strain softening response unlike similar sample with the same initial sample state but subjected to compression loading, which developed type 4 response (Fig. 4.1a). The sample loaded in extension experienced severe loss of shear resistance with accompanying large strain potential before it regained its strength due to dilation with further straining.

Ottawa Sand Test Results

Typical stress-strain and pore pressure response of initialy loose samples of Ottawa sand consolidated to low and high confining pressures are shown in Fig. 4.6a,b. The corresponding effective stress paths are shown in Fig. 4.7.

In contrast to the behaviour of tailings sand, all initially loose samples of Ottawa sand developed strain softening response with significant strain potential for the range of confining pressure and K_c ratio considered. Strain softening is particularly severe under low confining

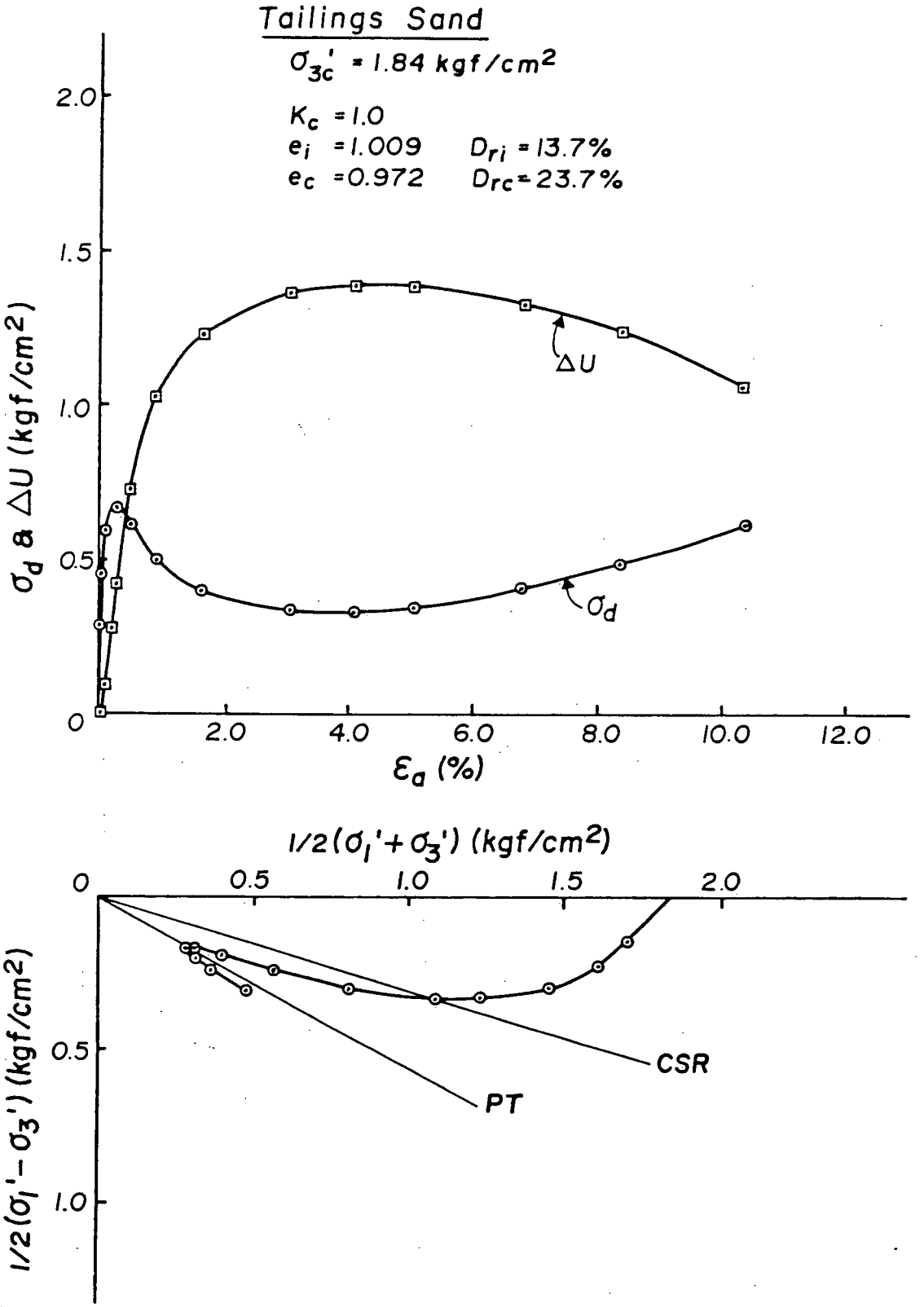

Fig. 4.5 Undrained monotonic extension loading behaviour of initially loose tailings sand.

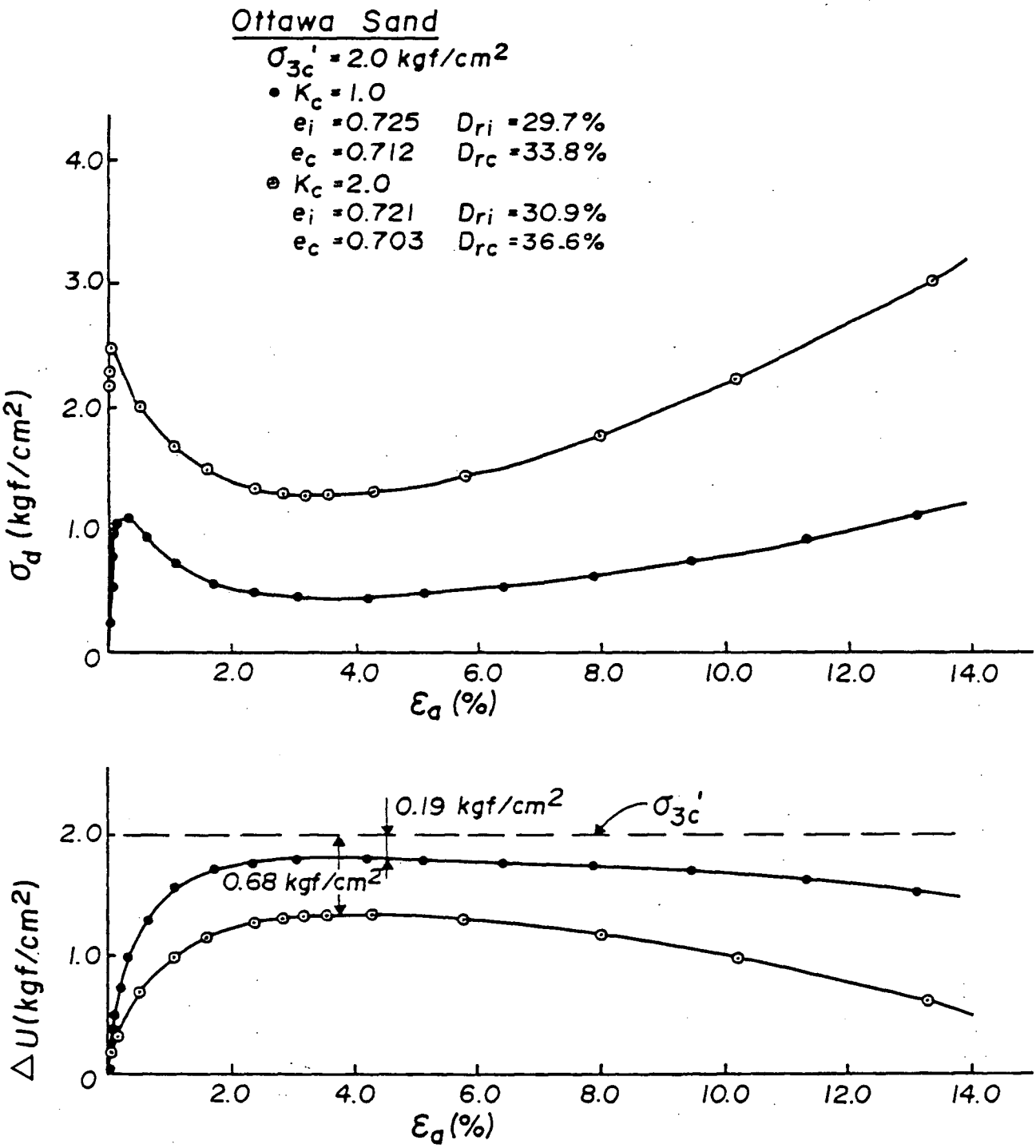

Fig. 4.6a Undrained monotonic compression loading behaviour of initially loose Ottawa sand under low confining pressure.

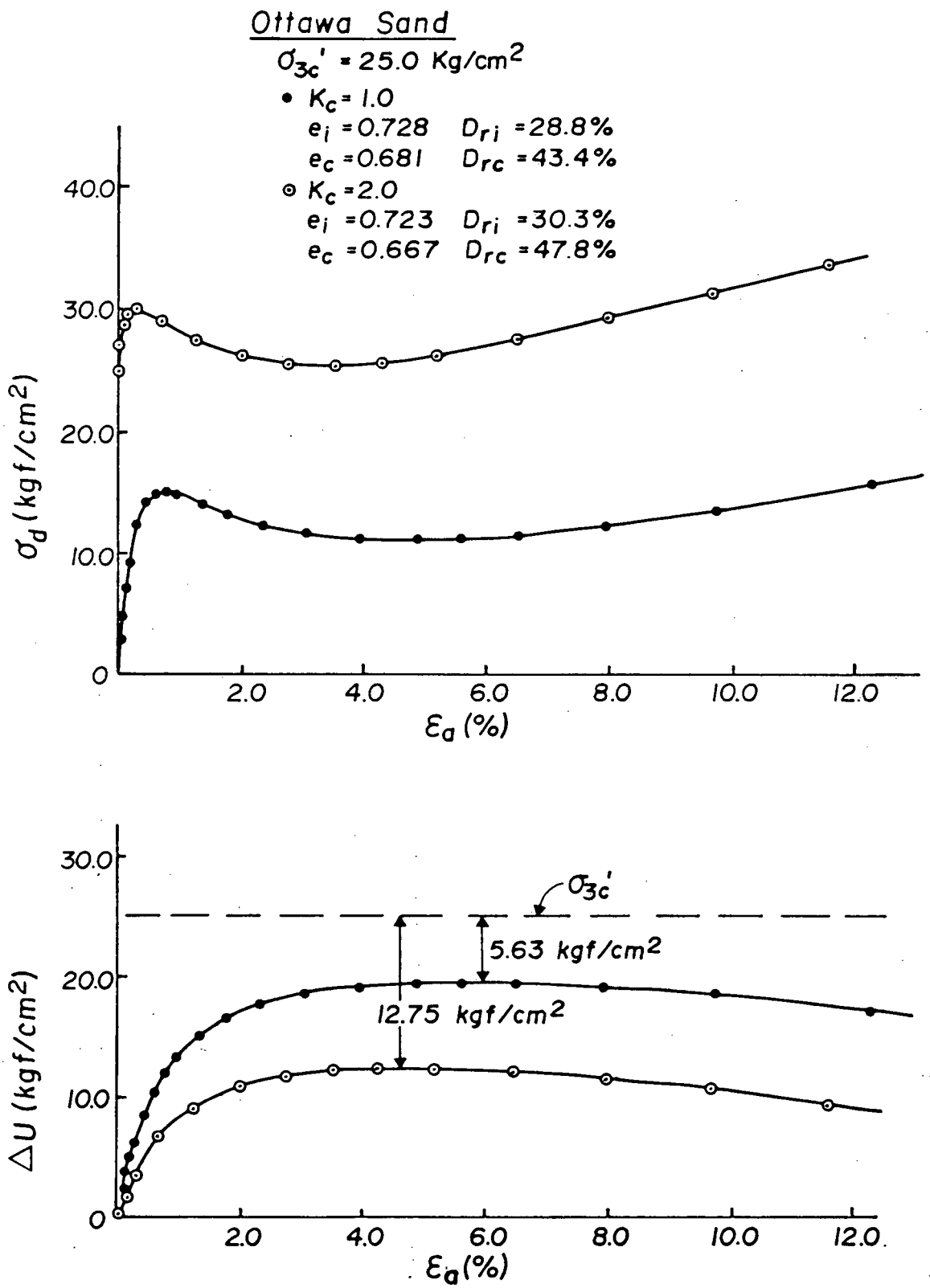

Fig. 4.6b Undrained monotonic compression loading behaviour of initially loose Ottawa sand under high confining pressure.

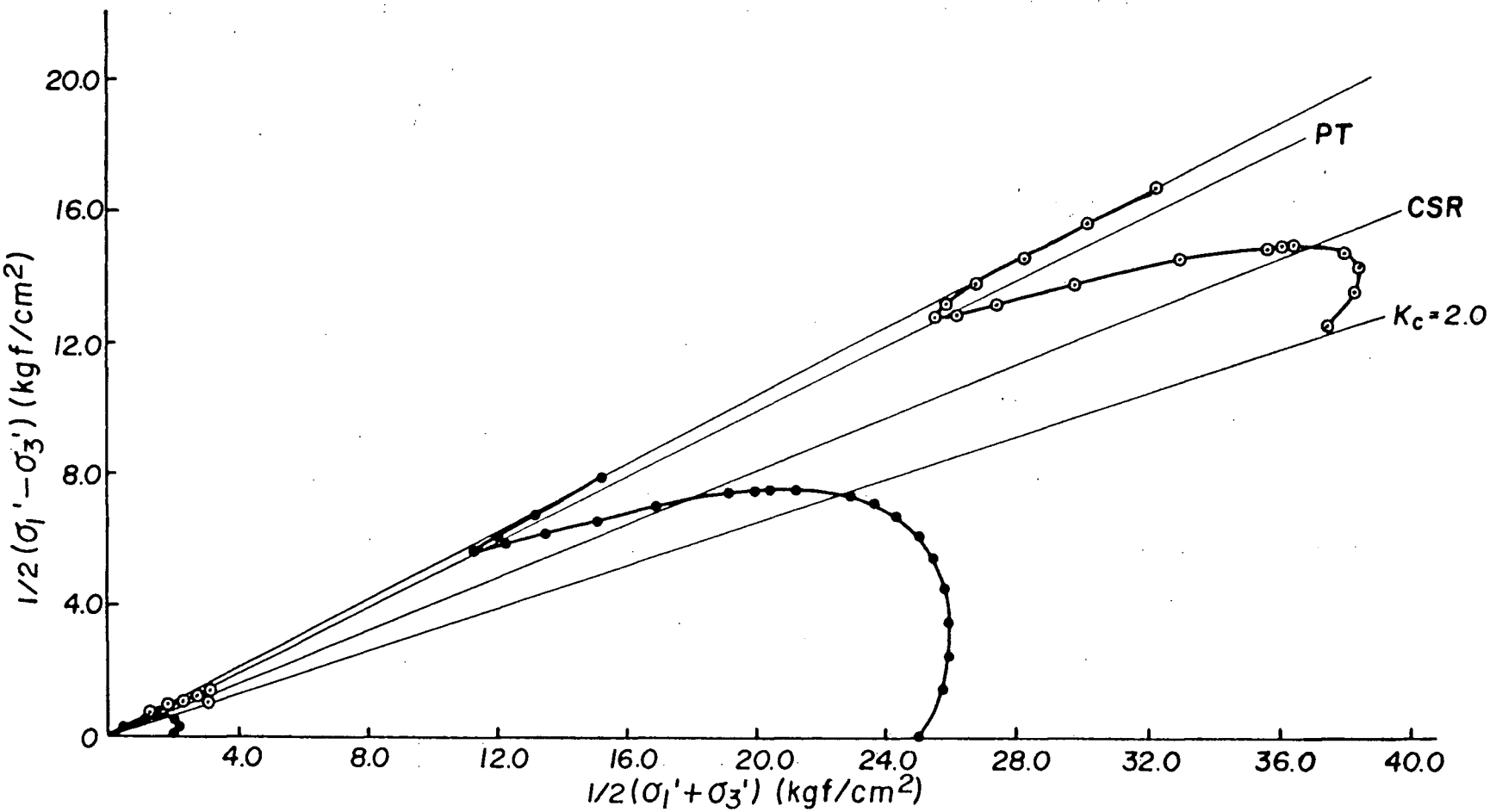

Fig. 4.7 Effective stress paths of monotonic compression loading response of initially loose Ottawa sand.

pressure (Fig. 4.6a). The sand lost much greater percentage of its resistance and developed much larger strain potential than those under high confining pressure. All samples developed type 2 response, which is typical of limited liquefaction, and no type 1 response typical of true liquefaction was observed.

For samples densified to initial relative density of 45%, however, completely different responses compared to those of the initially loose states were obtained. Instead of developing strain softening response, all samples developed strain hardening or type 4 response, regardless of the confining pressure. Typical test results for such response are shown in Figs. 4.8a,b and 4.9.

Typical test results for an initially medium dense sample under a confining pressure of 8.0 kgf/cm^2 (784 kPa) and K_c = 1.0 subjected to monotonic extension loading are shown in Fig. 4.10. Similar to the behaviour of tailings sand, samples with states which developed strain hardening response in compression developed strain softening response with significant strain potential under extension loading.

Comparison of Tailings and Ottawa Sand Response

From the test results of tailings and Ottawa sands presented above, it may be noted that the strain softening and strain hardening behaviour are similar for both sands. However, there are important differences in the factors which control the occurrence of strain softening or strain hardening response in the two sands. For tailings sand, it appears that the confining pressure and consolidation stress ratio are the most important factors. Samples with low relative density can develop strain hardening response under low confining pressure and low K_c ratio,

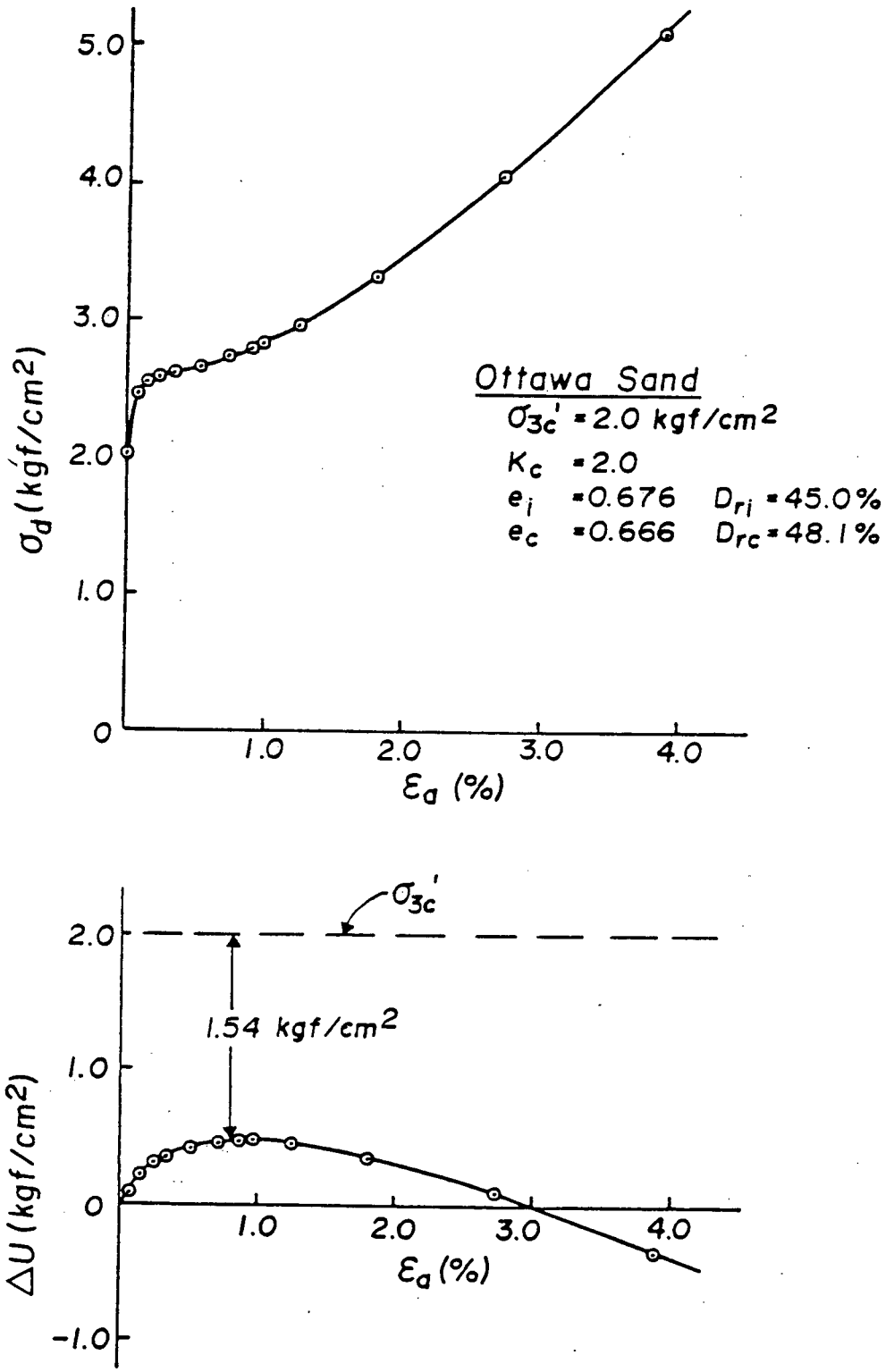

Fig. 4.8a Undrained monotonic compression loading behaviour of initially dense Ottawa sand under low confining pressure.

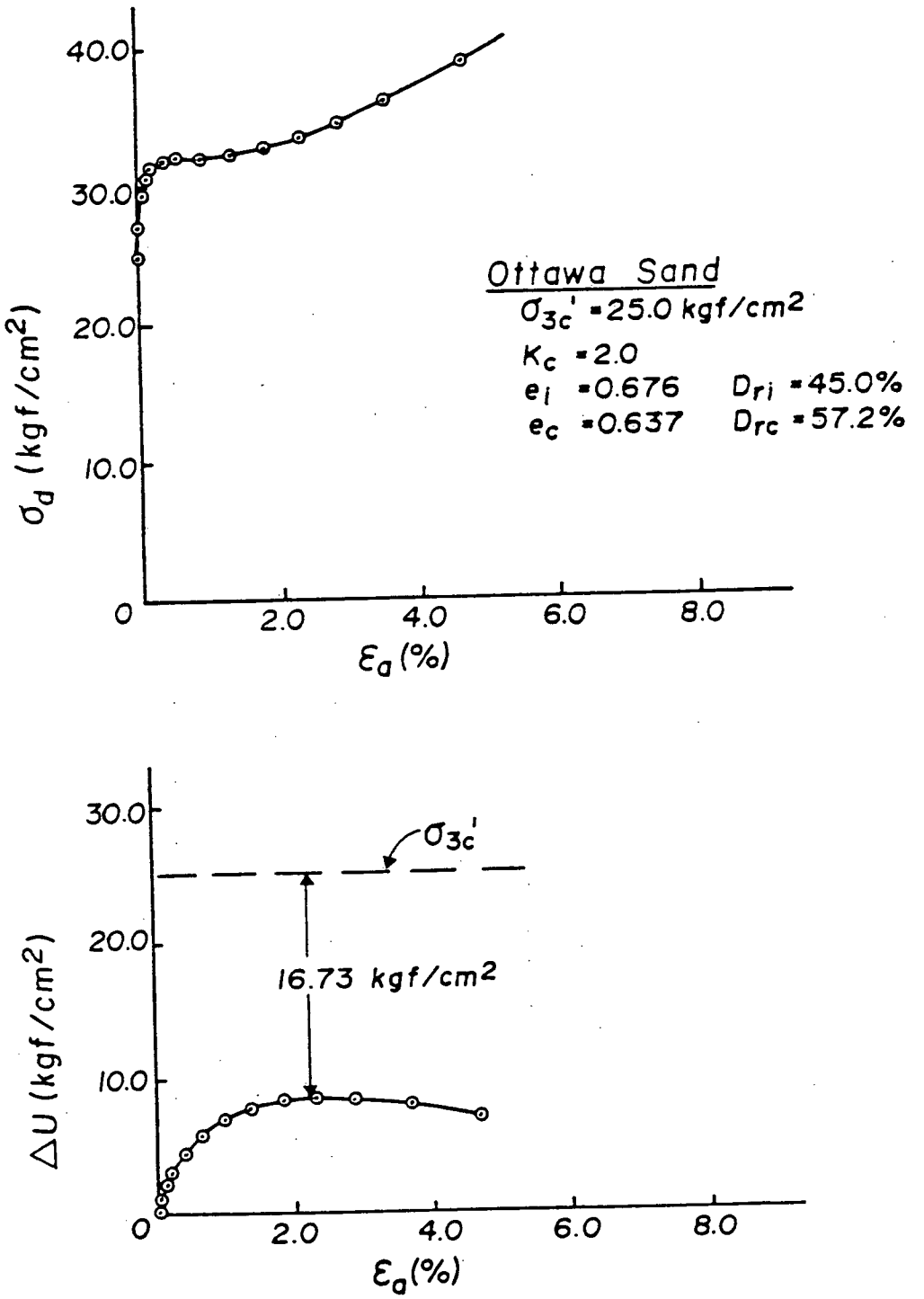

Fig. 4.8b Undrained monotonic compression loading behaviour of initially dense Ottawa sand under high confining pressure.

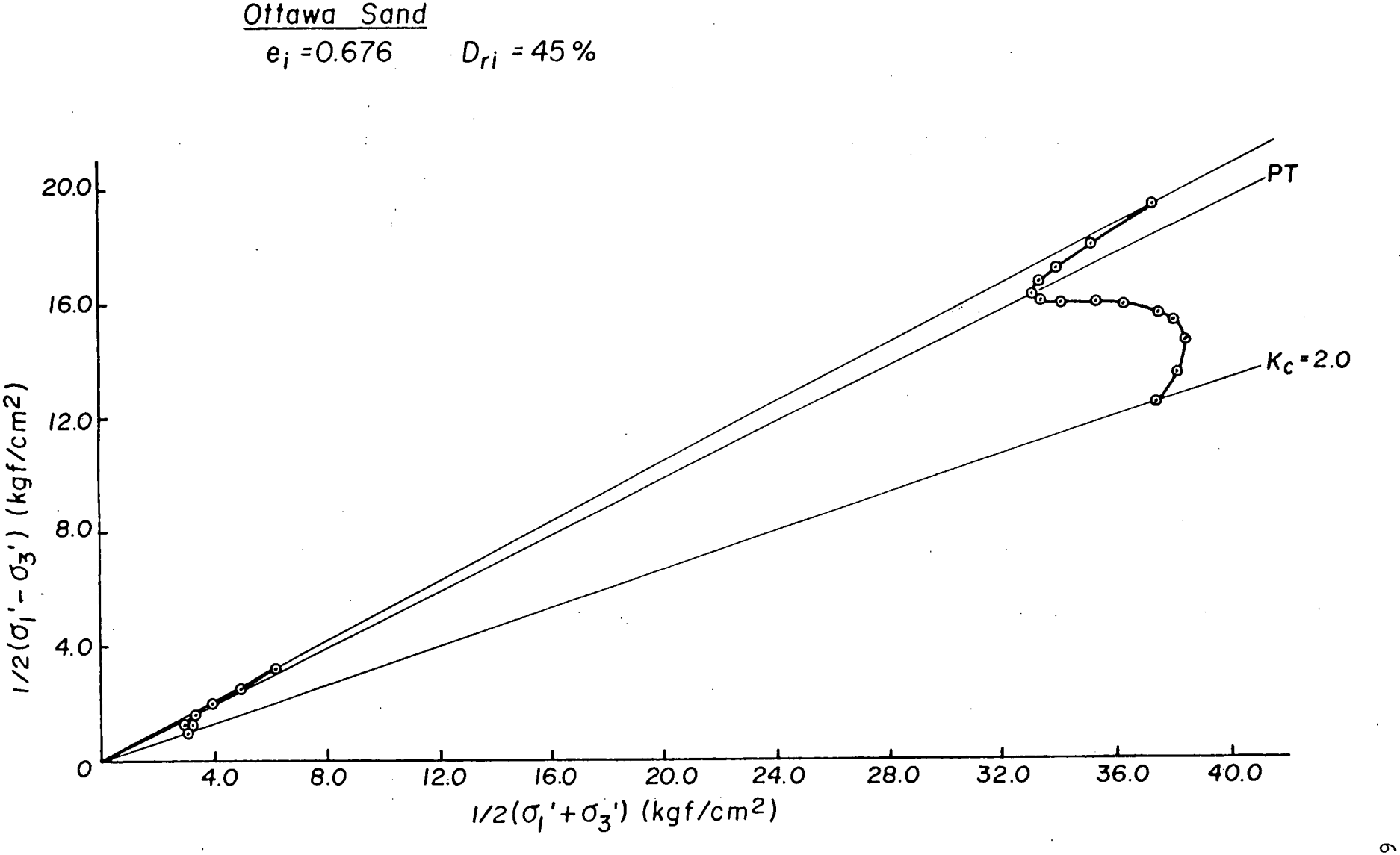

Fig. 4.9 Effective stress paths of monotonic compression loading response of initially dense Ottawa sand.

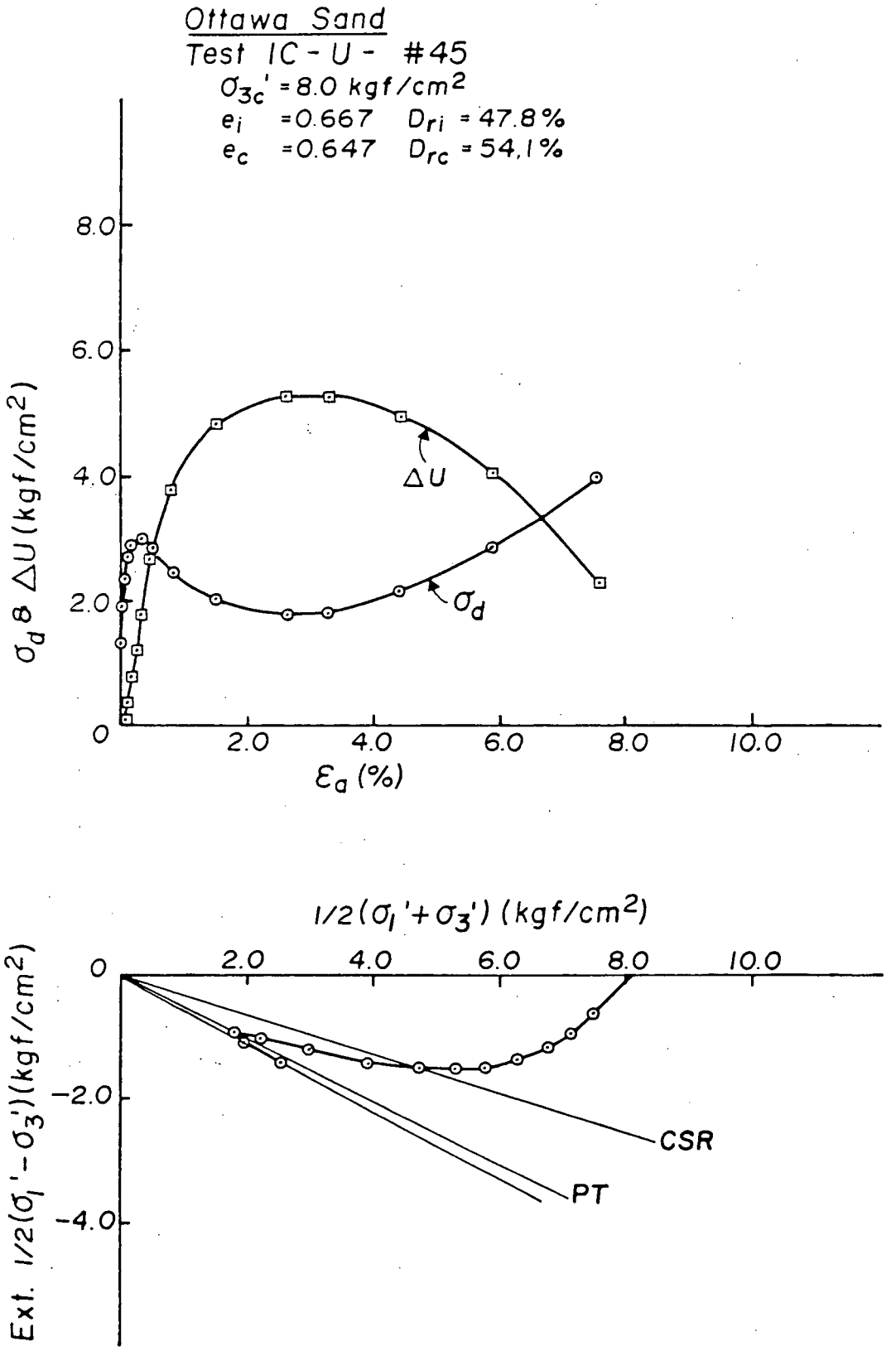

Fig. 4.10 Undrained monotonic extension loading behaviour of initially medium dense Ottawa sand.

whereas samples even with high relative density can develop strain softening response under high confining pressure and high K_c ratio. On the other hand, relative density seems to be the most important factor for Ottawa sand. All initially loose samples developed strain softening response over the range of confining pressure and K_c ratio considered, and all samples densified to an initial relative density large than about 45% developed strain hardening response, regardless of the confining pressure and K_c ratio. This difference in the factors controlling the undrained response of these two sands will be discussed further in Section 4.2.

It may also be noted that the modes of loading influence the undrained behaviour of both sands. Sand at given relative density may be safe against liquefaction (limited or true) under monotonic compression but may undergo liquefaction under monotonic extension. The range of relative density over which liquefaction can be induced in extension is larger than that in compression under the similar consolidation stress conditions. Also the degree of strain softening is more severe in extension than that in compression under similar initial sample states. These characteristics are true for both sands.

4.2 Strain Softening and Strain Hardening Responses

Traditionally, strain softening and strain hardening responses are described by the shape of the stress-strain curve obtained. In this way, only qualitative description as to the undrained behaviour, i.e., softening or hardening, can be obtained. Possible relationship of the type of response either to the soil parameter during deformation or to initial

state (e_c, σ'_{3c}, K_c) has not been investigated comprehensively. In the investigations reported herein, different types of response will be related to the sample state at phase transformation, and peak strength and to the initial sample state.

4.2.1 Classification of Undrained Responses

Test results relating void ratio after consolidation e_c versus effective confining stress σ'_3 at phase transformation state for tailings sand prepared at an initial void ratio e_i of 0.90 are shown in Fig. 4.11. The relationship between void ratio e_c and consolidation stress σ'_{1c} which is valid for any value of K_c (see Fig. 3.8) is also shown in the figure. Samples under low consolidation stresses, σ'_{1c}, developed strain hardening response. As the void ratio e_c decreases as a result of increasing consolidation stresses, the samples started to develop slight strain softening associated with small strain potential. As the consolidation stresses are increased further, the samples developed strain softening response with significant (>2%) strain potential or even true liquefaction. It should be noted that data points in Fig. 4.11 contain results for samples consolidated to various K_c ratios. A continuous unique relationship may be seen to exist between e_c and σ'_3 which describes the full spectrum of undrained response type 1 to type 5. This continuous line relating e_c and σ'_3 at PT state may be divided into two distinct regions of response, i.e., strain hardening region and strain softening region (Fig. 4.11). Due to the unique e_c-σ'_{1c} relationship, these two regions of response can also be related uniquely to consolidation stress σ'_{1c}, regardless of the K_c ratio. In other words, the undrained response is uniquely related to consolidation stress σ'_{1c}

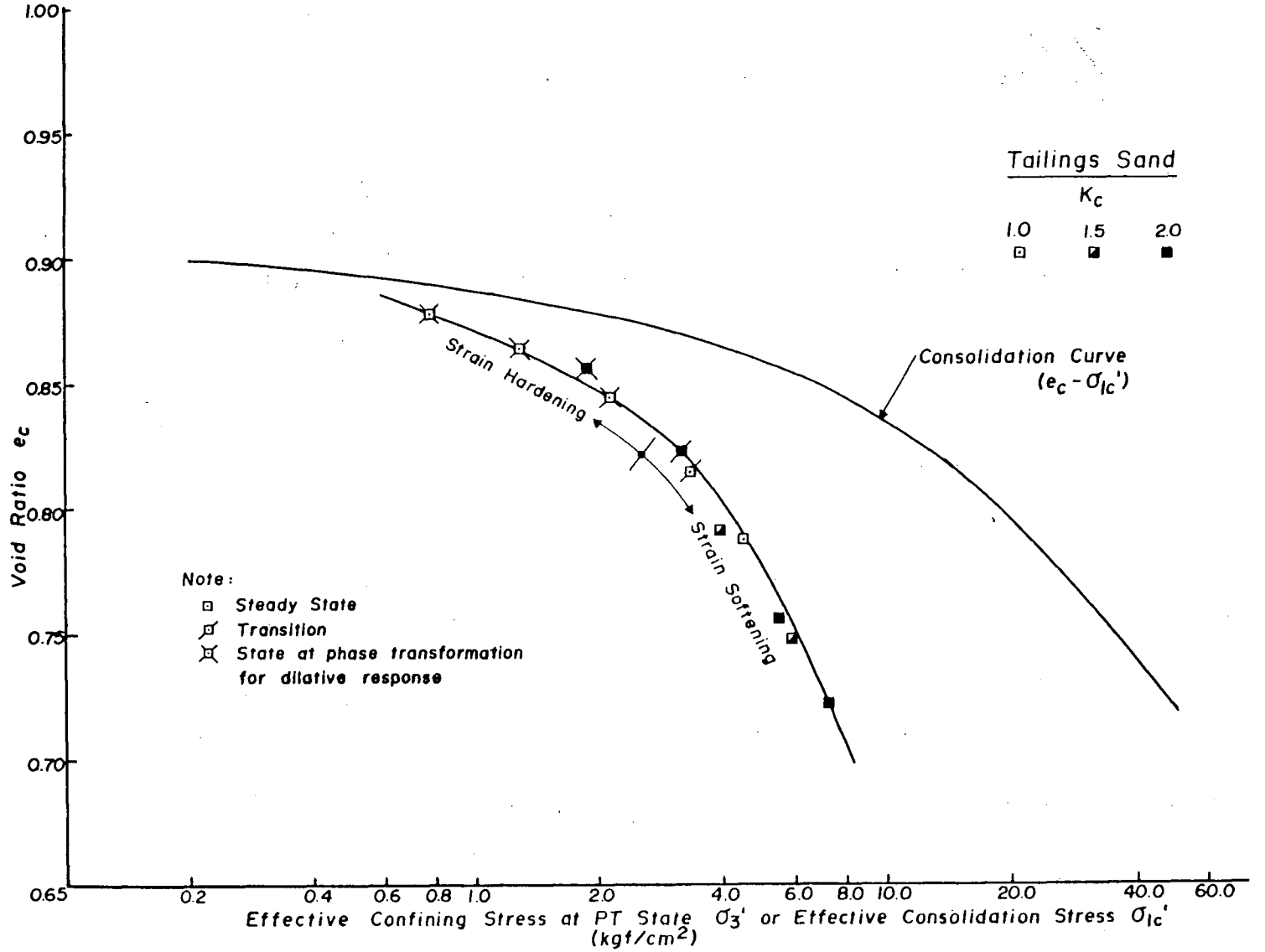

Fig. 4.11 Relationship between e_c and σ_3' at PT state for tailings sand at fixed e_i under undrained compression loading.

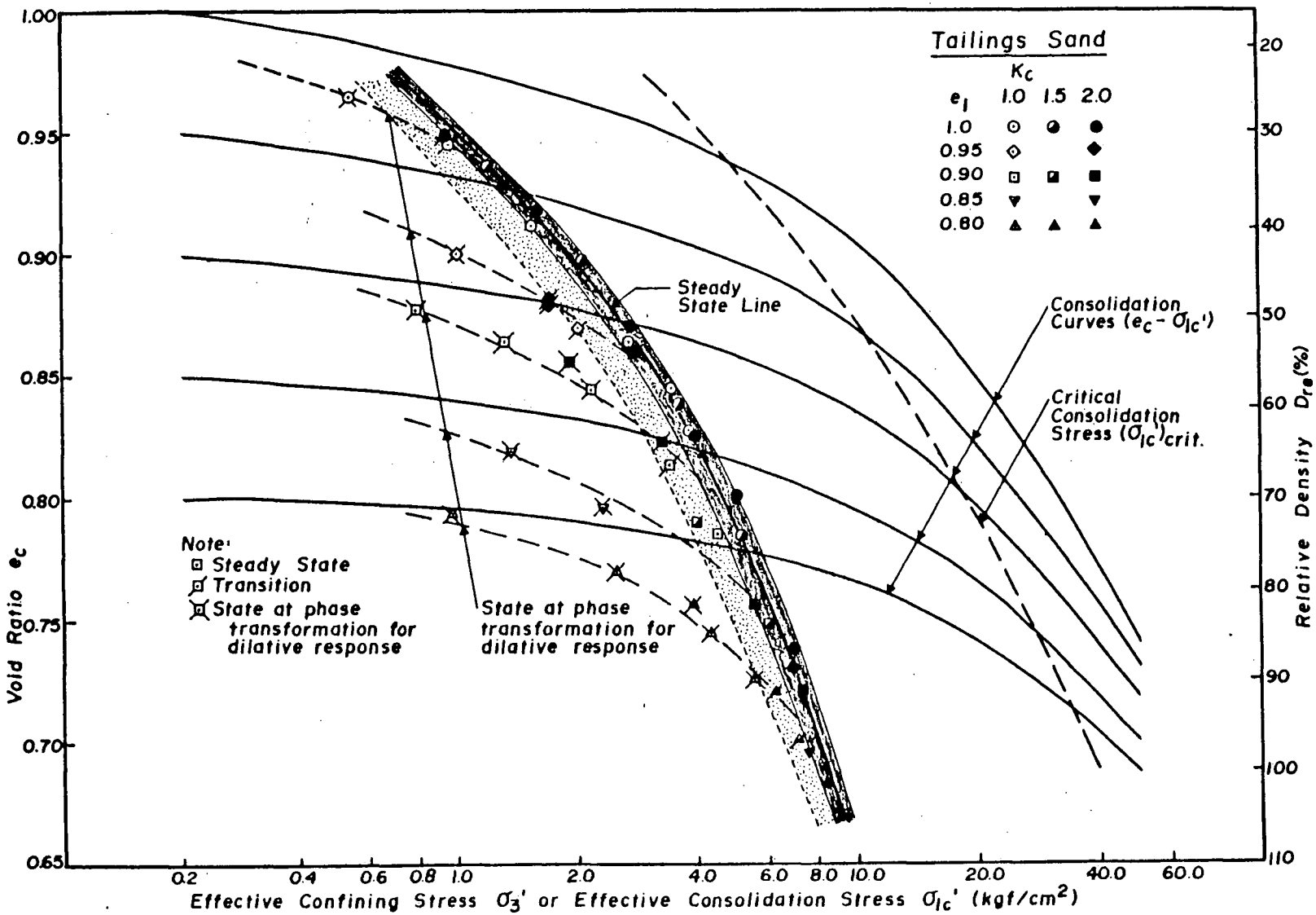

Fig. 4.12 Relationship between e_c and σ_3' at PT state for tailings sand with various e_i under undrained compression loading.

which is the product of K_c and σ'_{3c}.

Fig. 4.12 shows compilation of all test results relating e_c and σ'_3 at PT state for tailings sand with various initial void ratio e_i. The relationship between e_c vs. σ'_{1c} for various e_i is also shown in the figure. It may be seen in Fig. 4.12 that e_c-σ'_3 relationships for various e_i form a series of curves which merge into a unique line below a certain e_c, depending on e_i of the sand. It is found that this unique line describes the behaviour of all samples which developed strain softening resulting in true liquefaction or limited liquefaction with significant strain potential (greater than 2%), regardless of the e_i of the sand.

Thus, for those samples that developed limited liquefaction, the concept of a unique steady state line proposed by Castro (1969) may be used in the same manner as for samples that develop true liquefaction. This steady state line is shown in Fig. 4.12 by a darkened band. It should be emphasized that this steady state line comprises of results for limited liquefaction as well as true liquefaction.

If the sand developed slight strain softening with strain potential less than 2%, the e_c-σ'_3 relationship for each e_i starts to branch away from the unique steady state line. Immediately to the left of the steady state line, these relationships form a region characterized by slight strain softening. This is shown by the dotted area in Fig. 4.12 and is the region of transition from limited liquefaction, which fits within the concepts of unique steady state line, into the region of strain hardening response. The dotted line in Fig. 4.12 which separates the regions of strain hardening and slight strain softening response is only approximate. A precise determination of this line would require a much more comprehensive testing program.

From Fig. 4.12, it may be seen that there exists a limiting value of consolidation stress σ'_{1c} for each e_i such that sand with consolidation stress σ'_{1c} greater than this value would always develop strain softening response with significant strain potential and the e_c-σ'_3 at PT state relationships fits the unique steady state line. Hereinafter this type of response will be called liquefaction. In contrast, samples with consolidation stress σ'_{1c} less than this critical value would always develop either strain hardening or slight strain softening response and the e_c-σ'_3 at PT state relationship does not fit the unique steady state line. This limiting value of consolidation stress will be called critical consolidation stress $(\sigma'_{1c})_{crit}$. From the results for test at five e_i, a relationship betwen e_c and critical consolidation stress $(\sigma'_{1c})_{crit}$ may be obtained. This is shown in Fig. 4.12 by the dashed line to the right but more or less parallel to the steady state line. It may be noted that $(\sigma'_{1c})_{crit}$ increases with decreasing e_c.

This critical consolidation stress $(\sigma'_{1c})_{crit}$ separates regions of initial sample state (e_c, σ'_{3c}, K_c) which will develop liquefaction from those which will not. Any sample with a state after consolidation lying on or to the right of $(\sigma'_{1c})_{crit}$ line will result in liquefation, otherwise slight strain softening or strain hardening response will be developed. $(\sigma'_{1c})_{crit}$ line thus forms a quantitative criterion for separating regions of liquefaction from other types of response. It eliminates the arbitrariness of criterion proposed by Castro (1969) and Castro and Poulos (1977), which specifies that the initial state of sand has to be well above and to the right of the steady state line, in order to develop liquefaction. It should be noted that σ'_{1c} is the major consolidation stress, which is the product of minor consolidation stress

σ'_{3c} and K_c ratio, i.e., σ'_{3c} and K_c do not influence the liquefaction behaviour independently. Therefore, all sample states along the constant σ'_{1c} path will show the same response as long as conditions at PT state are concerned. It will be shown later that sand with a given e_c and σ'_{1c}, with $\sigma'_{1c} > (\sigma'_{1c})_{crit}$ will result in the same peak undrained strength and steady state strength under monotonic loading, regardless of the individual value of σ'_{3c} and K_c.

The results of void ratio e_c versus effective confining stress σ'_3 at PT state for Ottawa sand are shown in Fig. 4.13. The relationships between consolidation stress σ'_{1c} and e_c for three initial void ratios are also shown in the figure. As discussed in Section 4.1, all initially loose samples (upper consolidation curve) developed strain softening response with significant strain potential (>2%). The stress state at steady state vs e_c for these samples may be seen to form a well defined steady state line with slight scatter at around $e_c = 0.70$. No initial state gave rise to either strain hardening or slightly strain softening response. Initially somewhat denser samples (middle consolidation curve) under low initial stresses σ'_{1c} developed strain hardening response, but slight strain softening response was obtained under higher σ'_{1c}. For σ'_{3c} up to 25.0 kgf/cm^2 (2450 kPa) and $K_c = 2.0$ used in this study, there was no initial stress state which led to strain softening with significant strain potential and hence no data point on the steady state line. As the sand was densified initially to initial relative density of about 45%, all samples developed strain hardening response over the same range of σ'_{3c} and K_c values. It may be noted in Fig. 4.13 that the plots of void ratio versus σ'_3 at PT state for the two series of tests on initially denser samples formed two lines more or less parallel to the steady state

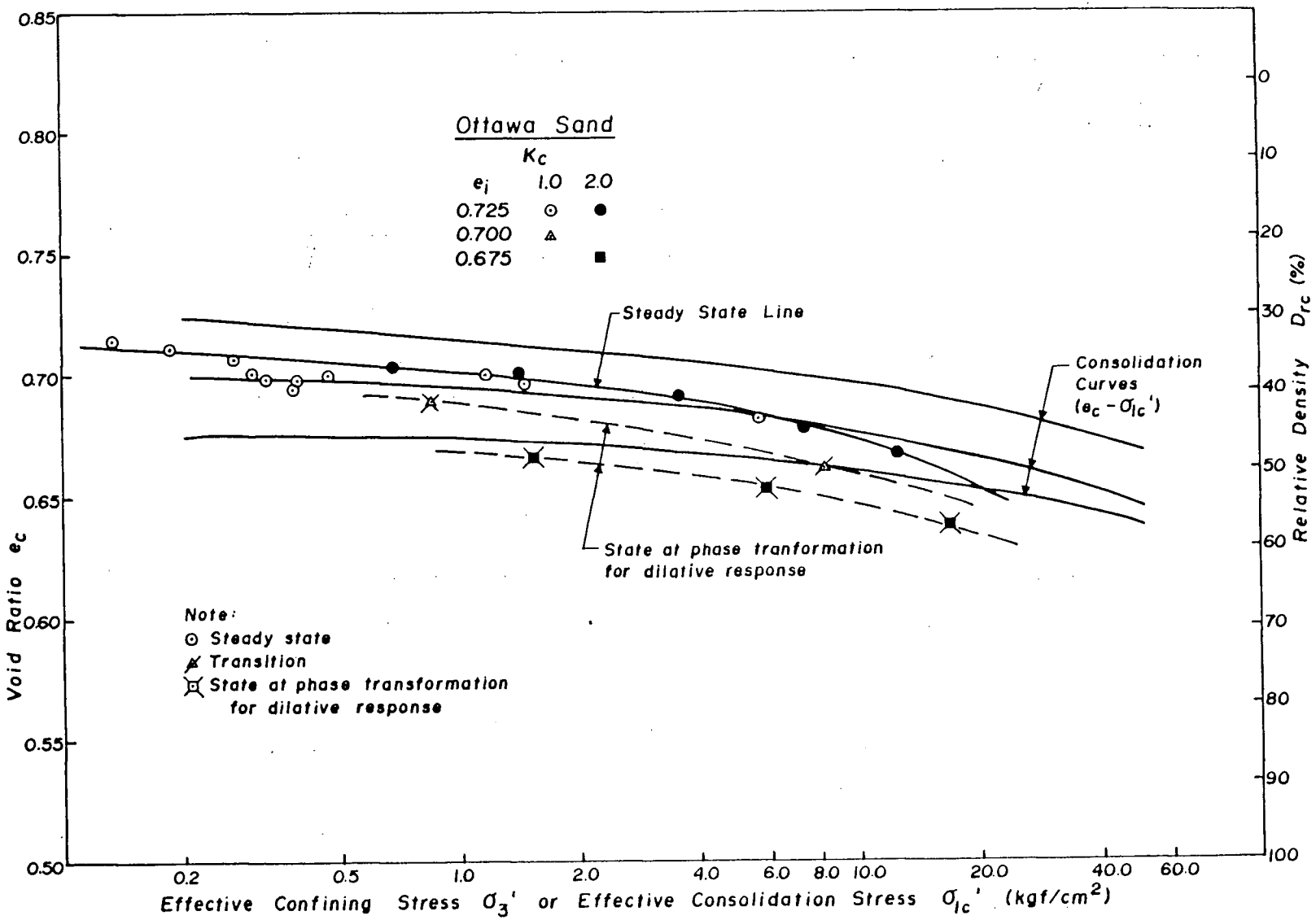

Fig. 4.13 Relationship between e_c and σ_3' at PT state for Ottawa sand with various e_i under undrained compression loading.

line obtained from initially loose samples. These lines tend to approach and may eventually merge into the steady state line at extremely high consolidation stress σ'_{1c}. This characteristics of Ottawa sand is similar to that of the tailings sand. From the results presented in Fig. 4.13 it appears that the PT state for $e_i = 0.70$ will merge into the steady line only when the consolidation stress σ'_{1c} is greater than the range considered here. Similarly for initially loose samples, it appears that strain hardening response can occur under very low consolidation stress only. Therefore, the critical consolidation stress $(\sigma'_{1c})_{crit}$ could not be obtained for the range of consolidation stresses and initial void ratio considered. However, as discussed in Section 4.1, sample with initial relative density greater than about 45% has little possibility of developing strain softening response. On the other hand, samples with initial relative density looser than about 40%, are highly susceptible to liquefaction.

Only limited test data were obtained for both sands in undrained extension loading. Only those samples which led to the development of steady state deformation were covered. Results of these tests for tailings sand are shown in Fig. 4.14a. For Ottawa sand, more comprehensive studies have been made by Chung (1984), and some of his test results are shown in Fig. 4.14b. From the limited data obtained, it is apparent that the steady state line in extension is not the same as that in compression for each sand. Furthermore, the extension steady state line for either sand is not as well defined as the compression steady state line. It is, however, clear that for the same e_c the steady state strength in extension is always less than that in compression because of smaller σ'_3 at steady state in extension. Moreover, the range of void ratio over which

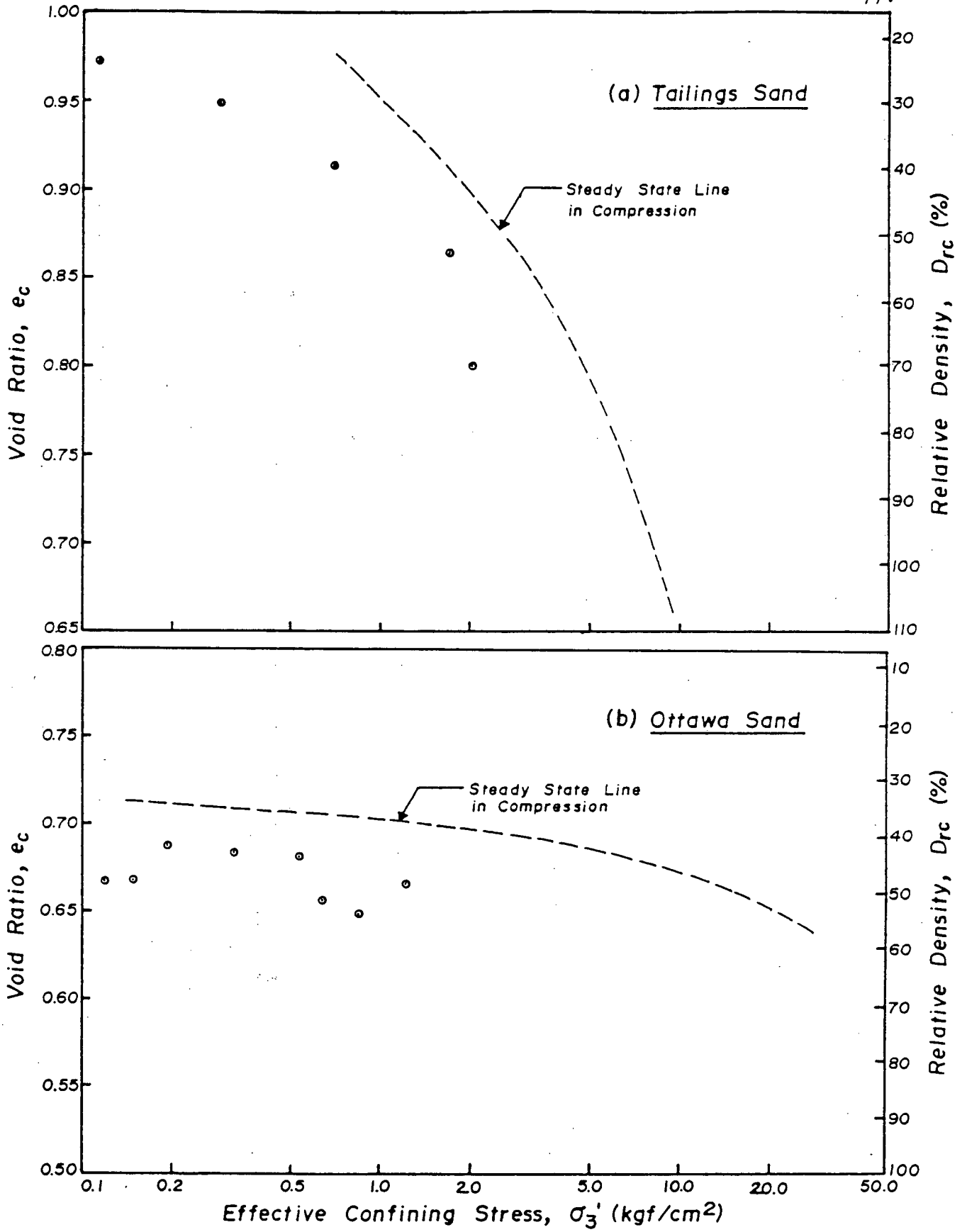

Fig. 4.14 Comparison of steady state condition under compression and extension.

liquefaction can be induced in extension is much larger than that in compression for the same range of consolidation stresses considered. This difference in compression and extension behaviour is believed to be a consequence of the inherent anisotropy in pluviated sand samples. However, these loading path differences may reflect certain situations in nature, such as the soil elements at the crest and near the toe of a potential failure surface. If such a situation occurs in nature, possible extension mode of loading should not be dismissed.

Effect of Particle Angularity

It was pointed out in Section 4.1 that Ottawa sand can not develop strain softening response once it is densified to an initial relative density above 45% for the range of consolidation stresses considered. However, tailings sand could develop strain softening response even though the final relative density was over 100%. From the consolidation characteristics (Fig. 3.8) it may be noted that angular tailings sand shows much larger compressibility under high consolidation stress. During shear deformation angular sand shows stronger dilative tendency under low consolidation stresses but stronger contractive tendency under higher consolidation stresses. This increased contractive tendency in shear and higher compressibility during consolidation to high consolidation stress are believed to be due to the breakage of sharp edges of angular particle (Vaid et al., 1983). It was found that the fines content (material passing No. 100 sieve) of angular sand after shearing increases with increasing consolidation stresses. Fig. 4.15 shows the comparative grain size distribution curves of a fresh untested sample and a sample after undrained shearing. An increase in fines content from less than 1% to about 6.5% may be observed when the confining pressure of 25.0 kgf/cm^2

Tailings Sand
Test AC - U - #6
$\sigma_{3c}' = 25.0$ kgf/cm^2
$K_c = 2.0$

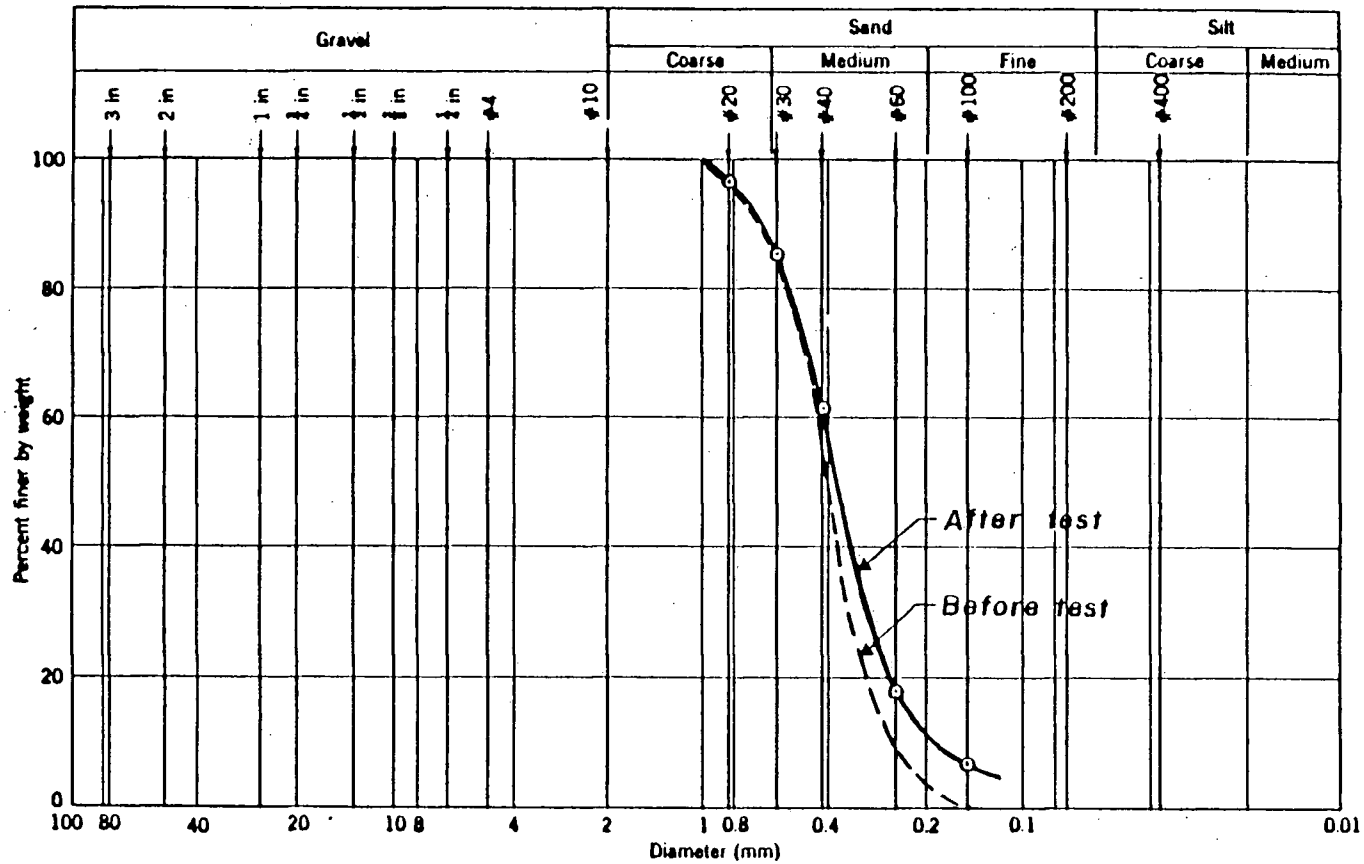

Fig. 4.15 Grain size distribution of tailings sand before and after test.

(2450 kPa) and K_c ratio of 2.0 were used in undrained shear. From the grain size distribution, it appears there was no major particle crushing. This may also be seen from the microphotographs of tailings sand samples before and after shear testing (Fig. 4.16). Very large amount of fines may be seen in the sample after testing, whereas there is hardly any particle with this size in the fresh sample. For Ottawa sand, on the other hand, no indication of particle breakage could be observed for the level of consolidation stresses considered. Therefore, it is conceivable that strain softening response in sand of rounded particles is related to initial loose structure. Although consolidation of initially loose sample to high stresses can result in high relative density, strain softening response can still develop due to the initial loose structure, which may be mostly preserved during consolidation. This seems to be true for other sands with rounded or subrounded particles, such as banding sand used in Castro's (Castro, 1969; Castro et al., 1982) studies. In such sands, liquefaction can develop only in states of low relative density. Thus, for sand with rounded particles, initial relative density provides a good single parameter defining its initial state for a prediction of its anticipated undrained response as long as no particle breakage occurs. However, if the consolidation stresses are high enough to cause particle breakage, it is believed that the behaviour of rounded sand would be similar to that of the angular sand, due to the added potential compressibility due to particle breakage.

It may also be noted in Fig. 4.12 and 4.13 that the steady state line for rounded Ottawa sand is much flatter than that of the angular tailings sand. This feature is another characteristic manifestation of the differences in particle shapes. Similar variations in slope of

Screened Brenda Mine Tailings

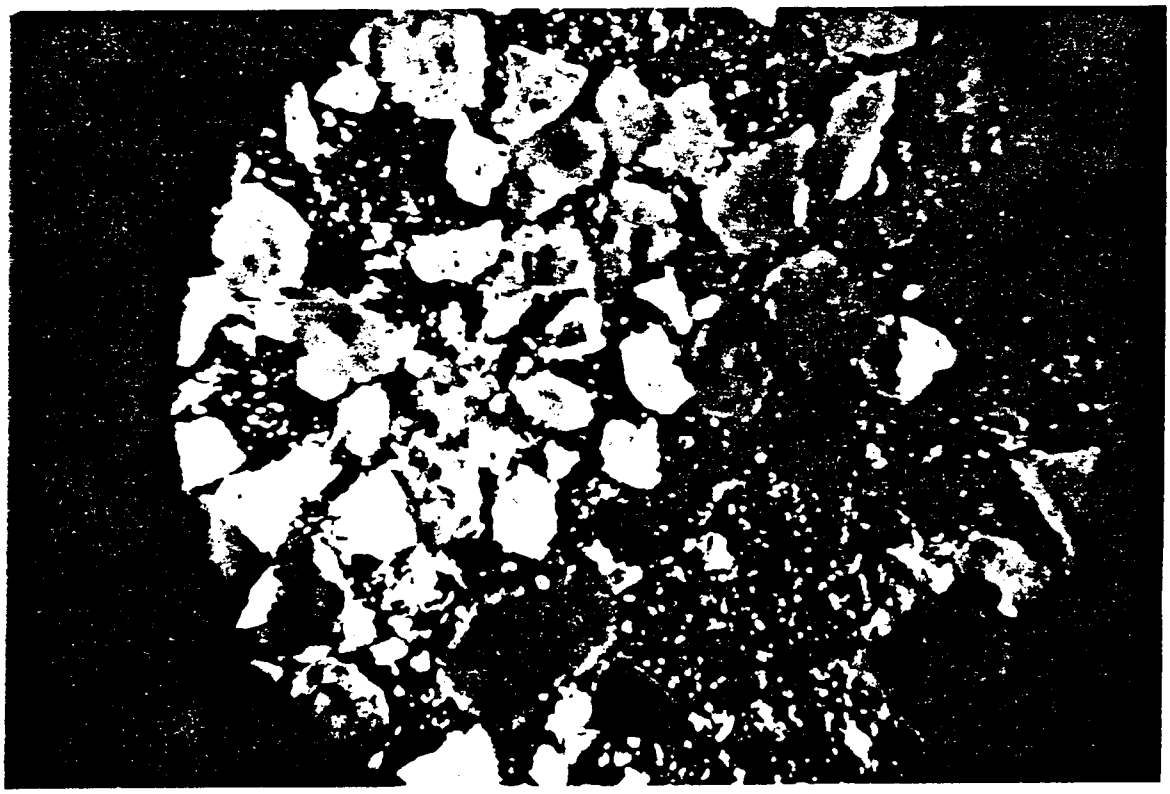

After Test (AC-U-#6)

Fig. 4.16 Microphotograph of tailings sand before and after test.

steady state line with changing particle angularity have been reported by Castro et al. (1982). One important significance associated with the flat steady state line is the extreme sensitivity to the magnitude of steady state strength with very small changes in void ratio. This aspect of sand behaviour will be discussed further in later sections.

While the discussions presented above are valid for hard, clean, uniform, medium quartz sand, particle characteristics which increases the compressibility of sand, such as friable particle or presence of fines, will increase the contractive tendency. Sand with such particle characteristics will have a steeper steady state line which is a direct reflection of its compressibility.

4.2.2 Characteristics of Strain Softening and Strain Hardening Responses

It has been shown in Section 4.2.1 that for any void ratio e_c there exists a critical consolidation stress $(\sigma'_{1c})_{crit}$ for tailings sand. Sand consolidated to initial states with void ratio e_c and consolidation stress σ'_{1c} equal to or greater than $(\sigma'_{1c})_{crit}$ develops liquefaction. The stress conditions at PT state then fit the unique steady state line when the sample is loaded monotonically. Otherwise only strain hardening response or slight strain softening response can be developed. This critical consolidation stress separates the initial sample state into regions which will develop liquefaction and other type of response. Typical undrained monotonic loading responses for samples consolidated to the same e_c above and below the $(\sigma'_{1c})_{crit}$ = constant line are shown schematically in Fig. 4.17.

For case A, i.e., the initial stress state ($\sigma'_{1c} = K_c \times \sigma'_{3c}$) lying on or to the right of $(\sigma'_{1c})_{crit}$ = const. line, the sand always develops type 2 response (limited liquefaction) or type 1 response (true liquefaction) in the extreme case. Many cases which fit this type of response have been shown by typical test results in Section 4.1. Initial stress state

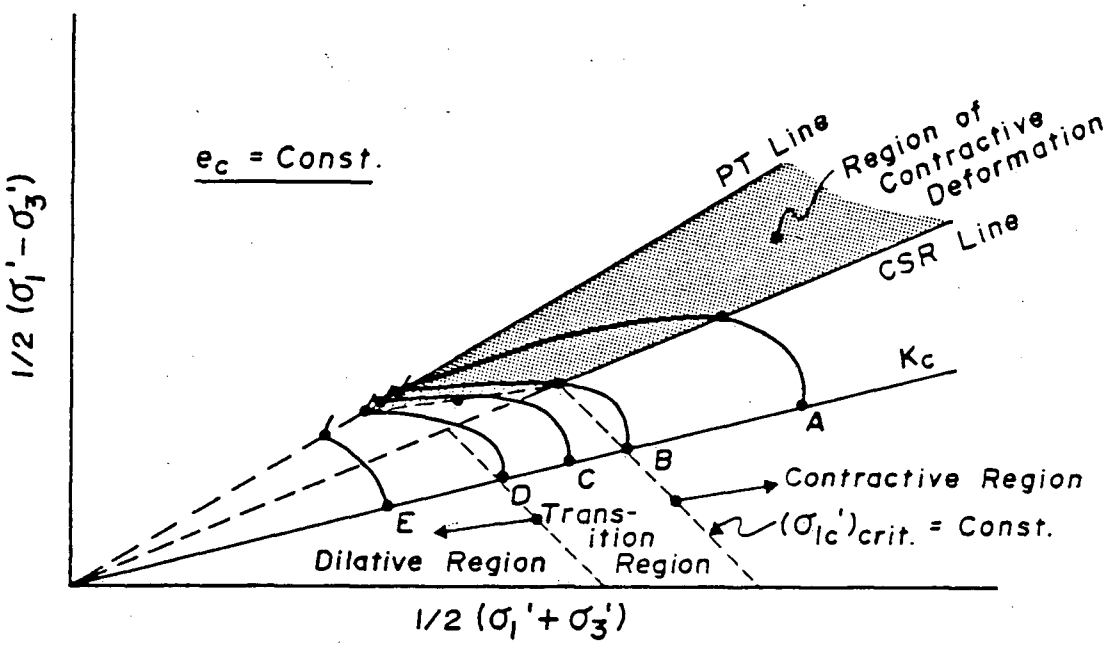

Fig. 4.17 Undrained monotonic loading response under various confining pressures.

represented by Case B is the limiting case for this category. The effective stress states at peak strength and PT state (same as steady state in this case) for all samples which show this type of response for tailings sand are shown in Fig. 4.18. It may be seen that regardless of the void ratio, confining pressure and consolidation stress ratio, the peak stress states or the stress states at which strain softening is initiated leading to steady state deformation lie essentially on a constant effective stress ratio line. This characteristic has also been reported by Vaid and Chern (1983[2]) based on results obtained for Ottawa sand under cyclic loading condition. This stress ratio will be called the critical effective stress ratio (CSR) in this thesis. The mobilized friction angle ϕ' at CSR (= 2.54) is about 25.1° for tailings sand. Fig. 4.18 also shows the effective stress conditions at PT states for tailings sand with initial states which give rise to liquefaction response. It may be noted that the PT states also lie on a constant effective stress ratio line, regardless of the void ratio, confining stress and K_c ratio of the sand. The mobilized ϕ' angle is about 36.5° for this tailings sand. This implies that the steady state line is a space curve lying on the phase transformation plane.

If the initial stress state lies to the left of $(\sigma'_{lc})_{crit}$ = const. (case C in Fig. 4.17), the undrained response starts to move into a transition region, which is characterized by the development of slight strain softening. The effective stress state at peak strength for such initial states was found to move closer and closer to the PT line as the degree of strain softening became less and less. Case D is the limiting case for this type of response which is typical of the type 4 stress-strain curve. The dotted line joining CSR state for Case B and PT state for case D (Fig. 4.17) forms the locus of peak stress state in this transition region at this particular e_c. The PT state for this type of response was found to have the same effective stress ratio as that for

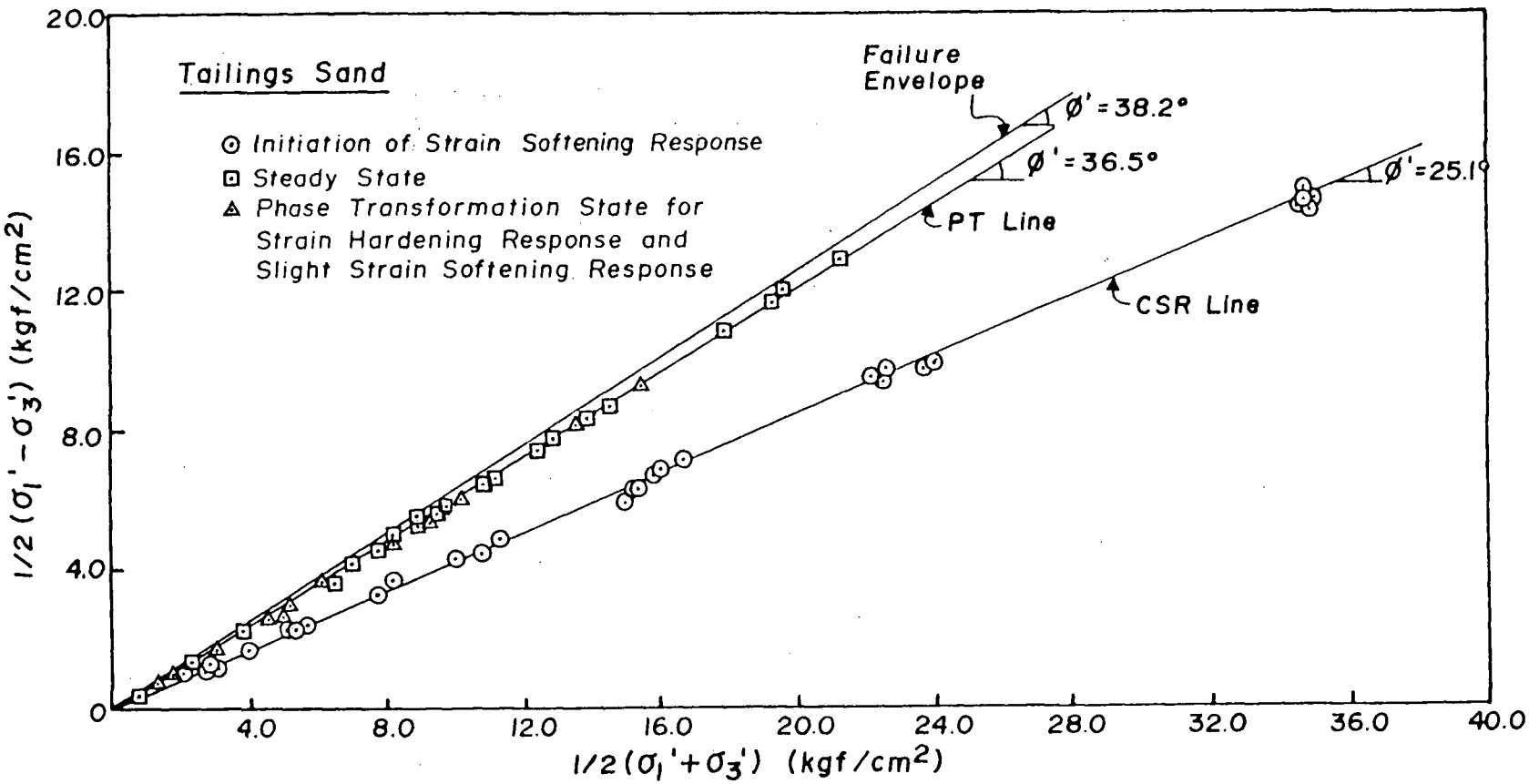

Fig. 4.18 Effective stress conditions at the initiation of strain softening response and start of dilation of tailings sand under undrained compression loading.

initial states which developed steady state deformation, regardless of the void ratio, confining pressure and K_c ratio. The actual results shown in Fig. 4.18 also include data points for test results characteristic of transitional response.

When the initial stress state lies further to the left of $(\sigma'_{1c})_{crit}$ = const. line (case E in Fig. 4.17), the sand develops strain hardening response with no peak strength developed. The PT state for this type of response, which corresponds to the maximum pore pressure condition, was also found to have the same effective stress ratio at PT states for states which developed liquefaction or limited liquefaction of the transition region type. The test results shown in Fig. 4.18 also incorporate results of samples which exhibited strain hardening response.

From the illustration in Fig. 4.17, the initial stress state for the chosen e_c to the left of $(\sigma'_{1c})_{crit}$ = const. line may be seen to constitute essentially a dilative region. Sand with initial stress states in this region will develop strain hardening or slight strain softening only. Region to the right of $(\sigma'_{1c})_{crit}$ = const. line including states on this line may be regarded as the contractive region. All initial sample states in this region will develop steady state deformation. The shaded area in Fig. 4.17 where actual strain softening occurs during shearing deformation may be called the region of contractive deformation. Before the stress state reaches the CSR, relatively small deformation is developed (0.2 to 0.7% for the sands tested) although considerable pore pressure can be induced and the sample is essentially stable. However, once the stress state reaches the CSR, preferred slippage between a majority of particle contacts starts to occur. Due to the initial loose arrangement of particles or breakage at sharp edges of particle in

angular sand under high confining pressure, the particles tend to rearrange themselves into a more compact form. High pore pressure then develops as a result of constant volume condition imposed with accompanying large deformation. This process continues until the effective confining stress becomes low enough to cause a tendency to expand in volume with further shearing deformation which occurs at the PT state.

All discussion presented above are based on test results with initial K_c ratio less than CSR only. It should be noted that the CSR simply represents the starting of major rearrangement of particles during shear. Samples consolidated to K_c values > CSR, i.e., to a state within the shaded area (Fig. 4.17) would be potentially unstable and strain softening response could be induced by slight disturbance. This may be seen from the results of the test shown in Fig. 4.19. The tailings sample was consolidated to σ'_{3c} of 8.0 kgf/cm^2 (784 kPa) and K_c ratio of about 3.0 which was greater than CSR. A slight increase in shear stress caused severe reduction in shear resistance and the sand deformed in a manner similar to the characteristic of true liquefaction. Thus, the sand consolidated in this shaded region of Fig. 4.17, although stable under drained conditions, is potentially unstable under undrained conditions. Such a region of contractive deformation exists for contractive sand only. Luong (1980) designated the region below the CT line (same as PT line) as the contractive domain and the region beyond the CT line as the dilative domain in the sense that positive pore pressure will be induced in contractive domain and dilation (reduction in pore pressure) will start beyond the CT line. This is consistent with the term dilative region used here, since the pore pressure reduction will not occur until the PT line is reached even if the sand develops strain

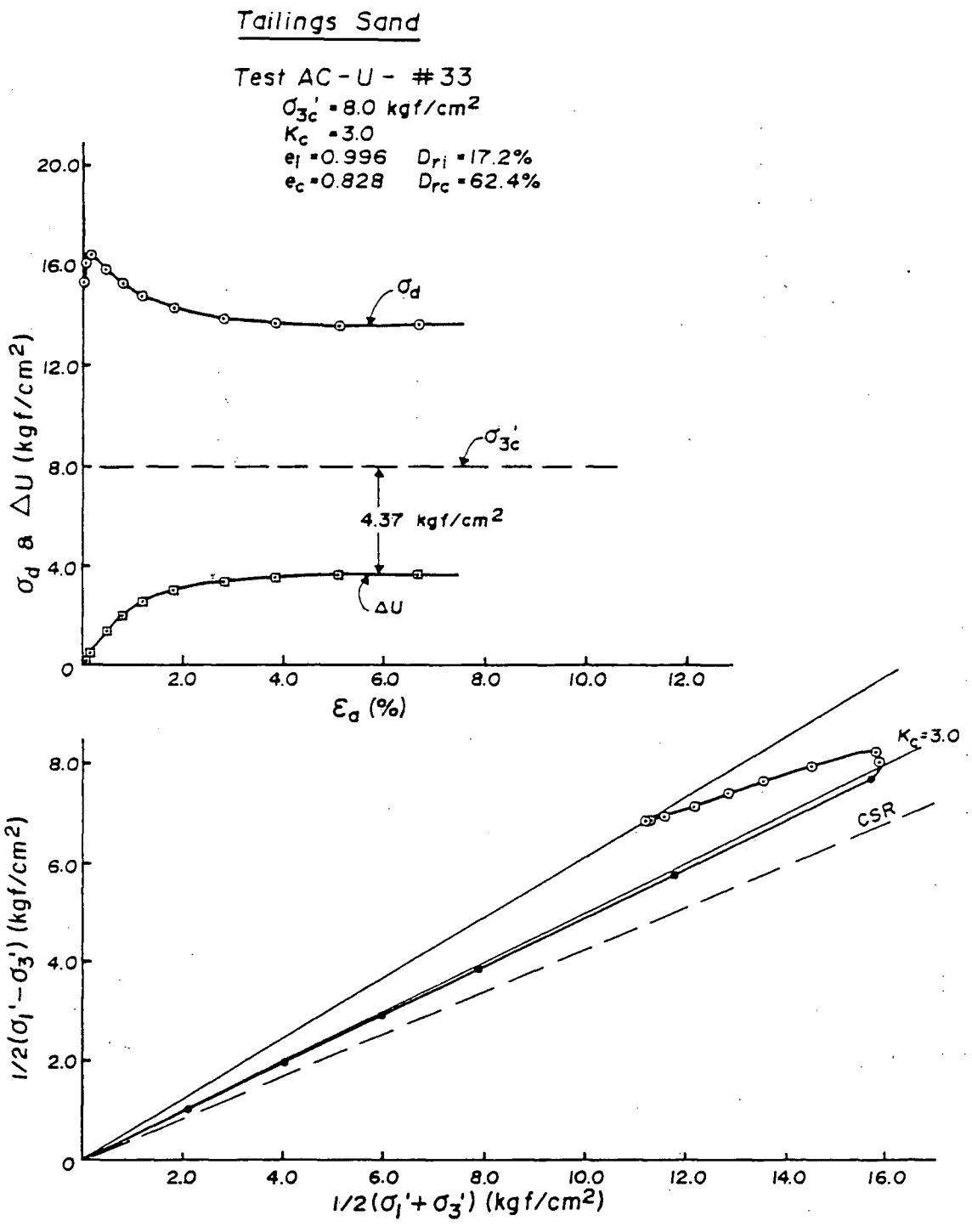

Fig. 4.19 Undrained monotonic loading behaviour of tailings sand consolidated into the region of contractive deformation.

hardening response. However, the terms contractive region and dilative region used herein refer to the type of response, i.e., strain softening or strain hardening expected in those regions of initial state of sand prior to undrained shear.

For Ottawa sand, test results similar to Fig. 4.18 for tailings sand representing the stress states at peak strength and steady state for those states that developed liquefaction are shown in Fig. 4.20. Similar to the behaviour of tailings sand, two constant effective stress ratio lines, one corresponding to CSR and the other PT were obtained, irrespective of the void ratio, confining pressure and K_c ratio of the sample. The stress state at PT state of sample that developed strain hardening or slight strain softening are also shown in Fig. 4.20. As in the case of the tailings sand, the PT state for strain hardening response may be seen to be the same as that of the strain softening response, regardless of the void ratio, confining pressure and K_c ratio of the sample. The mobilized ϕ' angles for CSR and PT states for Ottawa sand are 23.5° and 29.5° respectively.

It is interesting to note that the slopes of CSR lines for these two sands are nearly equal. The mobilized ϕ' angles are very close to the interparticle friction angle ϕ_μ of the quartz sand, which varies from 22.8° to 27° according to Horn and Deere (1962). It appears that preferred sliding at a majority of contacts would occur when the effective stress ratio reaches the value corresponding to ϕ_μ and thus marks the initiation of strain softening response.

Similar to the behaviour in compression, two distinct effective stress ratio lines corresponding to CSR and PT were found to exist in extension mode for both sands, as is clear from the results shown in

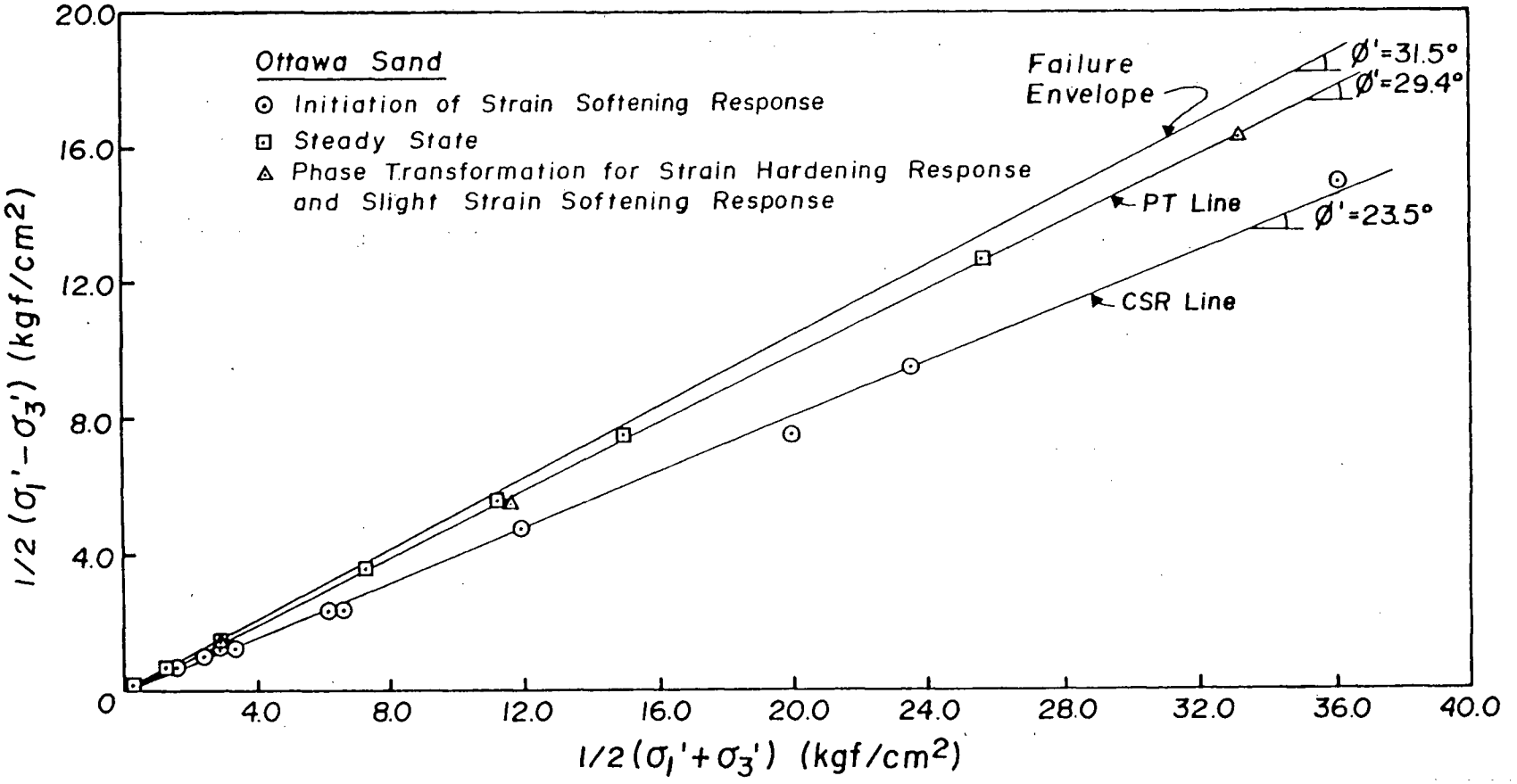

Fig. 4.20 Effective stress conditions at the initiation of strain softening response and start of dilation of Ottawa sand under undrained compression loading.

Figs. 4.21 and 4.22. For tailings sand, it appears that CSR may depend somewhat on the initial relative density of the sample, with mobilized ϕ' angle varying from 18° to 23° from the limited data obtained. Higher CSR appears to be associated with higher initial relative densities. For Ottawa sand, the mobilized ϕ' angle at CSR is about 15° (Fig. 4.22). The difference in CSR in compression and extension for each sand may be due to inherent anisotropy in pluviated sand. The implication of different CSR in compression and extension on the cyclic loading behaviour will be discussed in the next chapter. On the other hand, the PT line in extension has the same slope as that in compression for both sands (Figs. 4.21 and 4.22). Since PT state is a stress state after relatively large deformation, it is conceivable that inherent anisotropy may be erased as a consequence and hence the PT line will be the same in both deformation modes.

4.3 Undrained Strength Under Monotonic Loading

It has been shown in the previous sections that a sand can develop either liquefaction or strain hardening response under monotonic loading depending on its state (e_c, K_c, σ'_{3c}) after consolidation. For liquefaction the major concern is the strength loss and the associated excessive deformation, whereas for strain hardening response concern usually centres on limiting deformation to an acceptable level. Therefore, it would be useful to have strength estimation for these two cases in order to avoid strength loss and excessive deformation in contractive sand and excessive deformation in dilative sand.

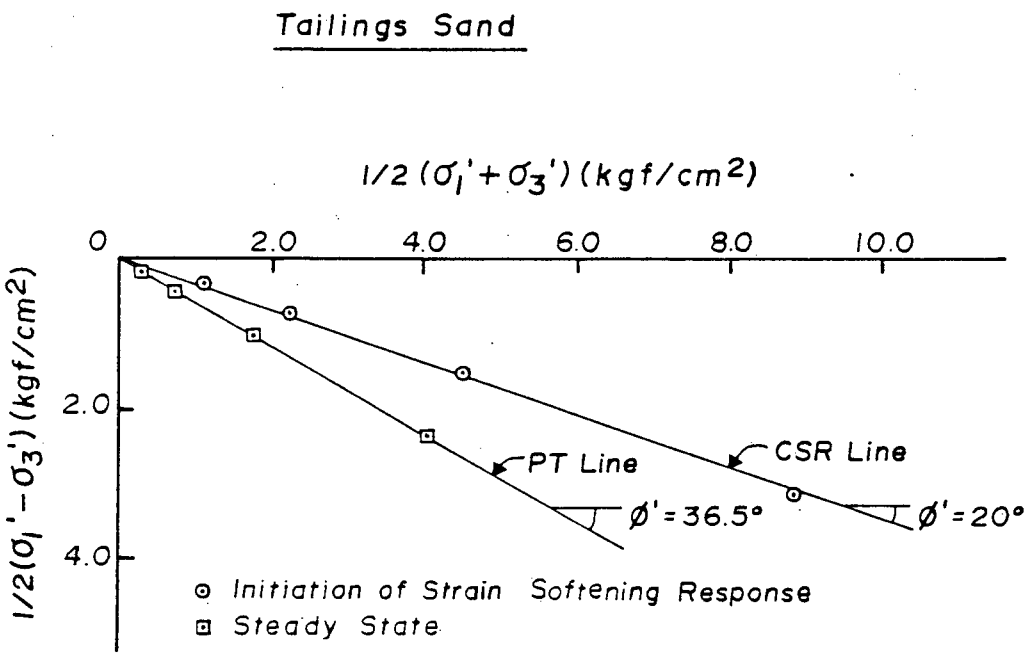

Fig. 4.21 Effective stress conditions at the initiation of strain softening response and start of dilation of tailings sand under undrained extension loading.

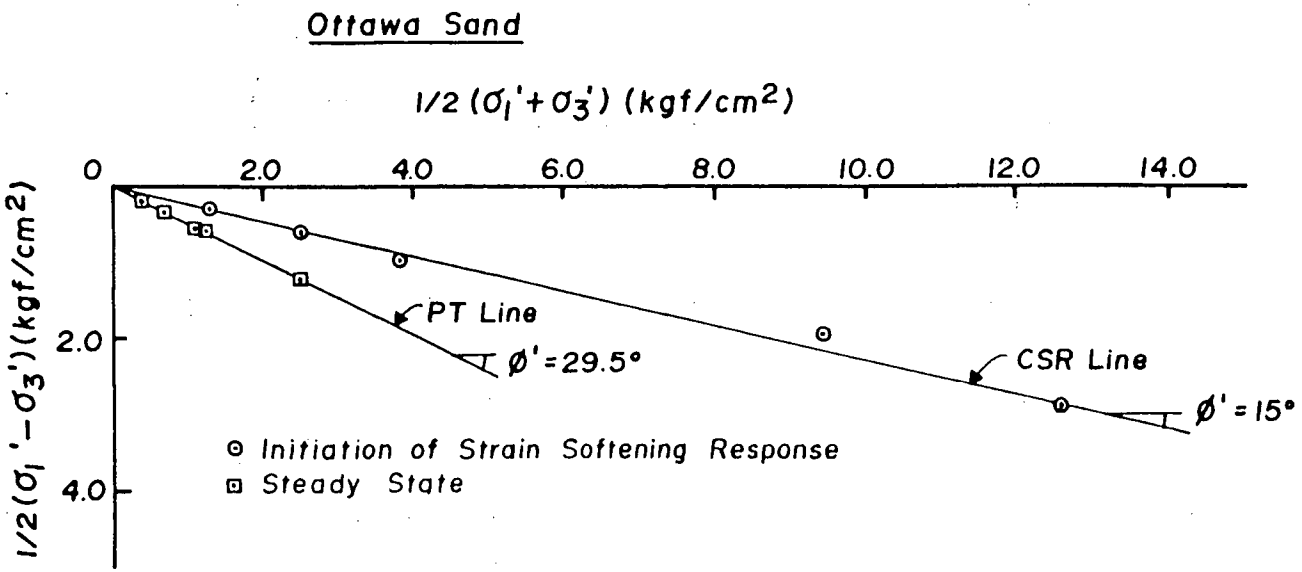

Fig. 4.22 Effective stress conditions at the initiation of strain softening response and start of dilation of Ottawa sand under undrained extension loading.

4.3.1 Peak Strength for States Which Developed Liquefaction

Tailings Sand

The minor effective confining stress at CSR state, σ'_{3p}, is plotted against minor consolidation stress, σ'_{3c}, for samples of tailings sand that developed liquefaction leading to steady state deformation in Fig. 4.23. It may be noted that the test results of samples with the same K_c ratio lie on a straight line passing through the origin, regardless of the void ratio of the sample. This implies similarity in effective stress path until the CSR is reached for samples with the same K_c ratio. Thus, the effective confining stress at CSR state is a function of initial consolidation stress σ'_{3c} and consolidation stress ratio K_c, and may be expressed as

$$\sigma'_{3p} = f(K_c)\ \sigma'_{3c} \qquad (4.1)$$

Plotting the slope of σ'_{3p} vs σ'_{3c} in Fig. 4.23 against K_c ratio, the function $f(K_c)$ can be obtained. Such a plot is shown in Fig. 4.24, which indicates that $f(K_c)$ may be approximated as a linear function of K_c as follows:

$$f(K_c) = 0.412\ K_c - 0.044 \qquad (4.2)$$

It is interesting to note that extension of the relationship of K_c vs $\sigma'_{3p}/\sigma'_{3c}$ to $\sigma'_{3p}/\sigma'_{3c} = 1.0$, i.e., the initial consolidation stress condition for which no excess pore pressure will be induced during undrained shear at the instant of initiation of strain softening corresponds to K_c ratio approximately equal to CSR for the sand (Fig. 4.24). This implies that strain softening response is imminent, if a sample is consolidated at CSR state prior to undrained loading. Slight disturbance

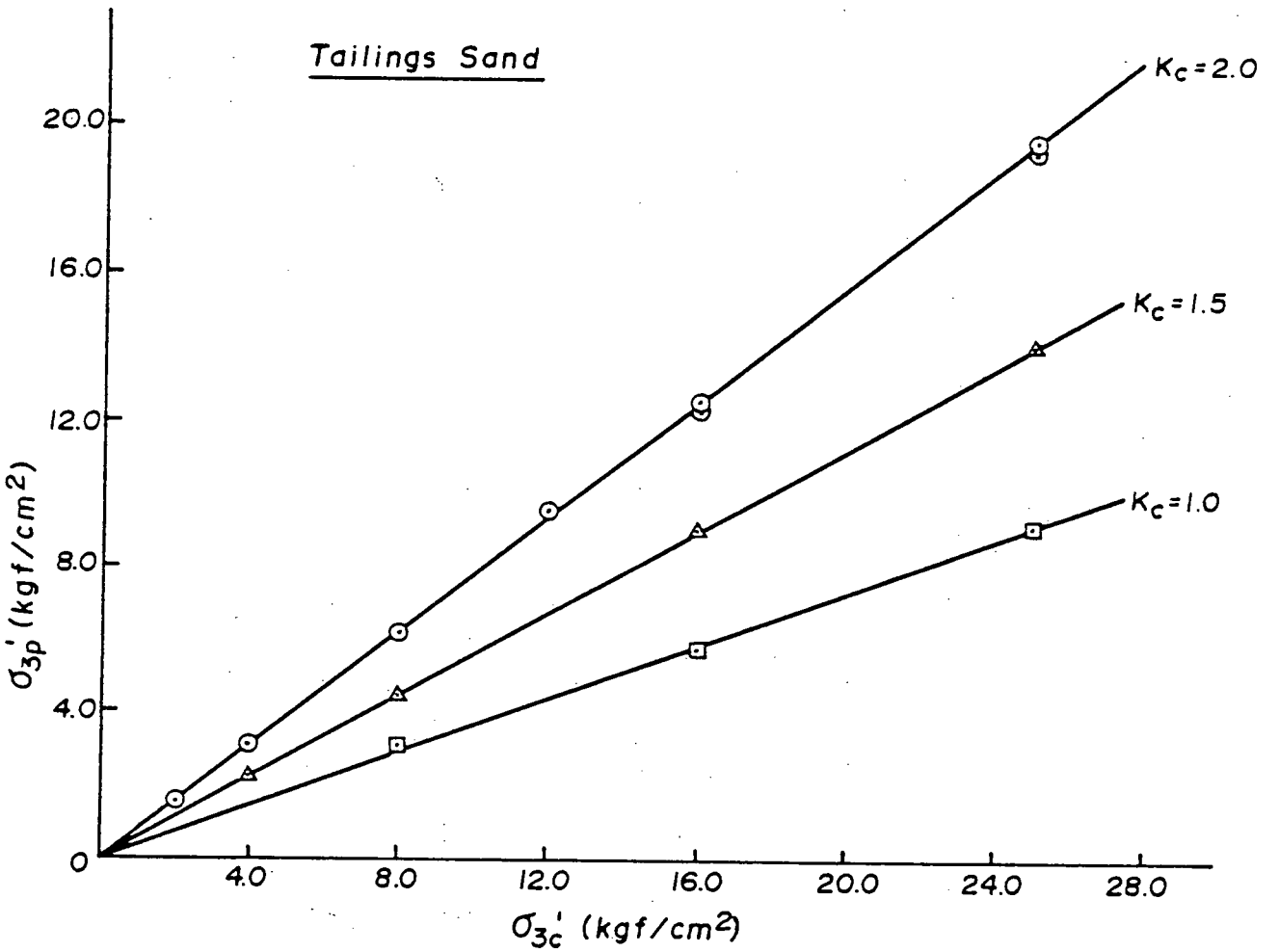

Fig. 4.23 Relationship between effective minor principal stress at CSR state and effective minor consolidation stress for tailings sand.

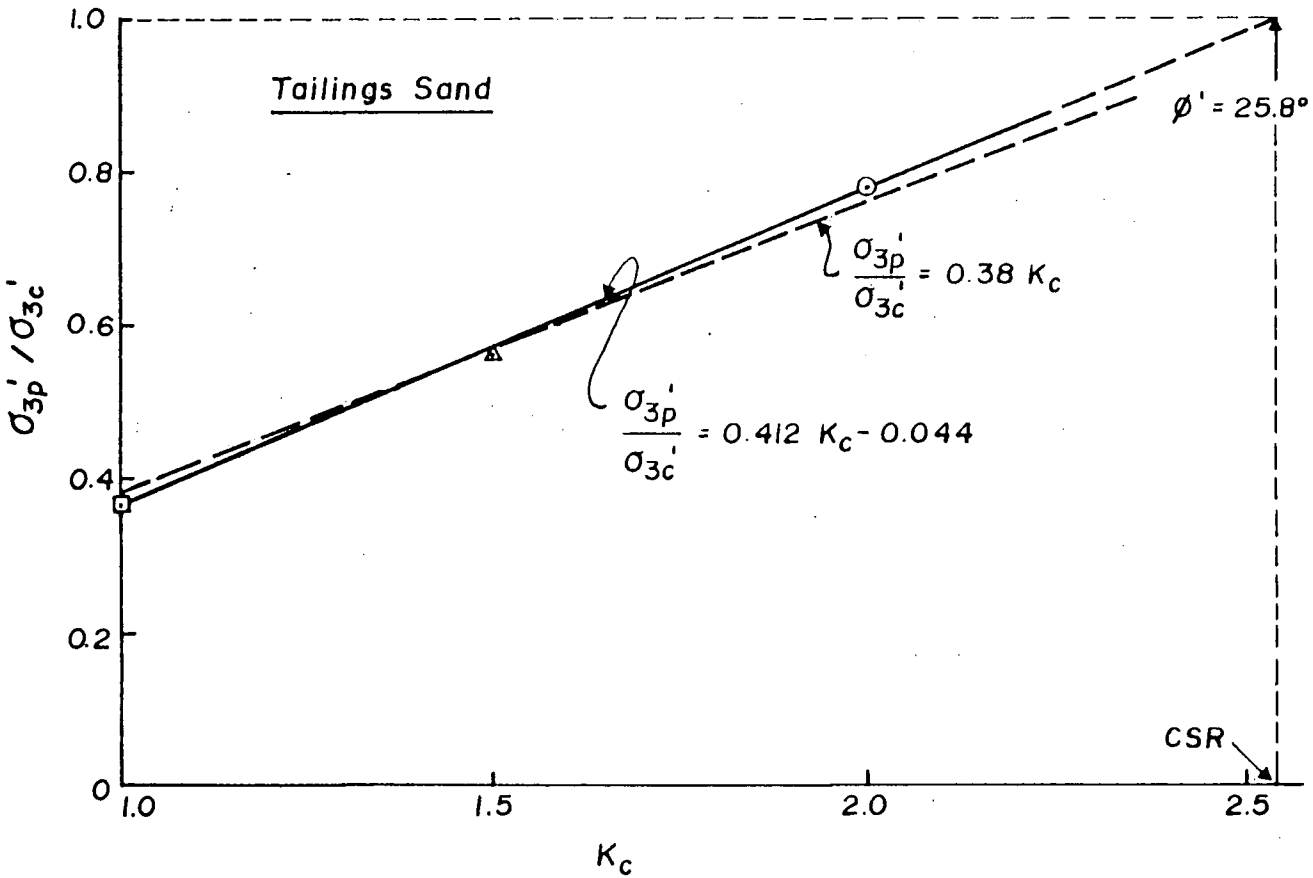

Fig. 4.24 Relationship between the ratio of effective minor principal stress at CSR state and effective minor consolidation stress vs K_c ratio for tailings sand.

could then cause the sample to develop strain softening, leading to steady state deformation. It should be emphasized that this is true for contractive sand only. This phenomenon will be discussed further in the next chapter in conjunction with spontaneous liquefaction.

It has been shown in previous sections that CSR for a given sand is a constant stress ratio, regardless of the void ratio, confining stress and K_c ratio. Therefore, the stress condition at CSR or peak strength can be expressed as

$$\sigma'_{1p} = c\ \sigma'_{3p} \tag{4.3}$$

where c is the CSR, which is a constant for the given sand (c ≃ 2.54 for tailings sand).

Substituting Eqs. 4.1 and 4.2 into Eq. 4.3, the peak shear strength, $S_{up} = 1/2\ (\sigma'_{1p} - \sigma'_{3p})$, may be obtained as follows:

$$S_{up} = \frac{1}{2}\ (c-1)\ \sigma'_{3p} \tag{4.4a}$$

or

$$S_{up} = \frac{1}{2}\ (c-1)\ (0.412\ K_c - 0.044)\ \sigma'_{3c} \tag{4.4b}$$

Hence the peak shear strength may be obtained as a function of initial stress state, σ'_{3c} and K_c. It was further noted that this function $f(K_c)$ in Eq. 4.2 may be approximated by

$$f(K_c) = 0.380\ K_c \tag{4.5}$$

with error less than ±3.0%. This line (Eq. 4.5) is the dashed line in Fig. 4.24. Use of Eq. 4.5 instead of Eq. 4.2 in Eq. 4.4b yields

$$S_{up} = \frac{1}{2} (c-1)\ 0.38\ K_c\ \sigma'_{3c}$$

$$= 0.19\ (c-1)\ \sigma'_{1c} \qquad (4.4c)$$

Eq. 4.4c implies that the peak strength which occurs at CSR is a function of major consolidation stress σ'_{1c} only. In other words, the peak stress condition at CSR state would be the same regardless of the K_c ratio, if samples were consolidated to the same σ'_{1c} but with different K_c and σ'_{3c}.

For a clearer illustration of the above conclusions, results of three sets of tailings sand samples each set consolidated to identical σ'_{1c} but samples within the set having different combinations of σ'_{3c} and K_c are shown in Fig. 4.25. It may be noted that, as postulated, S_{up} is a function of σ'_{1c} only at all three levels of σ'_{1c} considered. Thus, the undrained behaviour is mainly a function of σ'_{1c}, which is the product of K_c and σ'_{3c}. This may also be noted from earlier discussion in Section 4.2. Samples starting with the same e_i will result in the same e_c and the same PT state if the consolidation stresses σ'_{1c} are the same. It has now been shown further here that the peak stress state will also be the same provided the samples result in strain softening response, leading to steady state deformation.

Since for a given e_i the void ratio e_c after consolidation is a function of σ'_{1c} only, regardless of the K_c ratio, the peak shear strength in Eq. 4.4c can be expressed as a function of e_c instead of σ'_{1c}. The calculated peak shear strengths for five e_i as a function of σ'_{1c} and hence e_c are shown by the peak strength lines in Fig. 4.26. The actual peak strength test data are shown by the data points in the figure. It may be noted that the prediction of peak strength by using Eq. 4.4c is

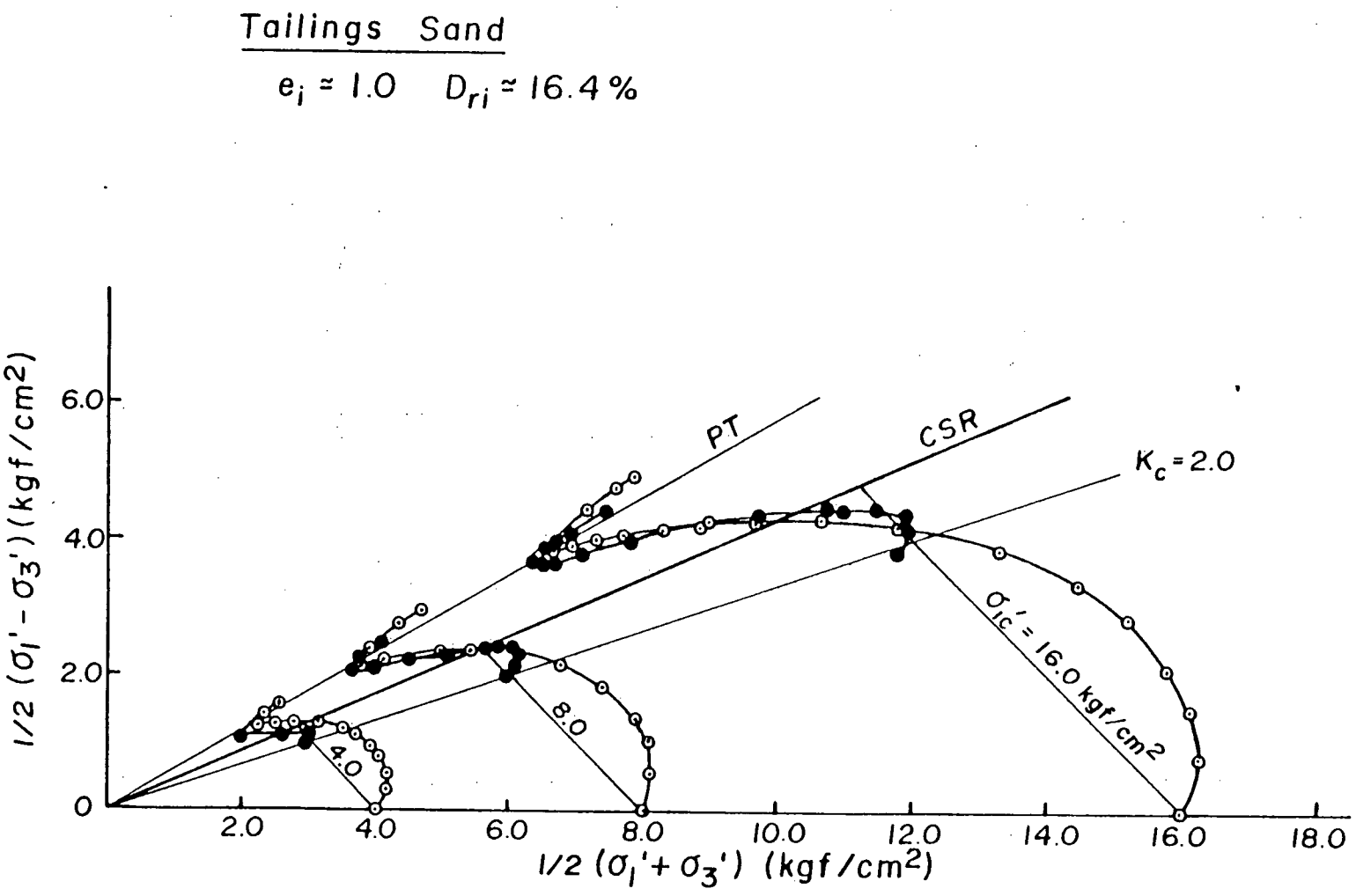

Fig. 4.25 Comparison of undrained monotonic loading response of tailings sand under the same major consolidation stress but with different K_c ratios.

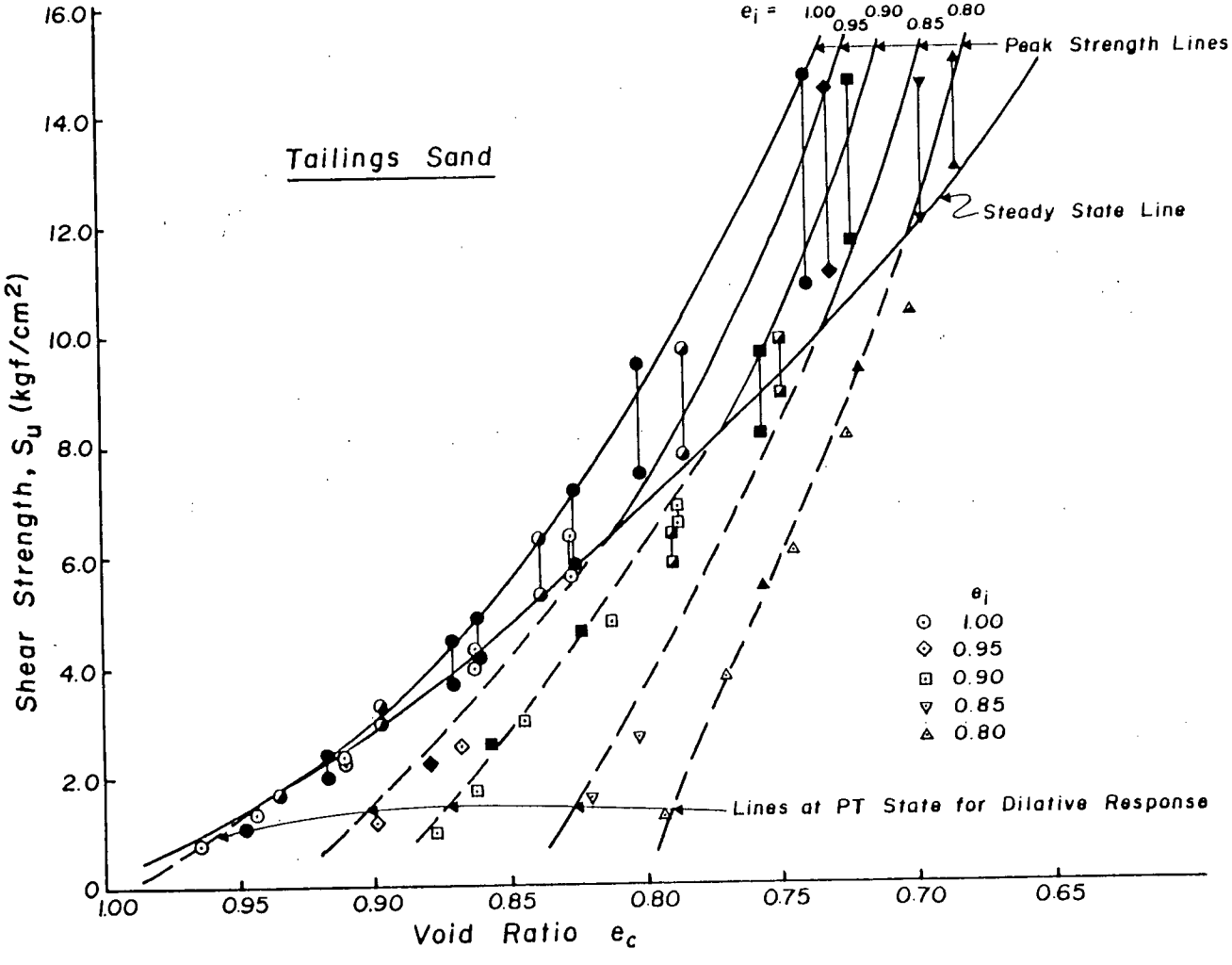

Fig. 4.26 Undrained strengths of tailings sand under monotonic compression loading.

very good for initially loose sample. For initially dense samples, strain softening response leading to steady state deformation could develop only under high consolidation stress. Very little test data were obtained in this range of high consolidation stresses. The paired data points connected by vertical lines represent the peak strength (upper one) and steady state shear strength (lower one), which will be discussed in the next section. The PT shear strength lines for strain hardening response lying below the steady state line will also be discussed later.

Ottawa Sand

For Ottawa sand, the relationship between σ'_{3p} and σ'_{3c} as a function of K_c ratio is shown in Fig. 4.27. Relationship similar to that for the tailings sand may be observed. Much less pore pressure is induced until CSR state for samples with high K_c ratio in comparison to low K_c ratio. This is illustrated in Fig. 4.28 in the plot of $\sigma'_{3p}/\sigma'_{3c}$ versus K_c value. It is again interesting to note that by assuming a linear relationship between $\sigma'_{3p}/\sigma'_{3c}$ and K_c ratio, the K_c ratio corresponding to no pore pressure generation until CSR state was found to be approximately equal to CSR. This also implies that the strain softening response leading to steady state deformation is imminent when the sand is consolidated to a state close to CSR. This illustrates the similarity in undrained behaviour of both sands if liquefaction is developed. However, due to very small range of e_c over which liquefaction can be induced, no attempt was made to relate peak strength to σ'_{1c} (or e_c) and hence no comparison made of predicted and observed S_{up} as a function of e_c, similar to Fig. 4.26.

It may be pointed out that the peak strength will be used later to

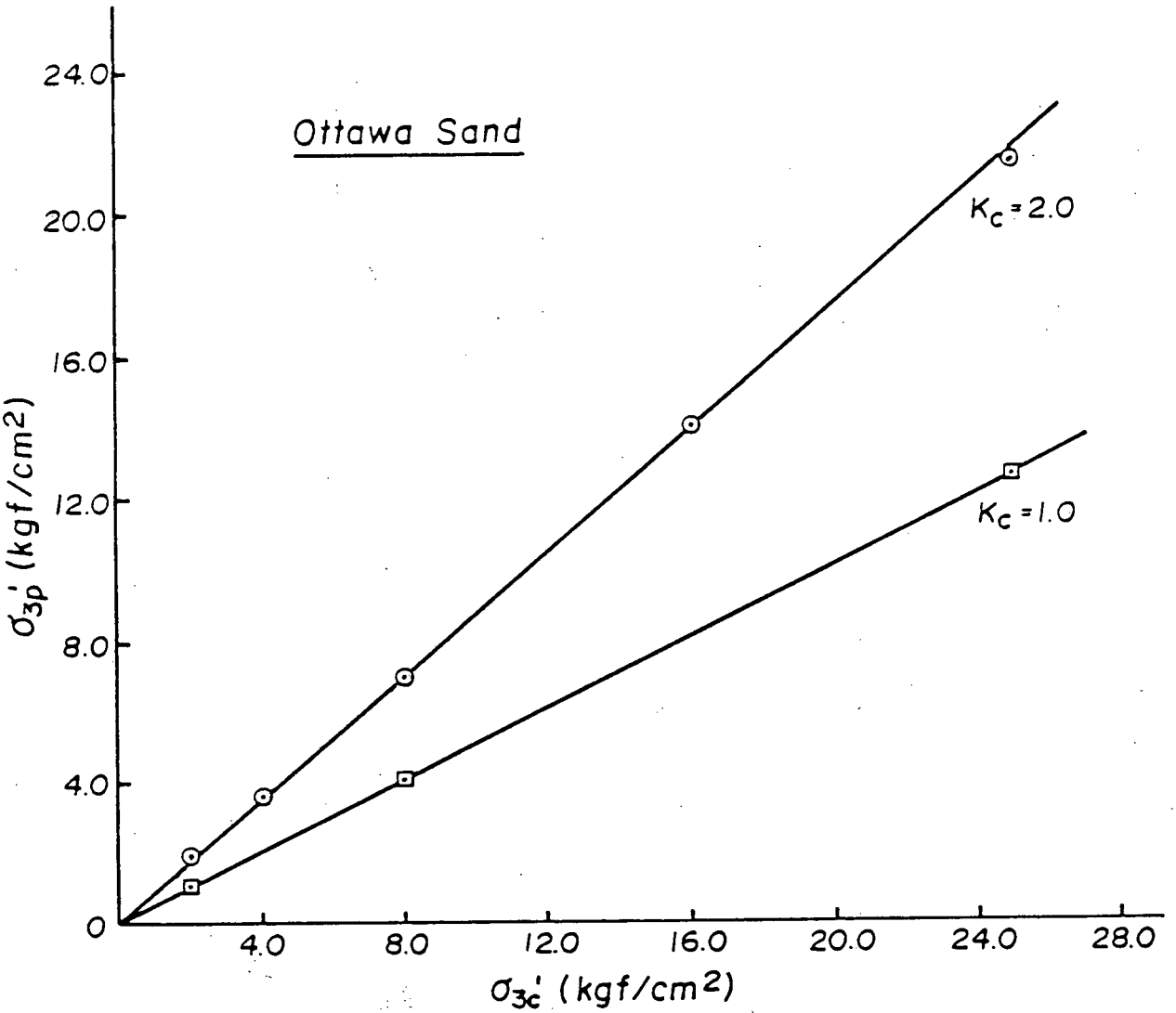

Fig. 4.27 Relationship between effective minor principal stress at CSR state and effective minor consolidation stress for Ottawa sand.

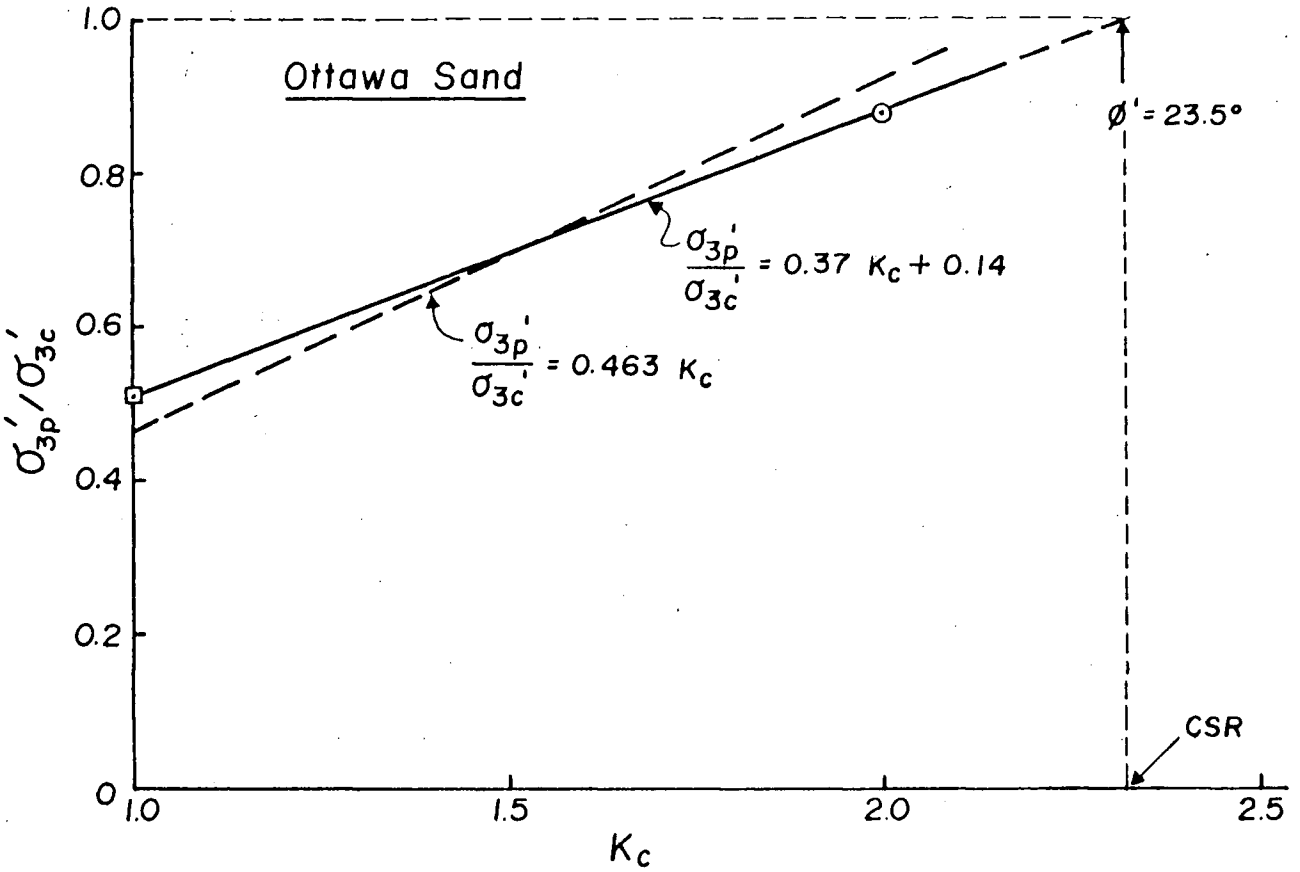

Fig. 4.28 Relationship between the ratio of effective minor principal stress at CSR state and effective minor consolidation stress vs K_c ratio for Ottawa sand.

construct the CSR plane in 3-D effective stress state diagram for a comprehensive illustration of the undrained behaviour of saturated sand only. The effective stress condition at this state may offer an explanation as to the influence of static shear or K_c ratio on the undrained response. Peak strength should not be used as a design parameter for sand which undergoes liquefaction since the sample is not stable at this state.

4.3.2 Steady State Strength

It has been shown in the previous section that the PT state coincide with the unique steady state line provided the sample develops liquefaction. Moreover, the minor effective confining stress σ_3' at steady state is a function of e_c only, regardless of the initial void ratio and consolidation stress conditions. Since the effective stress state at steady state lies on the phase transformation line which is a constant stress ratio line through the origin, the steady state shear strength S_{us} can be expressed as a function of e_c only. This predicted relationship between e_c and steady state shear strength based on the unique relationship between σ_3' and e_c at steady state is shown in Fig. 4.29 together with actual test results. The predicted values may be seen to be in good agreement with observed results. Similar unique relationships between steady state shear strength or steady state confining stress and void ratio e_c have also been reported by Castro et al (1982).

Relationship between e_c and S_{us} for Ottawa sand is shown in Fig. 4.30. It may be noted that the range of void ratio in which steady state deformation can be developed for Ottawa sand is very small for the range of consolidation stresses considered. The steady state shear strength

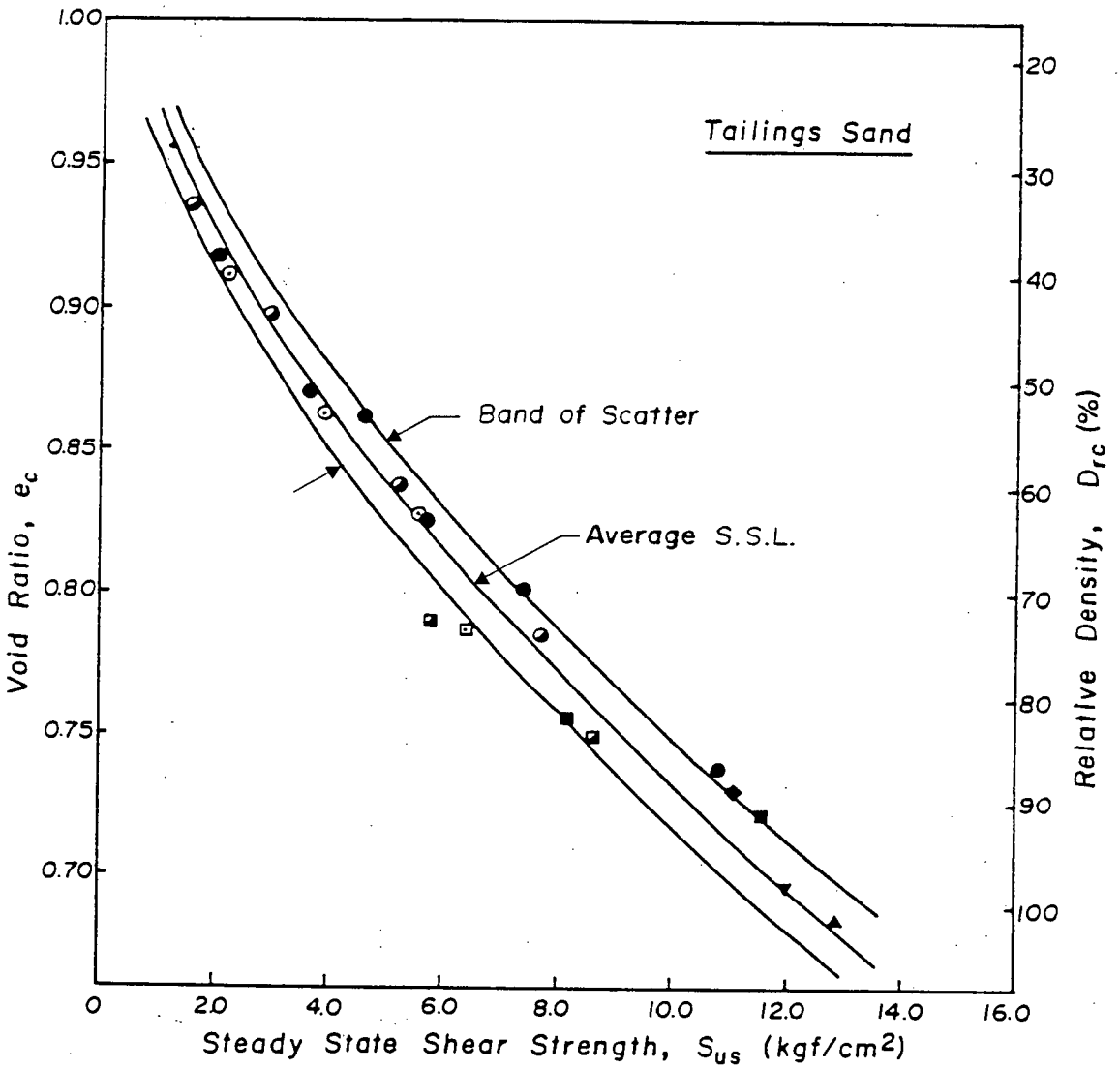

Fig. 4.29 Steady state shear strength of tailings sand.

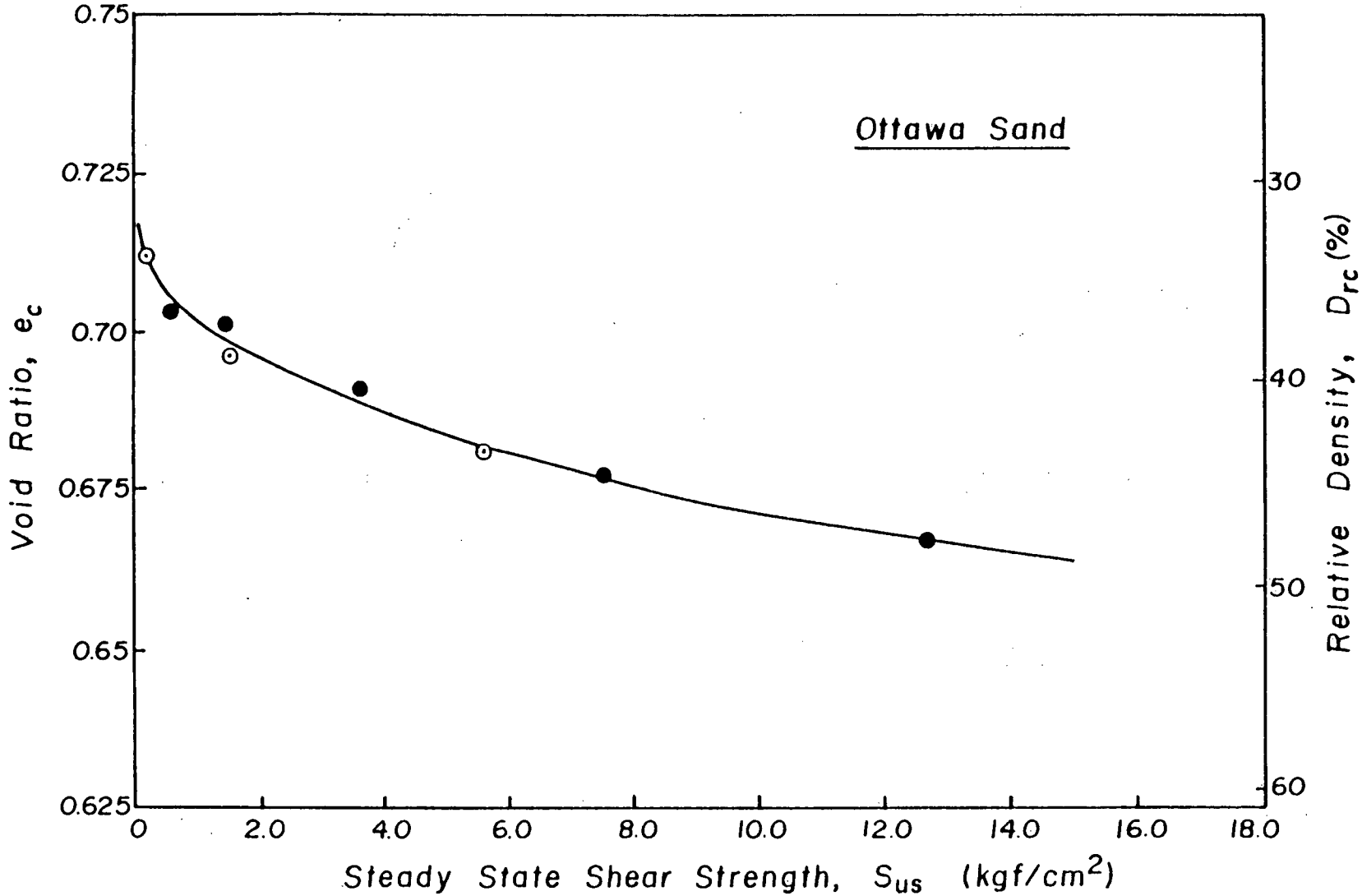

Fig. 4.30 Steady state shear strength of Ottawa sand.

increases rapidly with decreasing e_c when the relatively density is in excess of about 40%.

The steady state shear strength of sand may be regarded as the stable value of shear stress the sand can sustain. Sand subjected to a static shear stress greater than its steady state shear strength, which is substantially less than its drained shear strength, is potentially unstable under undrained conditions. Catastrophic failure could be induced if any type of undrained loading brings the stress state of sand to the CSR state. Therefore, the steady state shear strength should be used as the design parameter against liquefaction.

4.3.3 Phase Transformation Strength for Dilative Response

For dilative sand it was shown that σ_3' at PT state versus e_c form a series of curves depending on the e_i of the sand, regardless of the consolidation stress condition (Fig. 4.12). Due to a constant stress ratio at PT state, the phase transformation shear strength can be determined as a function of e_c and e_i. The predicted results based on σ_3' and effective stress ratio at phase transformation are shown by a series of lines in Fig. 4.26. All these lines lie below the steady state line. The data points correspond to actual test results. It may be noted that for fixed e_i the phase transformation shear strength increases with decreasing e_c and approaches the steady state shear strength as the sample becomes more contractive with increasing consolidation stresses. The lines for phase transformation shear strength merge into the steady state line when the consolidation stress is high enough to cause steady state deformation. It should be pointed out that these lines include test data in the transition region of sand, which results in slight strain softening and associated very small strain potential, and may be

considered to be the same category as the strain hardening region for design purposes.

From the earlier discussion of strain hardening behaviour of sand, it was noted that much flatter stress-strain curve develops after PT state (Figs. 4.3a and 4.8a,b). From the effective stress path (Fig. 4.4) it may also be noted that the phase transformation shear strength is much less than the corresponding drained shear strength. Furthermore, the phase transformation shear strength is much less than the ultimate undrained shear strength which can be mobilized only after very large deformation. Therefore, to design against large deformation for dilative sand, the phase transformation shear strength may be the more appropriate strength parameter to be used if undrained condition prevails. It should be pointed out that the strength estimation given here is good for sand that are not very dilative or are even slightly contractive which would have the most practical concern during undrained loading where limiting deformation are specified. For highly dilative sand, such as sand with high relative density under low consolidation stresses, the phase transformation shear strength is very close to the drained shear strength. The ultimate undrained shear strength will be very high and the strain involved is very small. Drained shear strength will then be appropriate for design purposes.

From Fig. 4.12, it may be noted that the series of lines which branch off the unique steady state line are very similar in shape. Therefore, relatively small number of tests have to be performed in order to establish the key aspects of undrained behaviour of sand; i.e., steady state line, branch off lines, consolidation characteristics and critical consolidation stress $(\sigma'_{1c})_{crit}$ line. The undrained strength parameters,

i.e., steady state shear strength and phase transformation shear strength can readily be obtained from e_c-σ'_3 plot and the effective stress ratio of PT line. For sand with a given e_i and consolidation stress conditions, the undrained response and its strength parameter can be determined. For sand with known e_c and consolidation stress condition, the undrained response, i.e., liquefaction or dilative response, can be determined from the $(\sigma'_{1c})_{crit}$ directly. If liquefaction occurs, the steady state shear strength can be determined from e_c directly. For dilative response, the e_i can always be interpolated from the consolidation curves (e_c-σ'_{1c}) as long as normal consolidation prevails. Knowing e_i, σ'_3 at PT state can always be interpolated from Fig. 4.12 and hence the PT shear strength estimated.

4.4 3-D Effective Stress State Diagram

Experimental evidence presented previously has indicated that sand can develop either liquefaction, slight strain softening or strain hardening response depending on its initial state (e_c, σ'_{3c}, K_c). Therefore, it would be of utmost importance to develop a method which would enable separation of the initial states into regions susceptible to liquefaction and strain hardening response, and explain the influence of initial state parameters on the occurrence of liquefaction and strain hardening response.

Since most of the studies on the undrained behaviour of sand have been performed on sands with rounded particles, it is generally believed that the relative density is the most important factor controlling the undrained response. Sand with low relative density may be considered to

be susceptible to liquefaction without any reference as to its consolidation stress conditions. Based on the results of present study it has been shown in Section 4.1 that this may be a sufficient guideline for sand with rounded particles but may be completely inadequate for sand with angular particles. Moreover, the use of relative density alone can not explain the influence of confining pressure and static shear on the occurrence of liquefaction.

Castro (1969, 1975) proposed the concept of steady state line in 2-D e_c-σ'_3 space. The concept of steady state deformation was used to explain the phenomenon of liquefaction. It was proposed that the initial state of the sample has to be well above and to the right of the steady state line in order to have the possibility of liquefaction occurring. Attention was focussed only on the soil behaviour during steady state. Specifically, no quantitative attempt was made to assess whether liquefaction could occur for a known initial state (e_c, σ'_{3c}, K_c). Also no rational explanation as to the influence of static shear on the occurrence of liquefaction was offered.

A comprehensive understanding of the undrained behaviour of sand can be obtained only by looking at the undrained behaviour over a whole spectrum of responses from strain softening to strain hardening under various consolidation stress conditions on different types of sand. Moreover, not only the sample state during steady state deformation but also at the initiation of liquefaction has to be examined in order to understand the influence of factors such as void ratio, confining stress and static shear, on the occurrence of liquefaction. This requires a 3-D effective stress representation of the most important stages, i.e., initial state (e_c, σ'_{3c}, K_c) and initiation of liquefaction and PT state

during undrained response. Although the type of undrained response can be predicted by using the e_c-$(\sigma_{1c})_{crit}$ relationship and the initial sample state in a 2-D plot, as described in Section 4.2, it can not explain the role of static shear on the occurrence of liquefaction. It will be shown further in the next chapter that a 2-D plot is insufficient to predict the occurrence of liquefaction under cyclic loading, even though it suffices to predict the occurrence of liquefaction under monotonic loading. Therefore, it requires a 3-D effective stress representation of state at CSR, steady state for strain softening response and phase transformation state for strain hardening response. This is shown schematically in Fig. 4.31, and will be called 3-D effective stress state diagram.

The state of sand is defined by a point in 3-D space given by void ratio after consolidation e_c, $p' = 1/2\ (\sigma_1' + \sigma_3')$ and $q = 1/2\ (\sigma_1' - \sigma_3')$. Other combination, such as e_c, σ_1', σ_3', may also be used. The initial sample state is given by the consolidation curve which lies on constant K_c ratio plane. For clarity of the diagram, the consolidation curves are not shown in the figure. The main features of the 3-D diagram are the existence of phase transformation (PT) and critical effective stress ratio (CSR) planes which are shown in the figure. The PT plane lies slightly below the undrained effective stress failure plane which is not shown in the diagram.

It was shown in Section 4.2.2. that the steady state for liquefaction and PT state for strain hardening response occur at a unique value of effective stress ratio corresponding to PT line (Fig. 4.18), regardless of the void ratio of the sample. Hence, the unique steady state line for liquefaction and PT state lines for dilative response shown in

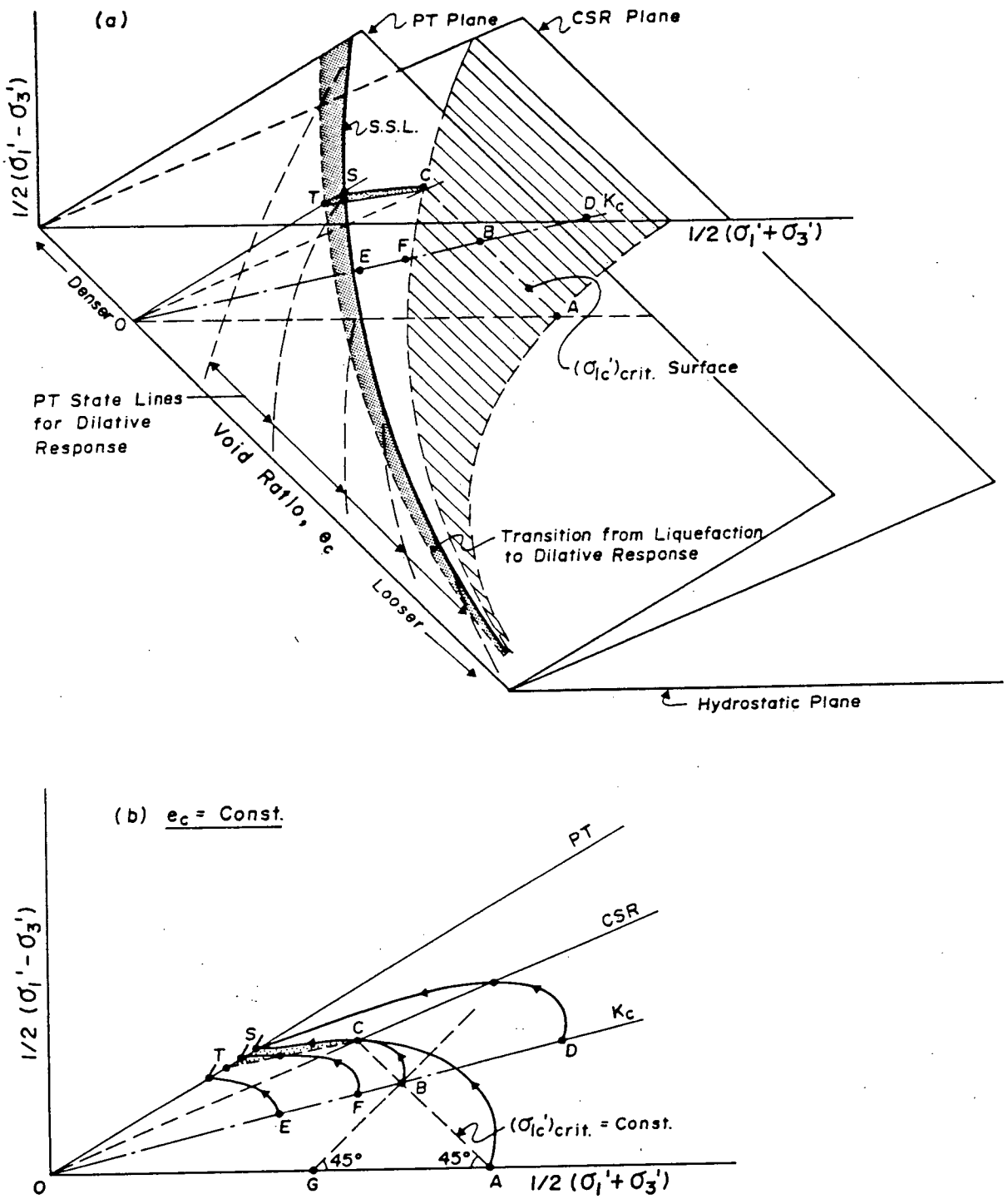

Fig. 4.31 (a) 3-D effective stress state diagram for tailings sand and (b) a typical section at constant e_c.

Fig. 4.12 are states on the PT plane. Therefore, the unique steady state line is a space curve on PT plane, which rises up above the hydrostatic plane as the void ratio decreases, as shown in Fig. 4.31a. The lines branching away from the steady state line are a series of lines corresponding to the loci of PT state for dilative response for several e_i. A small section of these curves near the eventual merger into the steady state line lies in the transition region (darkened area) of slight strain softening.

On the CSR plane, there exist another series of peak strength lines for various e_i, which are the loci of CSR states for those samples which developed liquefaction. For clarity of the diagram, these lines are not shown in the 3-D diagram. From the peak strength lines shown in Fig. 4.26, which are the projection of peak strength lines on CSR plane on e_c-q plane, these lines terminate at a certain state. In other words, CSR plane does not extend all the way to the origin as shown in Fig. 4.18. The state at which the of CSR plane ends are shown by the curve C in Fig. 4.31a. The construction of curve C will be discussed in the next paragraph.

As discussed in Section 4.2.1, for a given e_c there exists a critical consolidation stress $(\sigma'_{1c})_{crit}$ (Fig. 4.12). A sand consolidated to σ'_{1c} equal to or greater than $(\sigma'_{1c})_{crit}$ will develop liquefaction under monotonic loading. Otherwise, strain hardening or slight strain softening responses will be developed. The $(\sigma'_{1c})_{crit}$ was found to increase with decreasing e_c. Any combination of K_c and σ'_{3c} which results in $K_c\sigma'_{3c} = \sigma'_{1c} = (\sigma'_{1c})_{crit}$ is the critical consolidation stress. This is shown by the constant $(\sigma'_{1c})_{crit}$ paths AB in 3-D diagram (Fig. 4.31a) and in p'-q plot at constant e_c (Fig. 4.31b). It was also shown in Section

4.3.1 that all samples with state on path AB will result in the same peak stress state at C and steady state at S. The peak stress state C also corresponds to the upper limit of constant σ'_{1c} path AB at which liquefaction is imminent. This is also illustrated by the stress paths starting from initial states A, B and C in Fig. 4.31b. Therefore, the critical consolidation stress condition in 3-D diagram is a curved surface generated by translating the constant σ'_{1c} ($= (\sigma'_{1c})_{crit}$) path as the void ratio changes (Fig. 4.31a). The intersection of this curved surface with the CSR plane forms a limiting curve C which is the lower bound of the CSR plane. Below curve C the CSR plane does not exist. Liquefaction will be initiated when the sample moves into CSR plane in this region from below, e.g., sample D, during monotonic loading. The shear stress corresponding to the lower bound of CSR plane (curve C in Fig. 4.31a) has a very important implication in the occurrence of liquefaction under cyclic loading condition and will be discussed in the next chapter.

From the 3-D effective stress state diagram, a clear picture of the undrained monotonic loading behaviour can be obtained based on the initial state of the sand. For samples with initial states lying on or to the right of the $(\sigma'_{1c})_{crit}$ surface, liquefaction will be developed. Sample state will reach the CSR plane first and then undergo strain softening leading to steady state deformation, finally ending at steady state S (samples A, B, C and D). For initial states lying to the left of $(\sigma'_{1c})_{crit}$ surface, strain hardening response or slight strain softening response will be developed. The sample state will reach the PT plane directly (sample E) or reach the peak strength in the transition region and then undergo slight strain softening (sample F) depending on how

close the initial state is to the $(\sigma'_{1c})_{crit}$ surface.

It may be noted that the undrained behaviour obtained in Section 4.3, i.e., steady state line, phase transformation state lines and pore pressure generation characteristics, which are used to develop the 3-D effective stress state diagram, are similar for both sands. Therefore, similar 3-D effective stress state diagram as that of the tailings sand should exist for Ottawa sand also. However, due to a rather small range of relative density over which liquefaction can be induced for the range of consolidation stress considered, no similar 3-D diagram was developed for Ottawa sand. Nevertheless, the role of void ratio, confining pressure and K_c ratio on the undrained behaviour were found similar for both sands with only minor differences. These differences will be discussed in the next section.

4.5 Role of Void Ratio, Confining Pressure and Static Shear Stress on Undrained Monotonic Loading Behaviour

4.5.1. Void Ratio or Relative Density

Most of the understanding of the undrained behaviour of sand has come from tests on rounded sands. It is generally believed that relative density is the most important parameter dictating the undrained response with no reference as to the associated consolidation stress conditions and particle angularity.

From the consolidation characteristics discussed in Chapter 3, it may be seen that a sample with given void ratio e_c, can be achieved by various combinations of e_i and consolidation stress condition σ'_{3c} and K_c. The initial state of the sample can lie either to the left or to the

right of the critical consolidation stress surface (Fig. 4.31a). The response under these two conditions will be completely different. Therefore, specifying void ratio or relative density alone without reference to its consolidation stress condition will not give any indication as to the type of undrained response anticipated.

Generally, decreasing e_c will increase the critical consolidation stress level required to cause liquefaction. This may be seen from the increasing critical consolidation stress $(\sigma'_{1c})_{crit}$ as the void ratio decreases from the 3-D effective stress state diagram (Fig. 4.31a). This seems to be true for Ottawa sand also. However, for the range of consolidation stress considered, the initial void ratio alone of Ottawa sand gives a good prediction as to the type of undrained response, as discussed in the previous sections.

4.5.2. Confining Pressure

Undrained behaviour is normally studied by testing isotropically or anisotropically consolidated samples. The influence of confining pressure σ'_{3c} on undrained response is assessed by coupling e_c with σ'_{3c}, such as in Castro's 2-D, e_c-σ'_3 state diagram. As shown in the 3-D effective stress state diagram, it is the complete sample state, i.e., e_c, K_c and σ'_{3c}, which controls the undrained response. Specifying e_c and σ'_{3c} only is not sufficient to predict the undrained response. This may be explained clearly from the behaviour of sand along a constant σ'_{3c} path GB in Fig. 4.31b. Samples G and B have the same σ'_{3c} but different K_c ratio. As explained in Section 4.4.1, Sample B will result in liquefaction, whereas G will result in strain hardening response or slight strain softening response.

The general influence of increasing confining pressure on undrained response with other two factors e_c and K_c held constant is increasing contractive tendency (e.g. Sample E to D in Fig. 4.31b). However, the influences of σ'_{3c} on the occurrence of liquefaction in the contractive region and the stress increment required to reach PT state in the dilative region have to be considered separately due to different response developed in these two regions.

In the contractive region, the shear stress increment required to reach the CSR increases with increasing σ'_{3c}, but is proportional to σ'_{3c} due to the similarity of stress paths (with same K_c). However, the potential to develop steady state deformation increases with increasing σ'_{3c}. This may be seen from the response of Samples B and D in Fig. 4.31b. Sample D will develop much severe strength loss and larger deformation until steady state strength is mobilized than Sample B. Static shear stress on Sample D could be greater than its steady state shear strength if the confining stress is high enough. Sample under such a state is potentially unstable. This is especially serious for cases of high K_c ratio.

In the dilative region, the shear stress increment required to reach the PT state also increases with increasing σ'_{3c}, but the ratio of shear stress increment to σ'_{3c} decreases with increasing σ'_{3c} due to the increased contractive tendency. This will be reflected by the decrease in resistance to cyclic mobility with increasing σ'_{3c} in cyclic loading, which will be discussed in the next chapter.

For sand with rounded particles also, such as Ottawa sand, the sample will develop strain hardening response under very low confining pressures. As the confining stress increases, the sample develops strain

softening response similar to that for the angular sand. However, as stated in the role of void ratio, relative density is the most important factor controlling the undrained response of rounded Ottawa sand for the range of consolidation stress considered herein.

4.5.3. Static Shear Stress or Consolidation Stress Ratio

The increase in static shear or K_c ratio while maintaining e_c and σ'_{3c} constant could transform a sample from strain hardening response to liquefaction as discussed before. The influence of K_c ratio on the undrained response for samples in the contractive and dilative regions could be quite different due to different types of deformation developed. This may be illustrated by effective stress paths for samples in the contractive and dilative regions shown in Fig. 4.32.

In the contractive region (Sample C_1 and C_2 having same σ'_{3c}), the sample with higher K_c ratio develops higher peak shear strength. This may also be seen from Eq. 4.4b. However, the shear stress increment required to reach the peak strength starting from the initial static value always decreases with increasing K_c ratio. This may be shown by substituting Eq. 4.4b into the relation of $\Delta S_{up} = S_{up} - \tau_s$ where S_{up} = peak shear strength and τ_s = static shear stress.

$$\Delta S_{up} = \left[(1/2\ (c-1)(0.412\ K_c - 0.044) - 1/2\ (K_c-1) \right] \sigma'_{3c} \qquad (4.6)$$

Equation 4.6 implies ΔS_{up} decreases with increasing K_c ratio. For the limiting case, i.e., K_c = CSR (=c), the shear stress increment required to reach the peak strength is practically zero. In other words, the strain softening response is imminent when the sample is consolidated

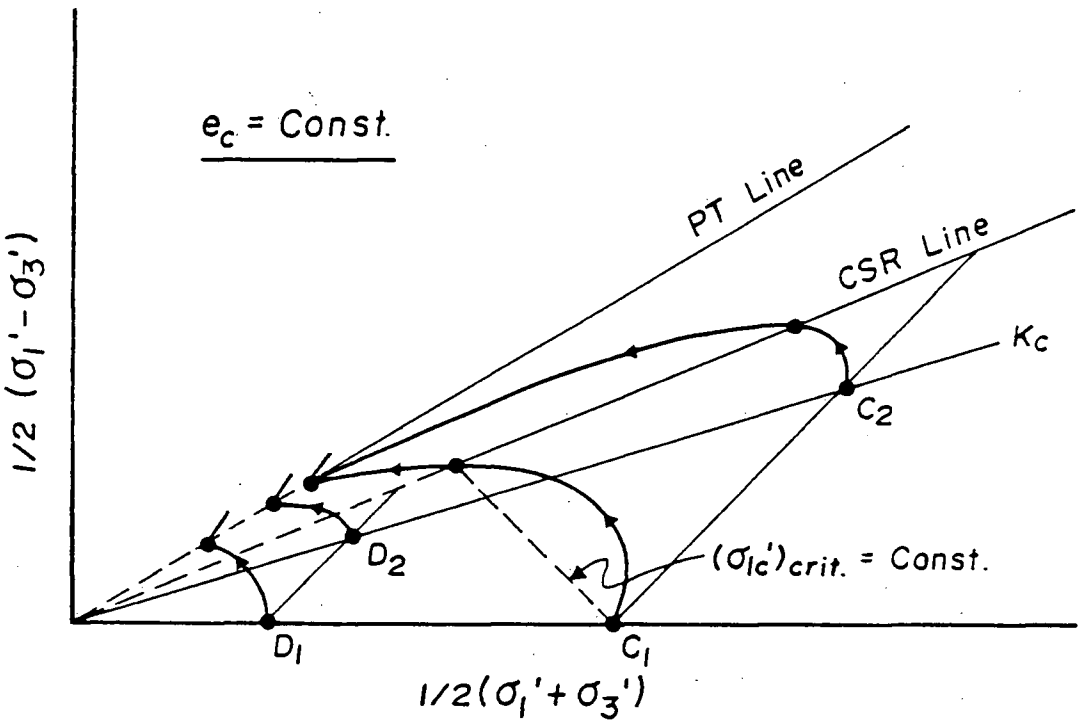

Fig. 4.32 Influence of static shear stress on the undrained monotonic loading behaviour.

under this effective stress ratio. This may also be seen from the relationship between the pore pressure generated untill the CSR state and K_c ratio as shown in Fig. 4.24. This case may correspond to the phenomenon of spontaneous liquefaction, which will be discussed further in the next chapter. Due to the unique steady state strength at constant void ratio e_c, the potential to develop steady state deformation increases with increasing K_c ratio. More severe loss of shear resistance accompanied by larger deformation will occur in sand with high K_c than with lower K_c ratios. Therefore, not only liquefaction is easier to occur but also the strength loss on liquefaction is more severe when the static shear stress is increased.

From the pore pressure generation characteristics and unique steady state line observed, it appears that the behaviour discussed above for tailings sand are also true for rounded Ottawa sand.

In the dilative region (Samples D_1 and D_2) also the sand with higher K_c ratio develops higher shear strength at PT state and the shear stress increment required to reach the PT state is smaller. This is similar to that observed in the contractive region. However, this similarity in monotonic loading behaviour in contractive and dilative regions can not be applied to cyclic loading behaviour, as will be shown in the next chapter.

The same conclusion concerning the influence of static shear to reach the PT state in the dilative region appears to be true for Ottawa sand also due to the similarity of undrained behaviour in the dilative region in both sands.

From the discussions presented above, it may be seen that using relative density or a 2-D e_c-σ'_3 representation is insufficient for

predicting the undrained response. Undrained response is mainly controlled by major consolidation stress σ'_{1c} for a given sand. The 3-D effective stress state diagram developed ties the effects of K_c and σ'_{3c} on the undrained response and also provides a method to predict the undrained response given the initial state of the sand. It also provides a general understanding as to the roles of void ratio, confining pressure and static shear stress on the undrained monotonic loading behaviour.

CHAPTER 5

UNDRAINED CYCLIC LOADING BEHAVIOUR

It was discussed in Chapter 2 that strain development during cyclic loading could be either due to liquefaction or cyclic mobility or a combination of two. Although both liquefaction and cyclic mobility result in large deformation which is unacceptable for engineering purposes, the mechanisms of strain development as a consequence of liquefaction and cyclic mobility are quite different. Therefore, the effect of factors on the strain development due to these two mechanisms could be quite different too. In order to understand the influence of factors, such as void ratio, confining pressure and static shear stress level, on the strain development under cyclic loading thus requires a clear understanding as to the mechanism which is responsible for the strain development. Moreover, it would be desirable to be able to predict whether liquefaction or cyclic mobility will be induced under cyclic loading given the initial state of the sand and the amplitude of cyclic load applied.

Although Vaid and Chern (1983[1,2]) made clear distinctions between liquefaction and cyclic mobility as the mechanisms of strain development during cyclic loading, the studies were limited to one sand and one confining pressure only. Therefore, no general guideline was offered to predict the occurrence of liquefaction or cyclic mobility under cyclic loading given the initial state of the sample and the cyclic loads applied.

This chapter describes tests on samples of both sands consolidated to various initial states to illustrate the mechanisms of liquefaction

and cyclic mobility for strain development under cyclic loading. The 3-D effective stress state diagram developed under monotonic loading conditions is then used, together with cyclic loading results to develop a comprehensive method for prediction of the occurrence of liquefaction or cyclic mobility given the initial state of the sand and the cyclic loads applied. A rational explanation as to the influence of factors affecting the resistance to strain development under cyclic loading is presented in an attempt to clarify some of the controversial aspects of cyclic loading response reported in literature.

5.1 Liquefaction Induced Under Cyclic Loading

In order to demonstrate occurrence of liquefaction during cyclic loading, a series of tests were performed on initially loose samples for both sands. All sand states (e_c, σ'_{3c}, K_c) after consolidation were so chosen that liquefactions were expected under monotonic loading conditions. Tests were performed under strain controlled conditions in order to avoid the influence of loading system on the post-peak stress-strain behaviour, as discussed in Chapter 3.

For isotropically consolidated sand, the cyclic stress ratio $\sigma_{dcy}/2\sigma'_{3c}$ required to cause liquefaction to occur is very high and close to the peak shear strength under monotonic loading. Moreoever, under this high cyclic stress ratio, liquefaction occurs invariably in the extension mode, which is not the main focus of study in these investigations. Therefore, only samples consolidated to high K_c ratio were used in this series of test. The results obtained in this series of tests were used to establish criteria for liquefaction to occur under cyclic loading conditions.

Another series of cyclic loading tests were performed in order to confirm the liquefaction criteria established by the earlier test series. These test results are also used to illustrate the influence of various factors on the resistance to strain development under cyclic loading (Section 5.4).

5.1.1 Liquefaction During Cyclic Loading

Typical results illustrating stress-strain relations and pore pressure response of tailings sand under various levels of confining pressure are shown in Fig. 5.1a,b,c, together with the effective stress paths. It may be seen that during the first few cycles of loading, pore pressure accumulated progressively and the effective stress path moved toward left. However, the sample accumulated very small strain before its state reached a certain effective stress ratio. Further straining beyond this effective stress ratio caused the sample to lose its shear resistance, which was accompanied by the development of large unidirectional deformation (characteristic of liquefaction) and pore pressure increase. The sample deformed continuously over a significant range of axial deformation in the same manner as the steady state observed under monotonic loading conditions. This continuous deformation was arrested in all samples after large straining except in the case under high confining pressure (Fig. 5.1c) which developed unlimited strain (true liquefaction) without causing dilation. The effective stress path then showed a sudden turnaround. The sample kept on strengthening with decreasing pore pressure while the effective stress path moved toward the undrained failure envelope until the peak cyclic load applied was reached.

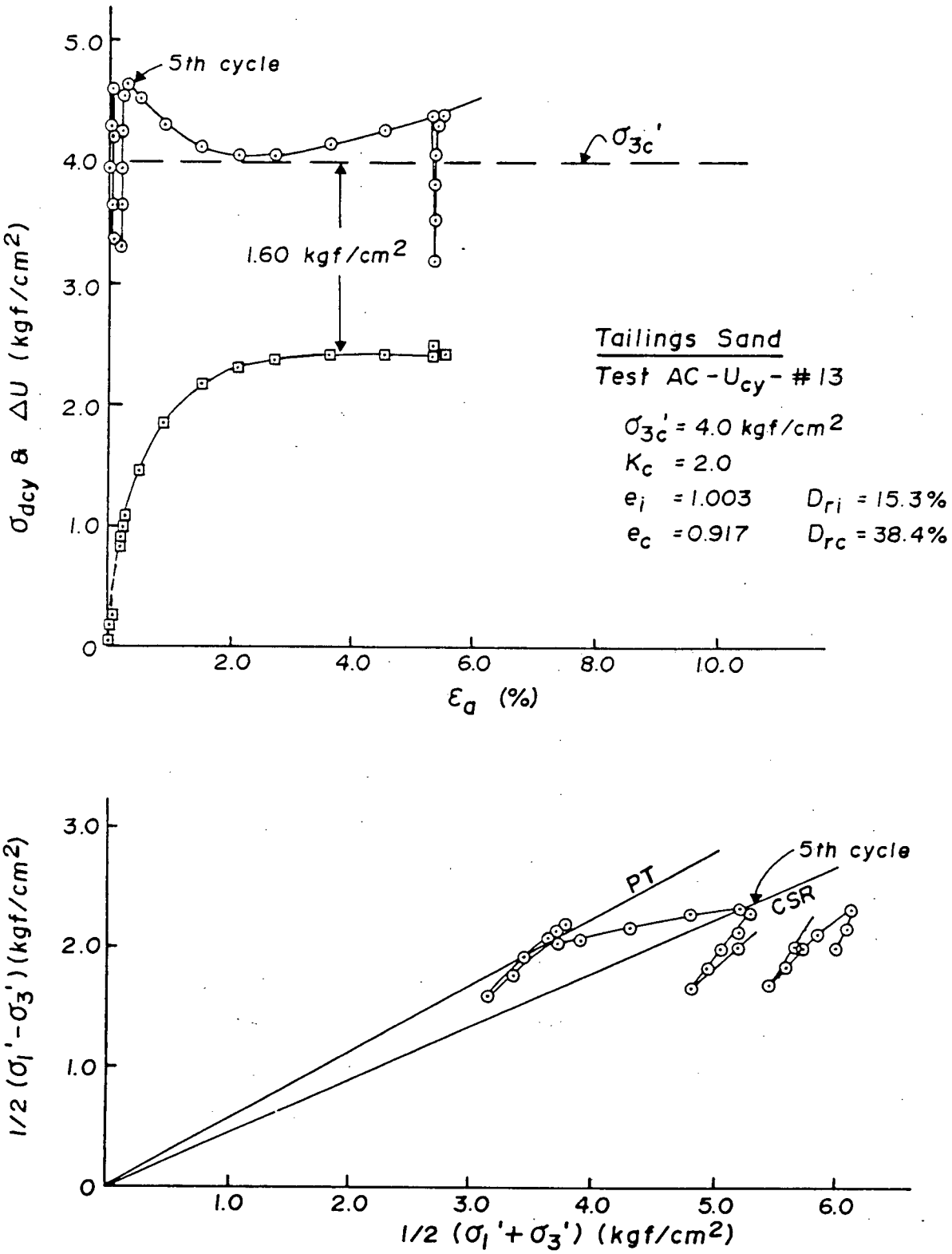

Fig. 5.1a Undrained cyclic loading behaviour of contractive tailings sand under low confining pressure.

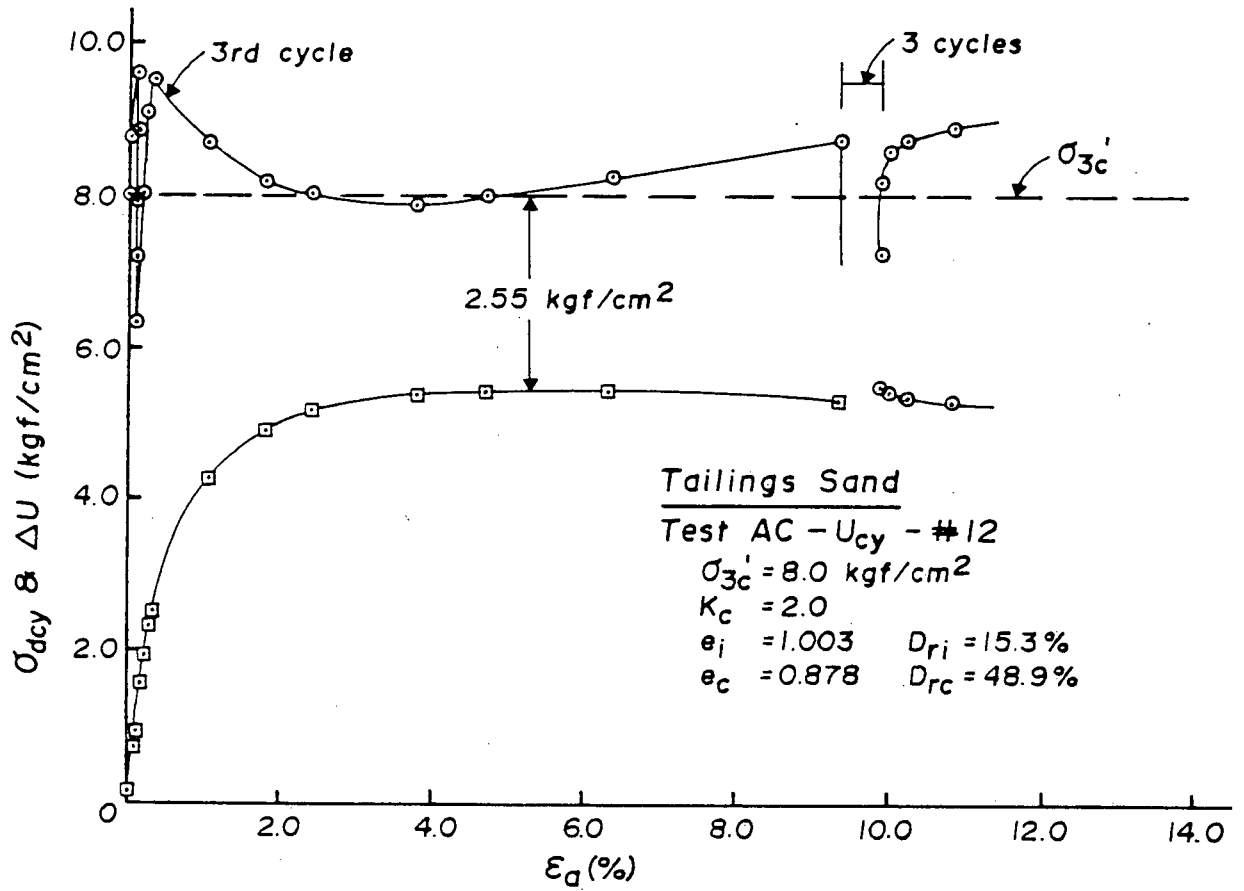

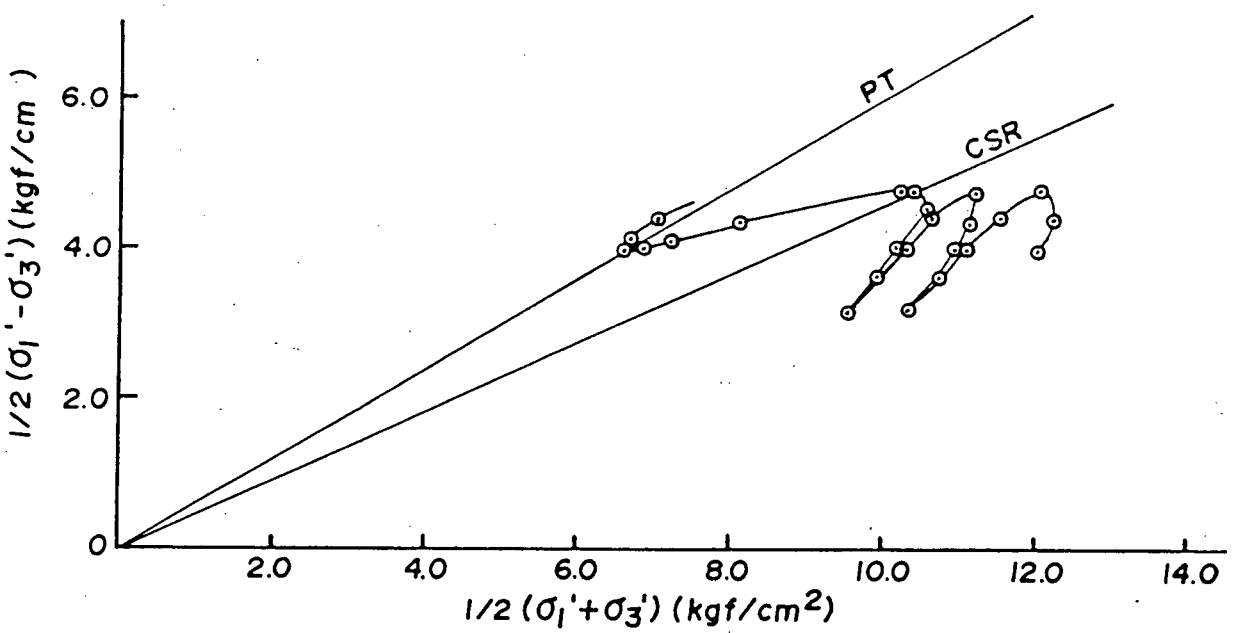

Fig. 5.1b Undrained cyclic loading behaviour of contractive tailings sand under moderate confining pressure.

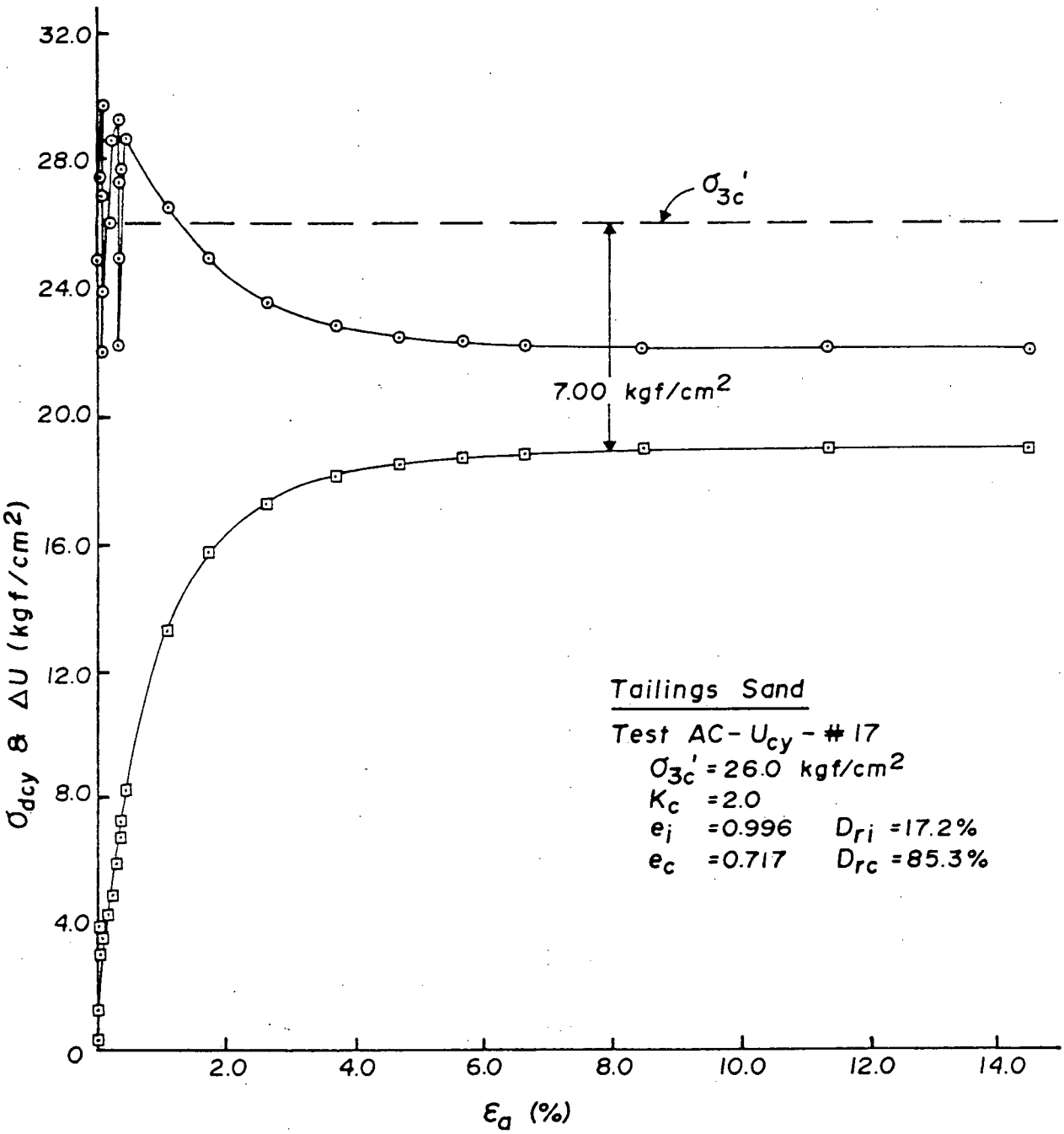

Fig. 5.1c Undrained cyclic loading behaviour of contractive tailings sand under high confining pressure.

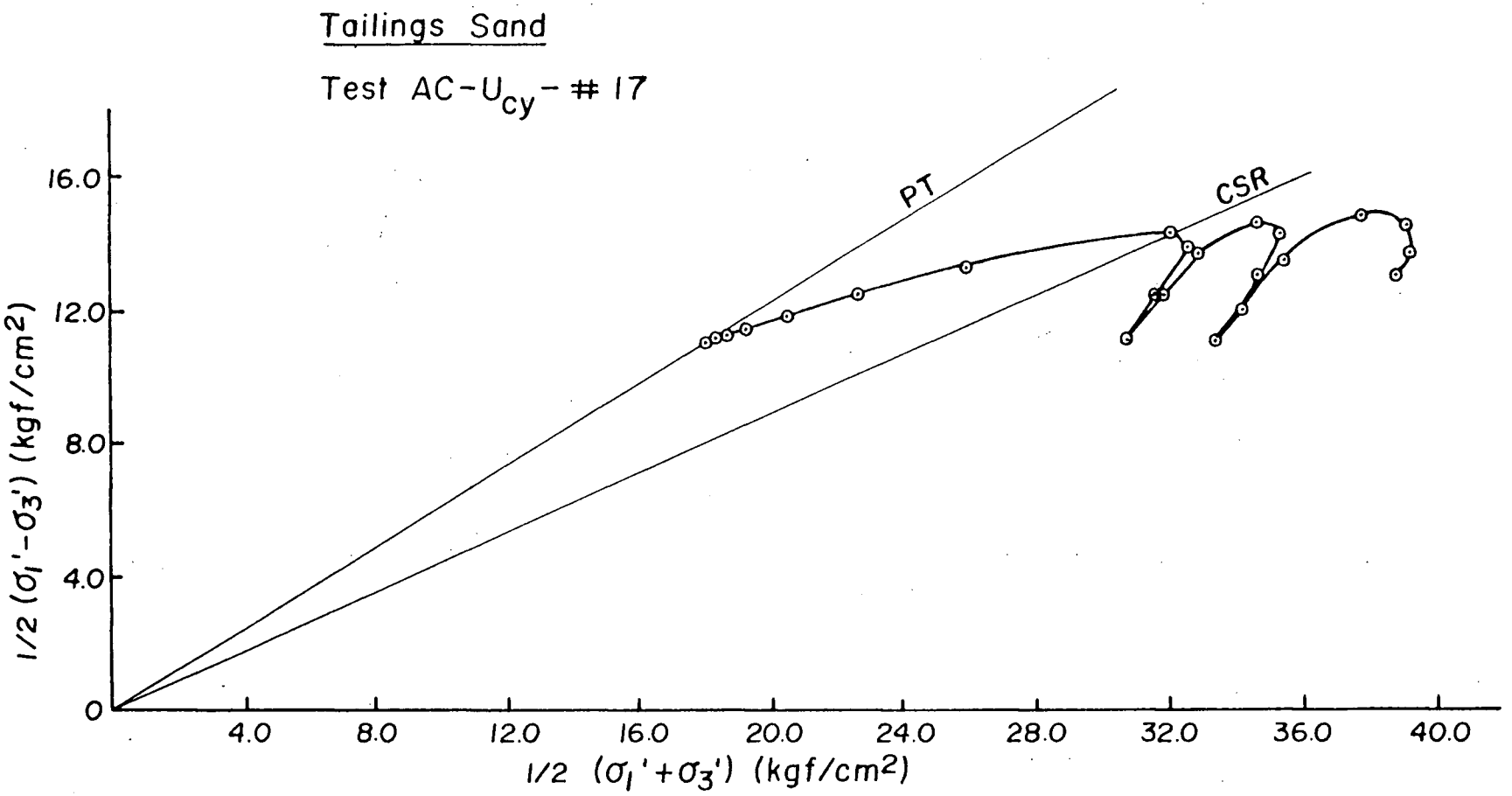

Fig. 5.1c (Cont'd) Undrained cyclic loading behaviour of contractive tailings sand under high confining pressure.

For Ottawa sand, behaviour similar to that for tailings sand was observed. Typical test results illustrating stress-strain curves and pore pressure response are shown in Fig. 5.2a,b,c, along with the effective stress paths. Unlike the behaviour of the tailings sand, all samples of Ottawa sand developed limited strains before the continuous deformations were arrested. No unlimited strain was developed even under high confining pressure. Such behaviour of Ottawa sand is similar to that observed under monotonic loading conditions.

The effective stress states at which strain softening response was initiated during cyclic loading are shown in Figs. 5.3 and 5.4 for tailings sand and Ottawa sand respectively. It may be seen that for both sands all data points lie essentially on the critical effective stress ratio (CSR) line obtained under monotonic loading conditions. This unique CSR line under monotonic and cyclic loading was also observed by Vaid and Chern (1983[2]) for Ottawa sand under low confining pressures.

5.1.2 Applicability of Steady State Concept to Liquefaction Under Cyclic Loading Conditions

Test results in the previous sections showed that the liquefaction occurs during cyclic loading in the same manner as observed under monotonic loading conditions. In order to consider the applicability of the steady state concept and the 3-D effective stress state diagram developed under monotonic loading conditions to predict the occurrence of liquefaction under cyclic loading conditions, the uniqueness of steady state under monotonic and cyclic loading conditions has to be examined.

The minor effective confining stress σ_3' at steady state under cyclic loading condition versus void ratio e_c are shown by data points in Figs.

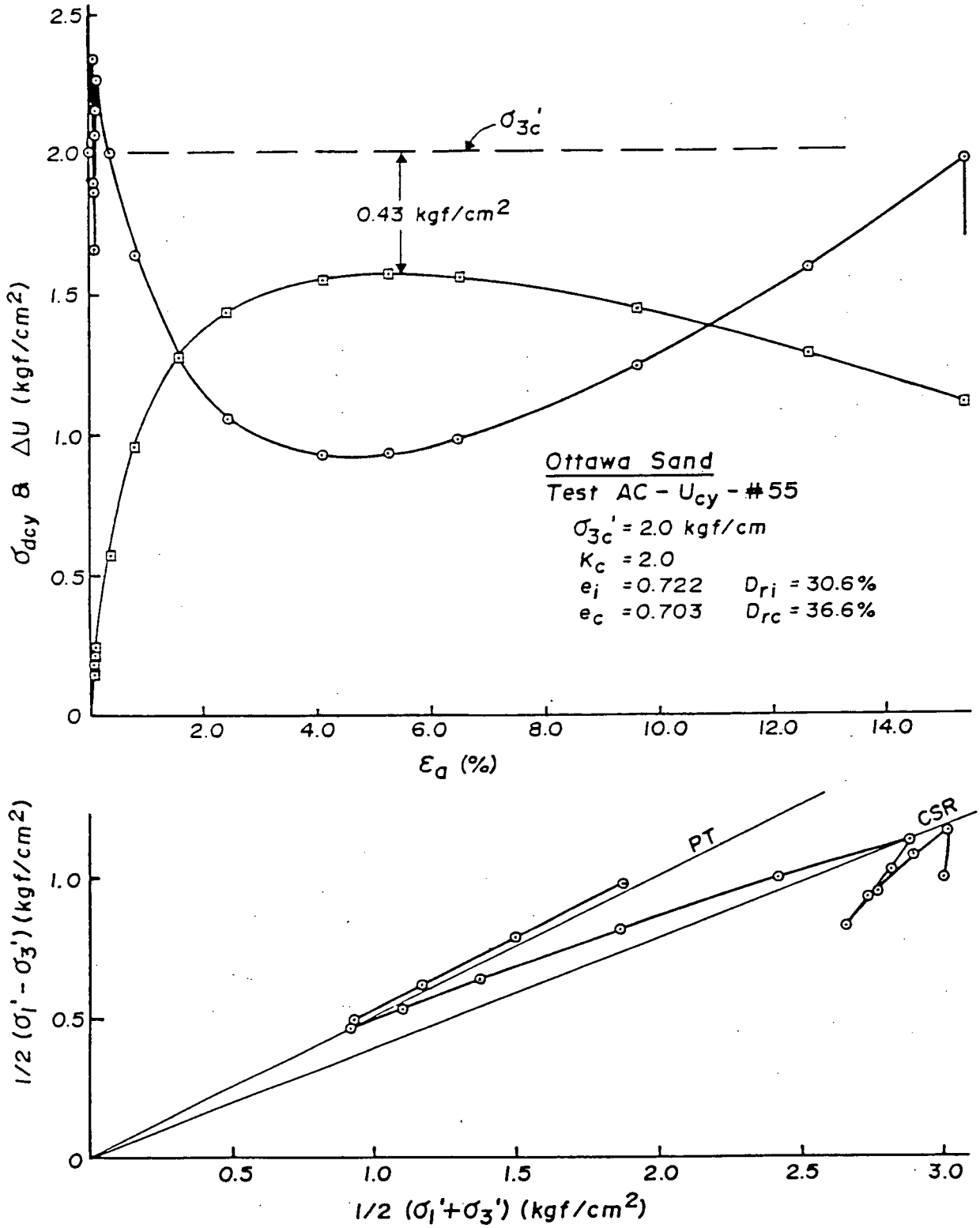

Fig. 5.2a Undrained cyclic loading behaviour of initially loose Ottawa sand under low confining pressure.

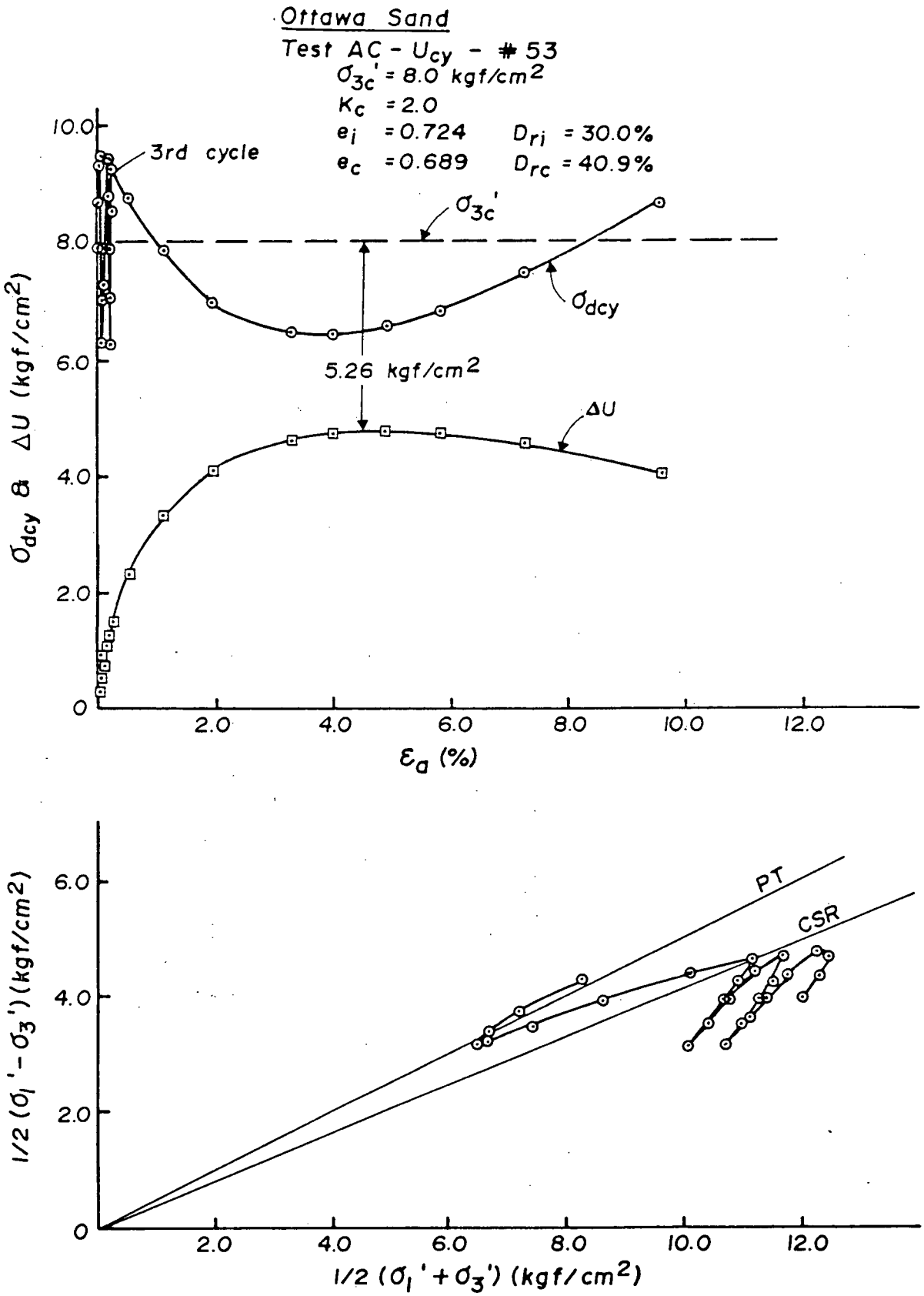

Fig. 5.2b Undrained cyclic loading behaviour of initially loose Ottawa sand under moderate confining pressure.

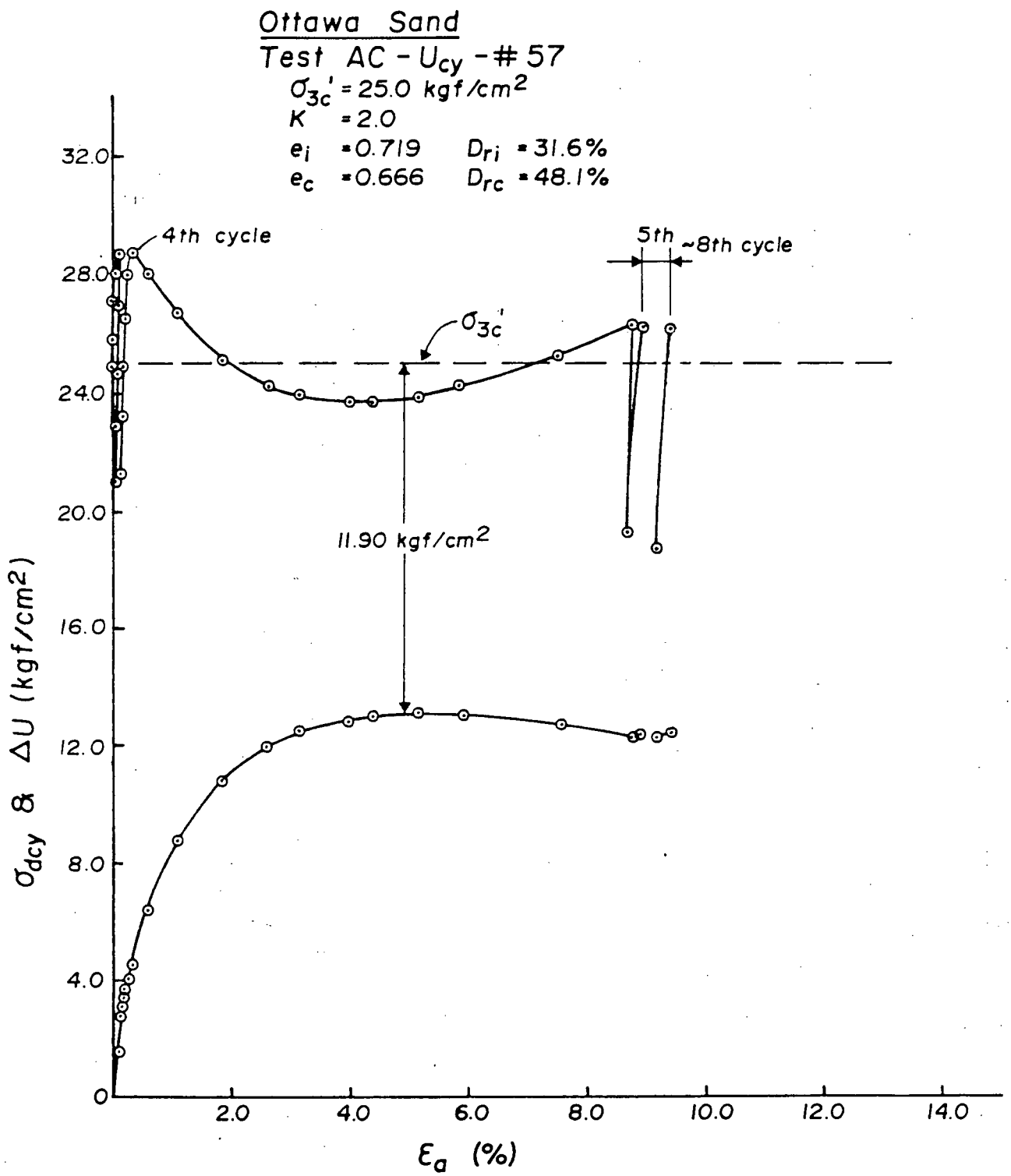

Fig. 5.2c Undrained cyclic loading behaviour of initially loose Ottawa sand under high confining pressure.

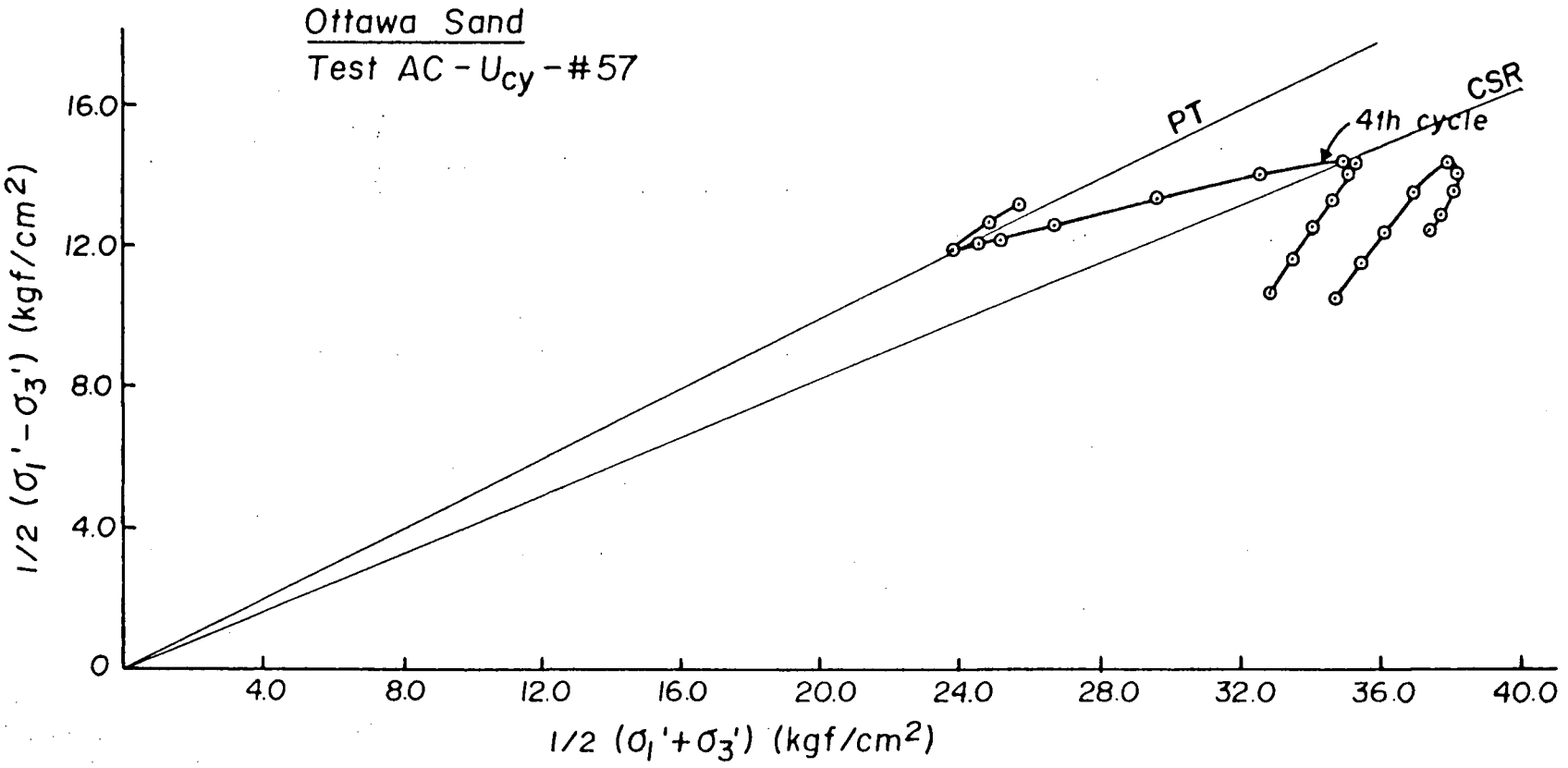

Fig. 5.2c (Cont'd) Undrained cyclic loading behaviour of initially loose Ottawa sand under high confining pressure.

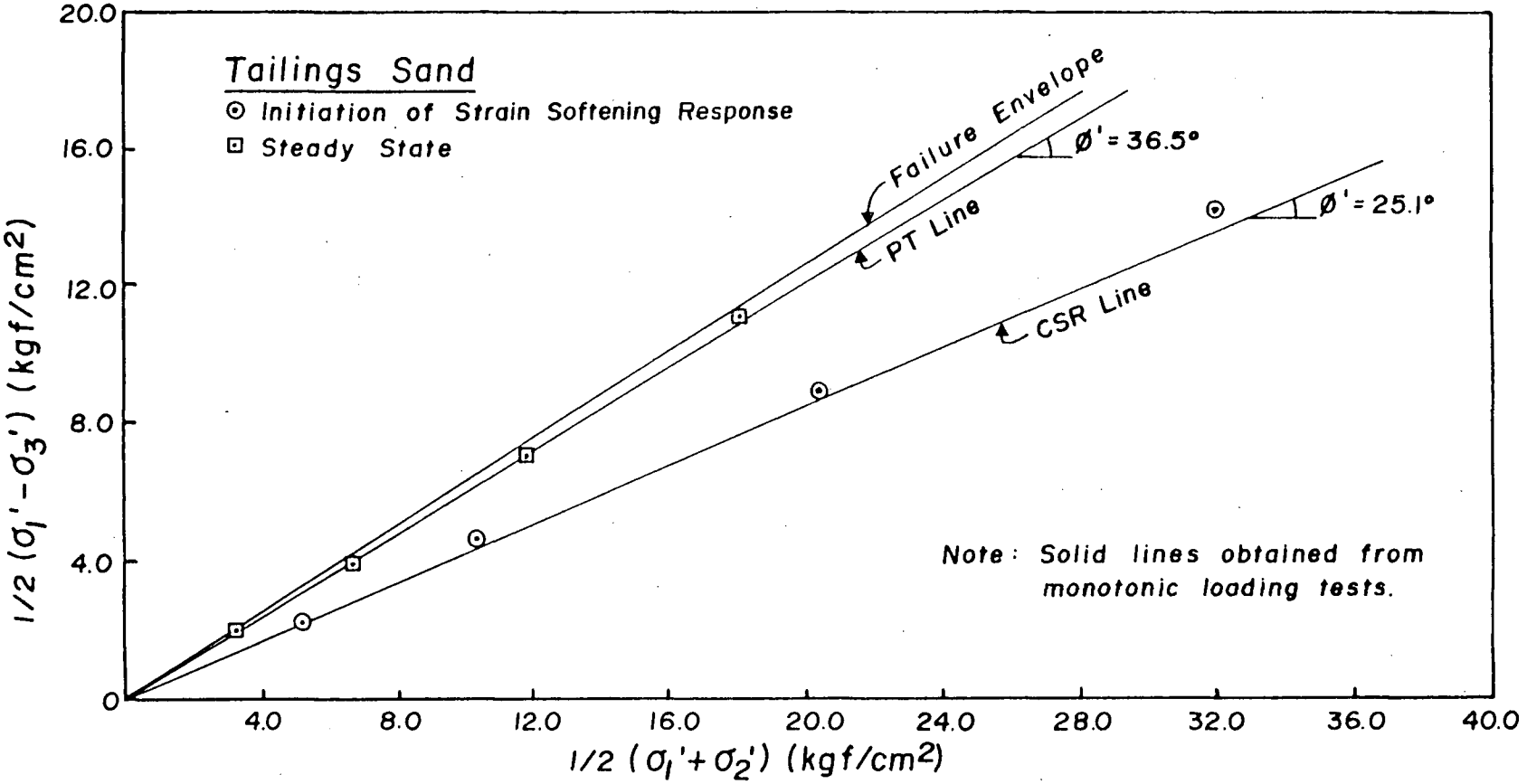

Fig. 5.3 Effective stress conditions at the initiation of strain softening response and start of dilation of tailings sand under undrained cyclic loading.

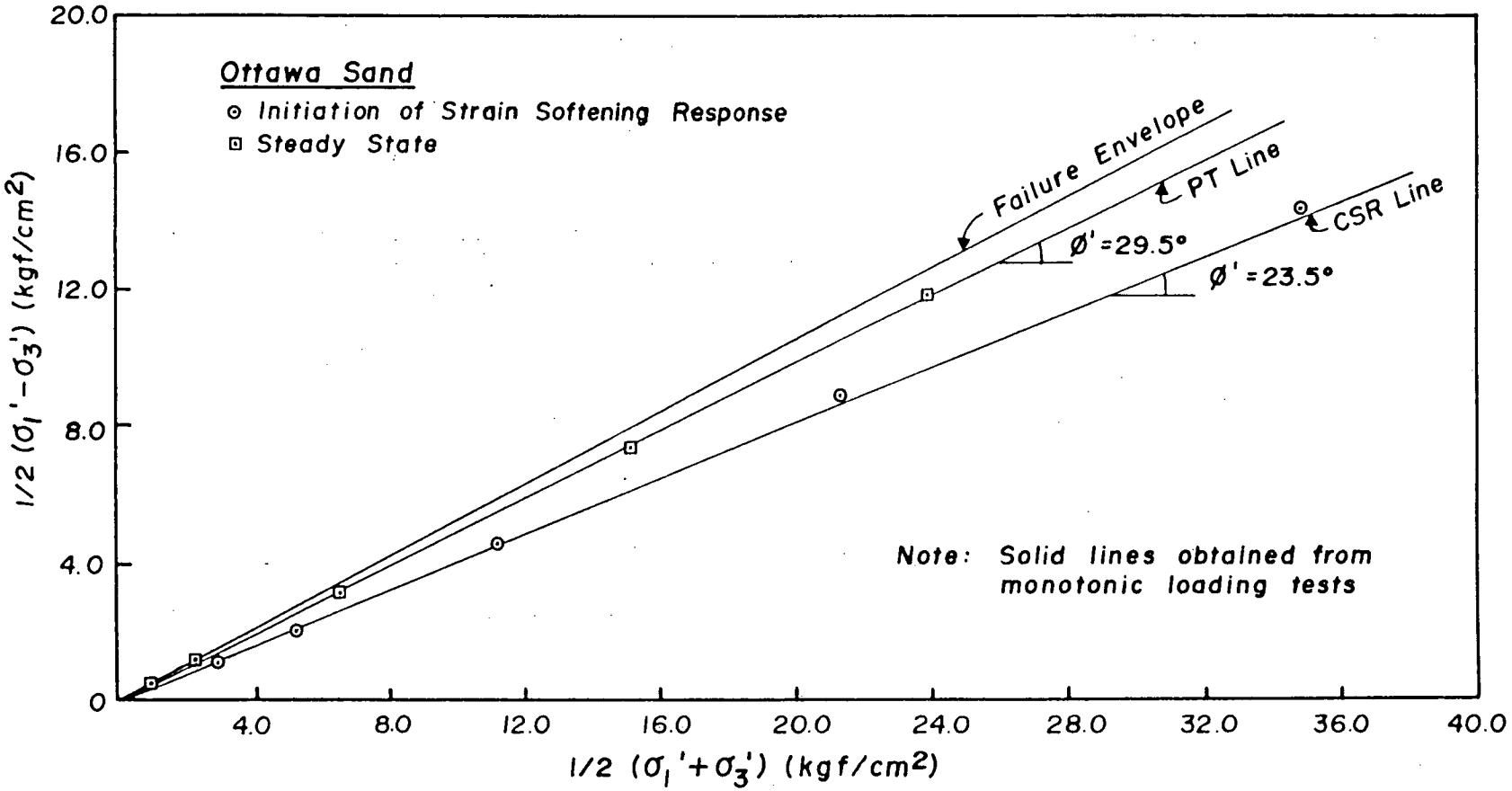

Fig. 5.4 Effective stress conditions at the initiation of strain softening response and start of dilation of Ottawa sand under undrained cyclic loading.

5.5 and 5.6 for tailings sand and Ottawa sand respectively. The range of σ_3' covered under cyclic loading spans the full range covered under monotonic loading. Average steady state lines obtained under monotonic loading conditions are shown by solid lines, and it may be noted that the cyclic loading results fit very closely the results from monotonic loading over the entire range of void ratio considered for both sands. Furthermore, the cyclic loading test data in Figs. 5.3 and 5.4 show that the effective stress states at steady state also lie on the same PT line obtained under monotonic loading. Therefore, the steady state is not affected by the loading paths which bring the sand to this state, and the steady state concept developed under monotonic loading conditions can be used for cyclic loading conditions also.

Due to the uniqueness of steady state line and PT line under monotonic and cyclic loading conditions, the steady state shear strength can be obtained as a function of e_c also. The results for tailings sand and Ottawa sand are shown in Figs. 5.7 and 5.8 respectively. Cyclic loading and monotonic loading results may be seen to be defined by a unique curve for each sand.

It may be pointed out that the existence of steady state for a sand with a given initial state does not necessarily imply that liquefaction will develop under cyclic loading. The criteria whether a sand with a given initial state will develop liquefaction under cyclic loading is discussed in the next section.

5.1.3 Criteria to Cause Liquefaction Under Cyclic Loading

It has been shown that the critical effective stress ratio (CSR) at which strain softening response is initiated leading to liquefaction

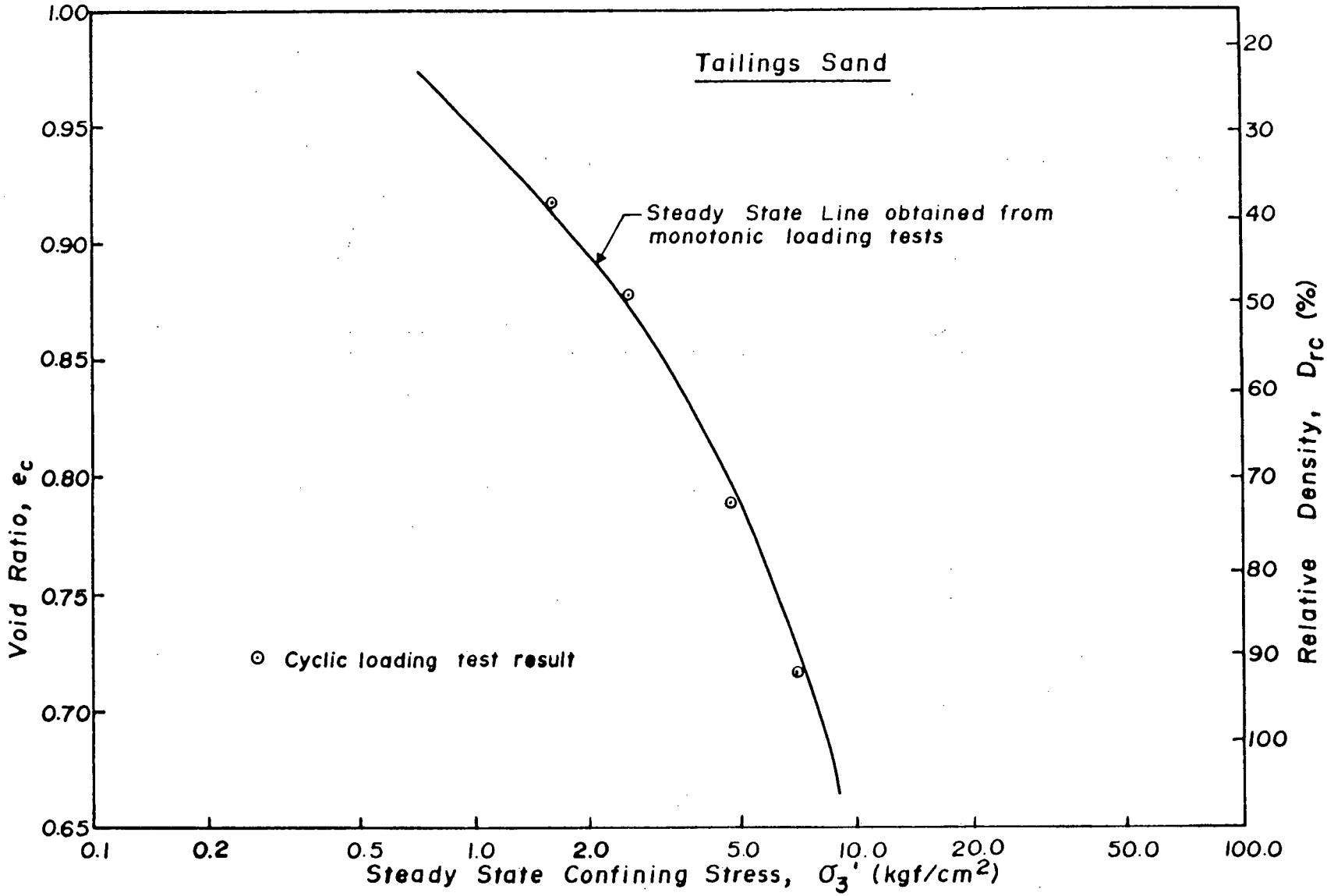

Fig. 5.5 Comparison of steady state confining stress of tailings sand under monotonic and cyclic loading conditions.

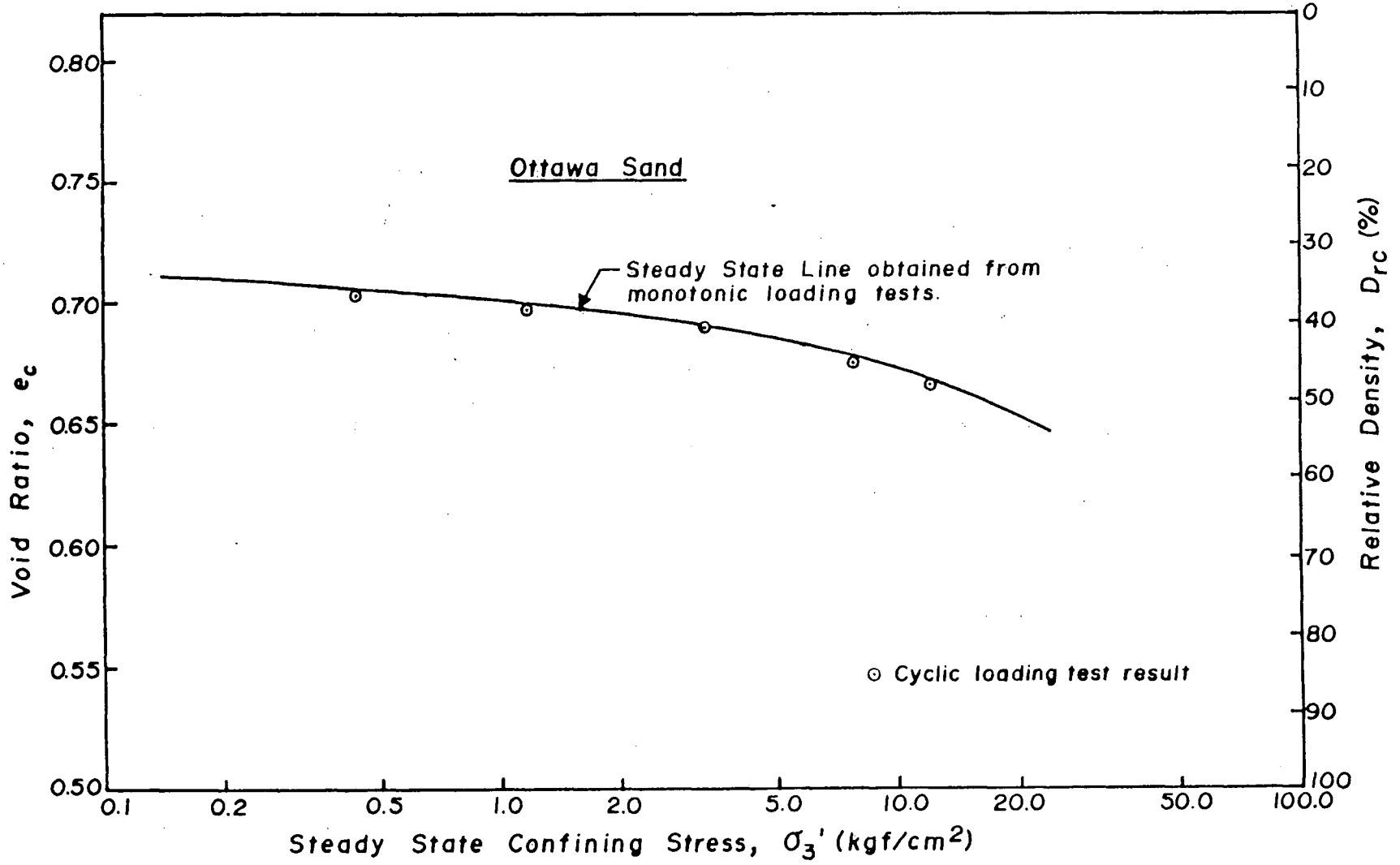

Fig. 5.6 Comparison of steady state confining stress of Ottawa sand under monotonic and cyclic loading conditions.

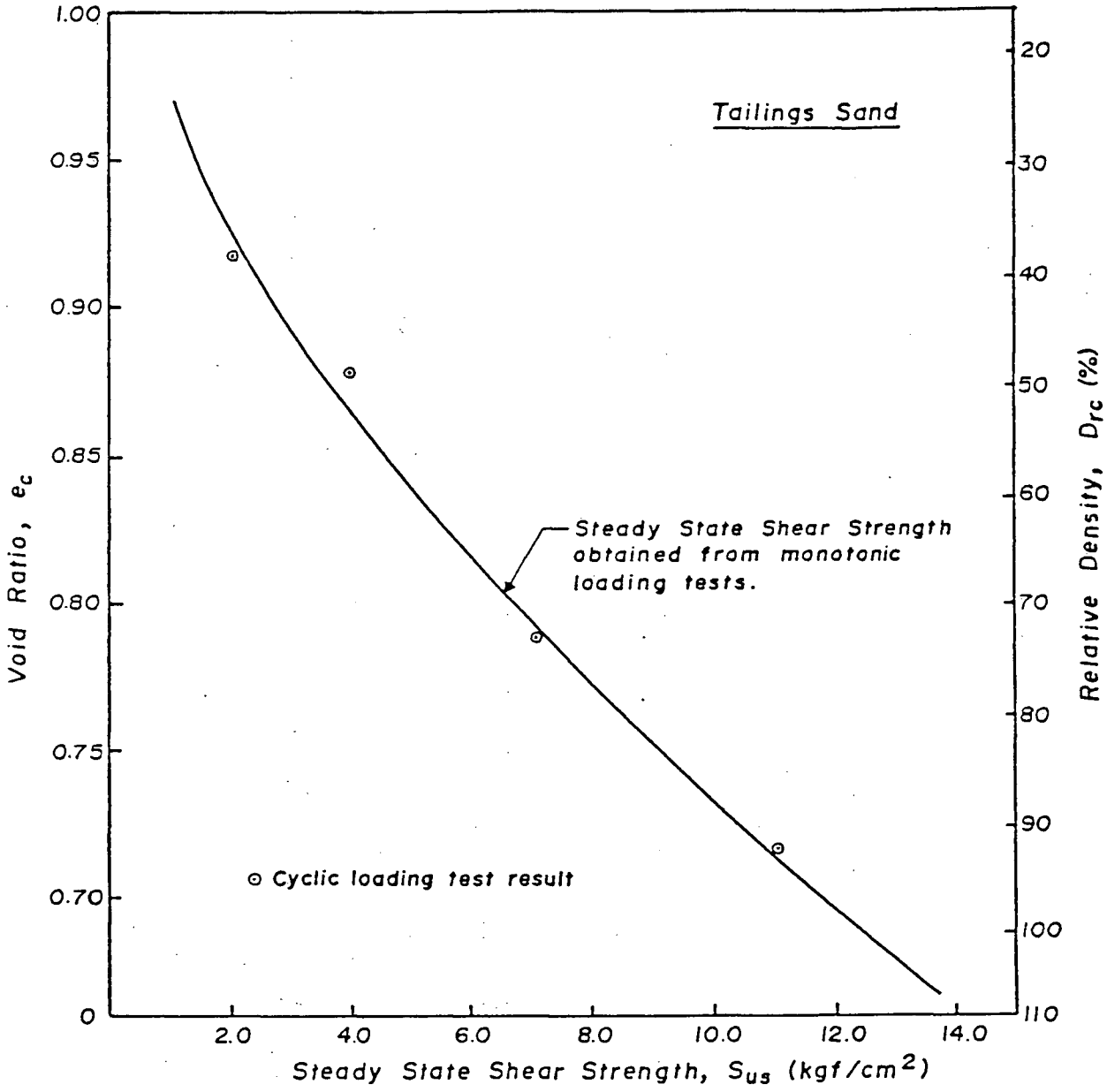

Fig. 5.7 Comparison of steady state shear strength of tailings sand under monotonic and cyclic loading conditions.

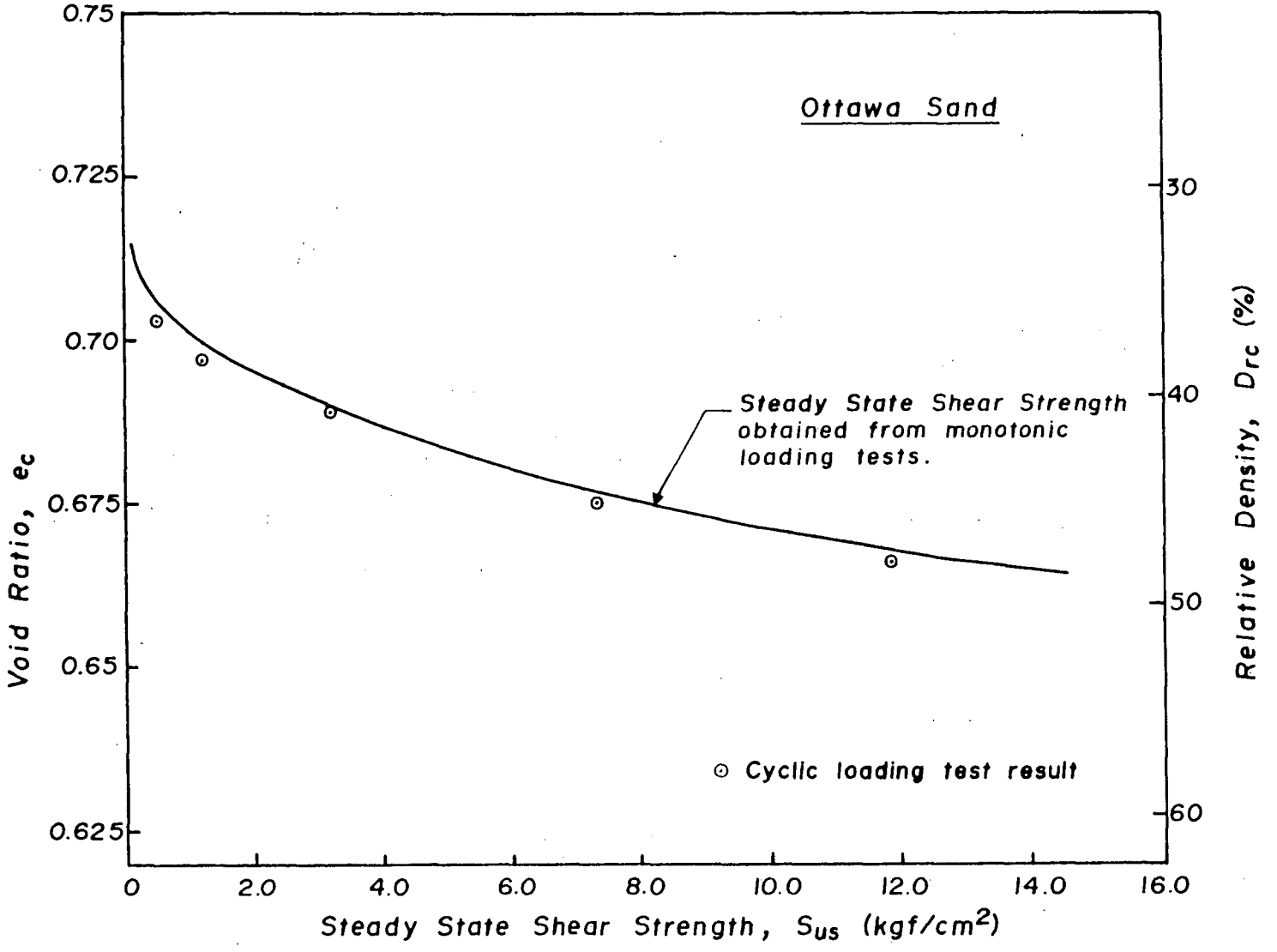

Fig. 5.8 Comparison of steady state shear strength of Ottawa sand under monotonic and cyclic loading conditions.

under cyclic loading conditions is the same as that under monotonic loading conditions. Moreoever, the steady state concept developed under monotonic loading conditions can also be applied to liquefaction under cyclic loading conditions. Therefore, the 3-D effective stress state diagram developed for monotonic loading may be used to develop criteria for liquefaction to occur under cyclic loading.

It was shown in Chapter 4 that for a given void ratio e_c there exists a critical consolidation stress $(\sigma'_{1c})_{crit}$ above which the sand develops liquefaction under monotonic loading, and below which only strain hardening response or slight strain softening can be induced (Fig. 4.12). Due to the demonstrated uniqueness of steady state under monotonic and cyclic loading, therefore, the first criterion for liquefaction to occur under cyclic loading is that the initial state of the sand (e_c, σ'_{3c}, K_c) must be above the critical consolidation stress $(\sigma'_{1c})_{crit}$ surface. In other words, the sand must at an initial state (e_c, σ'_{3c}, K_c) which has the potential to develop steady state deformation. Whether a sand with such an initial state can develop liquefaction or not then depends further on the cyclic loadings applied, which constitutes another criterion and is discussed in the next paragraph. For initial state that lie below the $(\sigma'_{1c})_{crit}$surface (Fig. 4.31), the steady state can not be achieved and hence liquefaction can not be induced.

As discussed in the previous chapter, the CSR plane exists only in the region above peak shear strength at critical consolidation stress $(\sigma'_{1c})_{crit}$ (state C in Fig. 5.9 for the fixed void ratio e_c) and the effective stress path CS is the lowest stress path over which strain softening response is developed leading to steady state deformation. Hence the peak shear strengh at $(\sigma'_{1c})_{crit}$ (strength at C) is the lowest

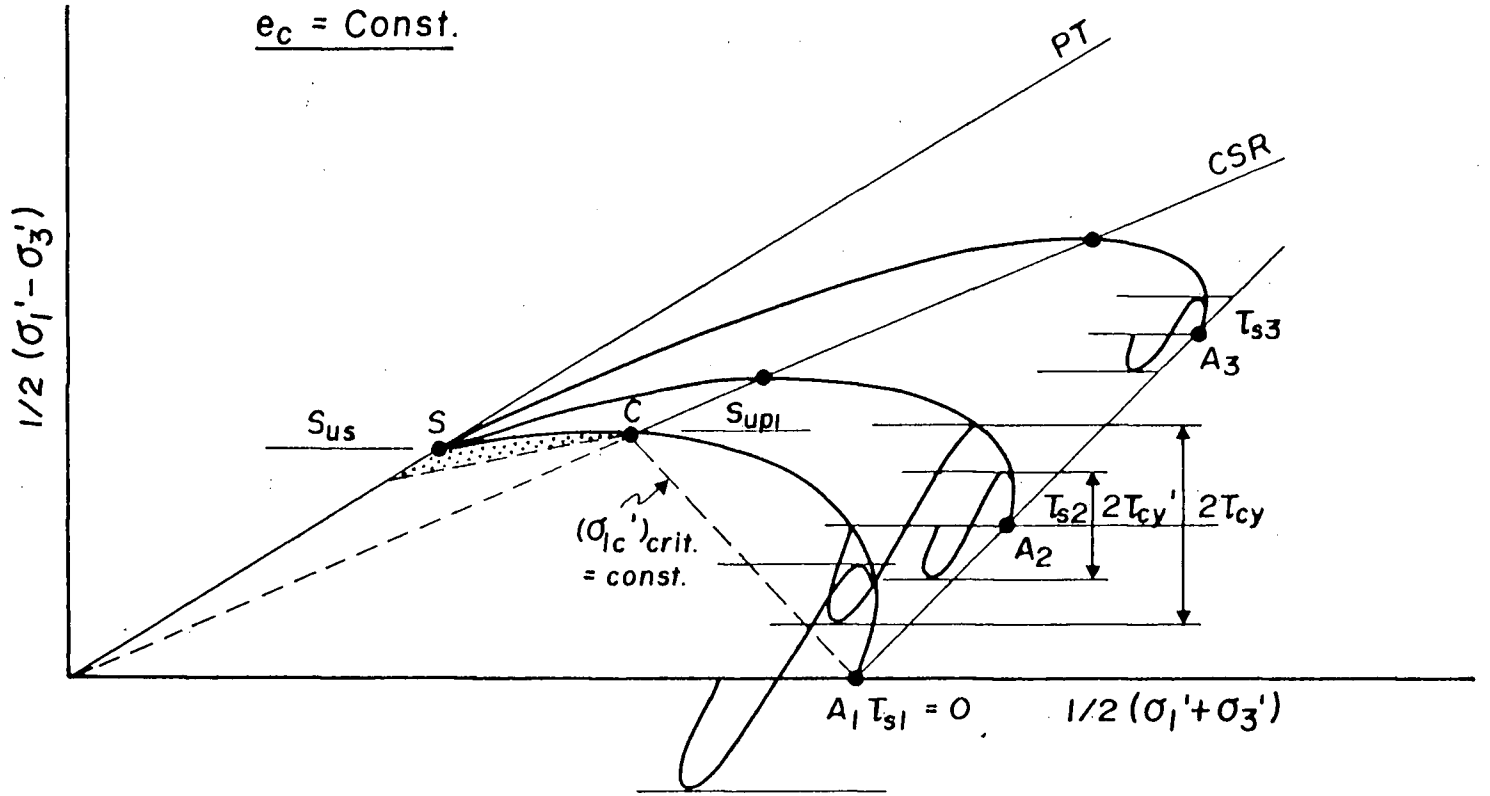

Fig. 5.9 Cyclic shear stress condition to cause liquefaction at fixed e_c.

level of shear stress to be applied in order to develop liquefaction. Due to the uniqueness of CSR and steady state, the cyclic loading applied must therefore result in peak stress state above state C. Only then the CSR line will be reached in order to have liquefaction initiated. Such a situation can be illustrated by the effective stress path plots of three samples at constant void ratio e_c and σ'_{3c} in Fig. 5.9.

For sand with no static shear stress (Sample A_1), although the potential to develop steady state deformation exists (first criteria satisfied) under monotonic loading, for the level of cyclic stress shown in the figure, the stress state of the sand with continued cyclic loading will reach the CSR line in the region where CSR state does not exist (dashed line below C). Hence, liquefaction can not be induced in this case. Cyclic loading will move sample state progressively toward the PT line and only cyclic mobility will develop, which will be discussed in Section 5.2. Liquefaction for state A_1 can be developed only by applying cyclic load with shear stress amplitude equals to the peak shear strength (S_{upl}) under monotonic loading. Under this condition, liquefaction will be induced in the first compression loading, which is identical to monotonic loading.

Increasing the static shear stress level while holding σ'_{3c} constant to a value less then the peak shear strength S_{upl} (Sample A_2), two conditions can occur, depending on the amplitude of cyclic loading applied. If the total shear stress is less than S_{upl}, i.e., $\tau_{s2} + \tau'_{cy} < S_{upl}$, the sample state with continued cyclic loading will reach the CSR in the region where CSR state does not exist, and hence liquefaction can not be developed. Under this condition, only cyclic mobility can be induced. However, if the amplitude of cyclic load is large enough such that the

total shear stress is greater than S_{upl}, i.e., $\tau_{s2} + \tau_{cy} > S_{upl}$, the sample state with continued cyclic loading will reach the CSR in the region where CSR state does exist. Liquefaction will then be initiated at CSR line, provided that the number of stress cycles is large enough to move the effective stress state of sample to the CSR state by the progressive development of residual pore pressure.

For sand with initial static shear stress greater than the peak shear strength S_{upl} at C (Sample A_3), the sand state will always reach the CSR in the region where CSR state exists. Hence liquefaction will always be developed provided the number of stress cycles is large enough to move the effective stress state of sample to the CSR state.

It should be noted that the peak shear strength S_{upl} at $(\sigma'_{lc})_{crit}$ for the chosen e_c is slightly greater than the steady state shear strength (S_{us}). Therefore, for practical purpose the steady state shear strength may be used as the minimum value of total shear stress instead of the peak shear strength value at C. Thus, the second criterion for liquefaction to occur is that the maximum shear stress (static + cyclic) must be greater than the steady state shear strength. That these two conditions must be simultaneously satisfied for liquefaction to occur under cyclic loading will be examined by actual tests in the later sections.

It may be pointed out that the two criteria specified above for occurrence of liquefaction under cyclic loading are the necessary conditions only. Whether actual liquefaction can be developed or not depends on the number of stress cycles applied. If the number of stress cycles is not large enough to move the sample state to the CSR state, no liquefaction can be induced, even though both criteria specified above

are satisfied. However, the combination of cyclic loading and pore pressure increase due to pore pressure redistribution in the soil mass following the termination of cyclic loading could move the sample state to the CSR state and initiate liquefaction. This is especially important if the initial static shear stress is greater than the steady state shear strength, since the pore pressure increase due to cyclic loading coupled with the pore pressure increase due to post cyclic pore pressure redistribution could lead to the occurrence of liquefaction. Therefore, an initial condition with $\tau_s > S_{us}$ should always be avoided in order to eliminate the possibility of liquefaction under cyclic loading.

For Ottawa sand also the CSR is unique, regardless of the loading paths which brings the sample state to the CSR, and the steady state is unique after liquefaction has been induced. Therefore, the criteria specified above for angular tailings sand can be applied to sand with rounded particles also. However, in order to examine the existence or non-existence of steady state, the initial relative density alone may be used for the range of consolidation stress considered herein, as discussed in Chapter 4.

It should be noted that the discussions presented above apply to compression deformation mode only. However, similar concept should apply to extension mode also. It will be shown later by actual test results that liquefaction can be induced in extension mode if these two criteria specified above are satisfied in extension mode.

5.1.4 Test Results

A series of cyclic loading tests on samples consolidated to the same e_c and σ'_{3c} but with various levels of K_c ratio were carried out to

examine the validity of the criteria established for liquefaction to occur for both sands. The initial sample states were so chosen that the sand would experience liquefaction under monotonic loading. These results will also be used later in Section 5.4 to illustrate the influence of e_c, σ'_{3c} and K_c on the resistance to strain development under cyclic loading.

Tailings Sand

For tailings sand, the minor effective consolidation stress σ'_{3c} of 16.0 kgf/cm^2 (1568 kPa) and relative density after consolidation D_{rc} of 70% were used. Four series of tests with consolidation stress ratio K_c of 1.0, 1.25, 1.5 and 2.0 were performed. The identical final void ratio under various consolidation stress conditions was achieved by consolidating samples prepared with initial void ratios e_i obtained by interpolating between the consolidation curves (Fig. 3.8). Extremely consistent final densities were obtained with variations in relative density less than ±1.6%. This also served as a check of the consolidation characteristics of sand discussed in Chapter 3.

The results of cyclic stress ratio $\sigma_{dcy}/2\sigma'_{3c}$ ($= \tau_{cy}/\sigma'_{3c}$) versus number of stress cycles to develop liquefaction or cyclic mobility are shown in Fig. 5.10. If cyclic mobility developed, the number of cycles refer to those needed to accumulate 2.5% axial strain. If liquefaction develops, axial strain in excess of 2.5% develops until steady state. It may be seen that not all samples developed liquefaction, although potential to develop liquefaction in monotonic loading existed for all initial states. A combination of initial stress conditions and cyclic loading amplitude dictated whether liquefaction or cyclic mobility would

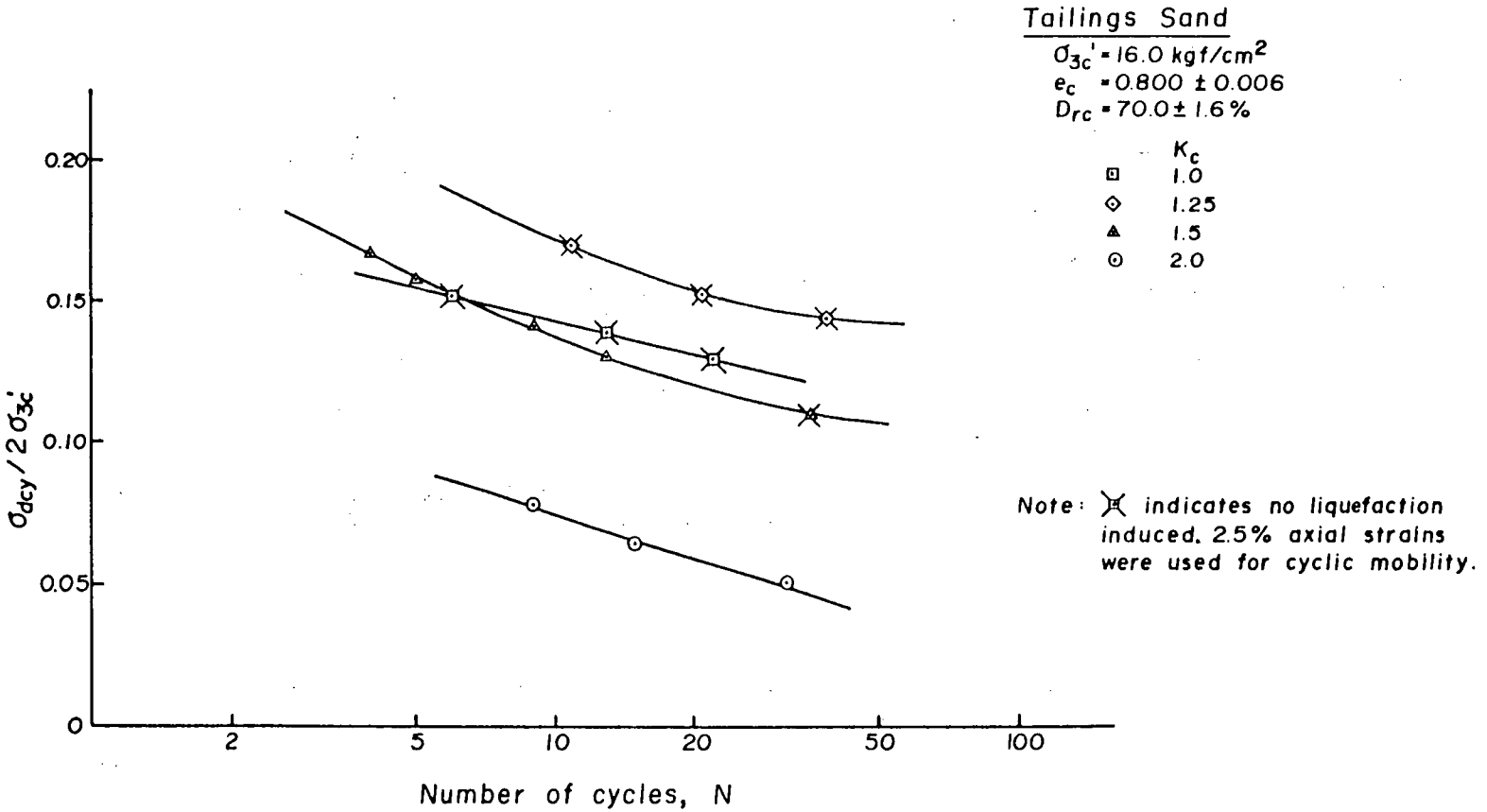

Fig. 5.10 Cyclic stress required to cause liquefaction or 2.5% axial strain for contractive tailings sand consolidated to various K_c ratios.

develop. Both liquefaction and cyclic mobility results are presented in Fig. 5.10 to facilitate discussion of the criteria to cause liquefaction under cyclic loading.

For isotropically consolidated states (K_c = 1.0) and anisotropically consolidated states with K_c = 1.25, all samples developed cyclic mobility. Typical strain developments and pore pressure responses during cyclic loading for such initial states are illustrated in Fig. 5.11. Since the maximum shear stresses (static + cyclic) were less than 2.4 kgf/cm^2 (235 kPa) and 4.7 kgf/cm^2 (461 kPa) for K_c = 1.0 and 1.25 respectively, which are substantially less than the steady state shear strength for the e_c selected (about 5.6 kgf/cm^2 lower bound), liquefaction could not develop.

For anisotropically consolidated state with K_c = 1.5, however, both liquefaction and cyclic mobility could develop depending on the amplitude of cyclic load applied (Fig. 5.10). For cyclic stress ratio greater than 0.13, liquefaction developed, whereas for cyclic stress ratio less than 0.13 cyclic mobility developed. These two cases are illustrated by the stress-strain curves and pore pressure responses in Fig. 5.12a,b. In Fig. 5.12a, the cyclic stress ratio results in maximum shear stress of 6.10 kgf/cm^2 (598 kPa) which is slightly greater than the steady state shear strength. About 2.5% axial strain was developed in the 5th loading cycle with accompanying pore pressure increase. In Fig. 5.12b, however, the maximum shear stress is slightly less than the steady state shear strength. Consequently no sudden development of strain associated with steady state deformation occurred. The strain developed progressively with number of stress cycles as a result of cyclic mobility. This may also be seen from the plot of strain development versus number of stress cycles in Fig. 5.13.

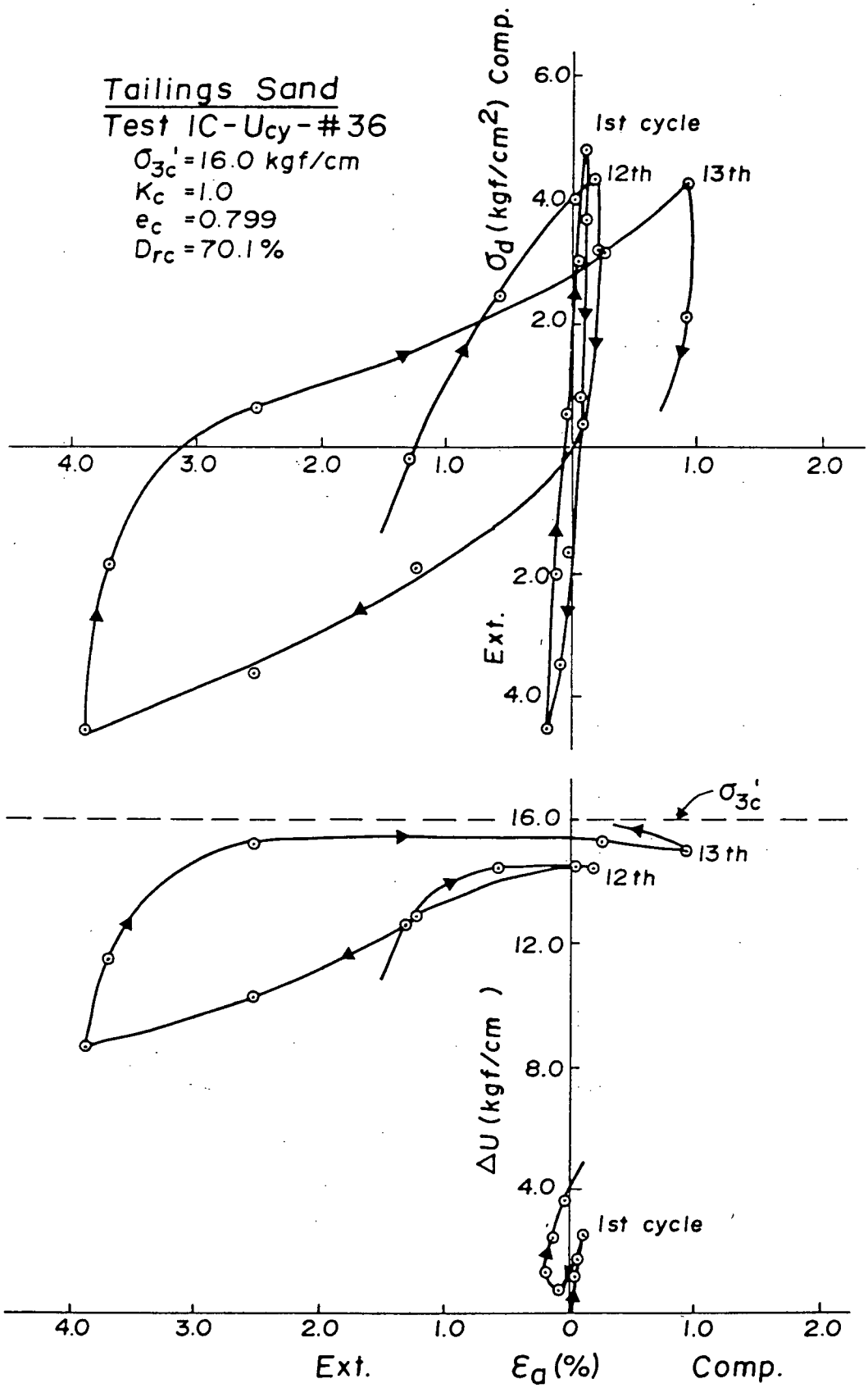

Fig. 5.11 Tyipcal undrained cyclic loading response for contractive tailings sand showing cyclic mobility.

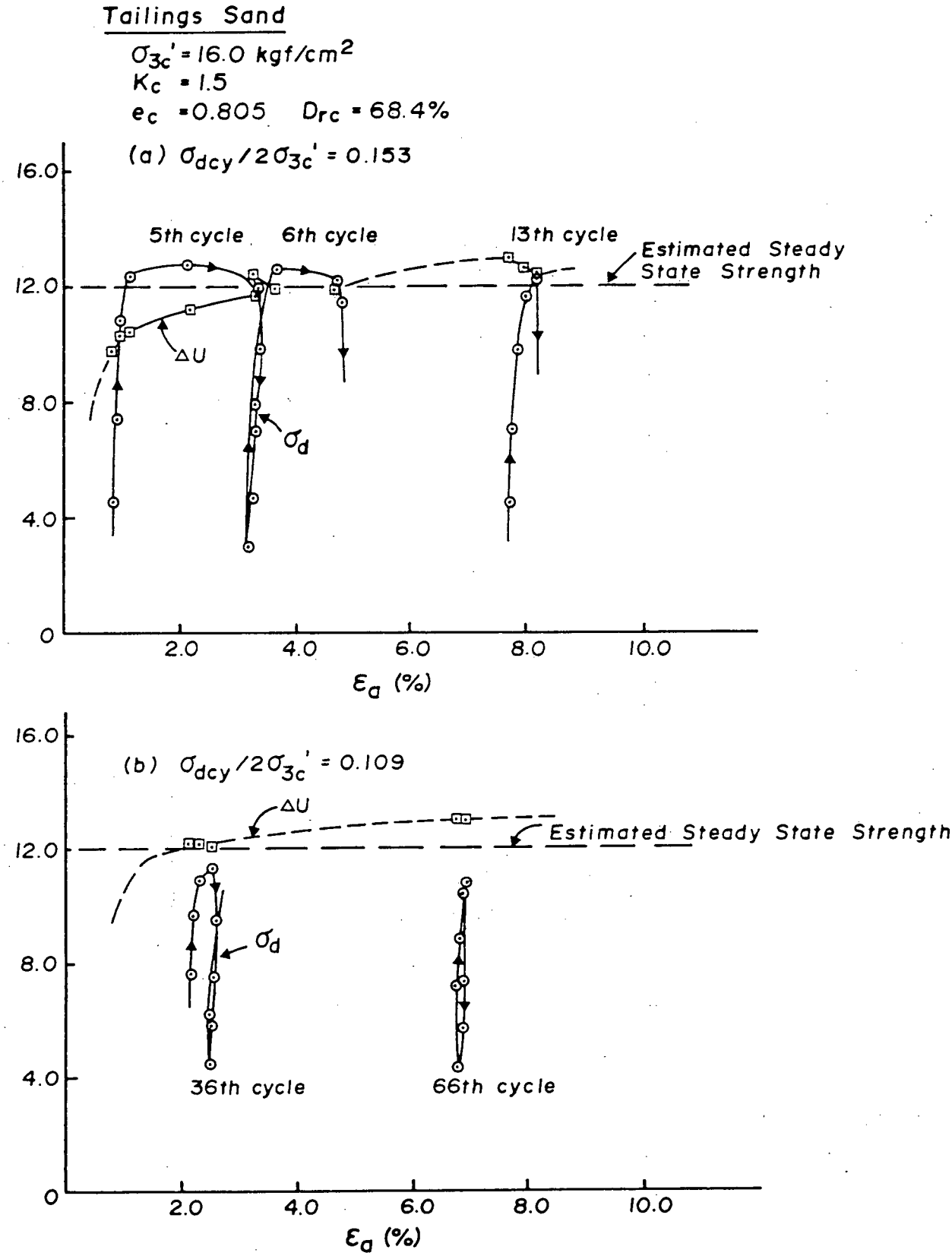

Fig. 5.12 Typical undrained cyclic loading response for contractive tailings sand showing (a) liquefaction, and (b) cyclic mobility.

From the two test examples shown above, both initial states satisfy the first criterion. But, the occurrence of liquefaction depends in addition on whether the maximum shear stress condition in relation to steady state strength is satisfied.

For anisotropically consolidated state with K_c = 2.0, all samples developed liquefaction (Fig. 5.10). In this test series, the static shear stress equals 8.0 kgf/cm^2 (784 kPa), which is substantially higher than the steady state shear strength. Thus, both criteria are satisfied, and hence liquefaction occurs in all samples. Typical strain development with number of stress cycles for such samples is shown in Fig. 5.13.

Ottawa Sand

For Ottawa sand, minor effective consolidation stress σ'_{3c} of 2.0 kgf/cm^2 (196 kPa) and relative density after consolidation D_{rc} of 35.5% were used. Three series of tests with K_c ratios of 1.0, 1.5 and 2.0 were carried out. Similar method as used in preparing the tailings sand sample was employed to achieve samples with identical final density. Again, very consistent final relative density was obtained, with variation less than ±1.0% from the desired target. All initial sample states chosen would develop liquefaction under monotonic loading.

The results showing cyclic stress ratio $\sigma_{dcy}/2\sigma'_{3c}$ versus the number of stress cycles to develop liquefaction are shown in Fig. 5.14. The results for K_c = 1.19 obtained from previous studies by Chern (1981) are also shown in the figure. In contrast to the behaviour of tailings sand, all samples developed liquefaction, regardless of the K_c ratio.

For isotropically consolidated state, although the cyclic shear stress applied (0.18 kgf/cm^2) to one sample was less than the steady

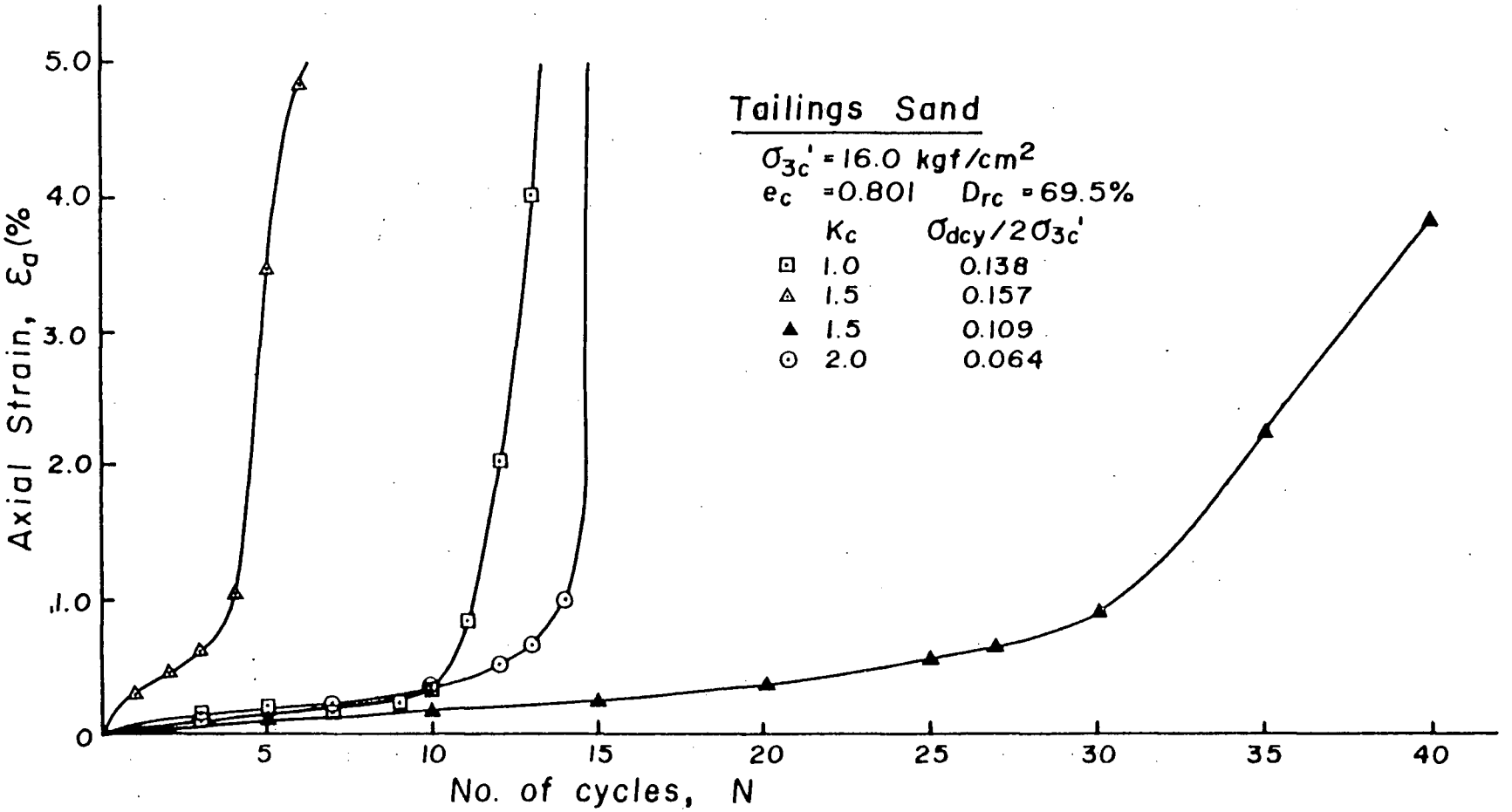

Fig. 5.13 Typical Strain development vs number of cycles for contractive tailings sand consolidated to various K_c ratios.

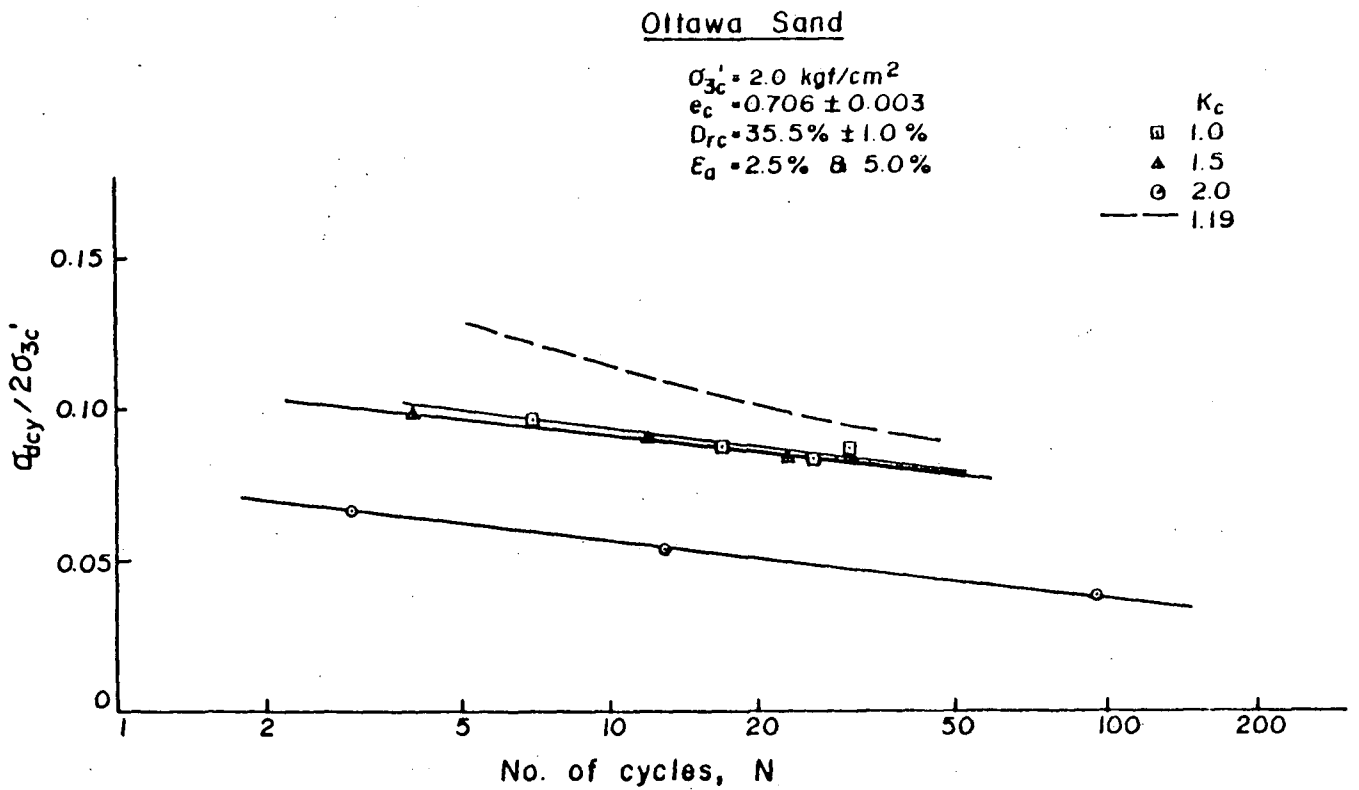

Fig. 5.14 Cyclic stress required to cause liquefaction for initially loose Ottawa sand consolidated to various K_c ratios.

state shear strength in compression (about 0.35 kgf/cm^2) at the chosen e_c, this cyclic shear stress was greater than the steady state shear strength in extension (less than 0.1 kgf/cm^2). Therefore, liquefaction occurred in extension mode. This is illustrated by the effective stress paths in Fig. 5.15. Typical strain development with the number of stress cycles is shown in Fig. 5.16.

As the K_c ratio increased to 1.19, although the static shear stress was less than the steady state shear strength in compression mode, the maximum shear stress (static + cyclic) was slightly larger than the steady state value. Therefore, liquefation occurred in compression mode. This is shown by the dashed line in Fig. 5.14. The corresponding strain development with the number of stress cycles is shown in Fig. 5.16.

For states with K_c ratios of 1.5 and 2.0, the static shear stresses were equal to or greater than the steady state shear strength in compression. Therefore, liquefaction occurred on the compression side in all cases.

From the results for both sands presented above, it may be concluded that both criteria must be met in order to develop liquefaction under cyclic loading. Liquefaction can not be induced if the maximum shear stress criterion in relation to steady state shear strength is not satisfied even though the sample has the potential to develop liquefaction. It will be shown in Section 5.2 that liquefaction can never be induced if the first criterion is not met, no matter what cyclic stress amplitude is applied. It should also be emphasized that these two criteria hold for liquefaction in compression as well as extension mode. Extension mode should be checked if cyclic loading results in significant shear stress reversal. In case both criteria are met in compression as well as

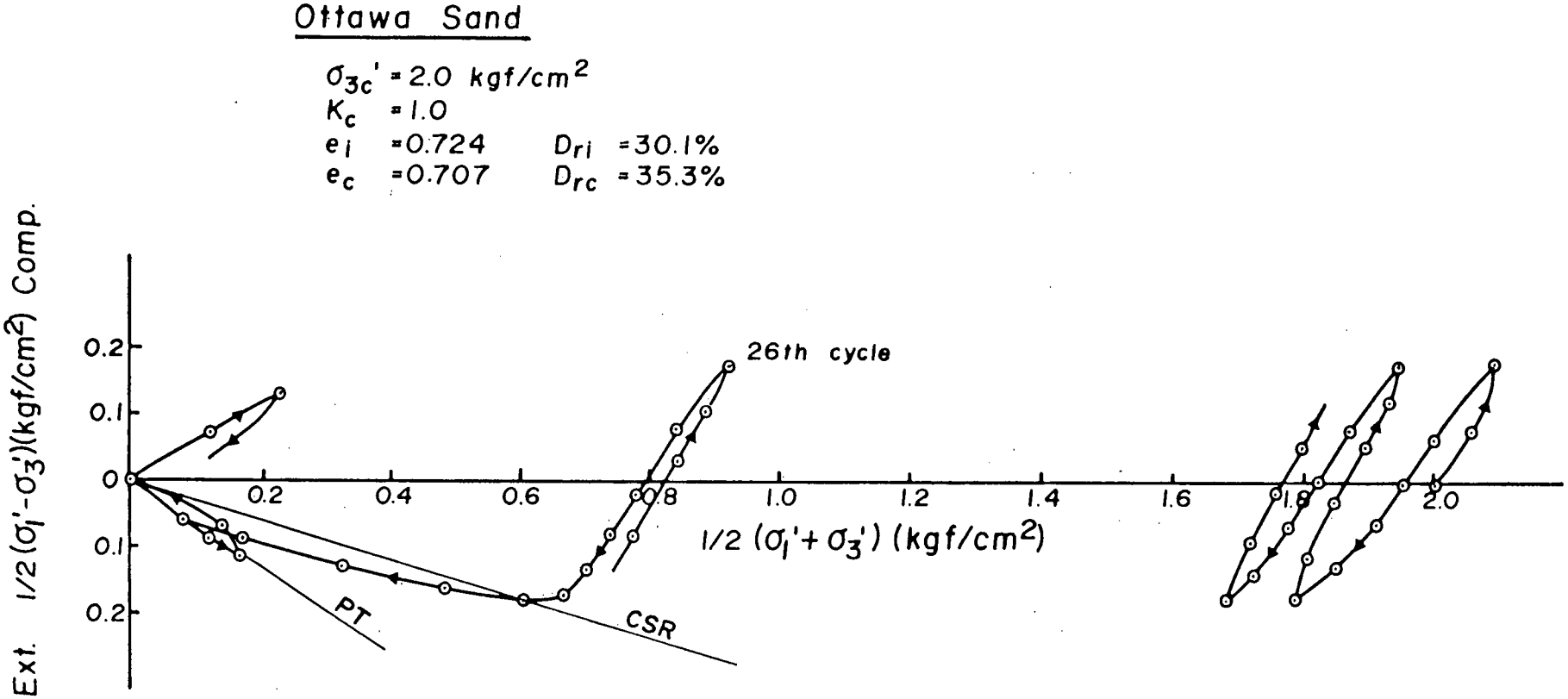

Fig. 5.15 Typical illustration of liquefaction of isotropically consolidated Ottawa sand under cyclic loading.

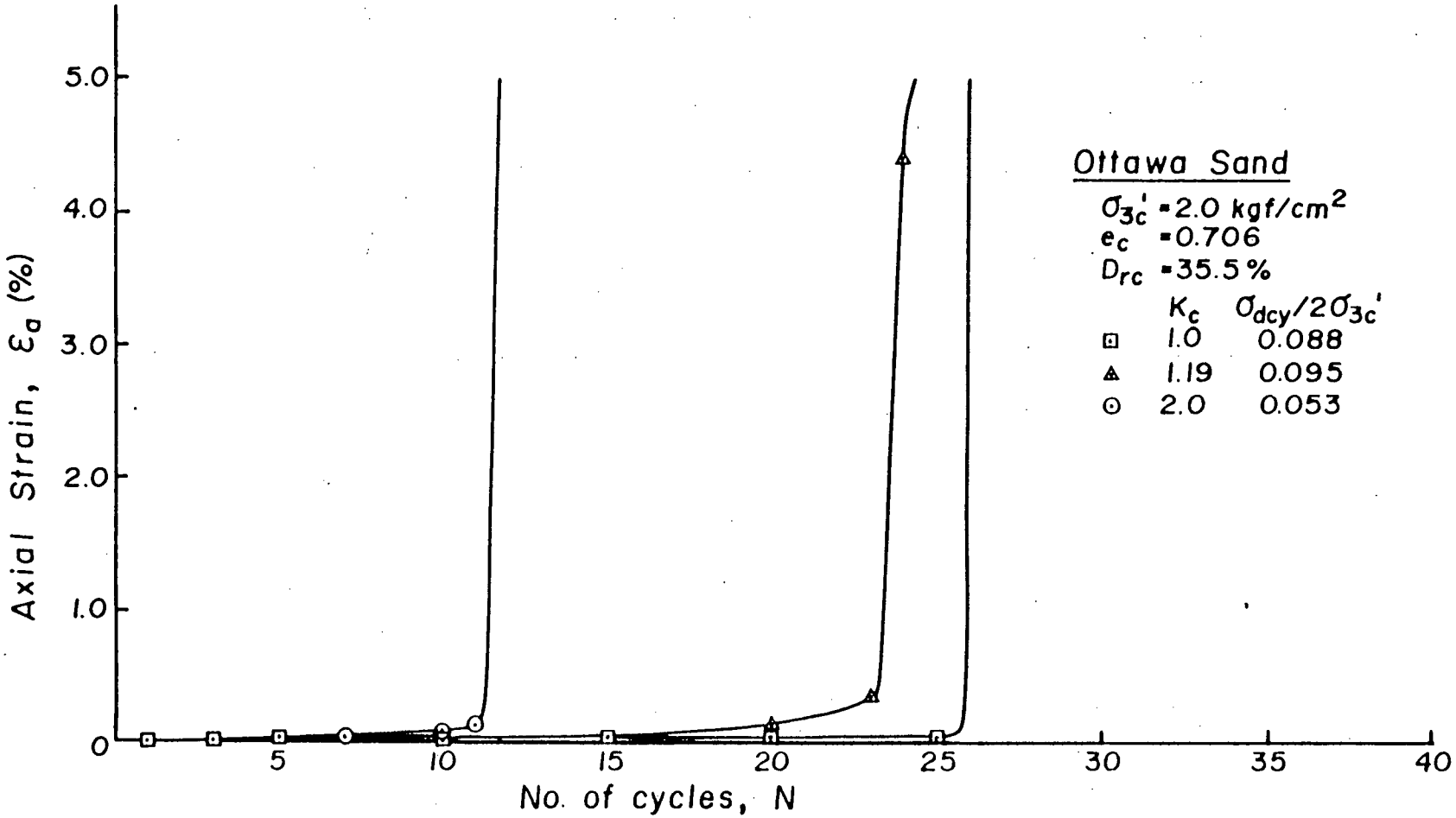

Fig. 5.16 Typical strain development vs number of cycles for initially loose Ottawa sand consolidated to various K_c ratios.

extension, liquefaction will always occur in extension mode due to a much lower CSR in extension as shown by test results in Section 4.2.2.

5.2 Cyclic Mobility Induced Under Cyclic Loading

It was shown in the previous section that a sand develops cyclic mobility if the shear stress criterion is not satisfied, even though the sand has the potential to develop liquefaction. In this section, it will be shown that a sand can develop only cyclic mobility if the steady state can not be achieved for the given initial state. A series of tests on both sands consolidated to initial sample states below the critical consolidation stress $(\sigma'_{1c})_{crit}$ surface will be used to illustrate this mechanism of strain development during cyclic loading. These results will also be used to illustrate the influence of various factors (e_c, σ'_{3c}, K_c) on the resistance to strain development under cyclic loading.

5.2.1 Strain Development Due to Cyclic Mobility

It was shown by Vaid and Chern (1983[2]) that dense Ottawa sand does not suffer liquefaction under cyclic loading. In such sand very small deformations are developed until the effective stress state of sand reaches the PT line. Significant amount of deformation is developed during the loading phase when the stress state crosses the PT line. Unloading thereafter causes large increase in pore pressure, bringing the sample close to the transient state of zero effective stress, but with very little change in deformation. Repetition of this phenomenon of stress state moving alternately into the region beyond the PT lines with cycles of loading ultimately results in a transient state of zero

effective stress, which is responsible for further accumulation of deformation. For tailings sand, typical stress-strain and pore pressure response and effective stress paths for isotropically and anisotropically consolidated samples are shown in Figs. 5.17 and 5.18. These two samples were consolidated to D_{rc} of 70% under σ'_{3c} of 2.0 kgf/cm^2 (196 kPa), such that their initial states lie well below the $(\sigma'_{1c})_{crit}$ surface. Therefore, the steady state can not be achieved, according to the results discussed in Chapter 4.

Isotropically consolidated sample (Fig. 5.17), accumulated very small deformation until its effective stress state reached the PT line. From the first cycle until 29th cycle of loading, the strain amplitude increased from 0.1% to 0.6% although the residual pore pressure reached 80% of the initial consolidation pressure. However, the application of 30th cycle of loading produced a disproportionate effect. The strain amplitude during this stress cycle increased to about 1.0%. The strain amplitude increased further from 1.0% to about 10% in the next eleven stress cycles. From the pore pressure response during the 30th cycle (Fig. 5.17b), it may be noted that sample showed a decrease in pore pressure when the maximum shear stress was reached (points 3 and 4). This feature is different from those observed in the previous loading cycles (e.g. points 1 and 2). The effective stress state at which the sample starts to dilate (decrease in pore pressure) was found to be essentially the same as the PT line obtained under monotonic loading. Thus, the attainment of PT state also signifies the onset of significant deformation of dilative sample during cyclic loading. It should be noted that the stress state at PT line moved closer and closer to the origin (Fig. 5.17c) as the cyclic loading continued. This concept of stress

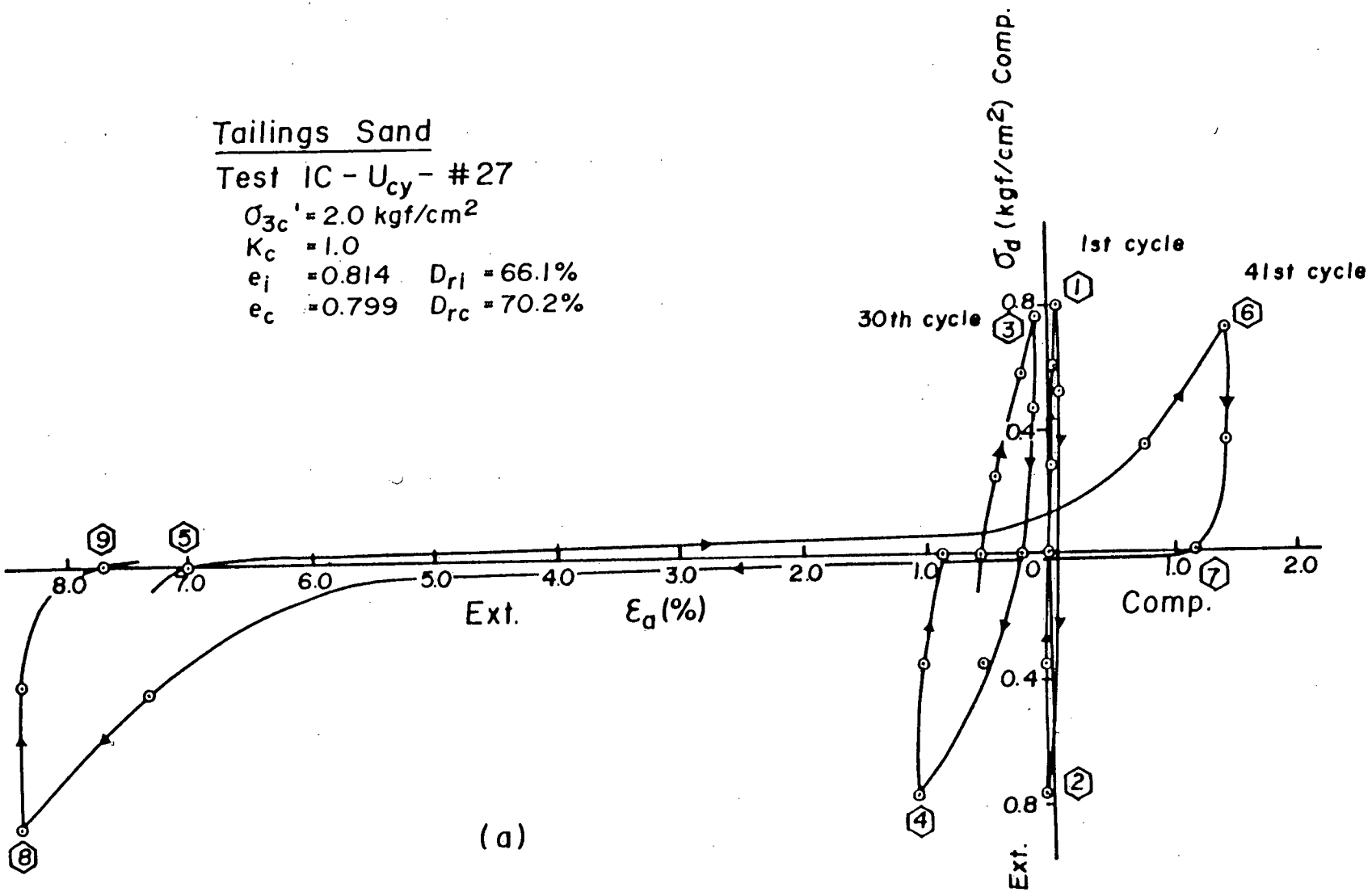

Fig. 5.17a Typical undrained cyclic loading behaviour of isotropically consolidated dilative tailings sand.

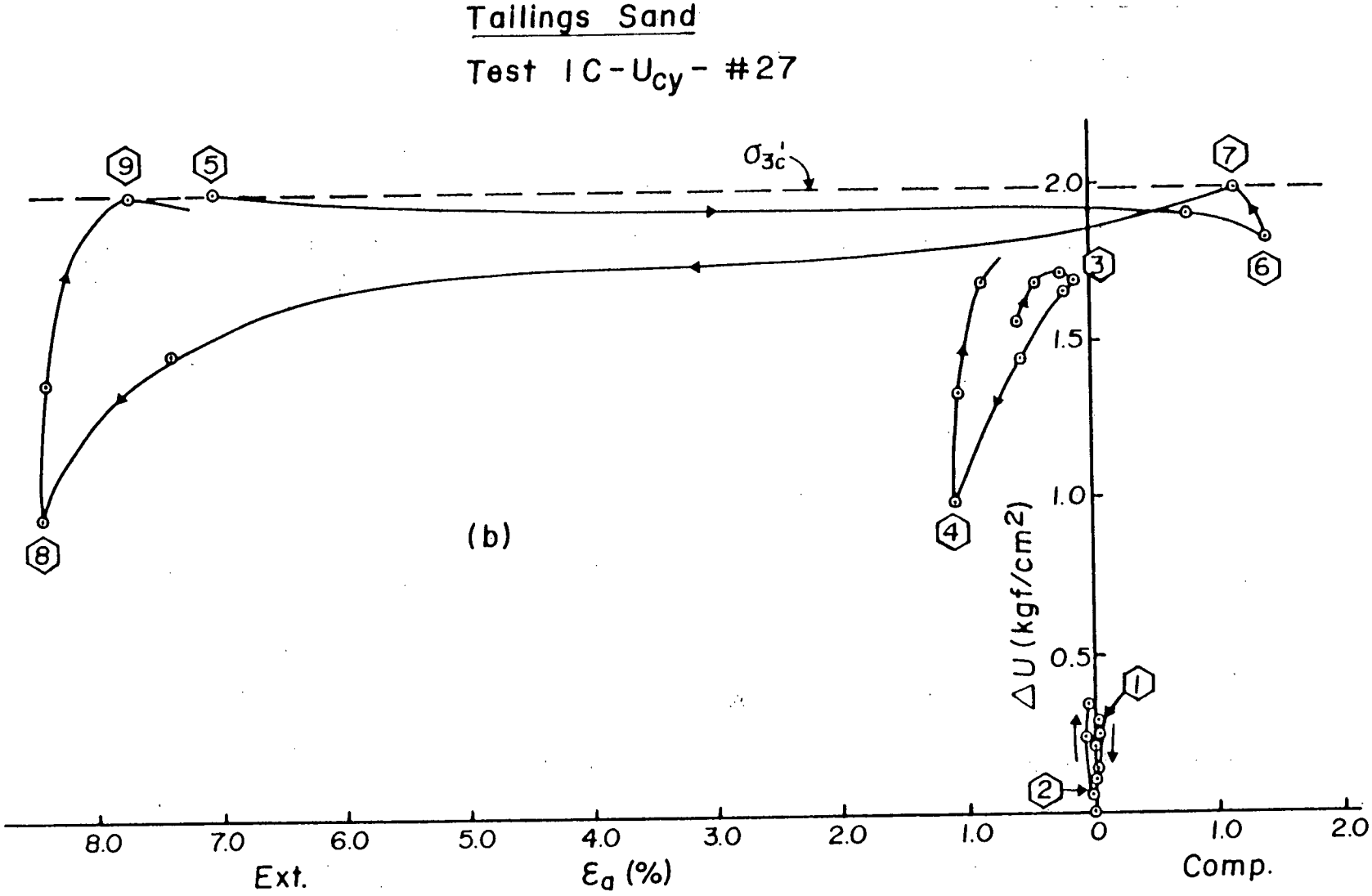

Fig. 5.17b Typical undrained cyclic loading behaviour of isotropically consolidated dilative tailings sand.

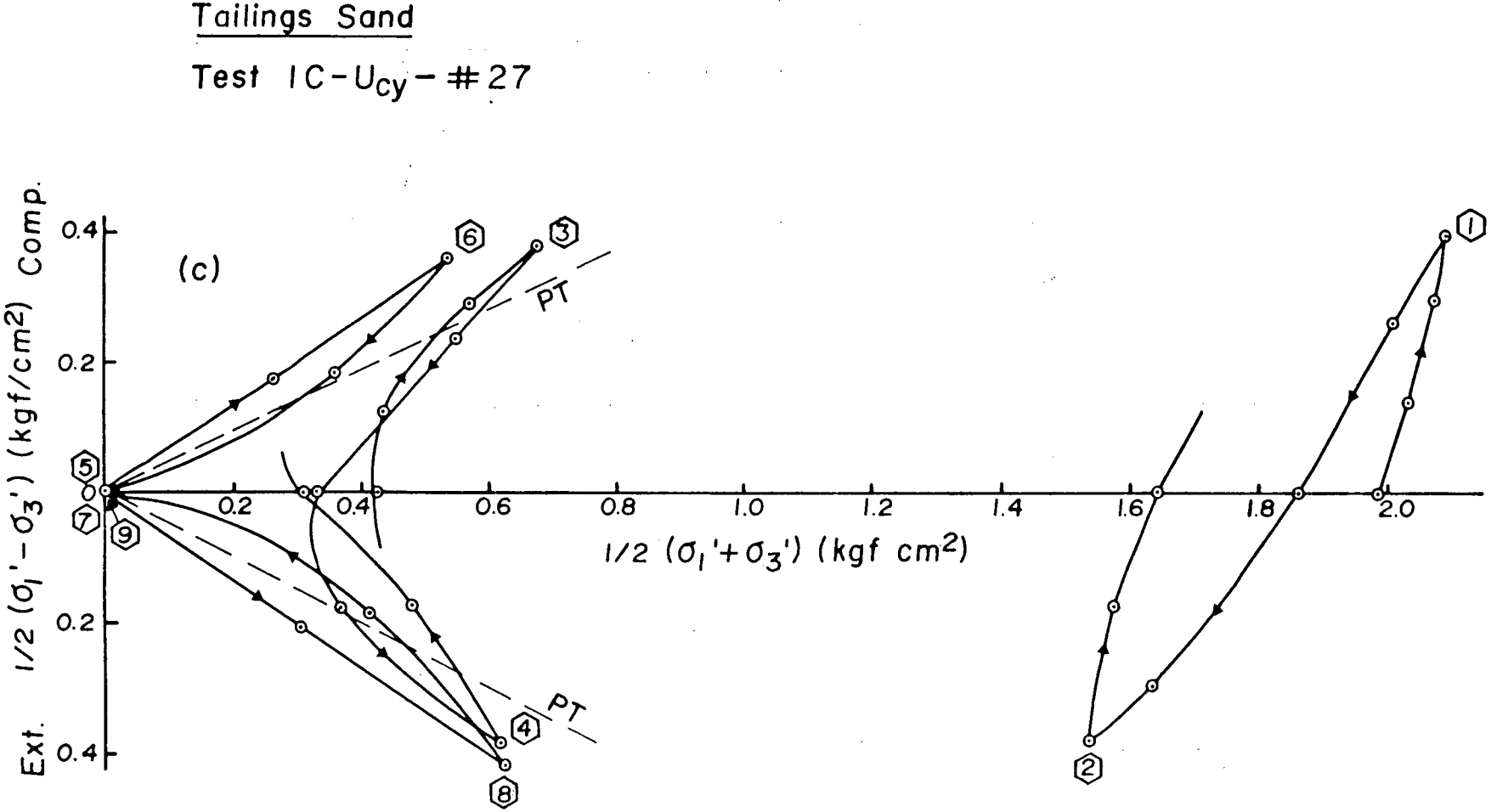

Fig. 5.17c Typical undrained cyclic loading behaviour of isotropically consolidated dilative tailings sand.

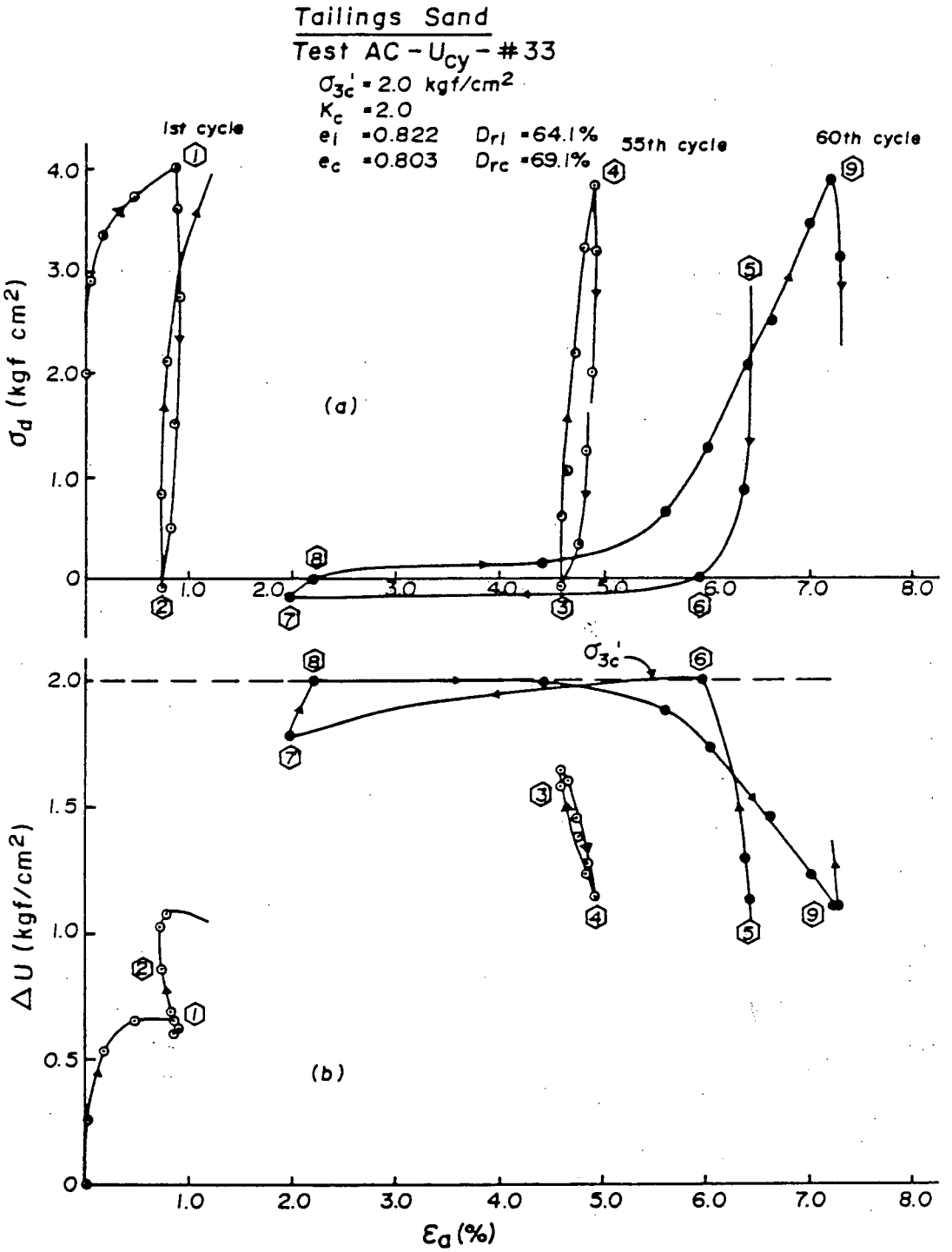

Fig. 5.18a,b Typical undrained cyclic loading behaviour of anisotropically consolidated dilative tailings sand.

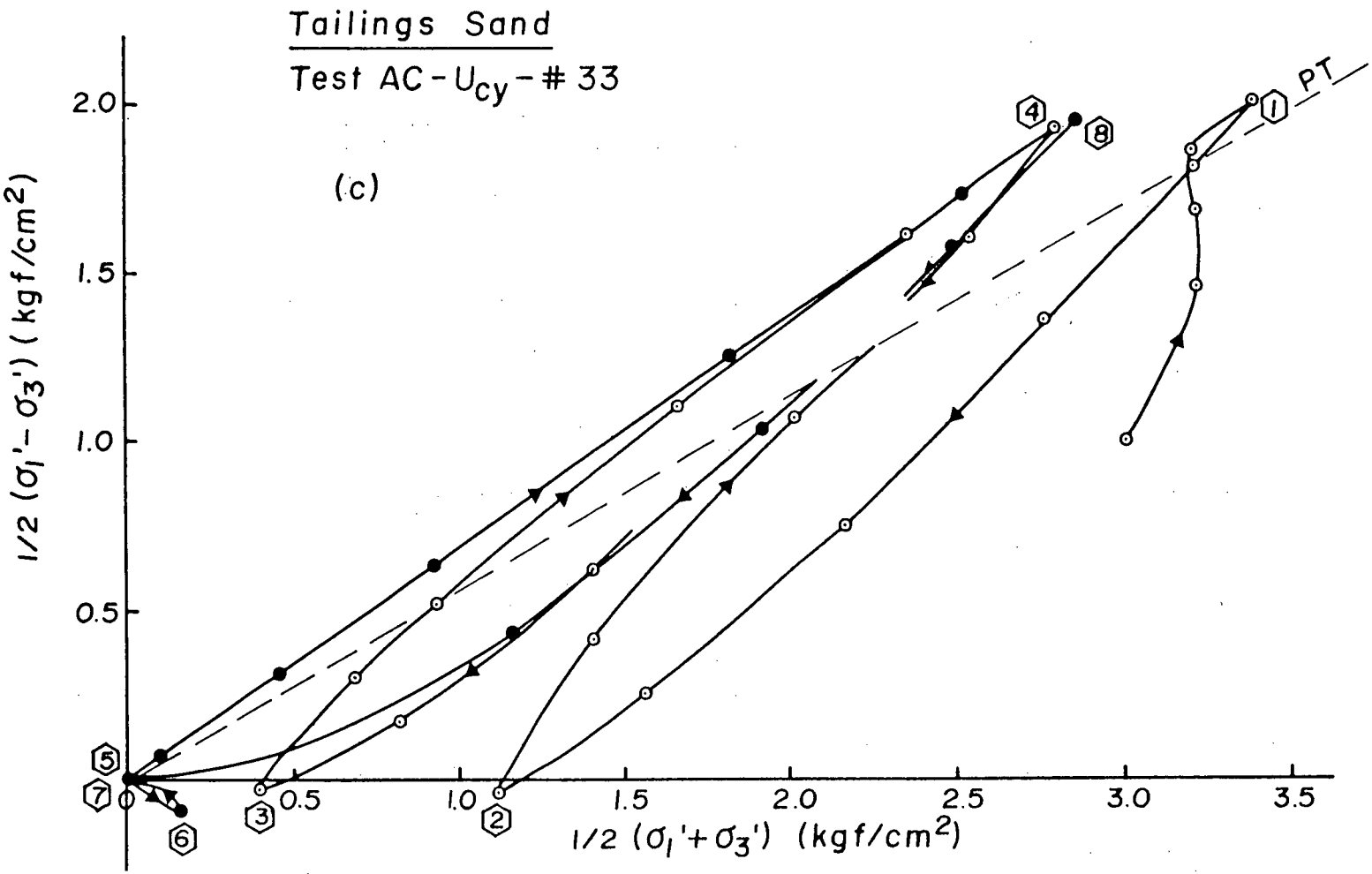

Fig. 5.18c Typical undrained cyclic loading behaviour of anisotropically consolidated dilative tailings sand.

path moving beyond the PT line in order to develop large deformation can still be applied when the transient state of zero effective stress is reached. Reloading in both the compression and extension regions caused dilation (points 5 to 6 and 7 to 8) with accompanying large deformation, particularly after attainment of transient states of zero effective stress. Unloading resulted in large increase in pore pressure (points 6 to 7 and 8 to 9) but with very little change in axial deformation.

For anisotropically consolidated sample (Fig. 5.18), the cyclic stress amplitude was selected so as to cause a slight amount of shear stress reversal. Significant amount of axial deformation was observed during the first cycle of loading. However, this deformation is not associated with liquefaction. The sample in fact dilated and showed a turnaround in effective stress path (Fig. 5.18c), a behaviour similar to that observed for dilative sand under monotonic loading. The effective stress ratio at the start of dilation (decrease in pore pressure) was found to be approximately the same as that of the PT line obtained before. Unloading of shear stress during the stress cycle caused increase in pore pressure with very little change in axial deformation (point 1 to 2). Reloading the sample beyond the PT line again caused significant amount of deformation and decrease in pore pressure. This behaviour is similar to that observed for isotropically consolidated sample once its stress state reached the PT line. However, due to only slight amount of shear stress reversal involved, the transient state of zero effective stress was never realized. Consequently, instead of deformations increasing with number of stress cycles, the accumulated deformations leveled off as the effective stress path got virtually stabilized with increasing cycles.

After 55 cycles of loading, the cyclic stress amplitude was increased slightly so as to cause 0.1 kgf/cm^2 (9.8 kPa) of shear stress reversal. The results of such loading cycles are shown by the data points in full dots in Fig. 5.18. In five additional stress cycles, the axial strain amplitude increased from 0.4% to 5.2% (Fig. 5.18a) and accumulated axial strain increased from 5% to more than 7%. Unloading of shear stress during the stress cycle caused the sample to reach the transient state of zero effective stress with very little change in deformation (points 5 to 6 and 7 to 8). On the other hand, loading caused the sample to develop large deformation with accompanying drop in pore pressure (points 6 to 7 and 8 to 9). This behaviour is similar to that observed for the isotropically consolidated case.

From the results presented above, it may be concluded that for dilative sand the deformation during cyclic loading is due to cyclic mobility instead of liquefaction associated with steady state deformation. Significant amount of strain can be developed only when the stress state reaches the PT line. Repetition of stress state moving into the region beyond the PT line is responsible for further accumulation of deformation. However, the rate of strain accumulation with number of stress cycles is generally slow if no shear stress reversal is involved. This has a very important implication on the effect of static shear stress on the resistance to strain development under cyclic loading, and will be discussed in Section 5.4.

The phenomenon of cyclic mobility was often attributed to the redistribution of water content within the test specimen during cyclic loading, especially in the case with shear stress reversal (Casagrande, 1975; Castro, 1969 and 1975; Castro and Poulos, 1977). It has been

argued that near the top of the specimen, the void ratio of sand increases, and near the bottom it decreases. Appearance of necking and bulging of samples under the top loading cap during cyclic loading has been advanced in support of this view. The pore pressure buildup and deformations measured in the laboratory were suggested to be due chiefly to the formation of such loose zone within the specimen. Hence the change in effective confining stress in state diagram during cyclic loading, such as shown in Fig. 5.19 for dilative sample, is considered fictitious in the sense that it represents average conditions. Therefore, the state point may not reach the condition of zero effective confining stress if the specimen were to remain uniform.

However, from the results shown above there is good direct and indirect evidence showing that this progressive softening may not be due to nonuniform deformation developed within the specimen. It has been shown in previous sections that progressive increase in pore pressure during cyclic loading causes very small strain until the stress state reaches the PT state (Fig. 5.17). Under this strain level, there is no evidence that redistribution of water content can take place within the specimen. Moreover, the progressive increase in pore pressure and deformations can also be induced if cyclic loading does not result in shear stress reversal, in which case the condition of transient zero effective stress (Fig. 5.18) never occurs - the condition which has been considered responsible for development of nonuniformities. Under this stress condition, densification in bottom part of the specimen and loosening in top part as suggested can not occur. It appears that necking can occur only in sample with nonuniform sample density or after very large strain has developed. By using the conventional procedures of

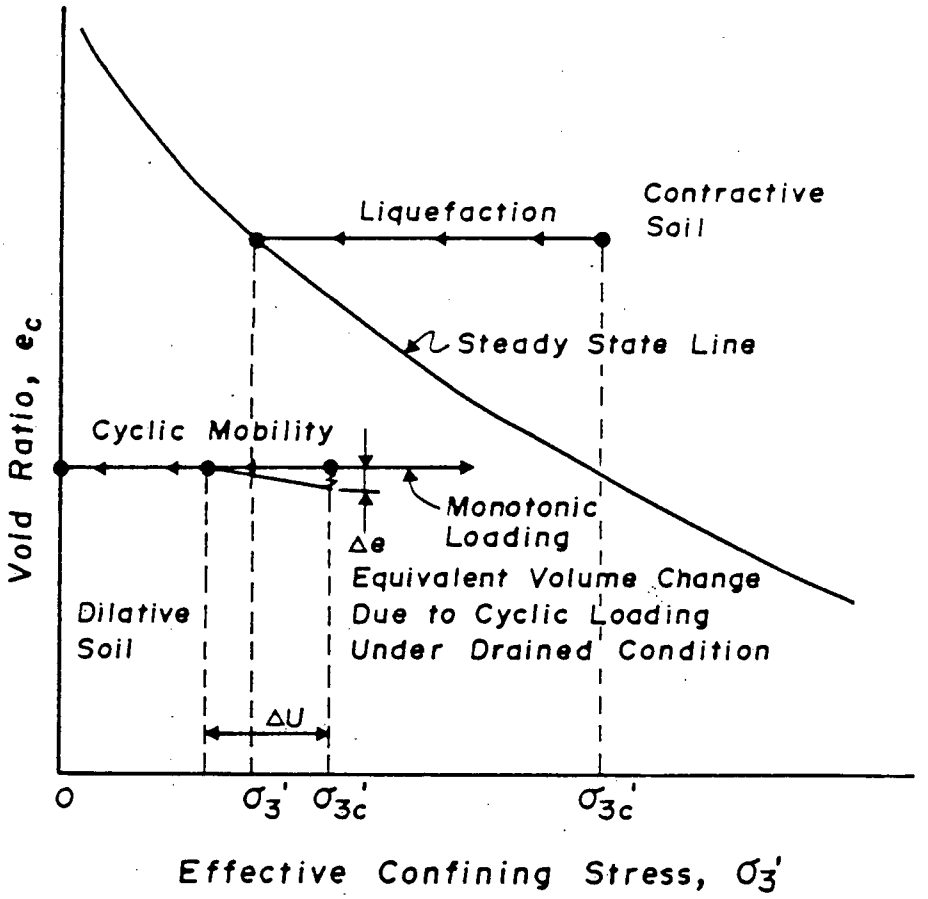

Fig. 5.19 Schematic illustration of monotonic and cyclic loading response of saturated sand in 2-D state diagram.

sedimentation and moist compaction, there is a tendency for reconstituted samples to achieve higher density in the bottom portion and lower density in the top. Consequently, in such specimens, nonuniform deformation tends to occur and reliable results may not be obtained. Therefore, it is very important to emphasize the sample formation techniques so as to yield sample with uniform density throughout. By using the improved sample preparation techniques described in Chapter 3, the sample did not develop necking even when the transient state of zero effective stress was reached.

It has been further inferred that dilative sand, which develops negative pore pressure after reaching PT state under monotonic loading (Fig. 5.19), can not develop progressive softening under cyclic loading similar to that of the contractive sample, if the specimen were to remain uniform (Castro and Poulos, 1977; Casagrande, 1975). As discussed in Chapter 4 and this chapter, dilation can occur only after the stress state reaches the PT line. Therefore, the development of negative pore pressure under monotonic loading is a behaviour after large deformation. However, cyclic loading behaviour is a small strain phenomenon until the stress state reaches the PT line. Therefore, dilative response after large deformations under monotonic loading (Fig. 5.19) does not imply that the same behaviour will occur under cyclic loading. It is well known that dense sample, which develops volume expansion under monotonic loading, causes volume reduction under cyclic loading. It has also been shown by Luong (1980) that cycling a sample under PT line causes volume reduction under drained conditions. Volume expansion can occur only when the sample is cycled in the region beyond PT line. Under undrained condition, this volume reduction results in rebound in soil structure to

the extent required to keep the volume constant. This may be illustrated by the schematic diagram in Fig. 5.19 proposed by Seed, Pyke and Martin (1975). This interplay of volume reduction and soil structure rebound results in build up of pore pressure as the cyclic stress application continues. Therefore, cyclic mobility is another class of problem under cyclic loading, and can occur in sand during earthquake loading.

5.2.2. Criteria to Cause Cyclic Mobility Under Cyclic Loading

It has been shown in Section 5.1.3 that sand with the potential to develop liquefaction, i.e., the steady state exists, will develop cyclic mobility if the maximum shear stress (static + cyclic) is less than the steady state shear strength. It was further shown in Section 5.2.1 that sand with initial state lying below the critical consolidation stress $(\sigma'_{1c})_{crit}$ surface, i.e., steady state can not be achieved, develops cyclic mobility only, regardless of the amplitude of cyclic load applied. Therefore, it may be concluded that sand with any condition that does not satisfy the criteria to cause liquefaction will develop only cyclic mobility. However, the criteria for liquefaction should be examined both in compression and extension regions if shear stress reversal is involved.

The above criteria for cyclic mobility to occur is verified by performing a series of tests on both sands consolidated below the $(\sigma'_{1c})_{crit}$ surface. These tests are discussed in the following section.

5.2.3. Test Results

A series of cyclic loading tests on samples consolidated to the same

e_c and σ'_{3c} but with various levels of K_c ratio were performed to examine the criteria for cyclic mobility to occur. The initial sample states were so chosen that the steady state can not be achieved in compression for both sands. For Ottawa sand, however, the steady state exists in extension mode at the chosen void ratio. These tests also serve to illustrate the importance of the mode of loading on undrained behaviour. Results from these test results will also be used later in section 5.4 to illustrate the influence of e_c, σ'_{3c} and K_c on the resistance to strain development under cyclic loading.

Tailings Sand

For tailings sand, the minor effective consolidation stress σ'_{3c} of 2.0 kgf/cm^2 (196 kPa) and relative density after consolidation D_{rc} of 70% were used. Three series of test with K_c ratio of 1.0, 1.5 and 2.0 were performed. Under these conditions, all initial sample states lie well to the left of the steady state lines (compression and extension). Hence the steady state can not be achieved in all cases.

The results of cyclic stress ratio $\sigma_{dcy}/2\sigma'_{3c}$ versus number of stress cycles to develop 2.5% axial strain for various K_c ratios are shown in Fig. 5.20. All samples developed cyclic mobility, regardless of the initial state of the sample and the amplitude of cyclic loads applied. Typical results of strain development versus number of stress cycles are also illustrated in Fig. 5.21.

Isotropically consolidated sample developed very small deformations until the stress state reached the PT line. The deformation increased rapidly thereafter due to development of transient state of zero effective stress (see Fig. 5.21).

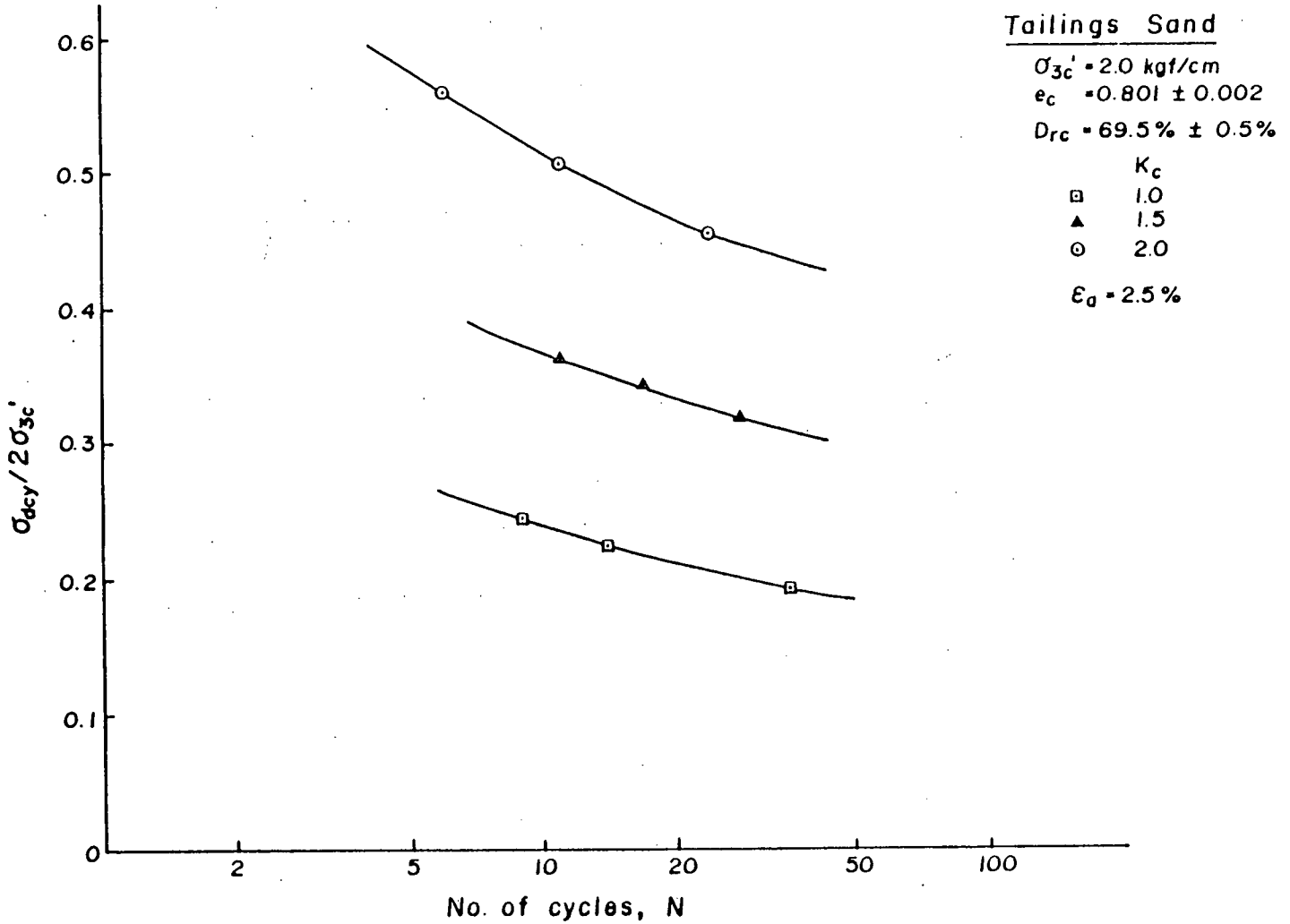

Fig. 5.20 Cyclic stress required to cause 2.5% axial strain for dilative tailings sand consolidated to various K_c ratios.

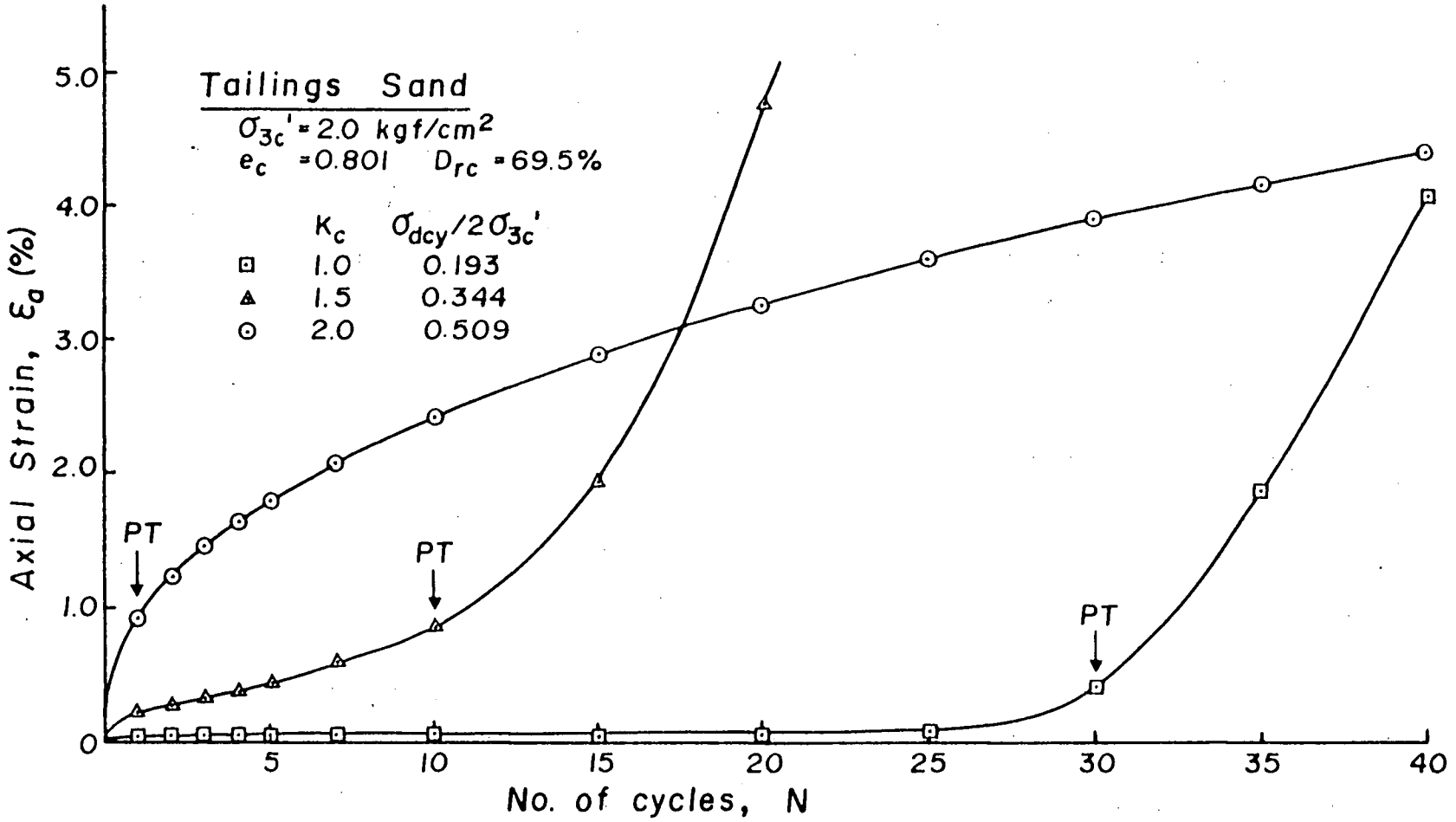

Fig. 5.21 Typical strain development vs number of cycles for dilative tailings sand consolidated to various K_c ratios.

For anisotrpically consolidated samples with K_c = 1.5, the strain development is similar to that for the isotropically consolidated case, except that the initial strain accumulation until the stress state reached the PT line is larger (Fig. 5.21). This may be due to the presence of initial static shear bias and much larger cyclic load applied. A small amount of strain was induced whenever the total shear stress approached its maximum value causing a small strain accumulation after each cycle of loading.

For sample with K_c = 2.0, the strain accumulation is quite different from the other two cases. Relatively large strain was developed during the first cycle of loading. This was due to the fact that the initial effective stress ratio was high. During the loading phase of the first stress cycle, the stress state reached the PT line and thus a rapid accumulation of strain was observed from the beginning of the test. However, the rate of strain accumulation decreased gradually because states of transient zero effective stress, necessary for rapid strain accumulation, did not occur due to no shear stress reveral. The sample accumulated 2.5% axial strain in 10 stress cycles, and it took another 45 cycles to accumulate additional 2.5% axial strain.

For sample with the same e_c but under higher confining pressure, it was shown in Section 5.1.4 that only cyclic mobility is developed when the maximum shear stress is less than the steady state shear strength. For such initial states the relationships between cyclic stress ratio versus number of stress cycles to develop 2.5% axial strain for K_c = 1.0 and 1.25 were shown in Fig. 5.10. Trends similar to those observed under low confining pressure (Fig. 5.20), i.e., increasing $\sigma_{dcy}/2\sigma'_{3c}$ with increasing K_c ratio, may be observed even under higher levels of

confining pressure.

Ottawa Sand

For Ottawa sand, minor effective consolidation stress σ'_{3c} of 2.0 kgf/cm^2 (196 kPa) and relative density after consolidation D_{rc} of 51.5% were used. Three series of test with K_c ratio of 1.0, 1.5 and 2.0 were performed. Under these conditions, the initial sample states lie below the steady state line in compression. Therefore, the steady state can not be reached in compression mode for these samples. However, it will be shown later that steady state in extension can be reached for these samples.

It was found that all samples developed cyclic mobility except the one with K_c = 1.0 which developed liquefaction in extension mode. The results of cyclic stress ratio $\sigma_{dcy}/2\sigma'_{3c}$ versus number of stress cycles to develope 2.5% axial train due to cyclic mobility or liquefaction in extension mode are shown in Fig. 5.22. The results for K_c = 1.19, which are interpolated from a previous study by Chern (1981), are also presented in the figure. The results for both liquefaction and cyclic mobility are presented here in order to facilitate discussion of the criteria for occurrence of cyclic mobility and liquefaction. Typical results of strain development versus number of stress cycles for these tests are shown in Fig. 5.23.

For isotropically consolidated sample, the cyclic stress applied exceeded the steady state shear strength in extension. Therefore, liquefaction occurred in extension mode. This illustrates the importance of examining the existence of steady state both in compression and extension

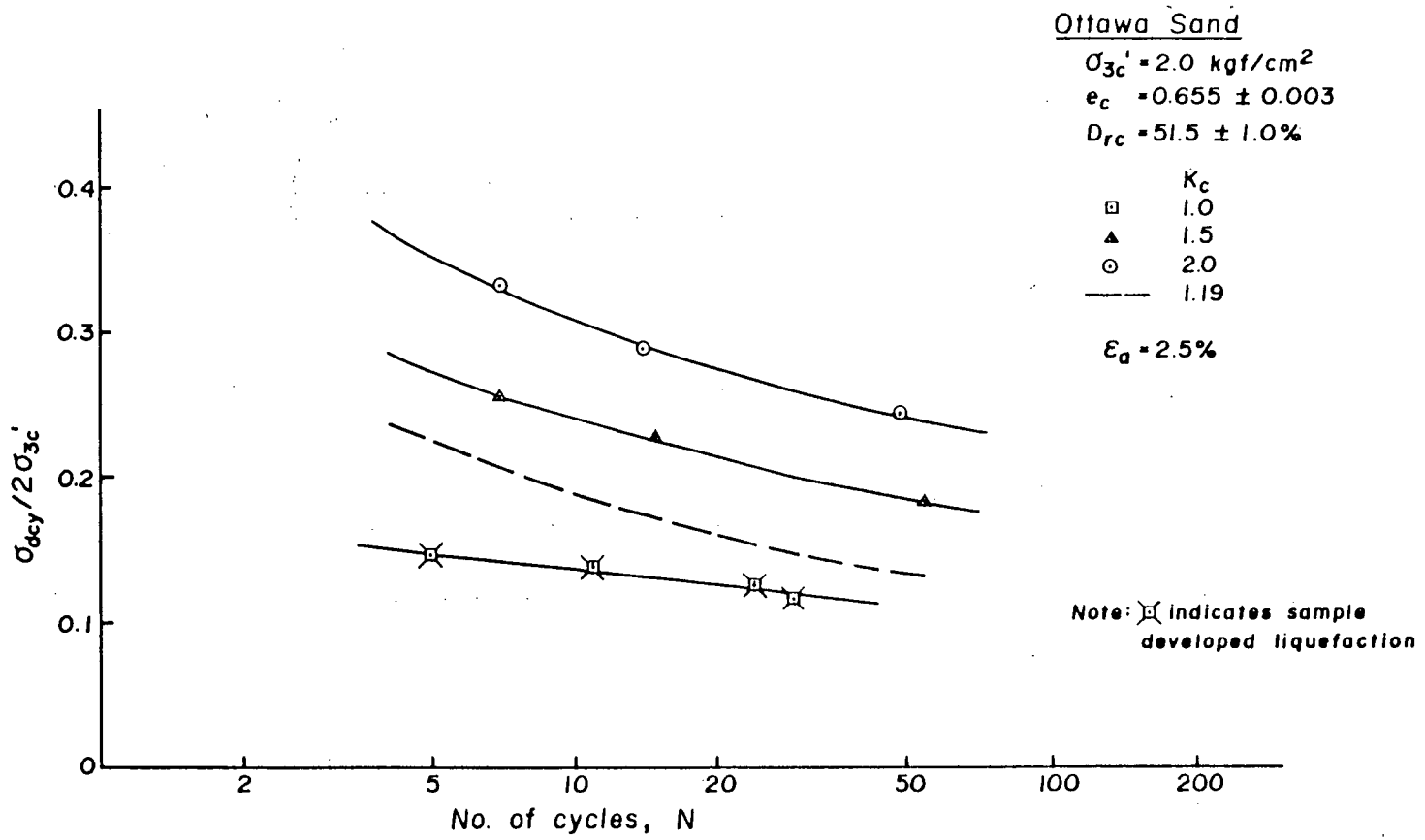

Fig. 5.22 Cyclic stress required to cause 2.5% axial strain for medium dense Ottawa sand consolidated to various K_c ratios.

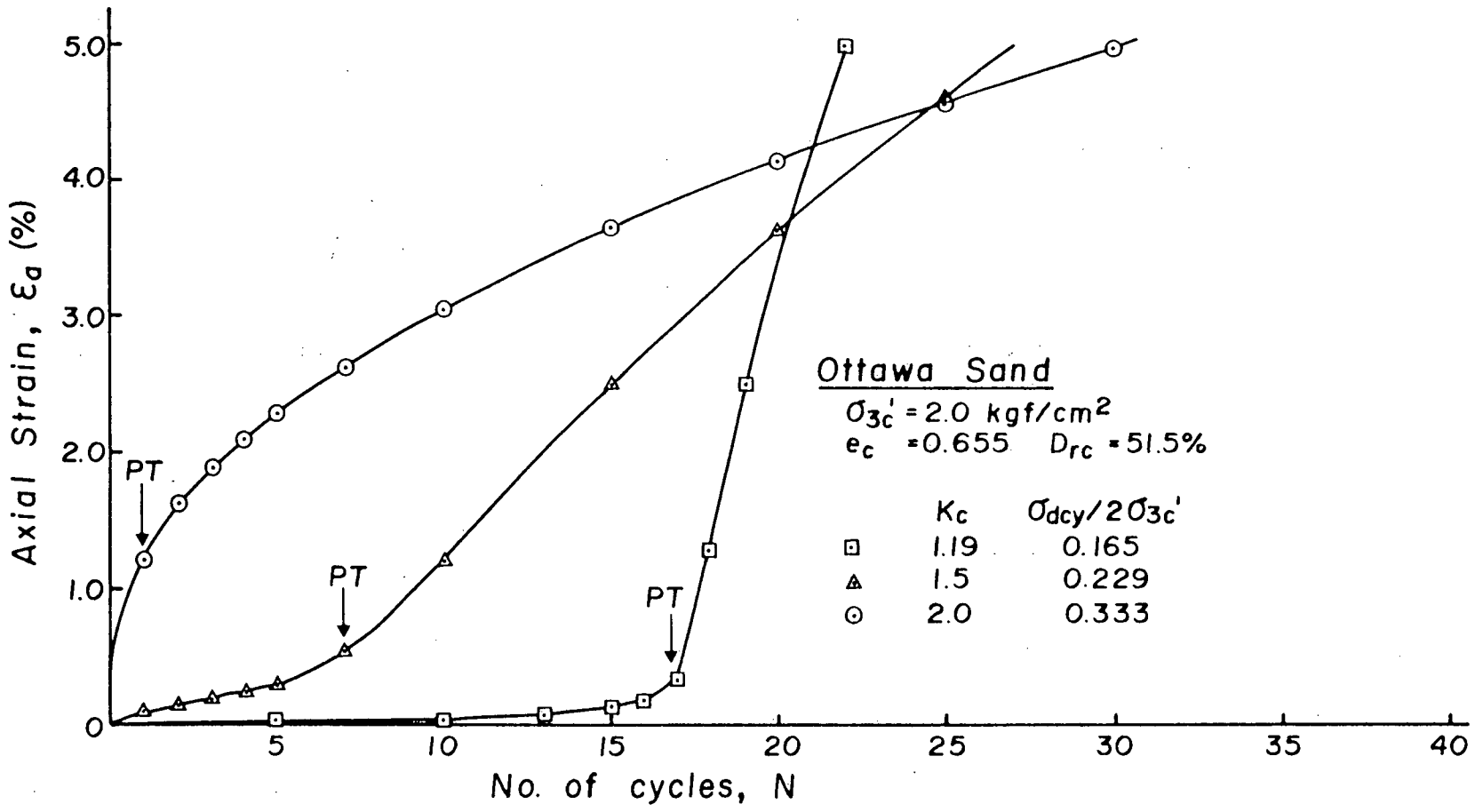

Fig. 5.23 Typical strain development vs number of cycles for medium dense Ottawa sand consolidated to various K_c ratios.

modes, if significant amount of shear stress reversal is involved.

All anisotropically consolidated samples (K_c = 1.19, 1.5 and 2.0) developed cyclic mobility (Fig. 5.22). The strain development versus number of stress cycles (Fig. 5.23) is similar to that for the tailings sand with similar K_c ratios. Accelerated increase in axial deformation was observed only if transient state of zero effective stress occurred after the sample state crossed the PT line. For the case with no shear stress reversal (K_c = 2.0), large deformation was developed in the first loading cycle when the stress state reached the PT line. However, the strain accumulation slowed down in the subsequent cycles because no transient state of zero effective stress developed for the cyclic load amplitude applied.

5.3 Resistance to Strain Development Under Cyclic Loading

It has been shown in the previous sections that large cyclic and residual strains are developed once the sand develops liquefaction or cyclic mobility particularly after reaching the transient state of zero effective stress. In the case of no shear stress reversal, the sand can never reach the condition of zero effective stress under cyclic loading. Nevertheless, large undesirable deformation could accumulate. If liquefaction develops, large deformations are inevitable. Hence, the accumulated strain is often used as the failure critierion against cyclic loading. The strain level considered as failure depends on the type and relative importance of the earth structure considered.

The accumulation of strain during cyclic loading may be due to liquefaction or cyclic mobility or a combination of both. Because of

different strain development mechanism in liquefaction and cyclic mobility, the influence of factors (e_c, σ'_{3c}, K_c) on the resistance to strain development under cyclic loading is likely to be influenced by the mechanism of deformation as well as the strain level of interest.

If liquefaction occurs, relatively large deformation (at least 2.5% axial strain for the sands tested) will be developed, once the liquefaction is induced. Therefore, if 2.5% axial strain development were used as the failure criterion, occurrence of liquefacton could be considered as failure. However, if higher strain level were specified, then the total strain to fialure could be the combination of liquefaction and cyclic mobility following liquefaction. Such a case may be seen from the strain development versus number of stress cycles for the tailings sample with K_c = 1.5 and cyclic stress ratio of 0.157 in Fig. 5.13. The sand accumulated about 3.5% axial strain at the end of stress cycle in which liquefaction developed. Further accumulation of strain was slowed down and only $1^{1/2}$% additional strain developed in the next stress cycle. Similar features of strain accumulation due to cyclic mobility following liquefaction may be seen in Figs. 5.1b and 5.2c. Due to the combination of these two mechanisms for development of specified level of strain, the influence of factors, e.g., static shear, on the resistance to strain development under cyclic loading may be different depending on whether liquefaction only or cyclic mobility only develops. It should be noted that 2.5% axial strain due to liquefaction is for the limiting case when total shear stress is slightly greater than the steady state shear strength. When total shear stress is considerably larger than the steady state strength, much larger deformation will be developed. This may be seen from the strain development due to liquefaction in Figs. 5.13 and

5.16.

For sand with state in the transition region (Fig. 4.17), the strain potential due to strain softening is very small. It is conceivable that the strain developed due to strain softening under cyclic loading would be very small as well. Thus, the strain development for such initial states may be regarded as due mainly to cyclic mobility.

5.4 Influence of Certain Factors on the Undrained Cyclic Loading Behaviour

The most important factors which influence the undrained cyclic loading behaviour of sand are void ratio, confining pressure and static shear stress. The role of these factors on the undrained cyclic loading behaviour of sands will be discussed in this section.

5.4.1 Void Radio or Relative Density

Most of the knowledge on undrained cyclic loading behaviour of saturated sand has been derived from studies on natural rounded sands. It is generally believed that relative density is the most important factor controlling occurrence of liquefaction and cyclic mobility. Sand with relative density less than about 40% has been suggested to always develop liquefaction, whereas sand with relative density greater than about 45% cyclic mobility, without reference to the particle characteristics and initial stress condition of the sand. It will be shown in the following that this may be a good approximation for rounded sand, but may not be true for angular sand.

Consider the effective stress state plot of the 3-D effective stress

state diagram at a constant void ratio as shown in Fig. 4.31b. From the consolidation characteristics of sand, it was noted that the sand can be consolidated to this void ratio by various combination of initial void ratios e_i and consolidation stress conditions σ'_{3c} and K_c. The sand with initial state to the left of the $(\sigma'_{1c})_{crit}$ = constant line has no possibility to develop liquefaction. It can only develop cyclic mobility except in a small transition region immediately to the left of $(\sigma'_{1c})_{crit}$ = constant line which may develop slight strain softening followed by cyclic mobility. On the other hand, sand with initial state on or to the right of $(\sigma'_{1c})_{crit}$ = constant line can develop liquefaction if the cyclic stress applied is large enough to cause total shear stress greater than its steady state shear strength. Occurrence of these phenomena was illustrated by cyclic tests on samples with the same void ratio in Figs. 5.10 and 5.20. It may be noted that all samples under low confining pressure (Fig. 5.20) developed cyclic mobility, whereas samples under high confining pressure could develop liquefaction if the shear stress criterion for liquefaction is satisfied. It may also be noted from Fig. 5.1c that liquefaction can be induced in samples with very high relative density (more than 85%) if the consolidation stresses are high enough.

For Ottawa sand with rounded particles the relative density seems to be the most important factor controlling the undrained cyclic loading behaviour for the range of consolidation stresses considered herein. For sample with initial relative density larger than about 45%, the steady state can not be achieved even under high confining pressure, and hence liquefaction is not expected under cyclic loading at least in the compression mode. However, for initially looser samples, liquefaction does occur under the same range of consolidation stresses.

Therefore, for sand with rounded particles the relative density gives a good indication as to the undrained cyclic loading behaviour since a limiting value of D_{ri} alone will suffice to separate regions of liquefaction and cyclic mobility. However, for sand with angular particles, specifying the void ratio or relative density alone without reference to the associated consolidation stress conditions is not sufficient to ascertain whether liquefaction or cyclic mobility will develop during cyclic loading.

The influence of void ratio or relative density on the occurrence of liquefaction is that increasing the relative density increases the critical consolidation stress $(\sigma'_{1c})_{crit}$ in order to have the possibility to develop liquefaction. This is shown by the increasing of $(\sigma'_{1c})_{crit}$ with decreasing void ratio in the 3-D effective stress state diagram (Fig. 4.31).

5.4.2. Confining Pressure

Even specifying e_c and σ'_{3c} for a sand is still insufficient for a prediction of the undrained cyclic loading behaviour with repsect to development of liquefaction or cyclic mobility. This may be illustrated by two samples with the same void ratio and confining pressure but with different K_c ratios (Samples G and B in Fig. 4.31b). For Sample G, the steady state can not be achieved, and hence liquefaction can not be developed. For Sample B, however, the steady state can be achieved, and liquefaction can be developed if the cyclic load is large enough to cause maximum shear stress greater than the steady state shear strength for the void ratio under consideration. This is also true when the initial sample state at G is to the right of the $(\sigma'_{1c})_{crit}$ = constant line. Such

a behaviour is illustrated by the test results shown in Fig. 5.10. Cyclic mobility occurred in samples with low K_c ratio, whereas liquefaction developed in samples with high K_c ratio even though they had identical e_c and σ'_{3c}. Furthermore, the occurrence of liquefaction depends on the amplitude of cyclic load applied. This is apparent from the undrained behaviour of sand with K_c = 1.5 in Fig. 5.10 in which the lowest level of cyclic stress amplitude caused cyclic mobility instead of liquefaction at higher stress amplitudes.

For Ottawa sand, however, as discussed in the previous section, the initial relative density appears to be the most important factor controlling the occurrence of liquefaction and cyclic mobility for the range of consolidation stress considered herein.

The effect of level of confining pressure on the undrained cyclic loading behaviour not only dictates the occurrence of liquefaction or cyclic mobility as discussed above, but also influences the resistance to strain development under either type of response. This may be illustrated by the response of samples with the same void ratio and K_c ratio but different confining pressures (Fig. 5.24).

For samples in the dilative region (D_1 and D_2), only cyclic mobility can be developed. An increase in confining pressure always results in increasing contractive tendency. Therefore, for the same cyclic stress ratio applied, the sample under higher confining pressure will show a faster pore pressure buildup with cycles of loading and reach the PT line earlier than that under lower confining pressure. Therefore, the resistance to strain development will always decrease with increasing confining pressure. Evidence for this argument may be seen from the cyclic loading test results shown in Figs. 5.10 and 5.20. For each K_c

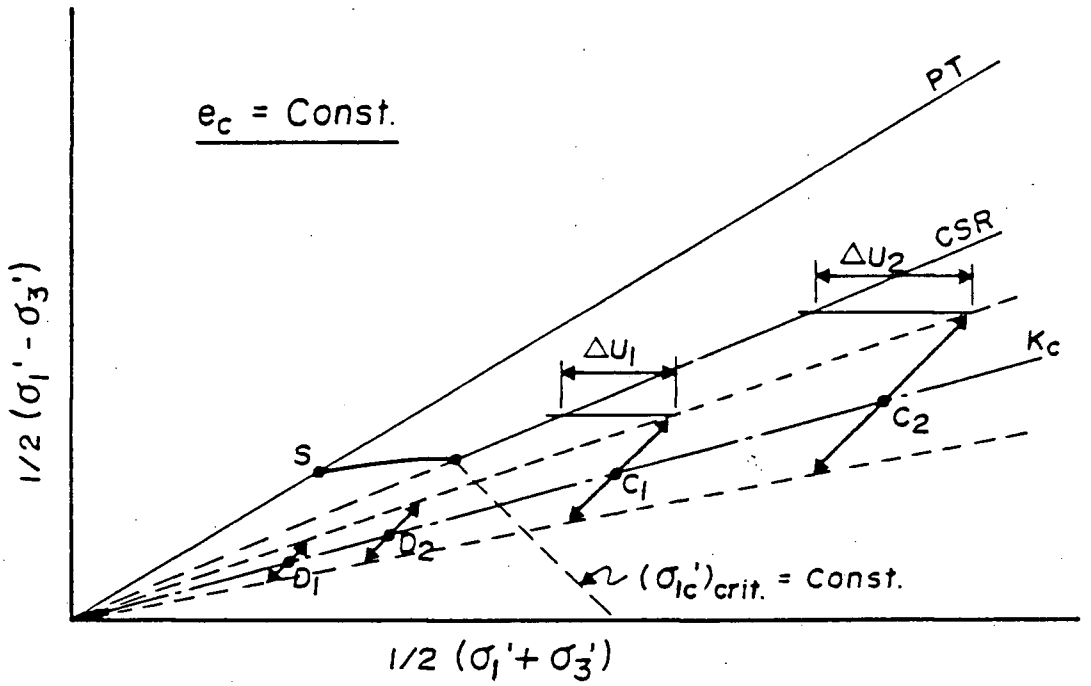

Fig. 5.24 Influence of confining pressure on the resistance to strain development under cyclic loading.

value for which cyclic mobility developed, the resistance curve $\sigma_{dcy}/2\sigma'_{3c}$ vs N for lower confining pressure is located higher than that for higher confining pressure. This reduced resistance to strain development due to increasing confining pressure has also been observed by Vaid, Chern and Tumi (1983) for both angular and rounded sands. In their investigation, sands were tested under simple shear conditions with no static shear and initial sand states which gave rise to only cyclic mobility.

For samples in the contractive region (C_1 and C_2 in Fig. 5.24), liquefaction will be developed, as discussed before. In this region, two aspects of the influence of the level of confining pressure may be noted. Firstly, due to the uniqueness of CSR, the pore pressure ratios $\Delta u/\sigma'_{3c}$ required to reach the CSR line will be the same under the same cyclic stress ratio. However, due to the increased contractive tendency under higher confining pressure in Sample C_2 than Sample C_1, it is conceivable that Sample C_2 will reach the CSR line faster (less number of cycles) than Sample C_1. In other words, the resistance to liquefaction ($\sigma_{dcy}/2\sigma'_{3c}$ required to reach CSR line in a fixed number of cycles) will be decreasing with increasing confining pressure. Secondly, the potential to develop steady state deformation and the associated loss in shear resistance for sample under higher confining pressure is always higher than the one under lower confining pressure due to the uniqueness of steady state strength (Fig. 5.24). Therefore, for sand under higher confining pressure not only the liquefaction is easier to be induced but also the deformation associated with liquefaction and the loss in shear resistance is more severe than those under lower confining pressure.

5.4.3 Static Shear Stress or Consolidation Stress Ratio

For sand with a given e_c and σ'_{3c}, increasing K_c ratio may transform the undrained cyclic loading behaviour of sand from cyclic mobility under low K_c ratio to liquefaction under high K_c ratio. This has been shown in earlier Fig. 5.10. Therefore, in order to predict the undrained cyclic loading behaviour of a sand sample, the shear stress component at the end of consolidation has to be considered in addition to the void ratio and confining pressure. In this regard the 3-D effective stress state diagram developed under monotonic loading conditions, together with the amplitude of cyclic loading imposed provides a complete description as to the expected mechanism of strain development during undrained cyclic loading of saturated sand.

Similar concept can also be used for Ottawa sand with rounded particles, with the difference that initial relative density may suffice to predict the existence of steady state for the range of consolidation stress considered herein.

The influence of static shear or K_c ratio on undrained cyclic loading behaviour may be illustrated more clearly by plotting the resistance to strain development ($\sigma_{dcy}/2\sigma'_{3c}$ required to cause $2^{1/2}$% and 5% axial strain in 10 cycles) at fixed values of D_{rc} and σ'_{3c} as a function of K_c ratio. Such test results for tailings sand are shown in Fig. 5.25a at D_{rc} = 69.5% and σ'_{3c} = 2.0 kgf/cm^2 (196 kPa) and in Fig. 5.26a at D_{rc} = 70% and σ'_{3c} = 16.0 kgf/cm^2 (1568 kPa). Similar results for Ottawa sand at σ'_{3c} = 2.0 kgf/cm^2 but different relative densities (51.5% and 35.5%) are shown in Figs. 5.25b and 5.26b. Because of the different mechanisms of strain development, the influence of static shear on the undrained cyclic loading behaviour should be considered separately in the

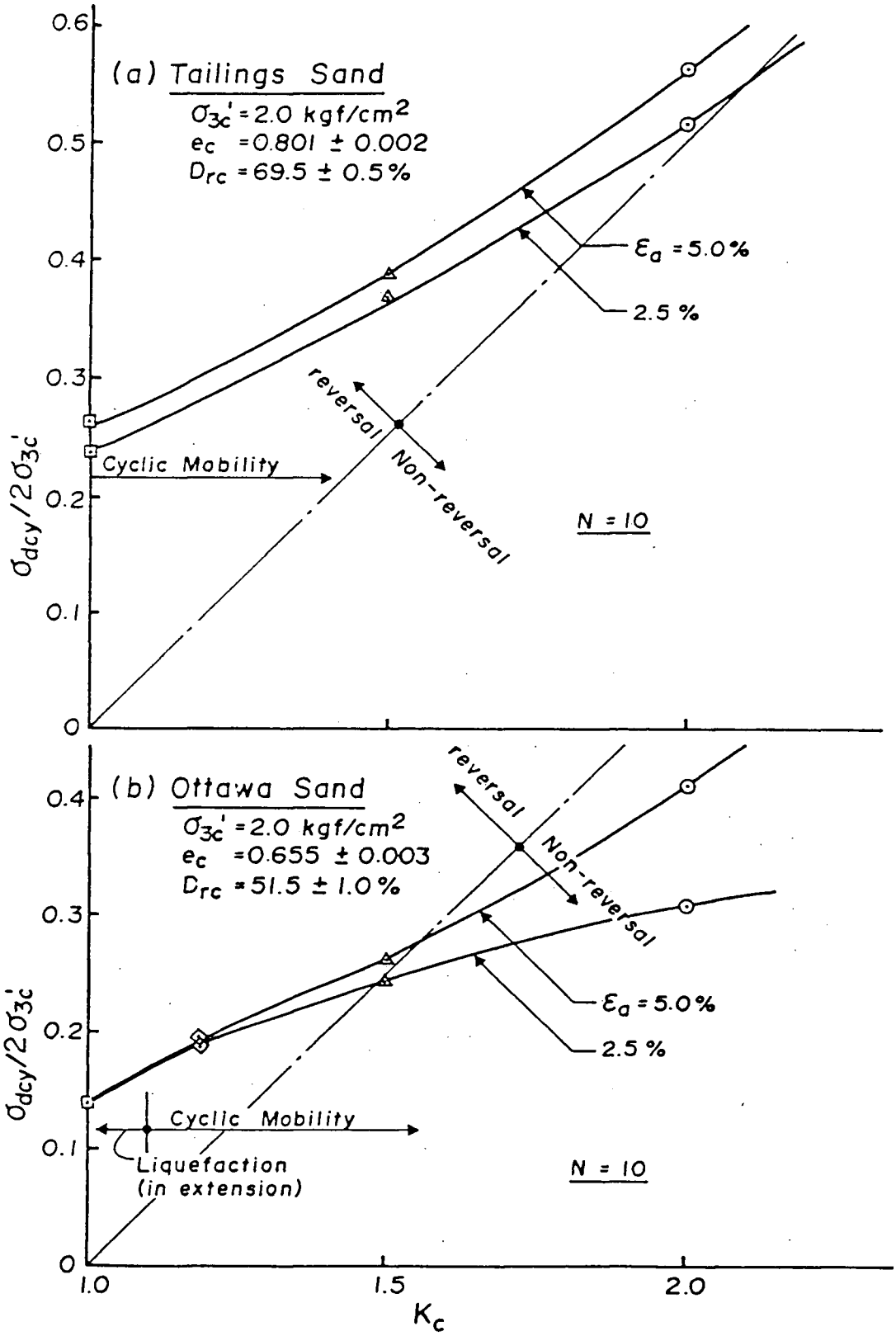

Fig. 5.25 Influence of static shear stress on the resistance to strain development under cyclic loading: (a) dilative tailings sand; (b) initially medium dense Ottawa sand.

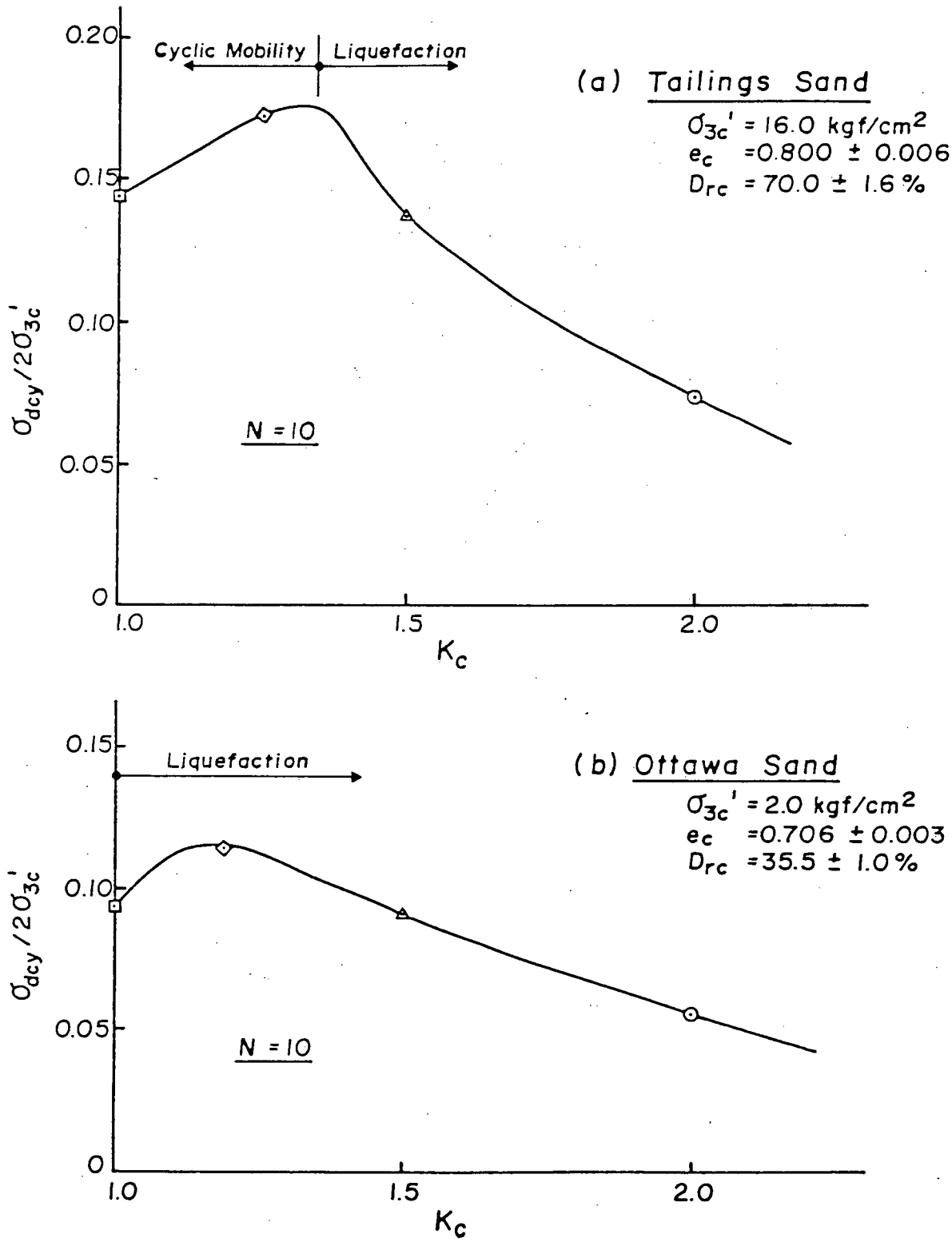

Fig. 5.26 Influence of static shear stress on the resistance to strain development under cyclic loading: (a) contractive tailings sand; (b) initially loose Ottawa sand.

contractive and dilative regions. For tailings sand under low confining pressure, the initial sample state was to the left of $(\sigma'_{1c})_{crit}$ = constant for the void ratio considered. Therefore, samples at all levels of K_c ratio being dilative developed cyclic mobility (Fig. 5.25a). It may be seen that the resistance to cyclic mobility (for 2.5% axial strain in 10 stress cycles) increased from 0.238 to 0.515 when the K_c ratio was increased from 1.0 to 2.0. Similar magnitude of increase in resistance to cyclic mobility may be noted for strain level of 5%. As discussed in Section 5.2.1, rapid accumulation of strain due to cyclic mobility is possible only when transient state of zero effective stress occurs during cyclic loading. Therefore, the higher the static shear, the higher is the cyclic stress amplitude required to cause this condition to occur and hence a consequent increase in resistance to cyclic mobility.

For Ottawa sand with D_{rc} = 51.5%, a trend similar to that for tailings sand under low confining pressure may be noted (Fig. 5.25b). However, unlike the tailings sand, which developed cyclic mobility regardless of the K_c ratio, Ottawa sand developed liquefaction at low K_c ratio. This has also been discussed earlier in Section 5.2.3. For this low K_c ratio, although the initial sample state is in dilative region in the compression deformation mode, it is contractive in the extension deformation mode. Therefore, liquefaction would be induced in extension mode, if the applied cyclic shear stress exceeds the steady state shear strength in extension. As the static shear stress in compression increases, the cyclic stress amplitude required to cause liquefaction in extension mode also increases. Thus the initial increase in resistance to cyclic strain developments at low K_c ratio in Fig. 5.25b is due to a

different strain development mechanisms. The limiting value of K_c in compression below which liquefaction could be induced in extension was found to be around 1.10. Beyond this K_c ratio, all samples developed cyclic mobility, and hence the resistance to cyclic mobility increased with increasing static shear stress, which is similar to the behaviour of tailings sand that developed cyclic mobility.

It may also be noted from the results shown in Fig. 5.25 that the resistance to cyclic mobility is influence by the strain level adopted. This is more significant in the region of high static shear. Sample under high static shear stress level may develop the lower level of prescribed strain in a specified number of stress cycle, but may take many more cycles to accumulate higher level of strain due to the slow down in the rate of strain accumulation in the case of non-stress reversal (Figs. 5.21 and 5.23). Therefore, the resistance curves diverge rapidly in the region of non-stress reversal.

For tailings sand under high confining pressure, i.e., initial state is to the right of $(\sigma'_{1c})_{crit}$ = const. line for the D_{rc} selected, liquefaction can not be induced at low K_c ratio and only cyclic mobility can be developed, as discussed in Section 5.1.4. The resistance to cyclic mobility may be seen to increase with increasing K_c ratio (Fig. 5.26a), which is similar to the behaviour of dilative sands. From the trend of the curve, this increase in resistance to cyclic mobility peaked at K_c ratio of about 1.35. At this K_c ratio, the sum of static and cyclic shear stresses approaches the lower bound of steady state shear strength for the D_{rc} considered. Therefore, liquefaction starts to develop for K_c values > 1.35 and the resistance to liquefaction decreases dramatically with increasing static shear.

For Ottawa sand at low relative density, similar trend as that of the tailings sand under high confining pressure may be noted (Fig. 5.26b). Relative values of the steady state shear strength and cyclic shear stress applied were such that the isotropically consolidated sample should not develop liquefaction. Therefore, the increase in resistance with initial increase in K_c should be the result of cyclic mobility developed. It was, however, found that this increase in resistance at low K_c ratio was due to the occurrence of liquefaction in extension mode and not the development of cyclic mobility. Increasing the static shear in compression increases the cyclic load amplitude required to exceed the steady state shear strength in extension. This trend continues until the static shear stress is high enough to cause liquefaction in compression mode. This level of static shear was found to be corresponding to K_c ratio of about 1.15. Beyond this static shear stress level, liquefaction always developed in compression mode, and the resistance to liquefaction decreased with increasing static shear stress level.

From the above results on both sands, it may be concluded that the resistance to liquefaction always decreases with increasing static shear stress level. This may be explained from the 3-D effective stress state diagram. As discussed in Sections 5.1.1, occurrence of liquefaction is due to the effective stress state of contractive sand reaching the CSR state and consequent initiation of strain softening response leading to steady state deformation. Therefore, the resistance to liquefaction is nothing but the cyclic stress ratio required to move the sample state to the CSR state in a fixed number of stress cycles. For easy visualization, this may be illustrated by the effective stress path plot of 3-D

effective stress state diagram at constant e_c as shown in Fig. 5.27. It may be noted in this figure that the stress space to be traversed to the left in order to reach the CSR state is less in the case of sand with higher static shear stress (case 2) than the sand with lower static shear stress (case 1). Therefore, the cyclic stress ratio or the number of stress cycles required to move the sample state from the initial state to the CSR state is less for higher K_c and hence the resistance to liquefaction is less. From the trend of the liquefaction resistance curves (Fig. 5.26), it appears that the resistance to liquefaction would be very low when a sand sample is initially consolidated to an initial state close to the CSR state. Slight shear disturbance or even a pore pressure increase could cause the sand to develop liquefaction. This would correspond to the phenomenon of spontaneous liquefaction, and will be discussed further in Section 5.6.

Comparing the stress states at CSR for Samples 1 and 2 in Fig. 5.27, it may further be noted that the potential to develop steady state deformation in Sample 2 is much higher than that in Sample 1. Much severe loss of resistance and larger deformation will be developed in Sample 2, once liquefaction is initiated. This may also be seen from the strain development due to liquefaction in Fig. 5.13.

Behaviour of sand anisotropically consolidated in extension mode was not within the scope of this investigation. Chung (1984) found that increasing the static shear in extension mode also causes decrease in resistance to liquefaction for Ottawa sand. The resistance curve in Fig. 5.26b can thus be extended in the extension region. Chung's findings are consistent with those reported herein and could be explained within the framework of steady state concepts.

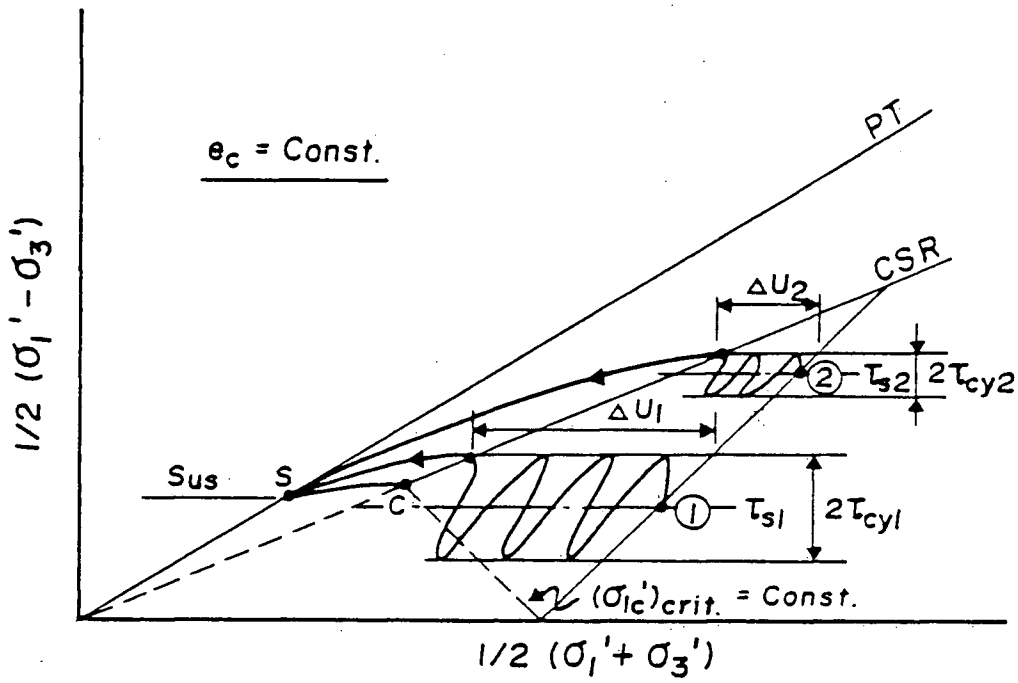

Fig. 5.27 Schematic illustration showing the influence of static shear stress on the resistance to liquefaction under cyclic loading.

From the examination of results for both sands in the contractive and dilative regions, completely different trends in liquefaction and cyclic mobility response may be noted. Increasing the static shear stress to the same level, e.g., K_c = 2.0, the resistance to cyclic mobility (for 2.5% ε_a) increased from 0.238 to 0.515 for tailings sand and from 0.167 to 0.308 for Ottawa sand (Fig. 5.25a,b), whereas the resistance to liquefaction decreased from 0.176 to 0.074 for tailings sand and from 0.114 to 0.056 for Ottawa sand (Fig. 5.26a,b). Therefore, it may be concluded that the resistance to strain development could decrease or increase depending on whether liquefaction or cyclic mobility is involved. It is often believed (Lee and Seed, 1967[2], 1970) that soil element in slope is more resistant to cyclic strain development than that under the level ground and suggestion is made that critical initial state would correspond to isotropic consolidation, which represent an initially zero static shear. This will be true for soil elements which develop cyclic mobility only. On the contrary, according to Castro and Poulos (1977) and Casagrande (1975), the resistance to strain development for soil element in the slope is always less than that under the level ground and the suggestion is made that tests be performed on anisotropically consolidated samples simulating appropriate initial static shear. Again, this will be true for soil elements which develop liquefaction only. Therefore, a clear understanding of the mechanism responsible for strain development is necessary for a rational assessment of influence of certain factors on the undrained cyclic loading response of sand.

It is also interesting to note that the influences of static shear stress on the undrained monotonic and cyclic loading behaviour are similar. Increasing the static shear stress level for fixed e_c and σ'_{3c}

can transform a sand from strain hardening response to liquefaction under monotonic loading conditions, and from cyclic mobility to liquefaction under cyclic loading conditions. The resistance to liquefaction (stress increment until peak in monotonic loading) was found to decrease with increasing static shear stress level under both loading conditions. However, this similarity can not be applied to monotonic strain hardening response and cyclic mobility. Under monotonic loading conditions, the shear stress increment ($\Delta\sigma_d/2\sigma'_{3c}$) required to reach the PT state is of concern, whereas the cyclic stress ($\sigma_{dcy}/2\sigma'_{3c}$) required to accumulate a specified amount of strain is of interest under cyclic loading conditions. The former constitutes a strength criterion, while the latter is a deformation criterion. The shear stress increment required to reach the PT line under monotonic loading was found to decrease with increasing static shear which is the reverse of the resistance to cyclic mobility.

5.5 Prediction of Undrained Cyclic Loading Behaviour

It was shown in Section 4.4.2 that 3-D effective stress state diagram gives a complete description of undrained behaviour under monotonic loading conditions, given the initial state (e_c, σ'_{3c}, K_c) of the sand. Under cyclic loading conditions, it has further been shown in Sections 5.1 and 5.2 that the undrained behaviour depends in addition on the amplitude of cyclic loads applied. The necessary criteria for liquefaction to occur under cyclic loading conditions are 1) the sand must have the potential to develop steady state deformation, i.e., the steady state can be achieved, and 2) the cyclic load amplitude applied must be large enough to cause the maximum shear stress (static + cyclic) greater

than its steady state shear strength and 3) sufficient number of load cycles are applied to move effective stress state of sand to the CSR line. Otherwise, only cyclic mobility or very small deformation can be developed.

From the consolidation characteristics of sand and the criteria mentioned above, a flow chart may be drawn to examine whether liquefaction can be developed in a sand with a given initial state and applied loads. This is shown in Fig. 5.28.

In order to examine the first criterion, the initial state of the sand is located in the 3-D effective stress state diagram. This initial state of the sand is obtained directly from the known void ratio e_c and the stress conditions in the ground or from the known initial void ratio e_i and the consolidation stress conditions. For sand elements with initial states below the critical consolidation stress $(\sigma'_{1c})_{crit}$ surface (Fig. 4.31), i.e., steady state can not be achieved, only cyclic mobility (together with slight strain softening for states slightly below $(\sigma'_{1c})_{crit}$ surface) can be induced, regardless of the cyclic loads applied. For sand elements with initial state on or above the $(\sigma'_{1c})_{crit}$surface, i.e., steady state can be achieved, potential to develop liquefaction always exists.

For Ottawa sand with rounded particles, the $(\sigma'_{1c})_{crit}$ is difficult to obtain. At loose e_i, $(\sigma'_{1c})_{crit}$ is extremely small (see Figure 4.13). In fact the strain softening and dilative branch off does not appear even at σ'_3 values as small as 0.13 kgf/cm^2 (12.7 kPa). And at slightly denser e_i, $(\sigma'_{1c})_{crit}$ is exceptionally large. However, the initial relative density alone gives a good prediction as to the potential to develop liquefaction.

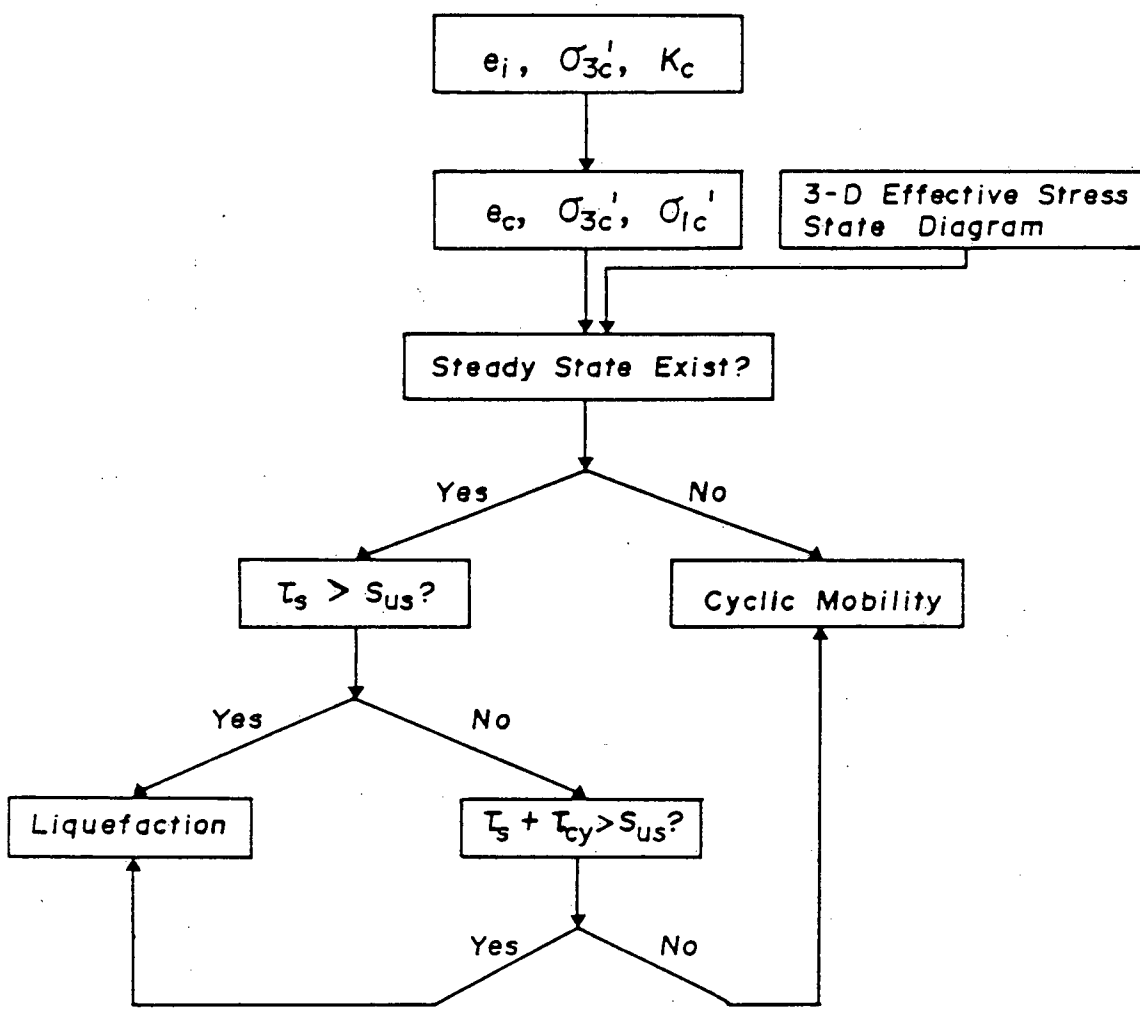

Fig. 5.28 Flow chart for assessing the potential of liquefaction or cyclic mobility.

Once the potential to develop liquefaction is determined and is found to exist, the second criterion has to be examined. Liquefaction is possible, regardless of the intensity of the cyclic loads applied, if the initial static shear stress is greater than the steady state shear strength of the soil element, which is a unique function of its e_c. This condition should always be avoided because combinations of pore pressure generated from cyclic loading and possible redistribution of pore pressure in the surrounding soil elements during and after cyclic loading may cause liquefaction and associated large deformations. However, if the static shear stress is less than the steady state shear strength, liquefaction is possible only when the maximum shear stress (static + cyclic) is greater than the steady state shear strength. Otherwise, only cyclic mobility can be developed.

It may be pointed out that very limited amount of monotonic loading tests have to be carried out in order to establish the 3-D effective stress state diagram of sand. The key aspects of the undrained cyclic loading behaviour of all soil elements in the earth structure can then be predicted from the 3-D effective stress state diagram and cyclic load applied, i.e., whether liquefaction or cyclic mobility will develop, thus enabling a first hand identification of the mechanism responsible for strain development under cyclic loading conditions.

5.6 Phenomenon of Spontaneous Liquefaction

As discussed in the last two chapters, liquefaction is the result of occurrence of strain softening response leading to steady state deformation when the effective stress state of sands is brought to the CRS state. This strain softening response can occur if potential for lique-

faction exists and when the total shear stress acting on the soil element is greater than its steady state shear strength. The change in state can occur on account of some shear disturbance applied to the soil element, which can be either static or cyclic in nature. If this disturbance is very small, the phenomenon is called spontaneous liquefaction.

The shear disturbance under static conditions can be caused by increases in shear stress due to erosion of toe of slope or surcharge applied on slope. It was shown by Eq. 4.6 in Section 4.4.2 that for tailings sand the shear stress increment to reach the CSR state under monotonic loading conditions decreases as the static shear stress acting on the sand increases. When the initial sample state is close to the CSR state, the shear stress increment required to initiate liquefaction is very small. This may also be seen from the relationship of pore pressure generated until the CSR state due to monotonic loading versus K_c ratio in Figs. 4.24 and 4.28 for both sands. For sand consolidated to even higher K_c ratio, i.e., in the region of contractive deformation (Fig. 4.17), a slight increase in shear stress can trigger strain softening response leading to steady state deformation. Such a phenomenon was illustrated by the example in Fig. 4.19. By an increase in shear stress less than 8% of the static shear stress, catastrophic failure was induced.

From the trend of resistance to liquefaction versus K_c ratio curves shown in Fig. 5.26, it appears that the resistance to liquefaction is very small when the sand is consolidated to a state close to the CSR state. For Ottawa sand consolidated to K_c ratio of 2.0, the resistance to liquefaction is about 0.056. The shear stress disturbance of this magnitude corresponds to earthquake with a_{max} of 0.05g according to the

simplified procedure proposed by Seed and Idriss (1971). Such a small change in shear stress required to cause instability is indeed a case of spontaneous liquefaction. For K_c ratio higher than 2.0, the shear disturbance required to cause liquefaction is even lower. For tailings sand, however, due to relatively high confining pressure involved, the cyclic stress ratio under this confining pressure corresponds to a relatively strong earthquake even though the cyclic stress ratio is very low.

Besides the shear stress disturbance discussed above, the change in sample state can also occur due to rise in pore pressure. This rise of pore pressure could be the result of fluctuation of ground water level or redistribution of excess pore pressure during or after earthquake shaking from the surrounding soil elements. To illustrate this mechanism of initiation of liquefaction, special tests were performed on both sands. An initially loose sample was consolidated anisotropically to K_c ratio of 2.0, and σ'_{3c} = 2.0 kgf/cm^2 (196 kPa) for Ottawa sand and 10.0 kgf/cm^2 (980 kPa) for tailings sand. Back pressure was then increased slowly while maintaining the static shear stress constant. By doing so the effective stress state of sand was moved horizontally toward the CSR line. After the effective stress state reached the state corresponding to the CSR state, the drainage line was closed. A slight increase in pore pressure was observed which was followed by a catastrophic failure in a manner similar to that observed during liquefaction. Typical results for both sands are shown in Figs. 5.29 and 5.30.

Thus spontaneous liquefaction will be triggered as soon as the sample state reaches the CSR state under undrained conditions due to a very small disturbance at which strain softening response leading to steady state deformation is initiated. This phenomenon can, however,

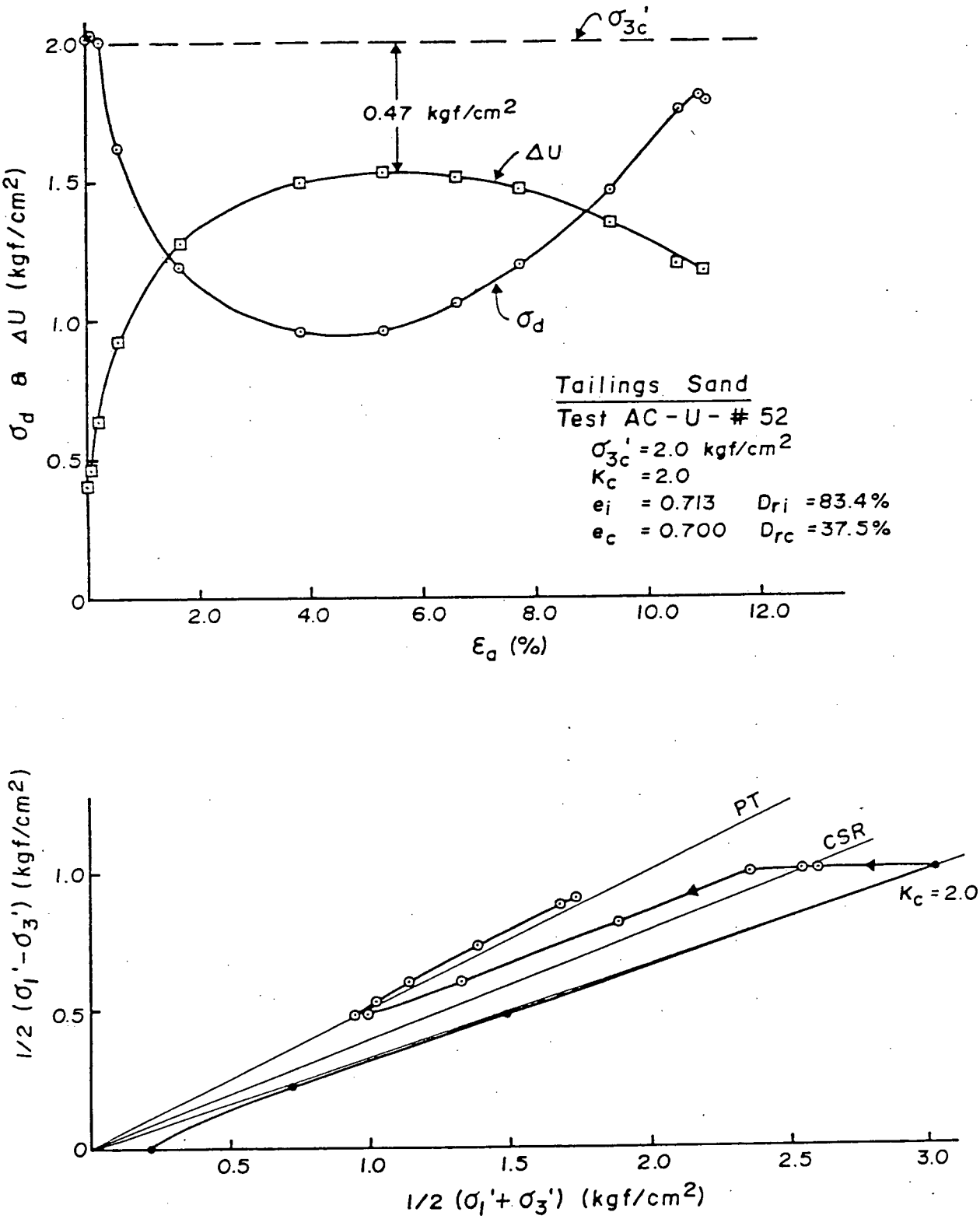

Fig. 5.29 Spontaneous liquefaction induced by pore pressure increase in initially loose Ottawa sand.

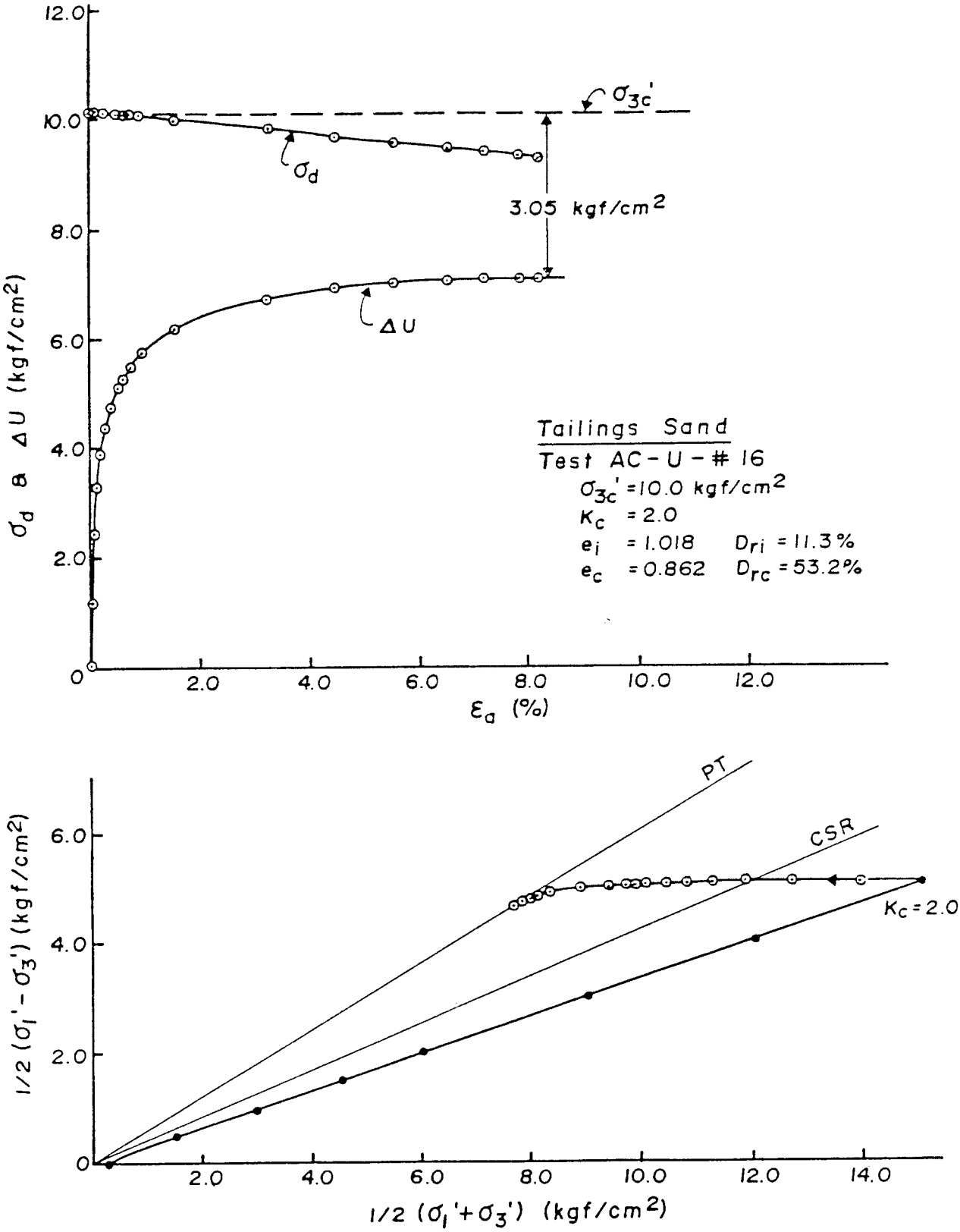

Fig. 5.30 Spontaneous liquefaction induced by pore pressure increase in contractive tailings sand.

occur only if the sand is subjected to static shear stress greater than its steady state shear strength. For tailings sand, this situation can exist only when an initially loose sample is consolidated to high confining pressure and high K_c ratio. This is shown in Fig. 5.31. It may be seen that for initially loose sample with K_c = 2.0 the confining pressure σ'_{3c} has to be greater than 7.0 kgf/cm^2 (686 kPa) in order to have static shear stress greater than its steady state shear strength. For sand with K_c = 1.5, the static shear stress is always less than its steady state shear strength for the range of consolidation stress considered. Therefore, under this K_c (= 1.5) ratio, sand is always safe against such kind of failure. Due to very high confining pressure required to have the condition discussed above to exist for K_c = 2.0, a very large pore pressure increase is required in order to bring about such a failure. In the example shown in Fig. 5.30, an increase in pore pressure by about 3.0 kgf/cm^2 (294 kPa), which corresponds to a rise of 30 m in water head, is necessary to trigger spontaneous liquefaction. Therefore, it appears there is rare possibility for such failure to be induced in tailings sand unless the sand is consolidated to K_c ratio close to or greater than the CSR.

Rounded Ottawa sand, however, behaves quite differently compared to the angular tailings sand. For initially loose sample under K_c ratio of 1.5 and 2.0, as shown in Fig. 5.32, the static shear stress is higher than its steady state shear strength under low confining pressure. The ratio of static shear stress to the steady state shear strength decreases with increasing confining pressure. The level of confining pressure below which the static shear stress is greater than its steady state shear strength depends on the K_c ratio of the sand. For initially

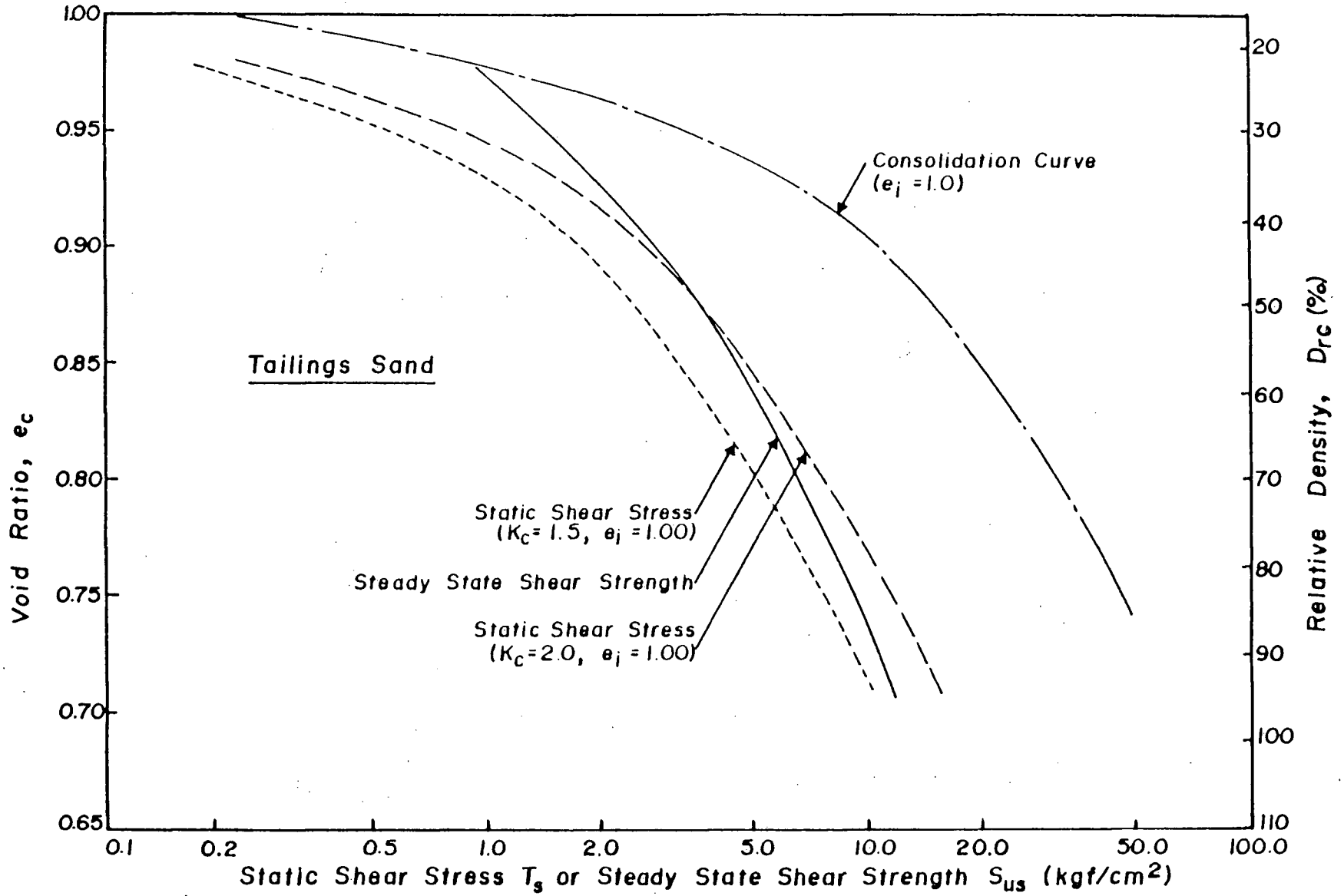

Fig. 5.31 Comparison of relative values of static shear stress and steady state shear strength for tailings sand at two K_c ratios.

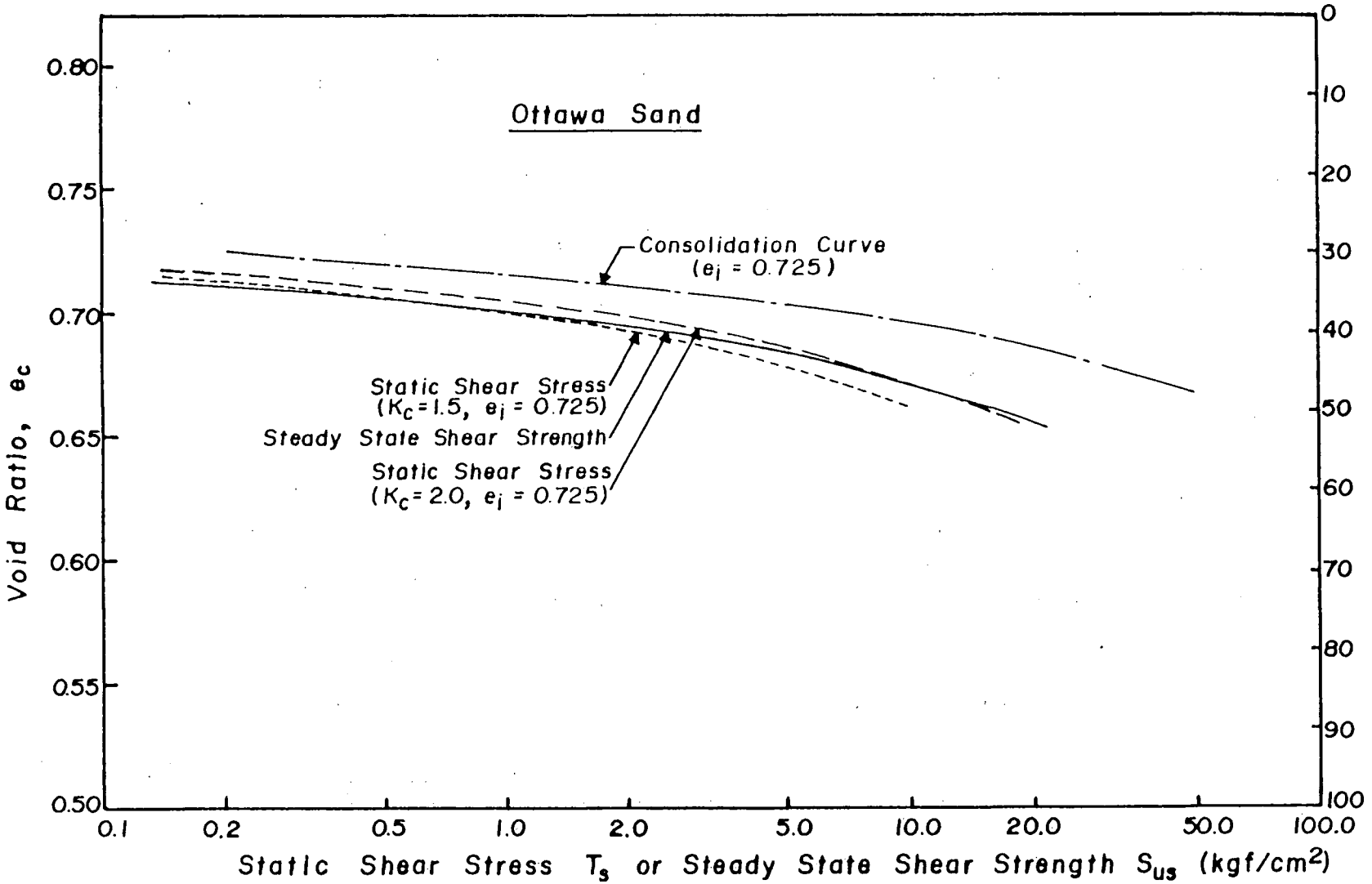

Fig. 5.32 Comparison of relative values of static shear stress and steady state shear strength for Ottawa sand at two K_c ratios.

loose sand, it is about 5.0 and 20.0 kgf/cm^2 (490 and 1960 kPa) for K_c ratio of 1.5 and 2.0 respectively. Therefore, sand with rounded particles is more susceptable to spontaneous liquefaction. Relatively small pore pressure increase has to occur in order to reach the CSR state and consequently trigger liquefaction.

CHAPTER 6

CONCLUSIONS

Undrained monotonic and cyclic loading behaviour of a saturated angular and a rounded sand has been studied under triaxial conditions over a confining pressure ranging up to 25.0 kgf/cm^2 (2450 kPa) and both isotropic and anisotropic consolidation histories. The range of behaviour under monotonic loading spanned between strain hardening at one end to various degrees of strain softening (termed liquefaction or limited liquefaction) at the other. Similarly, the range of behaviour responsible for development of strain under cyclic loading consisted of liquefaction or cyclic mobility or a combination of both. Cyclic mobility refers to the development of strain during cyclic loading which is not due to the occurrence of strain softening response. These definitions of liquefaction and cyclic mobility now enjoy a general acceptance among researchers. Based on test results on angular sand, the following conclusions may be drawn.

1) Under monotonic loading, the strain softening response is initiated at a critical value of effective stress ratio (CSR), regardless of the relative density and consolidation stress conditions of the sand.

2) The termination of strain softening response, which is characterized by the start of dilation (PT State), also occurs at a unique value of effective stress ratio, regardless of the relative density and consolidation stress conditions of the sand. When strain hardening response develops, the start of dilation, characterized by a decrease in pore pressure after a positive maximum value, also occurs at the same effective stress ratio as the PT state of strain softening response.

3) Under extension loading, the CSR is less than that in compression, but the effective stress ratios at PT state in compression and extension are the same.

4) Under monotonic loading, the stress conditions at PT state for strain hardening response form a series of lines in void ratio-effective confining pressure plot. These lines are function of initial void ratio only, regardless of the consolidation stress conditions. With increasing consolidation stresses, these lines for various initial void ratio merge into a unique steady state line representing strain softening response, characterized as limited or true liquefaction. This implies that the concept of unique steady state line can be used even when the sand develops strain softening response with significant strain potential (greater than about 2% for the sand tested) and is not necessarily restricted to unlimited strain characteristics of true liquefaction.

5) From the consolidation characteristics and stress conditions at PT state, a relationship between void ratio e_c and critical consolidation stress $(\sigma'_{1c})_{crit}$ emerges. Sand at a void ratio e_c under consolidation stress $\sigma'_{1c} \geq (\sigma'_{1c})_{crit}$ for e_c will develop liquefaction, regardless of the individual magnitudes of K_c and σ'_{3c}. For $\sigma'_{1c} < (\sigma'_{1c})_{crit}$, only strain hardening or slight strain softening response will develop. e_c - $(\sigma'_{1c})_{crit}$ line thus provides a quantitative division of initial states into regions of liquefaction and strain hardening response on undrained loading.

6) A 3-D effective stress state diagram for the sand characterizes comprehensively the anticipated monotonic loading response of sand from the knowledge of its end of consolidation state e_c, σ'_{3c} and K_c. This state diagram in e_c, $1/2(\sigma'_1+\sigma'_3)$, $1/2(\sigma'_1-\sigma'_3)$ space features a $(\sigma'_{1c})_{crit}$

surface which separates end of consolidation states of sand into regions of liquefaction and strain hardening response or slight strain softening response. A knowledge of the complete initial state of sand is necessary for assessment of the anticipated monotonic loading response. This response can not be predicted by specifying relative density alone or even the combination of relative density and confining pressure. The 3-D effective stress state diagram also offers a rational explanation as to the influence of relative density, confining pressure and static shear stress on the monotonic loading behaviour.

7) Under cyclic loading, the strain development could be due to liquefaction or cyclic mobility or the combination of both. If liquefaction develops, the CSR, effective stress ratio at PT state and steady state line are the same as those observed under monotonic loading. If cyclic mobility develops, the effective stress ratio at PT state is also the same as that observed under monotonic loading. Therefore, the stress conditions which characterize the key features of strain softening and strain hardening response are not influenced by the type of load (monotonic or cyclic) applied, and thus the 3-D effective stress state diagram provides a link between monotonic and cyclic loading behaviour.

8) The 3-D effective stress state diagram developed for monotonic loading can be used to develop the criteria for the occurrence of liquefaction and cyclic mobility. The criteria for the occurrence of liquefaction are: (1) the initial sand state must lie on or above the $(\sigma'_{lc})_{crit}$ surface, (2) the maximum shear stress (static + cyclic) is greater than the steady state shear strength, and (3) sufficient number of load cycles are applied to move the effective stress state of sand to the CSR line. Otherwise, only cyclic moblity or very small deformation

can be developed.

9) The influences of relative density and confining pressure on the cyclic loading behaviour are similar to those on the monotonic loading behaviour. However, the influence of static shear stress on cyclic loading behavior could be quite different depending on whether liquefaction or cyclic mobility is developed. If the sand develops liquefaction, an increase in static shear stress always results in a decrease in resistance to liquefaction. On the other hand, if it develops cyclic mobility, increasing static shear stress always results in an increase in resistance to cyclic mobility. These conclusions are in agreement with those suggested by Castro and Seed if a proper recognition of the mechanism of strain development under cyclic loading is made.

The conclusions drawn above are based on the results of tests on angular sand. These conclusions are also true for rounded sand. However, for the range of consolidation stress considered herein (the range of σ'_{3c} considered is larger than what would be encountered in most practical situations), the initial relative density alone provides a good single parameter for characterizing this initial state of rounded sand. For initially loose states, the sand always develops liquefaction, regardless of the initial stress conditions. The response, however, changes to strain hardening or slightly strain softening if initial relative density exceeds a certain minimum value (about 40% for the sand tested). It appears that the liquefaction response in rounded sand is related to an initial loose structure, which is not altered even after the application of large confining pressure.

REFERENCES

Bishop, A.W., Webb, D. and Skinner, A.E. (1965). "Triaxial Tests on Soils at Elevated Cell Pressure," Proc. 6th ICSMFE, Montreal, Vol. 1, pp. 170-174.

Bjerrum, L., Kringstad, S. and Kummeneje, O. (1961). "The Shear Strength of Fine Sand," Proc. 5th ICSMFE, Paris, Vol. 1, pp. 29-37.

Casagrande, A. (1936). "Characteristics of Cohesionless Soils Affecting the Stability of Slopes and Earth Fills," Jour. of the Boston Society of Civil Engineers, Jan. 1936.

Casagrande, A. (1975). "Liquefaction and Cyclic Deformation of Sands, A Critical Review," Proc. 5th Pan American Conf. on Soil Mech. and Found. Engng., Buenos Aires, Vol. 5, pp. 79-133.

Castro, G. (1969). "Liquefaction of Sands," Ph.D. Thesis, Harvard Soil Mech. Series, No. 81, Harvard University.

Castro, G. (1975). "Liquefaction and Cyclic Mobility of Saturated Sands," Jour. of the Geot. Engng. Div., ASCE, Vol. 101, No. GT6, Proc. Paper 11388, pp. 551-569.

Castro, G. and Poulos, S.J. (1977). "Factors Affecting Liquefaction and Cyclic Mobility," Jour. of the Geot. Engng. Div., ASCE, Vol. 103, No. GT6, Proc. Paper 12994, pp. 501-516.

Castro, G., Poulos, S.J., France, J.W. and Enos, J.L. (1982). "Liquefaction Induced by Cyclic Loading," Report Submitted to National Science Foundation, March, 1982.

Chern, J.C. (1981). "Effect of Static Shear on Resistance to Liquefaction," M.A.Sc. Thesis, The University of British Columbia, Vancouver, Canada.

DeAlba, P., Seed, H.B. and Chan, C.K. (1976). "Sand Liquefaction in Large-Scale Simple Shear Tests," Jour. of the Geot. Engng. Div., ASCE, Vol. 102, No. GT9, Proc. Paper 12403, pp. 909-927.

Dobry, R. and Alvarez, L. (1967). "Seismic Failures of Chilean Tailings Dams," Jour. of the Soil Mech. and Found. Div., ASCE, Vol. 93, No. SM6, Proc. Paper 5582, pp. 237-260.

Finn, W.D.L. (1981). "Liquefaction Potential: Developments Since 1976," Int. Conf. on Recent Advances in Geot. Earth. Engng. and Soil Dynamics, St. Louis, MO, pp. 655-681.

Finn, W.D.L. and Byrne, P.M. (1976). "Liquefaction Potential of Mine Tailings Dams," Proc. 12th Int. Conf. on Large Dams, Mexico City, Vol. 1, pp. 153-177.

Finn, W.D.L., Pickering, D.J. and Bransby, P.L. (1971). "Sand Liquefaction in Triaxial and Simple Shear Tests," Jour. of the Soil Mech. and Found. Div., ASCE, Vol. 97, No. SM4, Proc. Paper 2039, pp. 639-659.

Finn, W.D.L. and Vaid, Y.P. (1977). "Liquefaction Potential from Drained Constant Volume Cyclic Simple Shear Tests," Proc. 6th World Conf. on Earth. Engng., New Delhi, Session 6, pp. 7-12.

Green, G.E. (1969). "Strength and Compressibility of Granular Materials Under Generalized Strain Conditions," Ph.D. Thesis, University of London, Imperial College of Science and Technology.

Gueze, E. (1948). "Critical Density of Some Dutch Sands," Proc., 2nd ICSMFE, Rotterdam, Vol. 3, pp. 125-130.

Horn, H.M. and Deere, D.U. (1962). "Frictional Characteristics of Minerals," Geotechnique, Vol. 12, No. 4, pp. 319-335.

Ishihara, K., Tatsuoka, F. and Yasuda, S. (1975). "Undrained Deformation and Liquefaction of Sand Under Cyclic Stresses," Soils and Foundations, Vol. 15, No. 1, pp. 29-44.

Klohn, E.J., Maartman, C.H., Lo, R.C.Y. and Finn, W.D.L. (1978). "Simplified Seismic Analysis for Tailings Dams," Proc., ASCE Specialty Conf. on Earth. Engng. and Soil Dynamics, Pasadena, CA., pp. 540-556.

Koppejan, A.W., Wamelen, B.M. and Weinberg, L.J. (1948). "Coastal Flow Slides in the Dutch Province of Zeeland," Proc., 2nd ICSMFE, Rotterdam, Vol. 5, pp. 89-96.

Lee, I.K. (1966). "Stress-Dilatancy Performance of Feldspar," Jour. of the Soil Mech. and Found. Div., ASCE, Vol. 92, No. SM2, Proc. Paper 4734, pp. 79-108.

Lee, K.L. (1978). "End Restraint Effects on Undrained Static Triaxial Strength of Sand," Jour. of the Geot. Engng. Div., ASCE, Vol. 104, No. GT6, Proc. Paper 13838, pp. 687-704.

Lee, K.L. and Seed, H.B. (1967^1). "Cyclic Stress Conditions Causing Liquefaction of Sand," Jour. of the Soil Mech. and Found. Div., ASCE, Vol. 93, No. SM1, Proc. Paper 5058, pp. 47-70.

Lee, K.L. and Seed, H.B. (1967^2). "Dynamic Strength of Anisotropically Consolidated Sand," Jour. of the Soil Mech. and Found. Div., ASCE, Vol. 93, No. SM5, Proc. Paper 5451, pp. 169-190.

Lee, K.L. and Seed, H.B. (1970). "Undrained Strength of Anisotropically Consolidated Sand," Jour. of the Soil Mech. and Found. Div., ASCE, Vol. 96, No. SM2, Proc. Paper 7136, pp. 411-428.

Lee, K.L. and Vernese, F.J. (1978). "End Restraint Effects on Cyclic Triaxial Strength of Sand," Jour. of the Geot. Engng. Div., ASCE, Vol. 104, No. GT6, Proc. Paper 13839, pp. 705-719.

Lindenberg, J. and Koning, H.L. (1981). "Critical Density of Sand," Geotechnique, Vol. 31, No. 2, pp. 231-245.

Luong, M.P. (1980). "Stress-Strain Aspects of Cohesionless Soils Under Cyclic and Transient Loading," Int. Symp., Swansea, U.K.

Poulos, S.J. (1971). "The Stress-Strain Curves of Soils," Geotechnical Engineers Inc., Winchester, Mass., pp. 1-80.

Poulos, S.J. (1981). "The Steady State of Deformation," Jour. of the Geot. Engng. Div., ASCE, Vol. 107, No. GT5, Proc. Paper 16241, pp. 553-562.

Rowe, P.W. and Barden, L. (1964). "Importance of Free Ends in Triaxial Testing," Jour. of the Soil Mech. and Found. Div., ASCE, Vol. 90, No. SM1, Proc. Paper 3753, pp. 1-27.

Sangrey, D.A. Castro, G., Poulos, S.J. and France, J.W. (1978). "Cyclic Loadings of Sands, Silt and Clays," Proc., ASCE Specialty Conf. on Earthquake Engng. and Soil Dynamics, Pasadena, CA., Vol. 2, pp. 836-851.

Seed, H.B. (1979). "Soil Liquefaction and Cyclic Mobility Evaluation for Level Ground During Earthquakes," Jour. of the Geot. Engng. Div., ASCE, Vol. 105, No. GT2, Proc. Paper 14380, pp. 201-255.

Seed, H.B. (1981). "Earthquake-Resistant Design of Earth Dams," Int. Conf. on Recent Advances in Geot. Earthquake Engng. and Soil Dynamics, St. Louis, MO, Vol. 3, pp. 1157-1173.

Seed, H.B. and Idriss, I.M. (1971). "Simplified Procedure for Evaluating Soil Liquefaction Potential," Jour. of the Soil Mech. and Found. Div., ASCE, Vol. 97, No. SM9, Proc. Paper 8371, pp. 1249-1273.

Seed, H.B. and Lee, K.L. (1966). "Liquefaction of Saturated Sands During Cyclic Loading," Jour. of the Sol Mech. and Found Div., ASCE, Vol 92, No. SM6, Proc. Paper 4972, pp. 105-134.

Seed, H.B. and Lee, K.L. (1969). "Pore Water Pressure in Earth Slopes Under Seismic Loading Conditions," Proc. 4th World Conf. on Earth. Engng., Santiago, Vol. 3, A-5, pp. 1-11.

Seed, H.B., Lee, K.L., Idriss, I.M. and Makdisi, F.I. (1975). "The Slides in the San Fernando Dams During the Earthquake of February 9, 1971," Jour. of the Geot. Engng. Div., ASCE, Vol. 101, No. GT7, Proc. Paper 11449, pp. 651-688.

Seed, H.B., Pyke, R. and Martin, G.R. (1975). "Analysis of the Effect of Multi-Directional Shaking on the Liquefaction Characteristics of Sands," Report No. EERC 75-41, Earthquake Engineering Research Center, University of California, Berkeley, California.

Vaid, Y.P. and Chern, J.C. (1983[1]). "Effect of Static Shear on Resistance to Liquefaction," Soils and Foundations, Vol. 23, No. 1, pp. 47-60.

Vaid, Y.P. and Chern, J.C. (1983[2]). "Mechanism of Deformation During Cyclic Undrained Loading of Saturated Sands," Int. Jour. of Soil Dynamics and Earthquake Engng., Vol. 2, No. 3, pp. 171-177.

Vaid, Y.P., Chern, J.C. and Tumi, H. (1983). "Effect of Confining Pressure and Particle Angularity on Resistance to Liquefaction," Proc. 4th Canadian Conf. on Earthquake Engng., Vancouver, pp. 341-351.

Vaid, Y.P. and Finn, W.D.L. (1979). "Effect of Static Shear on Liquefaction Potential," Jour. of the Geot. Engng. Div., ASCE, Vol. 105, GT10, Proc. Paper 14909, pp. 1233-1246.

Yoshimi, Y. and Oh-Oka, H. (1975). "Influence of Degree of Shear Stress Reversal on the Liquefaction Potential of Saturated Sand," Soils and Foundations, Vol. 15, No. 3, pp. 27-40.